Geophysical Constraints on the Structural Evolution and Hazards of Masaya Volcano, Nicaragua

Thesis

Geophysical constraints on the structural evolution and hazards of Masaya volcano, Nicaragua

A thesis presented for the degree of

Doctor of Philosophy

By

Guillermo Caravantes González

Licenciado
Universidad Complutense de Madrid, Spain

Department of Environment, Earth and Ecosystems

The Open University

December 2013

"Geology isn't a real science!!!"

Sheldon Cooper

(The Big Bang Theory, Season 5, Ch. 1.)

ABSTRACT

Investigating the structural framework of active volcanoes is essential to understand the reasons for their past and present activity and the constraints on their future evolution. Potential field geophysical techniques can provide information on a number of physical parameters (density, conductivity, magnetic susceptibility) relevant for recognizing structures with influence on the evolution of a volcanic edifice. Masaya Volcano is a 11 km x 6.5 km basaltic shield caldera located in Nicaragua and the source of different types of volcanic activity in the past (including basaltic plinian eruptions). Considering the high population density of the area under the influence of Masaya Volcano (the largest in Nicaragua), understanding the implications of its structural framework for volcanic activity must be a high priority.

Geological and geophysical techniques were used to identify significant geological features within Masaya basaltic caldera and provide a complete picture of the relationship between structures and volcanic activity. A ≈3.5 km diameter ring fault found in the NW half of the Caldera connects most of the volcanic manifestations on the caldera floor (fumaroles, spatter cones, >50 m tall cinder cones and the active summit area). This fault has acted in historical times as a path for magma and the hydrothermal system. An elongated (NNW-SSE) intrusive body 1-3 km deep has been characterized using gravity methods. The spatial coincidence of this body (interpreted as a basaltic magma reservoir) below the ring fault is responsible for the concentration of erupted material in the SW section of the ring fault. This accounts for most of the volcanic material erupted in the last 1.8 ka in the caldera, thus contributing to partially emptying the reservoir and facilitating the current observable (using InSAR methods) 4 cm/yr subsidence of this part of the caldera floor (SW section of the lid inside the ring fault). The characteristics of this collapse resemble the end-member model of caldera trapdoor collapse. A NNE-SSW 1.5 km linear fissure, evidence for the connection between the caldera and the local graben, has been described. Our knowledge of the characteristics of a previously known (Metaxian 1994) dense intrusion NE of the caldera has also been improved, revealing that it partially underlies the caldera floor and its volume had been overestimated in previous studies.

Using the Very Low Frequency (VLF) method, a map using two orthogonal source transmitters of VLF waves has been completed in the summit area of Masaya Volcano. This map provides information on the size, shape and orientation of faults in the summit area and reveals that the main faults are currently occupied by the hydrothermal system. Using gravity methods, subsurface mass transfer processes in the summit area that occur on three different timescales (<1, 2-5 and >10 years) have been identified. A water-

bearing lava tube system has been discovered by a combination of Very Low Frequency (VLF), gravity and geological techniques. This combined approach yields a great potential for characterizing faults, voids, dikes and other features common in volcanic settings.

ACKNOWLEDGEMENTS

First, I would like to thank my supervisors (the best one could hope for) for their support and friendship through the last 4 years. In times of need, I could always find in them not only accurate comments on my writings (well, that too), but understanding, advice, and a sincere concern for my well-being. Hazel, thanks for believing in me from the beginning, and for your constant personal support. Steve, thanks for your patience and your unquenchable spirit of encouragement.

I would also like the members of my examination panel (Dave Rothery and Jenni Barclay) for making my Viva a pleasant (and very instructive) experience. Also, I can't help but remember at this point how everything started. Francisco Anguita has a big part of responsibility in instilling in me the love for Earth Sciences. I still remember how he played for us one of the episodes of the miniseries "From the Earth to the Moon" in my very first day of University, the one where geologist Harrison Schmitt (the only scientist to ever step on the Moon) is depicted. The words Professor Anguita uttered right after the episode finished have stayed with me my entire professional career: "Harrison Schmitt made it to the Moon. If you work hard enough, you can also fulfil your dreams". I must also express my gratitude to Javier Ruiz, who taught me almost everything I know about how science works, and has been a great friend over the years.

This thesis wouldn't have been possible without the support of the many friends and colleagues that offered their selfless help, time and resources, becoming the sword in the old Spanish aphorism: "Where a Spanish gentleman does not reach with his hand, it does with the tip of his sword" (Gregory Chavarri). I want to thank INETER for sharing with us their resources and expertise; and to Manuel (our driver) for a crash course on 4x4 extreme off road driving. Scary. I am extremely grateful to Masaya National Park Rangers for their support, company and professionalism. No one in the world knows the caldera better than them, and definitely no one in the universe can tell more jokes per unit of time (particularly useful if you are trying to learn Nicaraguan...). Thanks to Carlos Adan, Gabriel, Byron, Jaime Cárdenas and many others, and especially to Erico Manuel Tellez Jimenez, whose commitment to protecting Nicaraguan environment and wildlife is not only praiseworthy but inspirational.

Thanks to the owners of Hotel Regis, Don Carlos, Doña Juanita and their family, for making us feel at home, for many hours of interesting conversations on the political history of Nicaragua, and for the best *maduros* in the world. Thanks to Lola and her family in Colima, for proving to us that you can be young, pretty, warm and full of life after having lived a lifetime of experiences. Special thanks go to Sergio, Maria and Angel, that made of my time in Nicaragua an unforgettable experience, and embraced me (and my sister, from day one!) as part of their family. Thanks Sergio, my brother, for

teaching me what Nicaragua really is about, away from the glamour of volcanology expeditions and tourist spots. Thank you very much Jeff and Melanie for all those fun hours of fieldwork spent together.

I am very grateful to Jordi and Xiomara, my very best friends, who have been a constant reminder of what really matters in life, and with their support and friendship have made a very intense period of my life feel like a fun game. That includes the Supermanager, Olot, the calçots, the paragliding and swimming in rivers, the flights in helicopters... I will never forget how important your support has been guys. I totally and unconditionally love you.

I also want to thank my family, who have always fully supported me no matter what, and never stopped believing in me, even when I wasn't the best student out there. My mother Lola and my father Carlos are the greatest parents one could ask for, and have had a large and meaningful contribution to this thesis. Thanks for your advice on the *social sciences* chapter and your help with formatting and definitions; but above all thanks for being the best people to share life with, for teaching me almost everything I know, and for trying so hard to make a good person out of me. The list of things I have to thank you for is endless and I have written enough lately, so I'll keep the rest for our next family reunion in La Felicidad.

Yes Paloma, you deserve a paragraph apart. But instead of thanking you here, I've included this to apologize to you. Sorry for putting your life at risk quite a few times. Sorry about the killer bees. Sorry about the dehydration and the unexpected climbing. Oops. Now seriously, thank you, because it is such a great privilege having you as a sister. I consider myself incredibly fortunate to have you by my side, and I hope we can continue to share our lives -like we've done so far- for many, many years. Since I can't really express here how important you are for me, I'll let Will's words to Sloan do it for me ..."love you Sis!".

Last, but not least, I'd very much like to thank God, for looking at the Earth and making it tremble, and for touching the mountains and making them smoke (Psalm 104:32).

Por doquiera donde vaya,
el recuerdo irá conmigo
del corazón de Masaya,
tan hidalgo y tan amigo.

Son retorno y despedida
juntos en este momento;
Mas de Masaya florida
el nombre en mi pensamiento
irá por toda la vida.

A esta región hechicera
no quiero decir adiós
que la vea antes que muera
que esté siempre en primavera
y que la bendiga Dios.

Darío, Rubén, en un 7 de diciembre de 1907.

Table of Contents

List of figures

List of tables

1 Introduction

1.1 Masaya Volcano

Masaya Volcano is located in Central-Western Nicaragua, Central America, in an area of the country which is heavily populated. According to the socio-demographic census completed in the country in 2005, at least 4 of the 8 largest cities of Nicaragua (Managua, Masaya, Tipitapa and Granada) are located within 23 km of the volcano, which combined account for 1/3 of the country's population (ca. 6 million). Volcanic activity from Masaya has been highly varied over time, including passive degassing, fissure eruptions, lava flows, lava lakes, minor strombolian explosions and highly energetic basaltic Plinian eruptions that impacted the location currently occupied by the capital city of Managua, e.g. (Pérez and Freundt 2006). This wide range of potentially hazardous activity means that Risk Management Plans have to take into account a range of possible scenarios in order to be really effective. It is therefore essential that we have a deep understanding of the mechanisms that control Masaya's activity, so that high quality plans of preparedness can be adequately developed and put into action if they are needed.

1.2 Research questions

Main research questions:

- What role has Masaya Caldera's structural framework played in controlling its activity in the past?
- What role will it play in the future?

OBJECTIVES: the main objective of this thesis is to thoroughly characterize and describe Masaya Caldera's structural framework at different depths using new geophysical data gathered for this purpose (Chapters 3 and 4), and building on the work by Williams (1983), Metaxian (1994) , Rymer et al. (1998) and Girard and van Wyk de Vries (2005). The scope is to facilitate our understanding of the reasons for the type of activity that takes place in Masaya today and the constraints that the structural framework may impose on the evolution of future activity (Chapters 3 and 4).

It is also within the scope of this research to improve our knowledge on the extent and geometrical characteristics of Masaya Caldera's underlying magma chamber, and of any structures connecting it to shallower levels, which might be relevant for hazard assessment purposes (Chapter 5). Finally, making use of the favourable conditions that make Masaya Caldera a natural laboratory for volcanology studies (good accessibility, low risk, variety of volcanic structures), we have attempted to combine different types of geophysical data that measure different properties. The scope is to build a picture of sub-surface features and identify potentially useful multi-instrument techniques that can be applied in the future to the study of volcanic environments (Chapter 4).

1.3 Geological and tectonic setting

1.3.1 Tectonic context

Masaya Caldera is geodynamically related to the subduction of the Cocos Plate under the Caribbean Plate. The geometry of this subduction accounts for the crustal anti-clockwise rotation movement that dominates the Nicaraguan area. The Nicaraguan Depression (Figure **1-1**: ND), host to most of the Quaternary volcanoes in Nicaragua including Masaya, is almost certainly tectonically related to this rotation movement (La Femina, Dixon et al. 2002; Girard and van Wyk de Vries 2005). Today, this depression is dominated by a right-lateral strike-slip stress regime (Girard and van Wyk de Vries 2005).

The Managua Graben (Figure **1-2**, limited in the East by the Cofradias Fault and in the West by the Nejapa-Miraflores and Mateare Faults) is a very active structure within the Nicaraguan Depression, in the area between both of Nicaragua's major lakes, Lake Managua and Lake Nicaragua. It has been suggested in the past that the graben might be a pull-apart basin (Sebesta 1997), especially considering its rhomboid shape. In the vicinities of Masaya Volcano the graben is bounded by the Cofradías Fault to the East, the Nejapa-Miraflores, and Mateare Faults to the West, and Masaya Caldera and a set of faults between Masaya and Apoyo volcanoes to the South. It encompasses the Aeropuerto Depression, which is bounded by the Cofradías Fault to the East and the Aeropuerto

Fault to the West. Movements along the faults of the Managua Graben that connect Masaya Caldera and Lake Nicaragua are thought to be the cause for the destructive earthquake of 1972 (Brown, Ward et al. 1973), which severely damaged Managua City, killing over twenty thousand people and destroying most of the significant buildings in the centre of the town.

South of the Managua Graben, and probably acting as a boundary for it in the South, is the Las Sierras-Masaya Volcanic Complex, a complicated volcanic construct formed by an ignimbrite shield called Las Sierras that encompasses a system of overlapping calderas (van Wyk de Vries 1993; Sebesta 1997). The external limiting faults for some of the calderas in the area are still highly noticeable in the field and/or in aerial imagery, although it is not always possible to link them to a particular pre-existing volcanic edifice. Some of them seem to be the product of the 30000 years BP eruption which formed Las Sierras Caldera (van Wyk de Vries 1993). After the formation of Las Sierras Caldera, a high density intrusion centred directly beneath Nindiri Town emplaced in the area (Connor and Williams 1989; Metaxian 1994), to the NE of the present Masaya Caldera, although its boundaries are unclear.

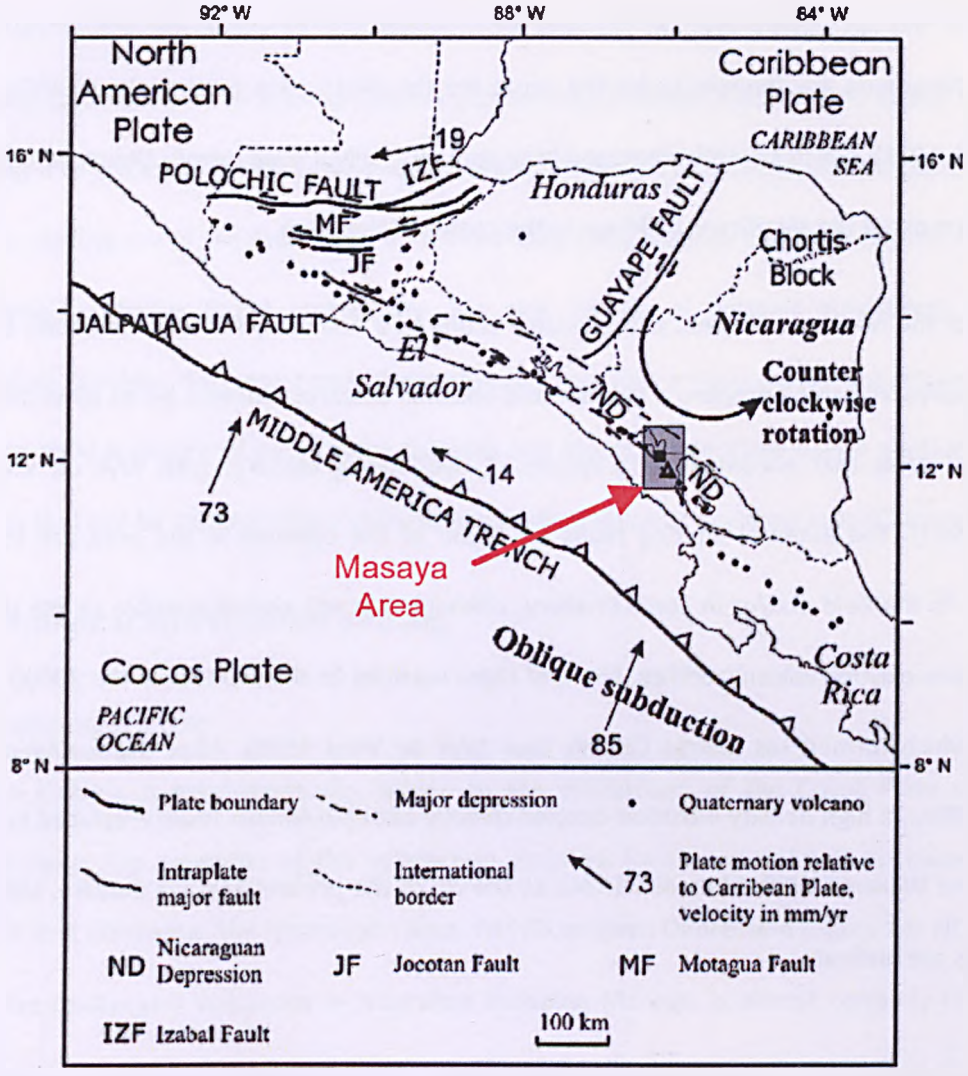

Figure 1-1: Regional tectonic map of the Nicaragua area, showing plate boundaries and the relative movement of the Nicaraguan crustal block at present (after Girard and van Wyk de Vries (2005)). The grey square shows the location of the study area.

It was within the boundaries of Las Sierras Caldera that a new basaltic volcano (the forerunner to Masaya), started to develop over a period of several thousand years, until a basaltic shield was formed. Interestingly, this shield produced several basaltic Plinian eruptions (Bice 1980; Williams 1983; Williams 1983; Pérez and Freundt 2006; Pérez Fernández 2007; Pérez, Freundt et al. 2009). According to Pérez and Freundt (2006), at least 4 Plinian eruptions with VEI of 3-4 have originated from Masaya in the last 6000 years. After the last one took place at 1800 BP, the present caldera boundaries were probably completely formed; and another basaltic shield volcanic edifice started to grow in the North-eastern half of the Caldera, which today is known as Masaya Volcano.

This complex tectonic setting holds most of the clues for understanding the development of Masaya Caldera. From the connection between the Nicaragua Depression and the generation of volcanic edifices within its boundaries in the Quaternary, to the extensional stress regime provided by the local pull-apart basin (Sebesta 1997), the tectonic environment has played a major role in the formation and present location of Masaya Caldera (Girard and van Wyk de Vries 2005). However, the clearest evidence of the interrelation between the surrounding tectonic features and Masaya Caldera is the presence of the Cofradías Fault, which has the same general orientation as several faults within Masaya Caldera (lineaments with a similar NNE strike South of Masaya Caldera have also been found that might be an extension of the Cofradías Fault (Girard and van Wyk de Vries 2005)). If this fault is, in fact, the eastern bounding fault of a pull-apart basin (Girard and van Wyk de Vries 2005), its connection to the Caldera complex could be even more important, since the dense underlying pluton that is inferred by Connor and Williams (1989) and Metaxian (1994), might have localized the faulting (Girard and van Wyk de Vries 2005) and those two contemporaneous structures (1 Ma, Sebesta (1997); van Wyk de Vries (1993)) might be inextricably linked.

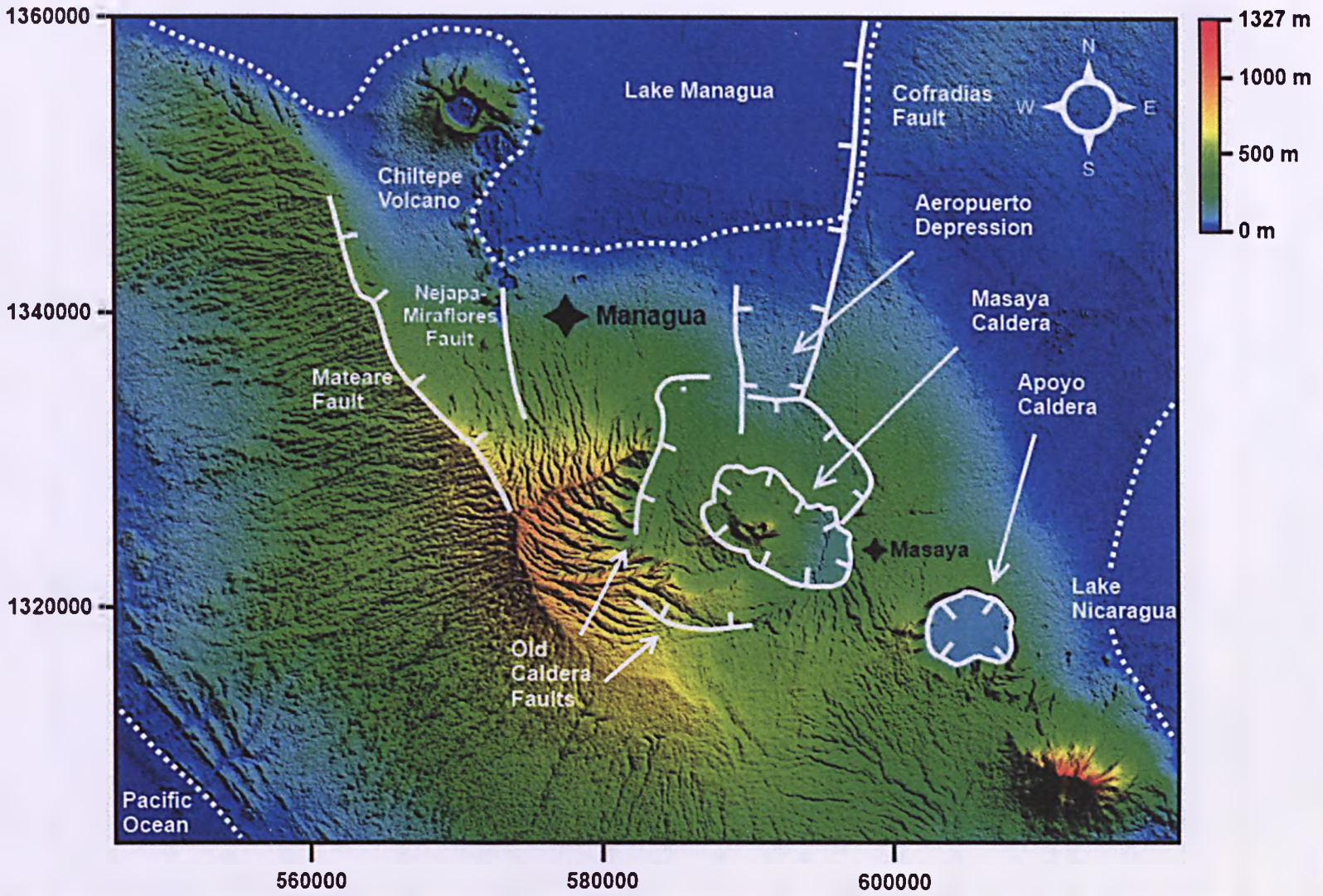

Figure 1-2: Regional topographic map built from a 30 m Aster DEM reflecting the main tectonic features in the area, after Bice (1980), Sebesta (1997); Girard and van Wyk de Vries (2005). Dotted lines show the boundaries of the water bodies in the area.

1.3.2 Physical aspects of Masaya Volcano and characteristics of the summit area

Masaya Caldera is a medium sized caldera 11 km long, 6.5 km wide and with an area of 58 km^2 (Figure **1-2**). Its long axis follows a N118°E orientation; while its short axis has a virtually perpendicular orientation of N207°E. The caldera bounding scarps define a total perimeter of 32 km.

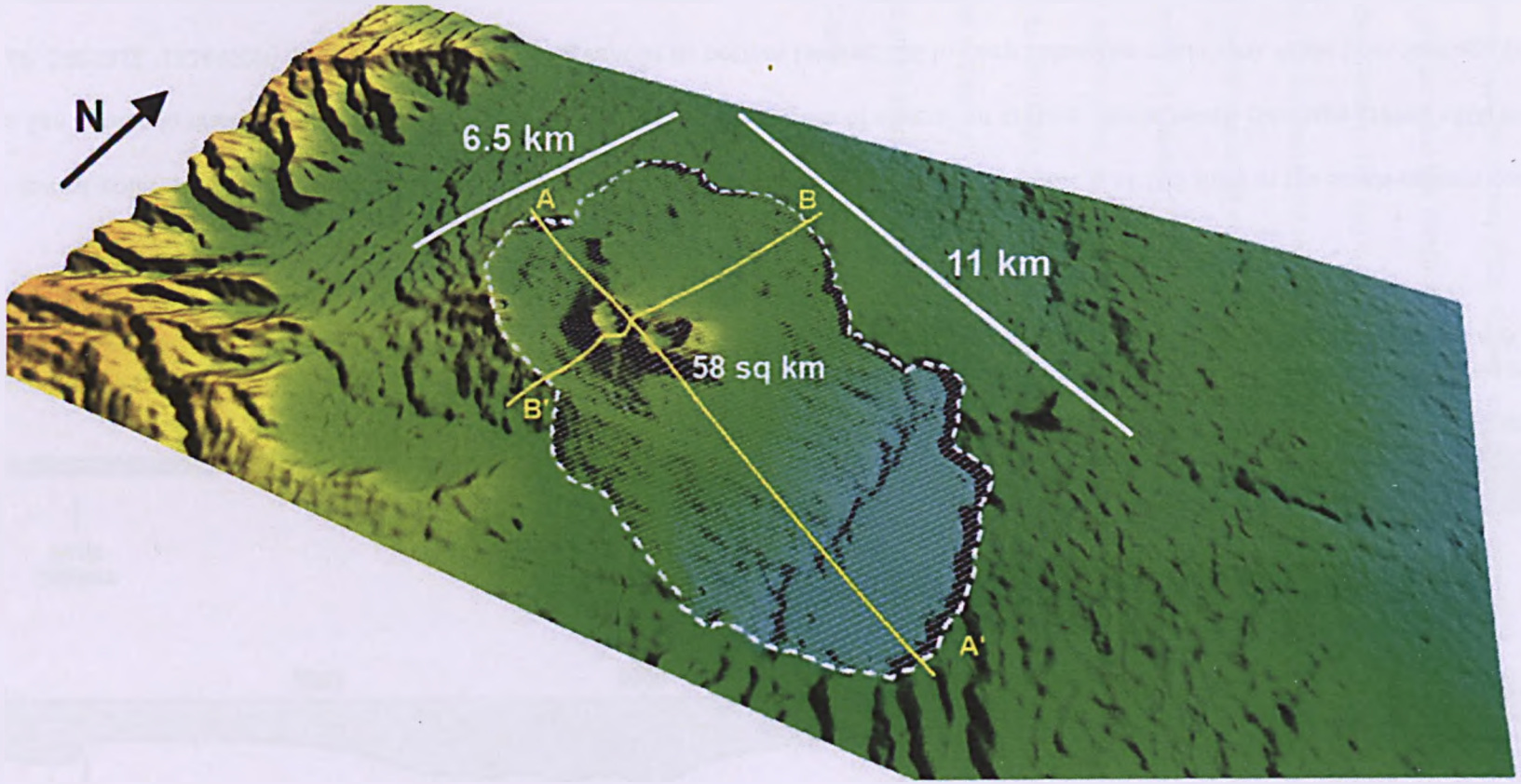

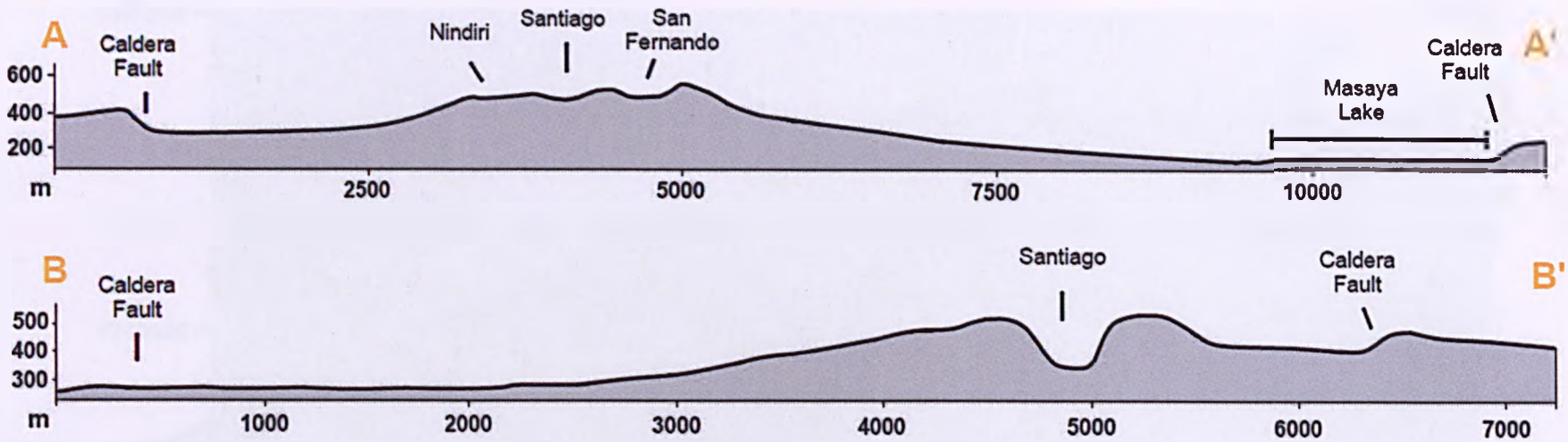

Figure 1-3: Masaya Caldera dimensions from a 30 m DEM. A-A' and B-B' topographic profiles (1:1 scale) cross the summit area of Masaya, where the main pit craters (Nindiri Crater, Santiago Crater, San Fernando Crater, and also San Pedro y San Juan, which are not traversed by the profiles) can be found today (Note: A-A' and B-B' have different scales).

The lowest point in the caldera is Masaya Lake, with a water surface at 137 masl, and the highest is at 596 masl in the south-eastern corner of the inactive San Fernando crater. The summit area (Figure 1-3 A-B, Figure 1-4) consists of several pit craters, one of which (Santiago Crater, ≈600 m diameter, UTM 16P, 590531E, 1324960N) hosts an actively degassing vent at its bottom (almost 200 m deep below the crater rim). Aside from Santiago Crater, from West to East we find first San Pedro Crater (Figure 1-4), a pit crater 400 m wide and 200 m deep. At present it is still unclear if San Pedro has been a centre for eruptive activity in the past, but it seems (Montessus de Ballore 1888; Rymer, van Wyk de Vries et al. 1998) to have formed in 1858-59, simultaneously with Santiago Crater. Nindiri Crater (Oviedo y Valdez 1851) has also been one of the most active in historical times.

It hosted a lava lake when the first Spanish Conquistadores arrived in Western Nicaragua (Oviedo y Valdez 1851), and has probably intermittently hosted lava lakes (including the one that generated the 1670 lava flow) since then (McBirney 1956; Rymer, van Wyk de Vries et al. 1998; Harris 2009). After 1670, normal faults formed in the Nindiri frozen lava lake and these can be seen on the walls of Santiago and San Pedro Craters. The most recent effusive eruption in 1852 still deposited some juvenile material within Nindiri crater (Montessus de Ballore 1888; McBirney 1956; Rymer, van Wyk de Vries et al. 1998). San Fernando pit crater, where the highest point on the caldera floor is, was formed after Oviedo's visit to Masaya (Rymer, van Wyk de Vries et al. 1998), and was also probably host to some of the most recent activity to have taken place within Masaya Caldera, the 1772 eruption. Linked with its formation, there was not only the 1772 lava flow that extended beyond the caldera (Figure 1-5) and spilled into the Managua Graben (McBirney 1956), (Girard and van Wyk de Vries 2005), but also a small eruption that generated a small lava dome, visible today at the bottom of the San Fernando Crater.

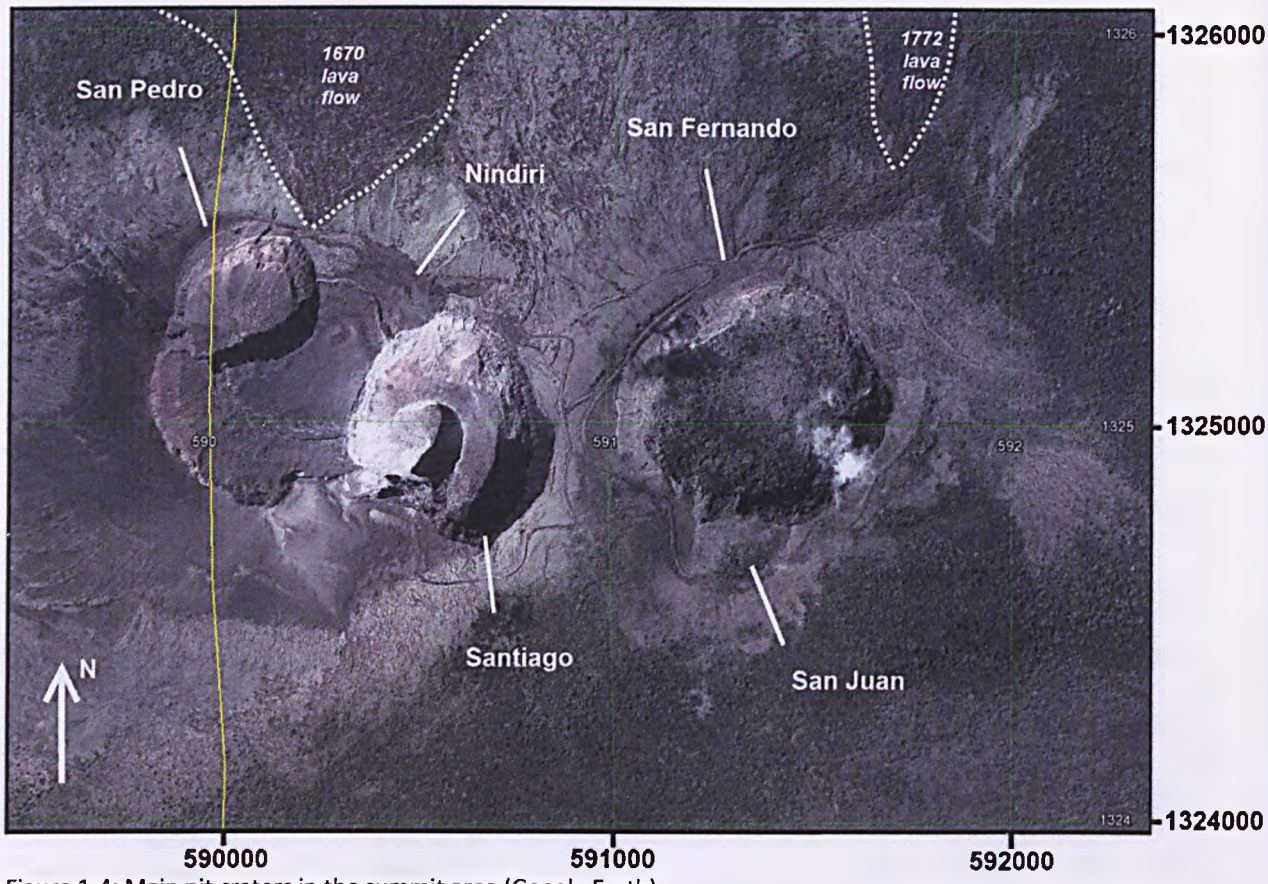

Figure 1-4: Main pit craters in the summit area (Google Earth).

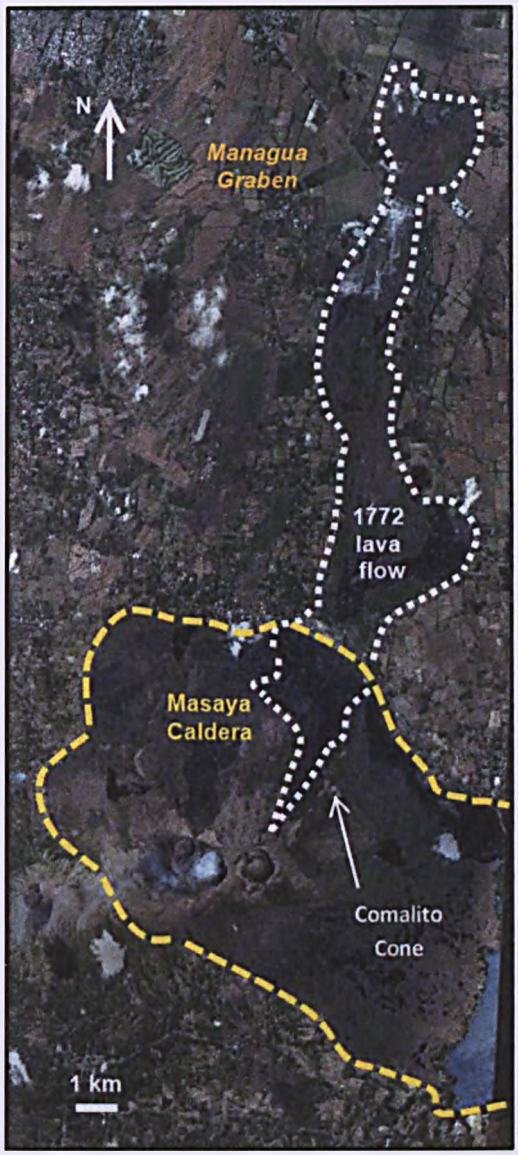

Figure 1-5: Extent of the 1772 lava flow.

1.4 Previous volcanological studies of Masaya

This section provides a general view of the types of research that have taken place at Masaya Caldera. Following a section on early historical observations, I have organized this section in paragraphs according to the aspects of the volcanic complex they deal with, and then review the evolution of research in that particular area, with special attention to the implications for understanding Masaya Caldera's evolution and processes.

1.4.1 Historical observations

The first surviving historical observations of Masaya in the written record date from 1529 (Oviedo y Valdez, published 322 years later in 1851) when Spanish explorer Gonzalo Fernández de Oviedo y Valdez climbed to the crater, later producing a detailed account of his observations that included a description of a lava lake that was active in Masaya at that date. He thoroughly described the morphology of the craters and the characteristics of the activity on Masaya Volcano, thus commencing a long history of observations. For three centuries after Oviedo's visit, the majority of the records that have survived are from Catholic priests who visited the area (Viramonte and Incer-Barquero 2008). For this reason, most interpretations of the volcanic phenomena at Masaya were focused on their relationship with theological matters. As McBirney (1956) commented, 1841 saw the dawning of a new era of more precise, and more scientific observations of Masaya, which has allowed us to understand the recent evolution of the morphology of the main vents (Stephens 1841; Squier 1856; Montessus de Ballore 1888; von Seebach 1892; Sapper 1925; Schönberg 1927).

1.4.2 Peer-reviewed research

Peer reviewed research in Masaya Caldera dates back only to 1956, when McBirney completed a geological study of the Caldera, proposing several explanations for the geological features he found and suggesting a preliminary evolution model of the pit crater area that has remained substantially unmodified until recent times. However, we can consider that the modern era of volcanology studies of Masaya did not truly start until 3 decades later, with the Doctoral studies of Stanley Williams (1983). Since then, the relatively easy access to Masaya's pit craters and active vents due to the road built in the 1950s inside Masaya's National Park (limited by Masaya Caldera's external boundary faults), and the remarkably intense volcanic degassing processes that take place at the summit area, have attracted researchers from all over the world, making Masaya one of the best known volcanic edifices in Central America.

1.4.2.1 Studies addressing different types of activity

1.4.2.1.1 Diffuse degassing

The first study on this topic (Crenshaw, Williams et al. 1982) dealt with the emanations of Ra and Hg from the caldera floor, and sought to detect buried structures and faults. Crenshaw et al. concluded that the Ra and Hg data did not support the presence of a ring fault inside Masaya Caldera (for more details on the ring fault, see Chapter 3), or the boundaries of 2 overlapping caldera collapse features, but did support the existence of old caldera boundaries lying outside Masaya Caldera. After that, Katie St Amand (1999) completed a MSc Thesis on the emissions of CO_2 and Ra from Comalito (**Figure 1-5**: Extent of the 1772 lava flow.), a small volcanic cone within Masaya Caldera source of constant gas emissions, suggesting the existence of a fault on the North Slope of San Fernando Crater. Lewicki (2005) and Chiodini (2005) also carried out CO_2 measurements in the Comalito area, reporting time dependent variations in the total flux. Lewicki (2003) and Lehto (2007) combined Self Potential and CO_2 measurements, suggesting a deep gas origin for the emissions. Finally, Shaw, Hilton et al. (2003) report measurements of the $^3He/^4He$ ratio from fumaroles in the Central American arc, including from the Comalito area. However, the anomalous results from Masaya (which are the only fumarole samples in the region with values lower than the typical MORB range, 8±1 $^3He/^4He$ ratio) are attributed to atmospheric contamination factors.

1.4.2.1.2 Plume degassing/volatile emissions

Masaya's gas plume is probably the most intensively studied aspect of the volcano. Over 40 studies have dealt with different aspects of the degassing from Masaya's main vent in Santiago Crater. The first research article on Masaya's plume was authored by Baxter and Stoiber (1982). Stoiber then went on to publish with S. N. Williams (Stoiber, Williams et al. 1986) a paper in which the first reliable measurements of sulfur and halogen gas flux at Masaya were reported. In their research it was also first suggested that there was a 25 year cycle for degassing crisis at Masaya Volcano, and the environmental impact and net contribution of Masaya to the total world output of SO_2 emissions (7%) were estimated. Maciejewski (1998), Horrocks et al. (1999), Burton et al. (2000),

Williams-Jones (2001; 2003) and Horrocks (2001) report COSPEC and FTIR measurements of the volcanic plume, pointing out its very stable composition (probably due to the open-vent system, Horrocks et al., 1999) and its high intensity. Burton et al. (2000) presented the first CO_2 and H_2O measurements conducted at Masaya. Richter (2000), Richter et al. (2002), McGonigle et al. (2002), Galle et al. (2003; 2010) experimented with new sensors, and Burton (2001) tested new methodologies (spectroscopic measurements of volcanic gas emissions by lunar occultation), taking advantage of the favorable meteorology, accessibility and topography that facilitate the study of Masaya's plume.

Several studies have provided an insight into the characteristics of Masaya's plume composition, also improving our understanding of the variations in the contents of the gas plume from daytime to nighttime, through specific gas measurements that had not been completed in the Central American Arc previously. Those include studies of particle emissions transported by the plume (Mather, Allen et al. 2003; Martin, Mather et al. 2009; Moune, Gauthier et al. 2010), evaluation of the Pb emissions from Masaya (Vallelonga and Mather 2003), comparative studies of nitric acid from several Latin American volcanoes (Mather, Allen et al. 2004), and an estimation of Hg and halogen emissions from Masaya and Telica Volcanoes (Witt, Mather et al. 2008; Kern, Sihler et al. 2009).

Baxter and Stoiber (1982), Johnson and Parnell (1986), Delmelle and Stix (2001), Mather et al. (2004) and Martin et al. (2010) have studied the impacts of the plume's fallout. Baxter and Stoiber (1982) studied the public health effects of Masaya's plume. Johnston and Parnell (1986) looked into the role played by plants in neutralizing the excess of acid supplied by acid rain. Delmelle and Stix (2001) calculated the rate of dry deposition of SO_2. Mather et al. (2004) looked into the particularities on how the global nitrogen cycle works using Masaya as an example, and Martin et al. (2010) studied element distributions around active volcanic vents determined by analyses of grasses.

The plume speed and dynamics have also been studied in detail. Branan (2007) and Branan et al. (2008) studied emissions in the first few seconds after being released in the vent, McGonigle et al.

(2004) argued that remote SO_2 flux measurements can be considered reliable proxies for source emissions for ash free tropospheric plumes not emitted into cloud or fog. McGonigle et al. (2005) and Williams-Jones et al. (2006) developed new methods to more accurately measure plume speed, and Nadeau (2004; 2009) characterized in detail the dynamics of propagation of Masaya's plume. Martin (2011) studied the aerosol size distributions, and reassessed the significance of atmospheric and dynamic factors in the formation of volcanic aerosols; and Martin et al. (2012) elaborated on the presence of trace elements in the plume. Finally, research articles compiling all present knowledge on the emissions from Masaya and the volcanic arc it belongs to have been published in recent years (Mather, Pyle et al. 2006; Carr, Saginor et al. 2007; Martin 2010).

1.4.2.1.3 Low energy eruptive activity

I define here low energy eruptive activity as eruptive events (including strombolian and hawaiian activity) which do not include highly explosive (Plinian) eruptions and degassing processes. Because of the increasing number of tourists visiting Masaya Volcano National Park (Parque Nacional Volcán Masaya) every year, assessing the hazards coming from this more common low energy activity is becoming an increasingly important task. With a few exceptions, research articles dealing with this type of activity from Masaya are scarce. Among the most significant studies is a thorough PhD Thesis that deals with the emission and spatial extension of lava flows on the caldera flow (Williams 1983). A paper by Duffell et al. (2003) reports a distinct change in plume gas compositions prior to a minor strombolian explosion. Martin (2007) deals with the differentiation of segregation veins during lava emplacement and degassing, and Moune et al. (2007) studied the other current and seemingly persistent activity from Masaya's active Santiago vent apart from the passive degassing; the emission of Pele's hairs and tears.

1.4.2.1.4 High energy eruptive activity

High energy eruptive activity at Masaya, which I define here as the Plinian eruptions that have taken place throughout its history, has been studied in 2 periods. The first (Bice 1980; Williams 1983;

Williams 1983; Bice 1985) described the surprising existence of Plinian eruptions of basaltic composition. This notion was a change in paradigm, since it showed that viscosity of the volcanic material is not the only factor of importance when a highly energetic, Plinian eruption is produced. Twenty years later, Pérez and Freundt (2006), Wehrmann et al. (2006), Kutterolf et al. (2007), Pérez (2007), Constantini et al. (2009), Pérez et al. (2009) and Goepfert and Gardner (2010) described in much more detail the deposits generated by these eruptions (see Table **1-1**), and have been able to produce much more precise estimations of column height, deposit dispersion, etc; contributing in turn to the improvement in our knowledge of the parameters for risk analysis to the most vulnerable communities to this type of activity.

Name/type of deposit	Deposit volume (km^3)	Age (ka)
Fontana Lapilli (uncertain origin)	2.9-3.8	60
San Antonio Tephra	14	6
Masaya Triple Layer	3.6	2.1
Masaya Tuff + Ticuantepe Lapilli	10	1.8

Table 1-1: Basaltic Plinian deposits from Masaya Caldera. Data from Pérez et al. (2009), Costantini et al. (2009), Kutterolf et al. (2008), Pérez (2007), and Wehrmann et al. (2006).

1.4.2.2 Studies focusing on the evolution of specific parts of the volcanic complex

1.4.2.2.1 Caldera structure and evolution

Several authors have investigated the implications of Masaya Caldera's structural framework for its evolution. McBirney (1956) was the first author to attempt to explain some of Masaya Caldera's morphological characteristics, such as its elongated shape, scalloped margins or near-vertical walls. He concluded that a process of downward subsidence as a result of magma withdrawal from depth is the most likely cause for many of those characteristics. McBirney was also the first author to mention the existence of a 3.5 km diameter ring fault within the caldera (which according to him was generated by an earlier collapse) based on the spatial distribution of vents on the caldera floor. Crenshaw et al. (1982) searched for faults on the caldera floor using a detection method that measures the spatial distribution of the concentration of Hg^0 and Rn. According to their study, more

than 75% of the measurements performed over suspected structures had anomalously high concentrations of these two gases.

From a structural data point of view, the most relevant study available is the doctoral thesis completed by Stanley N. Williams (1983). He studied the relationship of the caldera-bounding faults with regional fault lineaments, and provided a detailed map of volcanic features, faults and fissures that can be found within the caldera. He also argued that the alignment of vents on the caldera floor is structurally controlled, and alleged that they are aligned parallel to one of the regional fault directions, seeing no role for the ring fault structure suggested by McBirney (1956). Van Wyk de Vries (1993) studied some aspects of Masaya, including the morphology and origin of Cerro Montoso, a stratocone located within Masaya Caldera boundaries, and the morphology and origin of the Managua Graben, the regional structure that has likely conditioned the current location of the caldera (Chapter 5 this thesis). Šebesta (1997) completed a regional study that included an interpretation of the origin and role played by the Managua Graben, which was identified as a pull-apart basin. Šebesta's study also describes several fault scarps linked to some of the nested calderas in the area, providing information on the boundaries of Las Sierras Caldera, a large basaltic caldera encompassing numerous volcanic features (including Masaya Caldera). Finally, Girard and van Wyk de Vries (2005) published an investigation that deals directly with Masaya's geodynamical context. In their study, Girard and van Wyk de Vries consider Las Sierras-Masaya, the volcanic complex where Masaya Caldera is located, as a single evolutionary entity that plays a major role in the area's structural framework. According to the analogue modelling experiments they carried out, the large density of the intrusive body inferred by Connor and Williams (1989) and Metaxian (1994) has a major effect on the stress regime in the area. Girard and van Wyk de Vries also suggested that Masaya Caldera and the Managua graben might be tectonically linked and part of the same dynamic system, with the graben originating in response to a regional stress field being modified around the dense intrusive complex.

Adding information relevant for our understanding of Masaya's subsurface, Connor and Williams (1989) were the pioneers of the many gravity studies that have been done at Masaya, completing the first regional Bouguer map with sample points within the caldera boundaries. They concluded that a relative gravity high located to the NE of the Caldera corresponds to a dense intrusive body, elongated in shape. Metaxian (1994) supported this conclusion in the gravity study included in his doctoral thesis, suggesting also that this intrusive body is probably not completely solidified yet. However, both Metaxian and Connor and Williams employed barometric altimetry methods to calculate the position of the gravity stations, which are less reliable and accurate than the DGPS methods usually employed today. Bonvalot (1992; 1995) started the repetitive acquisition of gravity data at fixed points, a technique known as microgravity, in the early 90s and his network of stations was later occupied and extended by other authors to study the structure of the summit area of Masaya Volcano (Rymer, van Wyk de Vries et al. 1998; Williams-Jones 2001; Williams-Jones and Rymer 2002; Williams-Jones, Rymer et al. 2003), see Section 1.4.2.2.3.

From a geochemical and petrological point of view, Ui (1972) made a pioneer petrological study of Nicaraguan volcanoes, noting the distinct magma compositions for volcanoes in the vicinities of Masaya, with Mombacho and Apoyo erupting high-alumina basalts, and Masaya and Granada volcanic centers erupting Fe and Mg-rich basalts. Walker et al. (1993) made the first detailed petrological investigation of magma evolution at Masaya, proposing the existence of a large, shallow, open-system magma chamber, perhaps on the order of 10 km^3 in size. Atlas (2008), studying volatiles in melt inclusions in Masaya rocks, also provided some information on Masaya magmas and the dynamics of its magma chamber. In Atlas' thesis it is suggested that the magma that arrives near the surface at Masaya, after degassing, descends (due to its higher density values) to depths of 7-20 km mostly as an individual column, probably with some small batches of the same material also descending but independently from it. A fraction of this magma would be then re-enriched in CO_2 generated from exhumation from deeper parts of the magmatic plumbing system,

and eventually return to the surface. Sadofsky (2008) also provided data on volatile and trace element content from Masaya in a comparative study with other Central American volcanoes.

The most recent studies with structural implications include Mauri et al. (2012), who in their study on of the hydrothermal complex of Masaya volcano compiled data on the distribution of diffuse degassing structures on the caldera floor that might indicate the presence of a ring-like fault structure. Ebmeier et al. (2013) recently detected a region of slow subsidence at Masaya, Nicaragua, as part of a regional survey of Central American Volcanic Arc using 3 year L-band InSAR measurements.

1.4.2.2.2 Groundwater/hydrothermal system

For Masaya, scientific studies addressing the characteristics of the groundwater and hydrothermal systems did not take place until the year 2000. Since then, several researchers have completed investigations employing both classic and relatively new geophysical acquisition and processing techniques. Lewicki et al. (2003) completed a multi-parameter study in an area adjacent to Comalito Cone, a small volcanic edifice within Masaya Caldera. Their study provided an insight into the mechanisms controlling the transport and dynamics of the fluids that form the hydrothermal system, suggesting high temperatures and gas flow rates as responsible for the fluid disruption that causes the generation of positive self-potential anomalies. MacNeil (2006) and MacNeil et al. (2007) employed Transient Electromagnetic Methods (TEM) to study the interaction between the magmatic and the groundwater systems at Masaya, concluding that the latter was hydrologically isolated from the surrounding regions, and that the water table replicates the topography in the area. The presence of a small hydrothermal cell on the south flank of Nindiri cone is also suggested (MacNeil, Sanford et al. 2007). Mauri (2009) and Mauri et al. (2010; 2012) provided more detail on the dynamics and distribution of the groundwater and hydrothermal systems at Masaya. They concluded that a constant northward flow on the north flank of Nindiri cone and a southward flow on the south flank exist, with the water table being at 92±34 m depth (mean value)

over the area. Mauri et al. (2012) suggested that the hydrothermal activity in Masaya may be in stable state, with the diffuse degasing structures conditioning the path used by fluids to reach the Laguna de Masaya.

Pearson et al. (2008), Pearson (2010) and Pearson et al. (2012) studied the relationship between magmatic and groundwater systems using time series of soil temperature that show repetitive ≈5°C changes in temperature that the authors attribute to changes in volcanic activity. Through numerical modelling they show that the existence of relatively impermeable faults within Masaya Caldera has the potential of enhancing flow through the footwall. A 3-4 km radial fracture with the same orientation as the Eastern bounding fault of the Managua Graben that pierces the surface of the volcano is also identified as a centre of groundwater convection, resulting in a series of fumarole spots located along the fault.

1.4.2.2.3 Summit structure and dynamics

Due to the easy accessibility to Masaya's Santiago vent and the clear cut and lack of vegetation cover on Santiago's walls, many studies have addressed the geological history and formation of Masaya cones and pit craters, and the physical processes and governing dynamics of the vent. Rymer et al. (1998) gave the first comprehensive study of the sequence of geological events that resulted in the formation of Masaya's summit area as we can see it today. In their study, Rymer et al. use geological observations and gravity data to propose a structural model for Masaya pit craters that also suggests an interpretation of the processes taking place within Santiago, the currently active vent. Roche et al. (2001) discussed the collapse mechanism of pit craters and its relation with sub superficial structures, providing a comparison between the style of collapse that is taking place in Masaya active vent and the collapse occurring on other volcanoes (Telica, San Cristobal, Ubinas and Kilimanjaro).

Using gravity observations, Williams-Jones (2001) and Williams-Jones et al. (2003) studied the density changes that take place in Masaya over time in order to provide information of its internal

structure and dynamics. Combining the gravity data with observations of the SO_2 degassing in the area, they proposed two mechanisms to explain the observed cycles in the gas output. A temporary trapping and storage of gas in cavities before being erupted, or a staged convective overturn of shallow, degassed, cooled, magma and its periodical replacement by lower density, hot, gas-rich magma are the two main possibilities Williams-Jones et al. suggest as the origin for the fluctuations in gas emissions. Locke et al. (2003) also used gravity methods to look into the mass transfer processes (magma and gas) that occur beneath persistently active volcanoes. For Masaya, Locke et al. suggest that these mass transferences may be taking place at two different depths, a shallow one less than 500 m deep and another one at depths greater than 1-2 km. Stix (2007) completed a research study on vent dynamics, providing information on the characteristics and mechanisms controlling the magma foam layer sitting atop the free surface lava lake under Santiago vent. Stix also assessed the implications of this process for the stability of Masaya in the long term. Harris (2009) provided estimations of the thickness and volume for many geological units within Masaya, and produced a refined model to explain the formation of the currently solid and fractured lava lake in Nindiri crater.

Metaxian and Lesage (1997) and Del Pezzo et al. (2001) studied the permanent tremor in Masaya, providing information on its intrinsic characteristics and also on the implications for the lava lake source of the tremor. The depth to this source was estimated by Metaxian to be approximately 400 m below the NE rim of Santiago Crater, corresponding therefore to shallow magmatic activity.

1.5 Methodology

To study the structural framework that provides the geologic context for Masaya Volcano's activity, an approach involving the combination of several geological and geophysical methods has been chosen. The reason for employing a number of different techniques is the fact that any individual method is best suited to providing information on one or only a few aspects of the volcanic system. The integration of geophysical and geological datasets is an optimal methodology

capable of truly improving our understanding of a volcanic system. In addition, the aim of investigating Masaya Caldera at different depths requires the exploitation of different methods. Thus, gravimetric methods will be used in the main to investigate the deepest (>200 m) environments (although not only for that), Very Low Frequency (VLF) and magnetic methods for the shallower depths (<200 m), and geologic (both remote and ground-based) methods to study surficial features. Together, they should provide a holistic picture of the volcanic system as it is at the moment.

In addition, basic sociological research techniques have been used to describe demographic and sociological aspects of the area of study. This has allowed a good understanding of the evolution of the population in terms of numbers, distribution, and characteristics, thus improving the possibilities of adequately identifying elements and areas of increased risks.

1.6 Thesis outline

This thesis is organized in 6 chapters. Chapter 2 deals with the methods used to address the specific geological features investigated and explains the specificities of the procedures followed. Chapters 3 to 6 report the results. Chapter 3 deals with faults and other structures found at the intra-caldera level, and the implications of those for hazard assessment. Chapter 4 reports the results from VLF and gravity studies of the summit area and uses them to infer the shallow structure. This particular combination of geophysical methods is not very common in volcanic settings, but is argued to have the potential to become a powerful tool for monitoring active volcanoes. Chapter 5 reports the results from gravity studies that address the structure of the deeper levels of the caldera system, dealing with the location and geometry of the magma chamber and the pluton reported by Metaxian (1994) and Connor and Williams (1989), and the consequences for Masaya Volcano's activity in the future. Chapter 6 is the conclusion chapter, and summarizes the results obtained and provides information useful for planning of future work. Appendices contain all the data collected.

2 Methods

2.1 Recognition of relevant structural features

2.1.1 Introduction

The structural survey was carried out in order to provide evidence of the spatial distribution of fractures and other features, and their effect on the formation and possible future of the caldera.

2.1.2 Geological survey types

2.1.2.1 Ground based Survey

At Masaya Volcano, I have used a combination of traditional geological field techniques with the collection of digital photographs, and the employment of a Garmin eTrex handheld GPS to record the precise location of all data collected. The digital photographs have been obtained using a Fujifilm FinePix J27 camera, in order to illustrate different types of geological features.

Most of the ground survey observations have been collected during the course of the acquisition of geophysical data using the existing trail network that has been opened on the caldera floor over time by park rangers, illegal wood cutters, locals, researchers and tourists. Although this network improves the accessibility to many areas within the caldera boundaries, it fails at providing a complete coverage of the caldera floor, with the areas not serviced by the network usually being covered by dense and rough vegetation, collapsible ground, or any other form of difficult terrain.

This ground based structural survey was aimed at generating a complete database of relevant geological features to be found on the caldera floor, which could not only provide information on the structural features of the volcano, but that would also provide useful information to improve the efficiency and implementation of the geophysical study that was planned for Masaya. A particular effort was made to survey the areas within the caldera boundaries where structural observations are historically scarce even in the existing research papers and theses that specifically deal with structural aspects of Masaya Volcano, e.g. (McBirney 1956; Williams 1983; Walker, Williams et al.

1993; Rymer, van Wyk de Vries et al. 1998; Harris 2009). These areas have not been intensively surveyed in the past due to a number of reasons, such as the apparent lack of significant features, the difficult access, or the high interest generated by the summit area, Comalito hydrothermal zone and the other volcanic centres scattered on the caldera floor, which have concentrated the attention of most researchers. The best example for this is probably the north-western corner of the caldera, near Nindiri town, where previously unknown yet important structures within an aa lava field produced by the 1670 eruption have been found. The characteristics of the terrain here make particularly strenuous any attempt to perform a structural study in the area.

Structural observations were precisely located using a Garmin eTrex handheld GPS. Regarding accuracy and precision of this device, it must be stated that to calculate its minimum accuracy the manufacturer, after performing repetitive measurements with its GPS receivers and comparing them with Reference Stations, has been able to calculate the errors associated with the use of this particular model. Once these errors have been characterised, they can be combined with parameters such as strength of the signal, distance to satellites, etc. The magnitude of these parameters is then used by the receiver's software to perform estimations of accuracy levels when a new location is calculated in the field, and displayed in the "Estimated Location Accuracy" line within the Skyview Page of this handheld GPS' User Interface. The accuracy is provided in meters, making use of the RMS statistical method (which employs the square root of the mean square error of a set of measurements to express the difference between values predicted by a model or recorded as a reference, and values actually observed from the environment that is being modelled):

$$RMS = \sqrt{\frac{\sum_{i=1}^{n} (X_{obs,i} - X_{ref,i})^2}{n}}$$

where X_{obs} is observed values and X_{model} is reference values.

For our study, an average horizontal accuracy of <8m RMS has been calculated using the values supplied by the device, with recorded values consistently ranging from 3m RMS at best in open areas up to 15 m RMS in areas with dense canopy and topographic highs nearby. Furthermore, loss of lock has been very uncommon during the course of our survey, except for the interior of the lava tubes that can be found inside the boundaries of Masaya caldera, for obvious reasons. Apart from the company's routine testing, thorough studies (Rodríguez-Pérez, Álvarez et al. 2007) with the same handheld GPS model in locations with similar vegetation cover to our field area suggest accuracy levels (≈7.5-9.5m) consistent with our estimations, in this case using error bars with confidence intervals at 95% as the statistical preferred method to express accuracy.

Regarding other common geological methods, only geological sampling has been carried out to any significant extent here, with the aim of establishing general properties of the volcano such as average density or background magnetization levels.

2.1.2.2 Satellite Survey

The satellite structural survey has been a powerful tool to study the relationship between certain geological features located during the ground based survey, enabling us to precisely trace their geometrical characteristics on the surface. In this way, satellite imagery has never been used in isolation as a tool, but always in combination with other techniques.

Thus, to complement information acquired on the ground, satellite pictures compiled in the Google Earth application (version 6.2.2.6613) have been used to assess ground-based observations. Google Earth employs images provided by several corporations and institutions worldwide (CNES, DigitalGlobe, EarthSat, First Base Solutions, GeoEye, GlobeXplorer, IKONOS, Pictometry International, etc) to build a World Map in 3 Dimensions that can be used free of charge for research purposes. The quality of some of the imagery for certain areas rivals that of commercial providers, and often it is good enough to perform satellite-based basic structural feature identification.

The aerial imagery in the area compiled by Google Inc. for its Google Earth tool in the Masaya area was recorded on the following dates: 30/10/2004, 18/12/2004, 19/12/2004, 30/01/2011, 29/11/2011 and 31/03/2012. They were found to have enough quality to perform direct structural observations, particularly enhancing our ability to identify structures with a high degree of lateral continuity, which because of the chaotic and sometimes rough terrain were difficult to follow otherwise. All available scales were used. An aerial image collected before 01/01/1970 and also displayed in the application has been discarded due to poor image quality. For more details, see Chapters 3 and 5.

2.2 VLF Method

2.2.1 Introduction

The VLF method is a relatively old technique (Collett and Becker 1968; Hoekstra, Sellmann et al. 1975; Klein and Lajoie 1980) that has been widely used in recent years in the mining and exploration industries to detect buried electrically conductive bodies, being especially effective in the identification of long and straight faults filled with mineralization, water or clay (Ogilvy 1980; McNeill and Labson 1991). This technique uses receivers able to detect the signal emitted from remote radio stations operating in the VLF band of 15-25 kHz, interpreting the geometric effect on the signal after bouncing against buried electrical conductors. The VLF waves can travel thousands of kilometres on the Earth's surface, allowing us to select several transmitting stations (mostly military) to perform our measurements. This long travel distance of the waves with little dissipation of energy is due to the fact that low frequency waves never leave the atmosphere, being held between the ionosphere and the surface of the Earth. When those waves hit a conductive body buried underneath the VLF receiver, the magnetic field perpendicular to the surface generates eddy currents in the ground. The result is a secondary magnetic field out of phase and superimposed on the primary one (McNeill and Labson 1991). When added to the primary magnetic field, the resultant field is elliptically polarized, and a measurable tilt anomaly is generated (tilt angle mode of the VLF device). For a more detailed

explanation on the geometry of the electromagnetic field involved in VLF measurements, see (McNeill and Labson 1991; Parasnis 1995).

From mineralized to water bearing faults and fractures, this cost effective method is remarkably effective in areas where low background noises (normally associated with man-made structures) and high resistivity terrain are present. Volcanic environments with basaltic volcanic successions allow relatively deep (~100 m) penetration into the ground as a result of very low background noise levels. However, in spite of positive factors such as this high signal-to-noise ratio, its low cost and high speed of data collection, its use in the field of volcanology, e.g. (Zablocki 1978; Kauahikaua, Mangan et al. 1996; Zlotnicki, Vargemezis et al. 2006; Al-Oufi, Mustafa et al. 2008), is not common.

2.2.2 VLF instrumentation

The device employed to complete the VLF study is a VLF-2 receiver manufactured by Phoenix Geophysics (Figure 2-1). It is designed to detect VLF signals incoming from 2 different source fields, which in our case have been chosen to be approximately perpendicular to each other, allowing us to detect geological features with a certain degree of independence from their orientations. The direction of the incoming signal can be known by placing in a horizontal position the base of the detector and rotating it 180° until the maximum strength of the signal is reached. Placing the detector in a vertical position allows us to measure tilt angle and tilt direction (providing you with information on the characteristics of the feature in depth). The VLF receiver was also complemented by the use of a Garmin eTrex handheld GPS to record the position (see 1.2.1. in this chapter for more details) of each measurement, and a compass to precisely determine the direction of the incoming signal, and the direction of tilt. All data collected were recorded in field notebooks, and typed in Excel format after returning to base each day after fieldwork.

Figure 2-1: Performing a tilt angle VLF measurement on the south slope of the summit area. The position of the VLF receiver allows measurement of VLF tilt angle.

2.2.3 VLF Survey types

2.2.3.1 Gridding

The collection of data for the VLF grid was concentrated on the summit area, around the main pit craters. The selection of this part of the volcano to perform the VLF measurements is due to the fact that this area is where structural data could prove more useful to understand Masaya Volcano's present activity. Also, some of the structures that pierce the summit part of Masaya are partially visible in cross section because of subsidence and collapse of the pit craters, allowing us to correlate the geophysical signal with direct observations. This has proven essential to eliminate uncertainty, assess the validity of VLF as a method to study this particular survey area, and ultimately provide information about structure geometry elsewhere on the caldera floor, in places where the geometry of geological structures cannot be constrained independently. More than 600 stations were collected in a grid with a spacing of 25m (15 line kilometres) between measurements, and VLF maps have been limited to the areas with sample points. The software used to perform the gridding was Surfer 10.1.561., which uses a bilinear interpolation method to calculate Z values at points that do not coincide with grid nodes. The results of this study can be seen in Chapter 4.

2.2.3.2 *Profiling*

The VLF profiles completed for this project mainly correspond to areas on the caldera floor far away from the active summit area. The reason for this is that they were intended to provide information on the geometrical characteristics of structures that are relevant to understand the history of the formation of the caldera, and therefore scattered on the caldera floor. Due to the extent of the caldera and time limitations, we acquired these data in a last phase of the project, when most of the other survey types had been finished and therefore the locations for the VLF profiling could be selected on an informed basis. Due to time constrains, the profiles are restricted to the open trails and located mainly on the north-western corner of the caldera.

2.2.4 VLF Data Processing

To remove harmonic noise and improve the signal-to-noise ratio of the data, two main filters have been applied. The Fraser filter (Fraser 1969) constitutes the first derivative of the data, and its effect consists of enhancing the signal by removing the Nyquist frequency of noise. On the other hand, the Karous and Hjelt filter (Karous and Hjelt 1983) provides a display of apparent current densities at varying depths that would generate a magnetic field equal to the measurements. This results in apparent current cross sections that can reveal the geometry of conductive structures in depth.

2.3 Magnetic Method

2.3.1 Introduction

Techniques to measure the magnetic field on active volcanoes in order to detect faults and understand their structural framework are well known (e.g. Ozima and Kinoshita (1964), Henkel and Guzman (1977), Rathore and Becke (1980)). However, the variability of conclusions in these studies suggests that the magnetic signature is highly dependent on the geological characteristics of the region's lithology, as expected. That means that most conclusions derived from magnetic studies will only be applicable in geological contexts with similar lithological properties. Detailed and relevant

total magnetic field and structural studies can be found in Lopez-Loera et al. (2010), where the same methods have been applied to an active volcanic context with some similarities to the Masaya area. As shown by Lopez-Loera et al. (2010), total magnetic field methods can certainly be used to detect fault structures in volcanic environments.

2.3.2 Magnetometer instrumentation

Two Geometrics proton-precession magnetometers capable of measuring very small variations in the Earth's total magnetic field have been used in the course of this study. While one of them was used for fieldwork purposes, the other one was employed only for recording diurnal variations of the geomagnetic field. The antenna used during fieldwork was always mounted on a pole, to minimize disturbances induced by the operator's own field kit. Again, a Garmin eTrex handheld GPS was used to record the precise location of all data collected, and a compass was also used to ensure the orientation of the antenna remained constant throughout the survey. The operator in charge of the GPS, compass, and emergency radio systems kept at a distance of >5m from the operator of the magnetometer at all times, to minimize the effect of the electromagnetic field generated by any electronic equipment on the magnetometer. All magnetic data collected were digitally stored in the magnetometer's internal memory, and then downloaded after each day of fieldwork.

2.3.3 Magnetic survey types

2.3.3.1 Profiling

Magnetic measurements at 2577 stations with an average spacing of 25 m and subdivided into 17 profiles have been collected. That equals 64.425 line kilometres of magnetic study, that covers the caldera floor using the trails available, but is not enough to produce meaningful caldera-scale grid maps (with dimensions of ca. 11 km long and 6 km wide it is too big to be covered by a tight grid in the duration of this project). The profiles have been constructed without any previous design other than using all available trails, without specifically aiming at areas where we expected to find structures that were in some cases later revealed in the magnetic profiles. Through this trial and

error method, we have been able to identify a certain magnetic signature (a magnetic dipole with a low and a high peak) that corresponds to superficial evidence for faulting in many cases, or can be found where we expected structures to be located. For more details on the magnetic profiles built for this project, see Chapter 3.

2.3.3.2 Gridding

A data grid constructed using total field magnetic measurements from the summit area of Masaya was compiled in collaboration with Jeffrey Zurek, MSc (Simon Fraser University). However, topographic effects have been difficult to remove and may affect the quality of the data beyond reasonable. For more details, see Chapter 4.

2.3.4 Geomagnetic data processing

Diurnal geomagnetic variation effects have been monitored on about a quarter of the survey days (4 out of 15) in order to characterize the magnetic changes in this particular area. For that purpose, a magnetic base station (12°00'02.64706"N, 86°09'03.62968"W) was set up within Masaya Caldera, in an area where no magnetic anomalies could be induced by artificial structures. The results obtained can be found in Figure **2-2**. The data show that maximum changes of 250 nT were recorded (probably due to an unknown instrumental effect – see below) on the 13th of March 2010, while for the other 3 days, maximum diurnal variations in the magnetic values of 50 nT are found. In both cases, the size of the magnetic anomalies found in Masaya is larger than any diurnal variation recorded. For monitoring purposes, we have looked at the number of sunspots (which are an indication of intensity of solar activity) each of those days (see Table **2-1**) to see if there is any correlation with the diurnal variation of the total magnetic field. With 4 days record, we have found no effect on the record for normal solar activity.

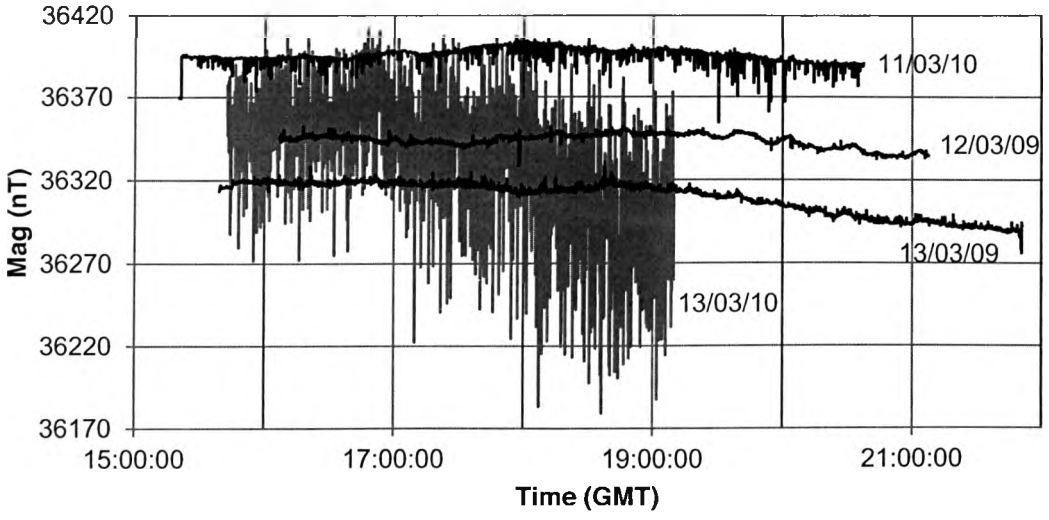

Figure 2-2: Magnetic diurnal variation recorded in Masaya Caldera on 4 different days.

Date	Total Number	North Sunspots	South Sunspots
12/03/2009	0	0	0
13/03/2009	0	0	0
11/03/2010	22	13	9
13/03/2010	20	20	0

Table 2-1: Number of sunspots (compiled by the Solar Influences Data Analysis Center - Royal Observatory of Belgium - http://sidc.oma.be/sunspot-data/dailyssn.php).

Due to the type of magnetic signatures found in correspondence with the outline of some of the faults under study (a sharp magnetic dipole), it was deemed not necessary to submit the data to processing methods such as the least-squares linear fit, or the application of a low pass filter, that might obscure the signal. For more details, see Chapter 3.

2.4 Gravity Method

2.4.1 Introduction

A variety of gravity methods have been employed in Masaya Caldera and its surroundings in order to obtain different pieces of information. We have constructed Bouguer anomaly maps that illustrate lateral changes in density, which in this context can be used to identify large scale buried structures such as large magma chambers, sharp lateral changes in lithology through fault boundaries, etc. We have also collected numerous microgravity measurements over the course of

this PhD, which build on previous microgravity data collected in Masaya since 1993 by Rymer et al. (Rymer, van Wyk de Vries et al. 1998; Williams-Jones, Rymer et al. 2003), which can provide information on mid to long term changes (years-decades) in volcanic activity. Finally, we have performed continuous gravity experiments using a permanent station on the edge of Nindiri pit crater with the scope of characterising activity over relatively short periods of time (hours to days). The intention behind this multi-experiment approach to study gravity signals in Masaya is to be able to integrate data that reveal information on different temporal and spatial scales of the volcano's present activity and history.

2.4.2 Gravity meter instrumentation

The instrumentation employed in the gravity study of this thesis has consisted of several devices to measure gravity, and equipment to accurately determine the position of each gravity reading. Four Lacoste and Romberg gravimeters, two G-meters (G-403, G-513) designed for discrete gravity measurements; and two D-meters (D-41, D-61) that can perform both continuous and discrete gravity measurements, have been used (Figure **2-3**). When employing D-meters for discrete measurements, an average of the readings over a certain period of time must be used as the appropriate value; and they also ought to be collected after the values have stabilized after being unclamped (the curve of the drift of gravity values becomes stable after approximately 4 minutes after the gravimeter is in position and recording). All gravity data collected were recorded on a notebook when a G-meter was being employed, or recorded in a storing unit connected to the RS-232 port of the gravimeters for processing purposes later on when working with D-meters. In this study we have also used a dual frequency Leica GPS differential system with the potential (depending on the satellite coverage and amount of time at each station) of recording positions with an error under 2 cm, which is more than appropriate for the purpose of a gravity survey (the repeatability of gravity readings has been estimated as ±5 μGals at the most, with the error induced by measuring the position in the same order of magnitude).

Figure 2-3: Lacoste and Romber gravimeter D-41 ready to perform a reading on a basalt lava flow in Masaya.

2.4.3 Gravity survey types

2.4.3.1 Bouguer Gravity

Bouguer anomaly techniques (e.g. Parasnis (1995)) give information on the internal density distribution of the terrain. After applying corrections for latitude, elevation, Bouguer, and terrain effects, Bouguer anomaly techniques can also be used to study volcanic settings, e.g. (Rymer and Brown 1986; Brown, Rymer et al. 1987; Rousset, Lesquer et al. 1989; Barberi, Cassano et al. 1991; Camacho, Vieira et al. 1991; Deplus, Bonvalot et al. 1995; Gudmundsson and Milsom 1997; Camacho, Nunes et al. 2007; Gottsmann, Camacho et al. 2008). In these environments, structures such as magma chambers, feeding conduits and lateral variations of underlying lithology can account for detectable changes of density in space, allowing us to reach meaningful conclusions regarding deep structures of volcanoes.

We have used a dual frequency Leica GPS differential system to accurately determine the position of the stations where gravity data were collected, in order to be able to perform precise corrections during the processing part of the study. Although Lacoste and Romberg G meters (G-513 and G-403) have also been occasionally employed, this Bouguer survey has been completed relying mostly on the D-meters (particularly D-61), due to efficiency and speed of use. In spite of the higher instrumental drift inherent to the D-meters (≈8 μGal/hour), the quality of the data is completely satisfactory for the purpose of this study (see Chapter 5 for more details).

Two different Bouguer gravity datasets have been collected in the course of this PhD project. The first one, with an average spacing of 100 m between stations and over 600 gravity measurements collected (60 line kilometres), covers most of the Caldera floor making use of the trail network that allows for rapid access of Park Rangers to the most remote/isolated parts of Masaya National Park. The scope behind the collection of this dataset is to assess anomalies at the whole caldera scale, including current and relict magma chambers, big scale collapses and regional faults and other structures. The second type of survey consists of a denser grid (50 m spacing) of gravity measurements collected in the summit area in collaboration with Jeffrey Zurek, MSc (Simon Fraser University), with the purpose of elaborating on the dynamics of Masaya's summit area (see Chapter 4).

2.4.3.2 Microgravity

Microgravity monitoring has been established for some time as a recognised method to study active volcanoes (Eggers and Chavez 1979; Johnson, Bjornsson et al. 1980; Yokoyama 1989; Berrino, Rymer et al. 1992; Rymer 1996; Rymer, van Wyk de Vries et al. 1998; Williams-Jones and Rymer 2002; Williams-Jones, Rymer et al. 2003). The technique employs repetitive discrete measurements of gravity over time, and combines them with precise high-resolution ground deformation studies to accurately determine the variations in the gravity field due to changes in sub-surface mass and density. As a reference point, a Survey base station outside the study area has to be established, in

order to provide an external frame of reference where gravity is stable over the years. For a more detailed description of the microgravity monitoring technique, see (Rymer 1996).

Microgravity measurements were performed in 2009, 2010, 2011 and 2012 making use of part of the monitoring network established by Bonvalot et al. (1992), Metaxian (1994), Rymer et al. (1998), and Williams-Jones et al (2003), with special attention to the summit area, which has proven to be the most active over the years and where most significant gravity changes have been detected. Lacoste & Romberg G-513 gravimeter was the main instrument used to perform the measurements (with Lacoste & Romberg D-41, D-61 and G-403 meters being employed to carry out occasional consistency checks to analyse the performance of G-513), thus using the same instrument that has been employed to occupy the microgravity network on Masaya since 1993, e.g. (Rymer, van Wyk de Vries et al. 1998). Furthermore, a dual frequency Leica GPS differential system was used to estimate the ground deformation at each microgravity station over the period 2009-2011. The reason for this is that changes in elevation have a direct effect in the gravity values, making essential to estimate any deformation effect in active settings like volcanic environments (an elevation change of 2 cm yr^{-1} exerts a -4 to -6 μGal yr^{-1} effect on gravity (Williams-Jones, Rymer et al. 2003)).

Interesting data that complement other geophysical datasets from the summit area of Masaya Volcano have been obtained. The results gathered using this method are extensively discussed in Chapter 5.

2.4.3.3 Continuous Gravity

Continuous monitoring of non-tidal variations of gravity was developed in the mid-80s by (Goodkind 1986). This method takes advantage of the small variations in the strength of the gravity field that occur when density distribution in the subsurface take place. However, the successful application of this technique on active volcanoes (pioneered by (Rymer and Brown 1987) in 1987, by using repetitive short term measurements) constitute a relatively recent advance e.g. (Jousset, Dwipa et al. 2000; Bonvalot, Diament et al. 2002; Carbone, Zuccarello et al. 2006; Carbone,

Zuccarello et al. 2008). Due to the low signal-to-noise ratio that results from studying such small variations of gravity over time, the evolution of data reduction and correction for external effects such as temperature and pressure variations plays a major role in the development of this technique e.g. (Tilling 1989; Andò and Carbone 2001; Andò and Carbone 2004; Andò and Carbone 2006).

Continuous gravity data have been recorded at Masaya in 4 different periods during 2010 and 2011 (12^{th}-13^{th} January 2010, 2^{nd}-5^{th} March 2010, 15^{th}-18^{th} February 2011, 1^{st}-7^{th} March 2011). A D-meter Lacoste and Romberg gravimeter and a Hobo atmospheric station were deployed inside a concrete bunker (1x1x0.5m) near the active Nindiri crater (Figure **2-4**). Due to nearly continuous presence of a corrosive gas plume emitted by Masaya's active crater in the area (with significant concentrations of SO_2, HCl and HF, e.g. (Delmelle, Baxter et al. 1999; Burton, Oppenheimer et al. 2000)), the installation was sealed with an iron lid. A 12V AC Delco car battery (periodically changed) was the main power source for the system at all times, with internal Li-Ion batteries supplying an extra 6 hours of life for the gravimeter if power supply from the Delco battery was lost, or when changes of battery took place. This was planned to avoid the corrosion of solar panels and electrical connections exposed to the effects of the gas plume.

However, detailed analysis of the collected data has been deemed impossible since several factors induced high noise levels, rendering this technique futile so far. The fact that the power source was a dischargeable car battery called for regular substitutions every 2.5-3 days, inducing in many cases a thermal tare in the gravity records that affected the data for several hours after the battery change had been performed, due to the difference in temperature between the air outside and inside the box. Furthermore, the extreme temperature changes (up to 25ºC) between day and night time dominate the gravity signal, with major pressure variation effects occurring in the central hours of the day, when the heat was most intense.

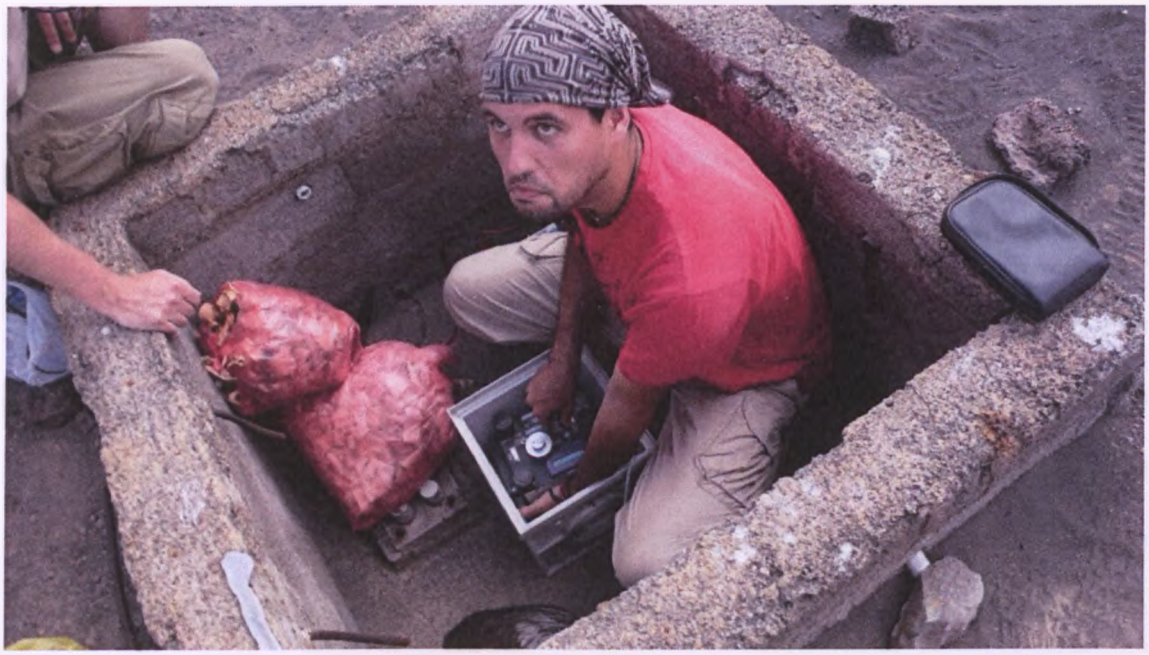

Figure 2-4: Deployment of D-41 Lacoste and Romberg gravimeter to record continuous gravity data near Nindiri and Santiago craters.

2.4.4 Gravity data processing

From the 3 gravity techniques employed in this thesis, the data acquired for the continuous gravity study have been discarded after the Quality Control phase was completed. As a result, the procedure to process it is not described in this section. Regarding the microgravity and Bouguer gravity techniques, in spite of the existing differences between them (see sections 2.4.3.1. and 2.4.3.2.), both are relative gravity methods that measure the difference in the value of gravity between a base station and multiple other gravity stations. Therefore, the gravity measurements acquired with these techniques are processed in a very similar manner, given the analogies between both techniques.

Discrete gravity measurements require a series of corrections to be applied in order to remove unwanted natural and artificial effects. The main natural causes for unwanted effects on the gravity data are the elevation of the gravity station, characteristics of local terrain, Earth tides and latitude. The main artificial effect on the gravity data is the drift of gravity values caused by the characteristics of the instrumentation used. After all corrections have been applied, they are normalized to a base station and can be then compared with other measurements in the same location at any other

moment in time to detect subsurface mass changes (microgravity technique), or can be used together with other measurements to build a map of density distribution on a large area (Bouguer gravity technique). Corrections applied:

a) Latitude correction: this correction is applied to the Bouguer data so that the effect of the Earth's irregular shape can be removed from the data. This correction is especially important for datasets collected over large areas, but has been applied in this case nonetheless.

b) Tidal correction: the Moon and the Sun have a detectable effect on the gravity values we record using gravity meters. These variations over time can be calculated using computer programs. We have employed Tidecalc (Broucke, Zürn et al. 1972) to predict the effect on gravity of these celestial bodies at the time and location of our gravity surveys, and then removed that effect from the data.

c) Terrain correction: the excess or deficiency of mass in the region where a gravity station is placed can have a significant effect on the data. The presence of pit craters, high cones, and in general any topographic high or low can exert an effect on the mass inside the gravimeter that is detectable by the instrument. The terrain correction is always positive with independence of the local topography being a low or a high. The topography data have been treated in 2 different ways using a Hammer's chart (Hammer 1939). For the terrain near the measurement station (up to 60 m), a visual estimation of average height relative to the gravity station has been determined. For more distant areas, a DEM and appropriate software (Oasis Montaj version 8.0, Geosoft Inc.) have been used to remove the terrain effect.

d) Drift correction: with small design variations, most current gravity meters measure gravity using a spring with a mass attached at the end. The material from which springs are made suffers from fatigue, and this has an effect in the gravity measurements. The Lacoste and Romberg meters we have used for this study are not an exception, and therefore measures had to be taken in order to remove this undesired effect. Repetitive gravity measurements at particular locations, coupled with

repetitive measurements at the base station at the beginning and end of the day allowed us to establish a drift curve that was later used to remove the drift effect from the gravity data.

e) Free Air correction: the different attraction of the Earth's gravitational field depending on the distance of every gravity station to the centre of the Earth must also be corrected. The free air gradient (FAG), with a theoretical value of -306.8 μGals m^{-1}, can be defined as the rate at which the attraction exerted by the Earth's gravitational field decreases with distance from its centre. However, this value can be measured and can change depending on topography or density variations (Berrino, Rymer et al. 1992). The procedure to apply the Free Air correction involves multiplying the elevation of each station with the FAG in the location of the study. In our case, small anomaly values and relatively small elevation differences in the survey area (<250 m) make the error induced by using the theoretical FAG minimal, which has been selected as the appropriate value to apply Free Air corrections to all gravity stations in the survey.

f) Bouguer correction: the Bouguer anomaly correction generates an infinite horizontal slab of a given density (a regional average density has to be determined as accurately as possible for the site of investigation) in order to remove the effect of an increase/decrease of material at different elevations. After this correction has been applied to the data, a Bouguer Anomaly value is obtained, that can be then used to build a Bouguer Anomaly Map.

3 Structures controlling volcanic activity within Masaya Caldera, Nicaragua

NOTE: this Chapter is the text of a research paper about to be submitted to Bulletin of Volcanology.

Authors contributions:

- Guillermo Caravantes González is the main author, conceived the idea for the paper, carried out most of the acquisition, processing and interpretation work included in it, and prepared the manuscript.
- Jeffrey Zurek helped conceive the idea for the paper and had a meaningful contribution in the acquisition of geophysical and geological data on the caldera floor.
- Dr Susanna Ebmeier is the sole author of the section on InSAR data.

3.1 Abstract

Detailed geophysical and geological studies have been completed in Masaya Caldera to define and characterise the structural framework of the volcano. A thorough field survey has been carried out in order to build a database of geological features present on the caldera floor. Magnetic and Very Low Frequency (VLF) data have been collected to detect buried bodies with high remnant magnetization and high electrical conductivity respectively. The results show anomalous values where faults have been detected on the surface, or have been inferred from the geological survey. The distribution of all these features approximates a circular shape of 3.5 km diameter and is interpreted to be a ring fault generated at some point in the last 1800 years (after the last Plinian eruption took place). InSAR measurements from 2007-2009 show steady subsidence (~2 cm/yr) at the southern end of the area enclosed by the ring fault. VLF profiles show inwards dip of this fault, which can thus be considered a caldera nested within Masaya's Volcanic Complex. Evidence for the influence of the Managua Graben on the Volcanic Complex can also be seen on the Caldera floor. The Managua Graben, the most active tectonic structure of the Nicaraguan Depression, is a pull-

apart basin responsible for the extensional stress regime that is dominant in the area. Several faults with similar orientation to the graben's easternmost fracture (Cofradías Fault), including the source for the fissural eruption of 1772 and other eruptions in the heavily fractured northern section of the caldera, suggest that the stress field related to this family of fractures is the other main component in the structural framework of Masaya.

Therefore, the structural framework that controls activity from Masaya Caldera depends on the interplay between the extensional stress regime associated with the Managua Graben, and subsidence along the ring fault. The high spatial resolution survey completed on Masaya also allows us to suggest several previously overlooked locations (mostly along the northern section of the ring fault) where eruptive, non-highly explosive activity might take place in the future.

3.2 Introduction

Masaya Volcano is one of the best known volcanic edifices within the Nicaraguan volcanic chain due to its accessibility and relatively non-hazardous regular activity. However, this basaltic caldera has also been the source of 3 basaltic tephras over the last 6000 years, produced by highly explosive basaltic eruptions that have spread pyroclastic deposits over a large area of Western Nicaragua (Williams 1983; Pérez and Freundt 2006; Kutterolf, Freundt et al. 2008; Pérez, Freundt et al. 2009). Its importance derives from the fact that it is located less than 15 km from Managua, the biggest city in Nicaragua (1.142.456 inhabitants, 2005 census), and one of the most populated urban areas in Central America. Morphologically, Masaya Caldera is a medium sized caldera, 11 km long and 6 km wide, with a shield volcanic cone 300 m high above its surroundings located in the middle of its north-western portion. This cone, composed of four pit craters (Fig. 1-4, from west to east: 1. San Pedro, 2. Nindiri, filled by a frozen lava lake, 3. Santiago, which contains the presently active vent, and 4. San Fernando or Masaya) is also the source for most of the degassing that takes place within the caldera. There is also an important number of other volcanic centres on the caldera floor, some have been named (Cerro Montoso, Cerro Arenoso, Sastepe, Comalito, Bejucal, etc), while others

remain nameless, mainly due to their small size. Most of them are distributed along suspected or inferred structures, such as a ring fault, faults geometrically related to the Eastern fault of the Managua Graben and others. The boundaries of Masaya Caldera consist of a series of scalloped and straight margins (the difference in height between the inner and outer block separated by these boundaries ranges from 0 to 200 m), with a short section (approximately 2 km out of 40 km perimeter) north of the caldera covered by lavas emitted from the central volcanic edifice. A shallow lake covers the easternmost side of the caldera, bordering Masaya Town, which uses the lake both as a water storage resource and waste disposal site.

Past studies of Masaya Caldera provide important background information on many aspects of volcanic activity in the area. Studies such as (Stoiber, Williams et al. 1986; Burton, Oppenheimer et al. 2000; Williams-Jones, Rymer et al. 2003; Lewicki, Bergfeld et al. 2005; Mather, Pyle et al. 2006; Witt, Mather et al. 2008; Nadeau and Williams-Jones 2009; Pearson 2010) have characterised in detail the chemical signature and characteristics of Masaya Volcano's gas plume and provided information on degassing occurring elsewhere on the caldera floor. (Duffell, Oppenheimer et al. 2003; Moune, Faure et al. 2007; Stix 2007; Branan, Harris et al. 2008) have looked into vent structure and dynamics. Several gravity studies e.g. (Connor and Williams 1989; Metaxian 1994; Bonvalot, Metaxian et al. 1995; Rymer, van Wyk de Vries et al. 1998; Locke, Rymer et al. 2003; Williams-Jones, Rymer et al. 2003) have revealed information on the sub-surface density structure of Masaya. There are geological studies that deal with Masaya's structure and eruptive history, e.g. (McBirney 1956; Williams 1983; Rymer, van Wyk de Vries et al. 1998; Roche, van Wyk de Vries et al. 2001; Girard and van Wyk de Vries 2005; Harris 2009). The role and effects of explosive activity from Masaya have also been investigated, e.g. (Williams 1983; Pérez and Freundt 2006; Fernández 2007; Pérez, Freundt et al. 2009). The groundwater and hydrothermal systems at Masaya have been studied by e.g. (Lewicki, Connor et al. 2003; MacNeil, Sanford et al. 2007; Pearson, Connor et al. 2008; Pearson 2010; Mauri, Williams-Jones et al. 2012).

Despite all this research, insufficient structural and geophysical data have been collected from the caldera floor in order to unequivocally establish the characteristics and geometry of its structural framework and assess its influence on Masaya Volcano's magma plumbing and hydrothermal systems. Although the existence of a ring fault in the area has been discussed based on the distribution of vents on the caldera floor and other evidences, e.g. (McBirney 1956; Viramonte 1972; Crenshaw, Williams et al. 1982), some of its sections remain relatively unknown due to factors such as the small size of the volcanic centres, or its relative inaccessibility. Also, evidence for the geometry of the faults at depth, the specific role they play regarding volcanic activity, and the rate and style of deformation, is missing. In this paper we provide the first magnetic, VLF and InSAR survey data of Masaya Caldera, allowing the study of subsurface and surface structures, and permitting active deformation to be described and related to the rest of the observations. The objective of this research is also generating a comprehensive model that explains the long term behaviour of Masaya Caldera's structural framework. A deep knowledge of this framework would allow us to identify the mechanisms that control eruptive activity at present, and also to correlate past eruptive events with present day structures, providing a better understanding of the evolution of the caldera. It is also a key element to improve the probabilities of adequately forecasting Masaya Volcano's future eruptive behaviour. In addition, the fact that mineralized/hydrothermal fluids in volcanic settings are usually channelled through weaknesses and openings (such as the faults and fractures that constitute most young calderas' structural framework), makes the study of these features crucial for identifying potentially interesting targets such as sources of geothermal power (Heiken and Goff 1983; Goff and Gardner 1988) and accumulation zones for ore deposits (Lipman 1984; Elston 1994; Rytuba 1994).

The present article will first offer a brief overview of the tectonic setting, the stress regime, and recent volcanic activity in the area. Then, evidence for the presence of significant structures contained within Masaya Caldera boundaries, collected using a variety of geological and geophysical

methods, will be presented. Finally, we will elaborate on the characteristics and role these structures play in the evolution of the caldera.

3.3 Tectonic background and recent activity

Masaya Caldera (Figure 3-1) is the most recent nested caldera within the Las Sierras-Masaya Volcanic Complex, an ignimbrite basaltic shield volcano which is the largest Quaternary volcano of Nicaragua (van Wyk de Vries 1993; Sebesta 1997; Girard and van Wyk de Vries 2005). Masaya Caldera is also associated in close proximity with a relatively dense intrusion to the NE (as suggested by gravity studies, (Connor and Williams 1989; Metaxian 1994)), and a similarly sized relict caldera further to the NE. This relict caldera, called Las Sierras Caldera by van Wyk de Vries (1993) and Las Nubes by Sebesta (1997), was probably generated 30000 yBP by the eruption of a large basaltic ignimbrite (Bice 1980; Sebesta 1997). It has been suggested that the presence of the volcanic complex in the area is linked tectonically with the Managua Graben (Girard and van Wyk de Vries 2005), an active pull-apart basin (Sebesta 1997; Girard and van Wyk de Vries 2005). This extensional volcanic setting has had major effects on the structural framework of the volcano. One effect of the extensional stress regime in the area is probably the continuous supply of magma that feeds volcanic and degassing processes taking place on the summit area at present (Stoiber, Williams et al. 1986; Burton, Oppenheimer et al. 2000; Williams-Jones, Rymer et al. 2003; Witt, Mather et al. 2008; Nadeau and Williams-Jones 2009). Several fracture systems parallel to the local stress regime (NNE-SSW) are visible on the caldera floor, and can be correlated in certain cases with different phases of activity at the volcano. For example, the 1772 effusive fissure eruption came from a fracture geometrically linked with the Cofradías Fault, the easternmost bounding fault of the Managua Graben (Crenshaw, Williams et al. 1982; Williams 1983; Mauri, Williams-Jones et al. 2012)

Masaya Volcano's activity has been characterised by a combination of major explosive activity including 4 Plinian eruptions in the last 6 ka (Williams 1983; van Wyk de Vries 1993; Pérez and Freundt 2006; Pérez, Freundt et al. 2009), the last one having taken place at around 2000 years BP;

and lower activity cycles that include periods of inactivity and periods when the dominant activity mainly consists of minor explosive, effusive activity, or passive degassing, or a combination of these processes. In the last 160 years 4 major degassing cycles have been recorded: 1852-1859, 1902-1906, 1919-1927, 1947-1959, (Stoiber, Williams et al. 1986). In 1993, the most recent degassing period in Masaya Volcano started (Rymer, van Wyk de Vries et al. 1998). Since then, activity has mainly consisted of persistent degassing from a small sized vent that fluctuates in intensity over time (in the rainy season, the input of rainfall makes the gas column grow substantially, due to the amount of water vapour present in it). For the period 1972–2007, (Nadeau and Williams-Jones 2009) estimated that an average of ~1,100 metric tonnes of SO_2 were emitted daily. Low energy explosive activity is also much more common during the rainy season, when the extra supply of meteoric water percolates through the porous mix of ashes and blocks that constitutes the roof and comes in contact with the shallowest part of the magma plumbing system, rendering activity more dangerous. The luminosity generated by the incandescence of a lava lake, or (less common) the free surface of the lava lake itself can be seen at times in one or both deep mouths in Santiago Vent. In addition to this, several spots where fumarolic emissions occur are scattered over the caldera floor. Regarding seismic activity, a continuous tremor presumably generated by the convection of magma reaching the upper part of the shallow magma chamber and releasing the gas it bears, can be recorded (Métaxian 1997; Del Pezzo, Bianco et al. 2001).

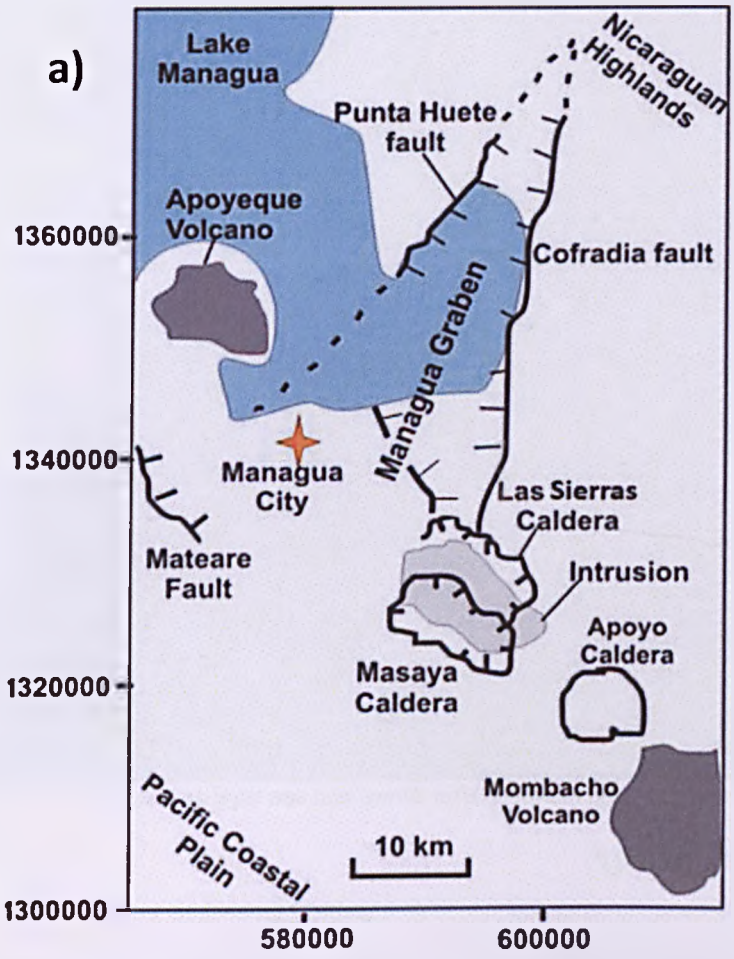
a)
Lake Managua
Nicaraguan Highlands
Punta Huete fault
Apoyeque Volcano
Cofradia fault
Managua Graben
Managua City
Las Sierras Caldera
Mateare Fault
Intrusion
Apoyo Caldera
Masaya Caldera
Mombacho Volcano
Pacific Coastal Plain
10 km
1360000
1340000
1320000
1300000
580000
600000

Figure 3-1: a) tectonic setting, modified after Girard and van Wyk de Vries (2005), b) Masaya Caldera area.

3.4 Structural survey

3.4.1 Ground based survey

A thorough geological and topographical survey was conducted within the limits of the caldera in January-March 2010 and 2011, with the aim of detecting any structures that might have played an important role in controlling Masaya Volcano's activity. Large scale/active structures are also the most likely to produce recognizable disruptions on the surface through lateral displacement and subsidence. The most common materials on the floor of Masaya Caldera are successions of ashes and lavas -and locally, sparsely vegetated recent lava flows. Several types of structural and volcanic features have been identified (**Figure 3-2**), many of which are relevant for reconstructing the geological history of the caldera and understanding its structural framework at present. Cooling fractures, lava tubes, and prominent edges of lava flows are not described in this Chapter as they provide little or no information on the volcano's structural framework. Structures directly related to the volcano's fault network include:

3.4.1.1 *Openings and cracks*

Caldera openings are defined here as fractures without displacement of any of the blocks on either side of the fracture. Their shape and characteristics are variable, from narrow and deep fractures to V-shaped openings. The area of the caldera where they are found has a decisive influence on their morphology. O1 openings (**Figure 3-2**, confined to the heavily fractured terrain in the northern part of the caldera) tend to follow a braided pattern, have typical widths between 0.1 and 2 m, depths between 2 and 10 m and lengths that range from 2-5 m for the shortest ones to 100s of metres for the longest (**Figure 3-3a**). After recognizing them in the field, data on their location, lateral extent and orientation were compiled using Remote Structural Survey techniques (see next section for further details). O2, O3 and O4 groups all have depths that range from 2 to 10 meters, and a V-shaped morphology with a bottom deeper than their surroundings that suggests they are unrelated to volcanic deposits in the area.

3.4.1.2 *Fumaroles*

In addition to the persistently degassing Santiago vent on the summit area (F1, Figure **3-3b**), 6 other sites (Figure **3-2**, from west to east, F2-F7) with intermittent (F2-F3-F5-F6) or persistent (F1-F4-F7) fumarolic activity have also been identified on the caldera floor. These include F2 – Rift Valley Site, a fumarole area within the rift valley on the slope to the west of San Pedro pit crater, with sulphur deposits and intermittent fumarolic activity over the period 2009/2012; F3 – Bee Site, a fumarole spot active since 2011 on the northern fault that limits Nindiri lava lake in the summit area, where the presence of humidity has attracted a bee colony (Figure **3-3g**); F4 – Hilltop Site, a well-known fumarole field on the Northern slope of San Fernando cone (Lehto 2007), F5 – Fumarole Field Site, a small fumarole field in the middle part of the fissure on San Fernando's North slope, source for the 1772 eruption (Lehto 2007), F6 – Road Site, a 10 m long, 0.2 m wide fumarole area along the main road that connects the entrance with the summit area, with 80-100°C temperatures recorded and hardly visible gas-steam emissions; and F7 – Comalito Site (Figure **3-3c**), a well-known hydrothermal area (Lewicki, Connor et al. 2003; Lewicki, Bergfeld et al. 2005; Pearson, Connor et al.

2008; Witt, Mather et al. 2008) classified in the past as a diffuse degassing structure (DDS) by (Chiodini 2005). F3 and F6 were previously undescribed in the literature. Those are superficial manifestations of Masaya's hydrothermal system, which uses the fault network as a communication path for fluids.

3.4.1.3 Rift valleys

Rift valleys are defined here as V-shaped valleys significantly larger than the openings with similar shape found on the caldera floor (>3 m deep, >10 m wide) which are always associated with fissural eruptive materials and hydrothermal manifestations. At least three relatively deep (3-20 m depending on the valley and section) and wide (10-40 m) rift valleys, coming down from San Pedro (RV1, Figure **3-3f**), San Fernando (RV2) and San Juan (RV3) Craters, with NW-SE, N/NE-S/SW and N-S orientations respectively, are the most important linear structures (relatively long, up to 1.5-2 km) within Masaya Caldera, and also three of the most prominent features within its boundaries. The first two have been the source of historic fissural eruptions, including the one in 1772 for which an erupted volume of ~$2.3x10^7$ m^3 was suggested by (Williams 1983), who also proposed a volume of $1.1x10^7$ m^3 for the 1670 lava flow that overflowed Nindiri crater. The valley going down from San Juan Crater (RV3) presents big spatter cones and ramparts along its path. This proves that these fractures have acted as an open path with a connection at depth with the magma chamber that has been active in historical times.

3.4.1.4 Eruptive centres

Eruptive centers within Masaya Caldera reflect the eruptive activity in the area after the last Plinian eruption 1.8 ka ago (Pérez, Freundt et al. 2009). They range in size from 300 meters high volcanic edifices to small-scale (less than 1 metre) lava constructs. All these features reflect by themselves the operative connection of an underlying magma chamber with the surface, and can be classified according to their eruptive style:

- Main pit craters (MC) are defined as the deep craters found on the summit area of the volcano which are the result of a complex eruptive history. Collapses, explosive and effusive eruptions have shaped the current morphology of these pit craters. They are part ofa semicircular alignment of cones and pit craters that form the most significant volcanic centre within the caldera, traditionally called Masaya Volcano. From West to East (Figure 3-2), we find San Pedro Crater (MC1), Nindiri Crater (MC2), Santiago Crater (Figure 3-2: MC3, Figure 3-3b) and San Fernando Crater (MC4). There is also a smaller crater to the South of San Fernando, called San Juan (MC5). For a more detailed description of these craters, see (Rymer, van Wyk de Vries et al. 1998; Harris 2009).
- Medium sized cones (MS) are monogenetic volcanic edifices (or polygenetic cones produced by a low number of eruptions) scattered on the caldera floor and composed mainly of ashes and spatter lava products(Figure 3-2, MS). They mark the location of eruptions that have taken place away from the present centre of activity. These include the relatively big (>50 m high over the caldera floor) Comalito (MS1), Visitor Centre (MS2) and Cerro Montoso (Figure 3-2: MS3, Figure 3-3d) cones, but also the smaller Cerro Arenoso (MS4), Sastepe (MS5) and Bejucal (MS6) cones.
- Spatter cones and ramparts (SC) are small mounds (heights between 1 and 10 m, and very short lateral extension) product of short-lived, local lava emissions. They are secondary volcanic centers generally associated with larger fissural eruptions but have also been found isolated on the caldera floor. In some cases (Figure 3-2, SC1) they are associated with newly formed fractures that cut through the historically recorded lava flows (1670 and 1772). At least 4 areas outside the volcanic centres already mentioned host these types of features: spatter cones found in the North Fracture Field (SC1) are the most important, since at least 5 centres can be found in the area, generally clearly associated with openings and cracks. One single spatter rampart has also been found South of Cerro Montoso (SC2). And some more cones and ramparts associated with rift

valleys (RV2 and RV3) and fissures (O3) have been found North of San Fernando (SC3), South of San Juan (SC4) Craters, and between Cerro Montoso (MS3) and Cerro Arenoso (MS4) being an indication for fissural eruptions in the area. This relatively uncommon phenomenon in Latin American volcanoes seems to have been repeated over time in Masaya.

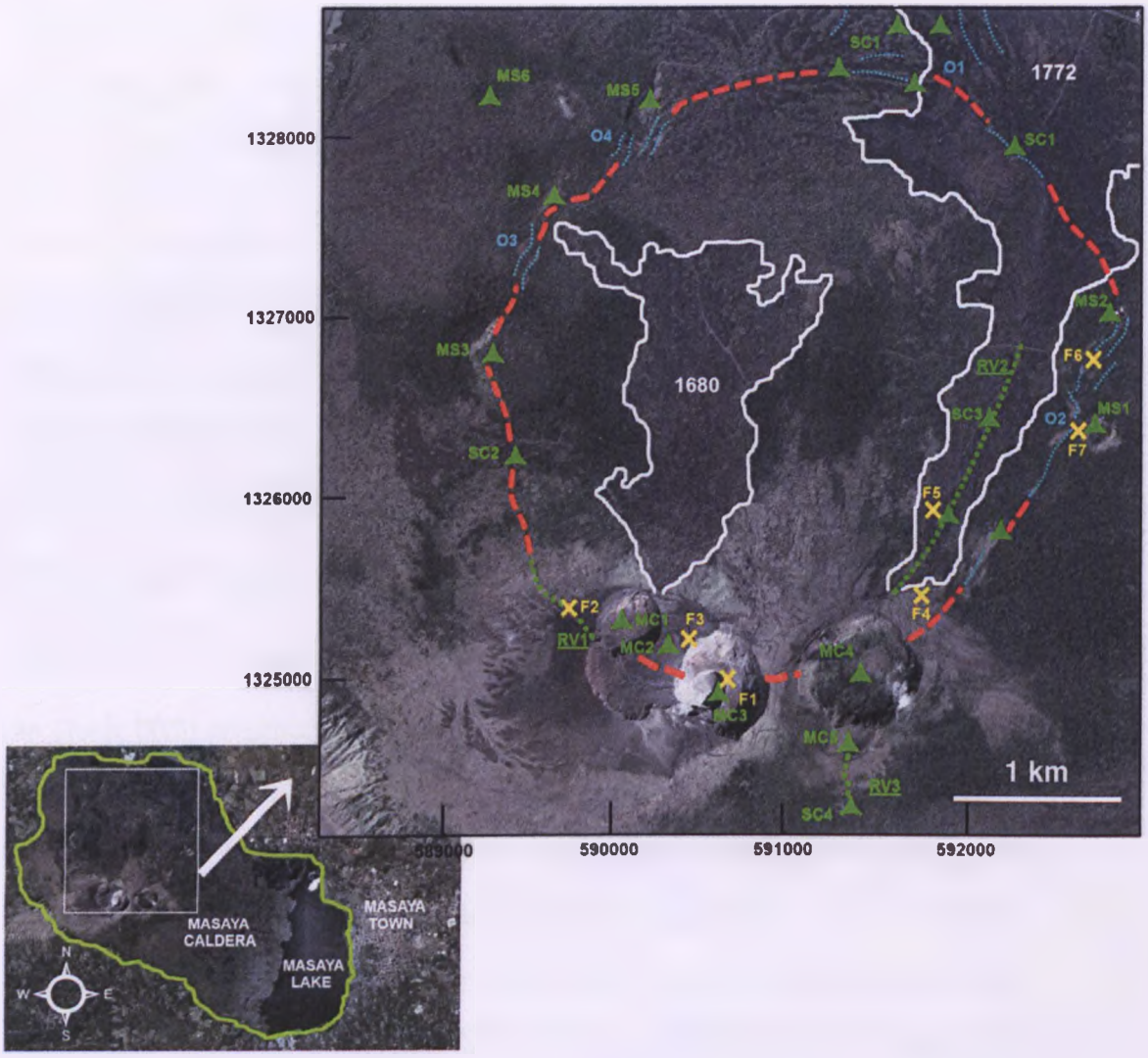

Figure 3-2: Location of relevant structural features within Masaya Caldera. Red dashed line approximates the surface trace of a ring fault based on the alignment of structural evidence. For identification of elements, see **Table 3-1**.

		Volcanic centres – green triangles			***F*** *(Fumaroles, degassing centres) – yellow crosses*	***RV*** *(Rift Valleys – green dotted lines, underlined)*	***O*** *(Openings, cracks– light blue lines)*
		MC *(Main Pit Craters)*	***MS*** *(Medium Sized cones)*	***SC*** *(Spatter Cones – ramparts)*			
1	Feature Name	San Pedro Crater	Comalito Cone	North Fracture Field SC (5 features)	Santiago Vent	San Pedro Valley	North Fracture Field Openings
	UTM Coord. / Bearing	590082/1325271 ≈370 m wide (W), 200 m deep (D)	592605/1326386 ≈360 m wide (W), 80 m high (H)	a) 591118/1328467 b) 591549/1328467 c) 591549/1328467 d) 591118/1328467 e) 591549/1328467	590497/1324861	589773/1325325 N135°E	591456/1328685
2	Feature Name	Nindiri Crater	Visitor Centre Cone	South of Cerro Montoso SC	Rift Valley Site	San Fernando Valley	Visitor Centre Openings
	UTM Coord. / Bearing	590267/1325124 ≈700 m W, 100 m D	592708/1327077 ≈270 m W, 50 m H	589277/1326109	589687/1325415	591942/1326348 N030E°	592630/1326863 N035°E
3	Feature Name	Santiago Crater	Cerro Montoso Cone	North of San Fernando SC	Bee Site	San Juan Valley	Cerro Arenoso Openings
	UTM Coord. / Bearing	590586/1324968 ≈530 m W, 300 m D	589028/1326803 ≈800 m W, 80 m H	a) 592118/1326809 b) 591949/1326379	590540/1325261	591487/1324119 N150E°	589290/1327358 N025°E
4	Feature Name	San Fernando Crater	Cerro Arenoso Cone	South of San Juan SC	Hilltop Site		Sastepe Cone Openings
	UTM Coord. / Bearing	591420/1325038 ≈700 m W, 150 m D	589464/1327814 ≈430 m W, 40 m H	591463/1324213	591924/1325457		589972/1328094 N035°E
5	Feature Name	San Juan Crater	Sastepe Cone		Fumarole Field Site		
	UTM Coord. / Bearing	591332/1324679 ≈250 m W, 50 m D	589916/1328272 ≈280 m W, 20 m H		591859/1325952		
6	Feature Name		Bejucal Cone		Road Site		
	UTM Coord. / Bearing		589009/1328360 ≈110 m W, 20 m H		592521/1326830		
7	Feature Name				Comalito site		
	UTM Coord. / Bearing				592461/1326594		

Table 3-1: Code Names of the structural features displayed in **Figure 3-2**. The columns represent type of feature (the initials are used in the map to identify them) and the lines assign a number to every particular feature so they can be individualized in the map. The UTM coordinates (UTM zone 16P) correspond with the center (or midpoint in linear features) of the respective structures, with predominant bearing specified if appropriate.

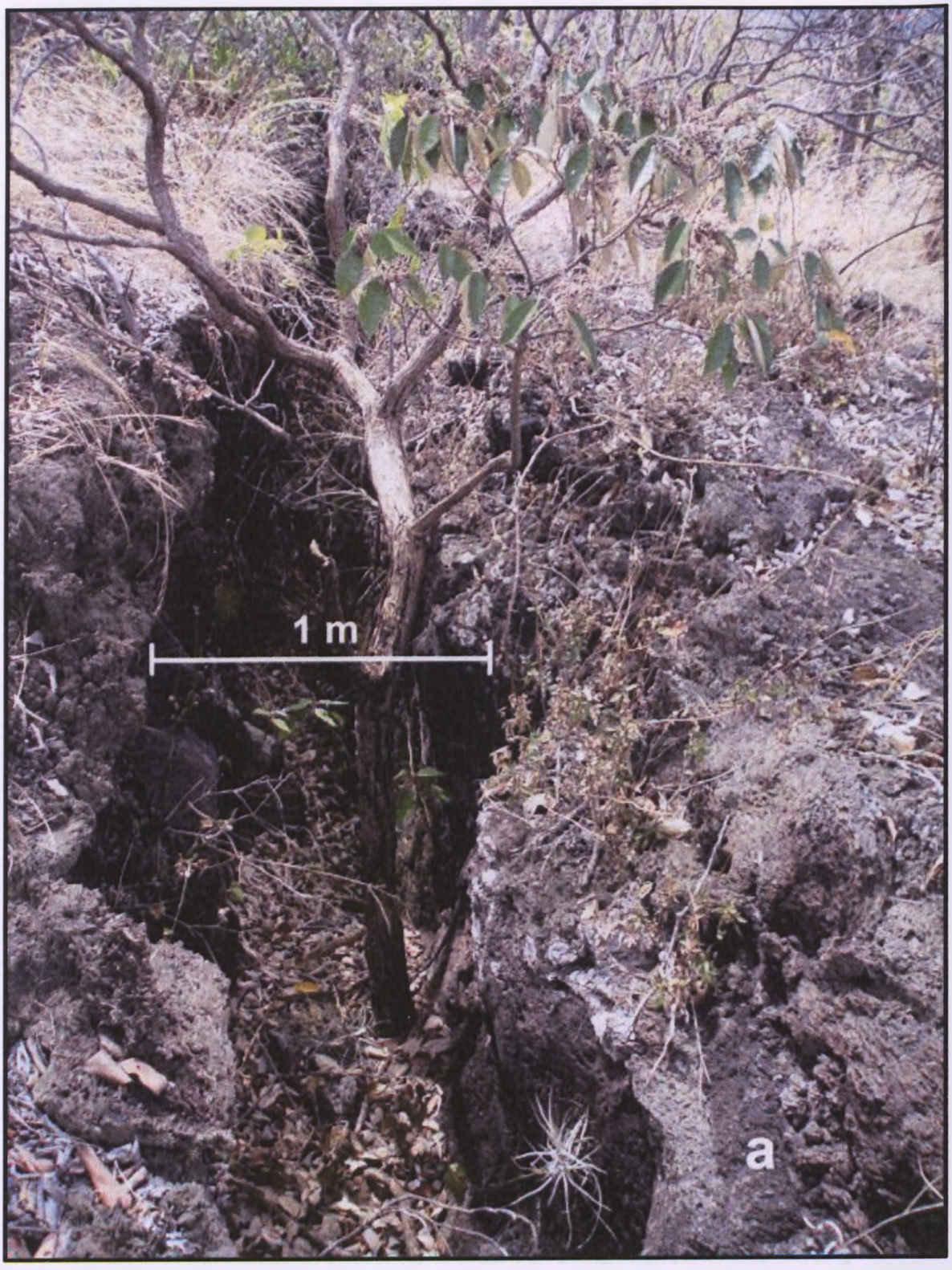
1 m
a

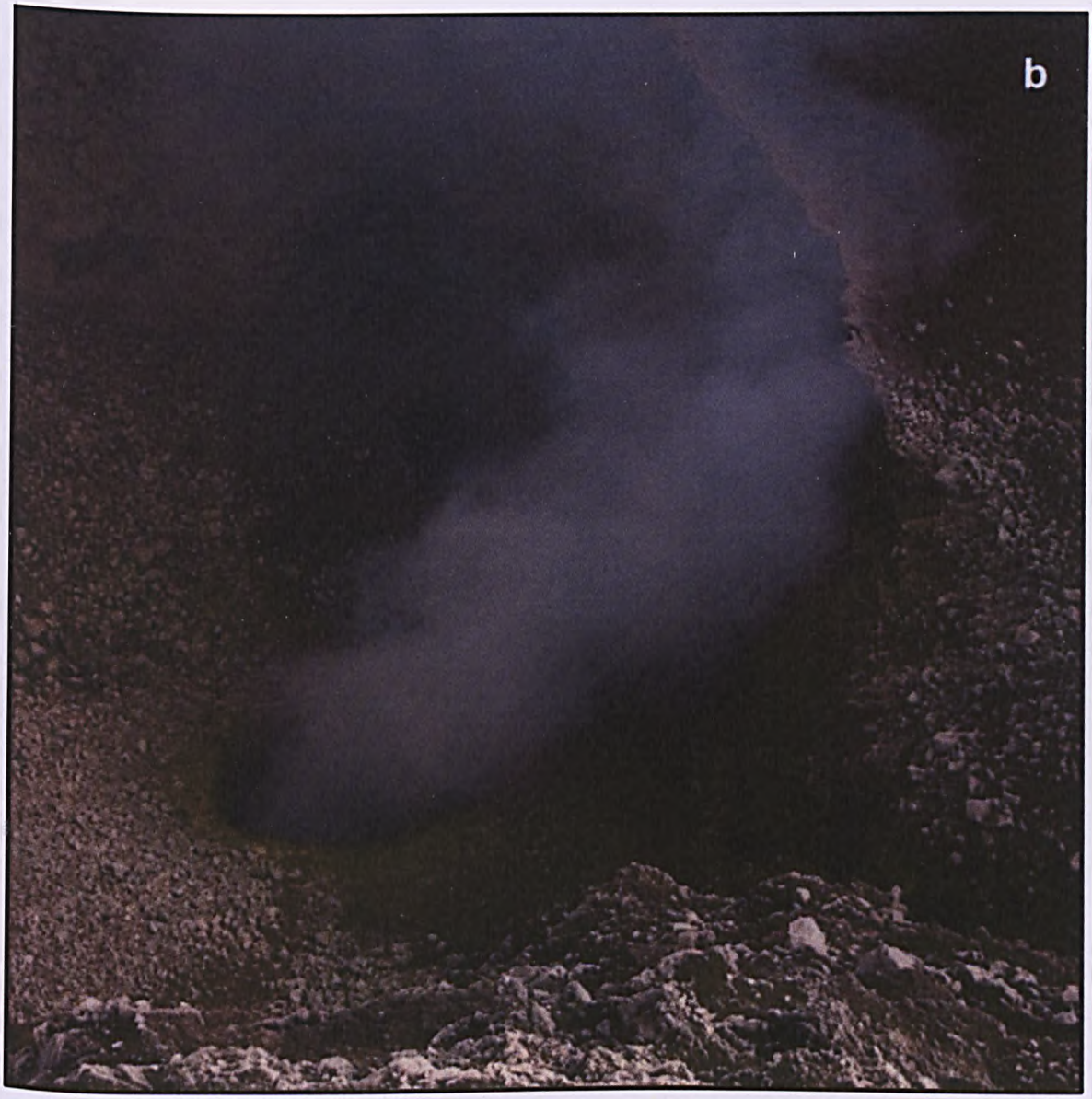
b


C
0.5 m


d

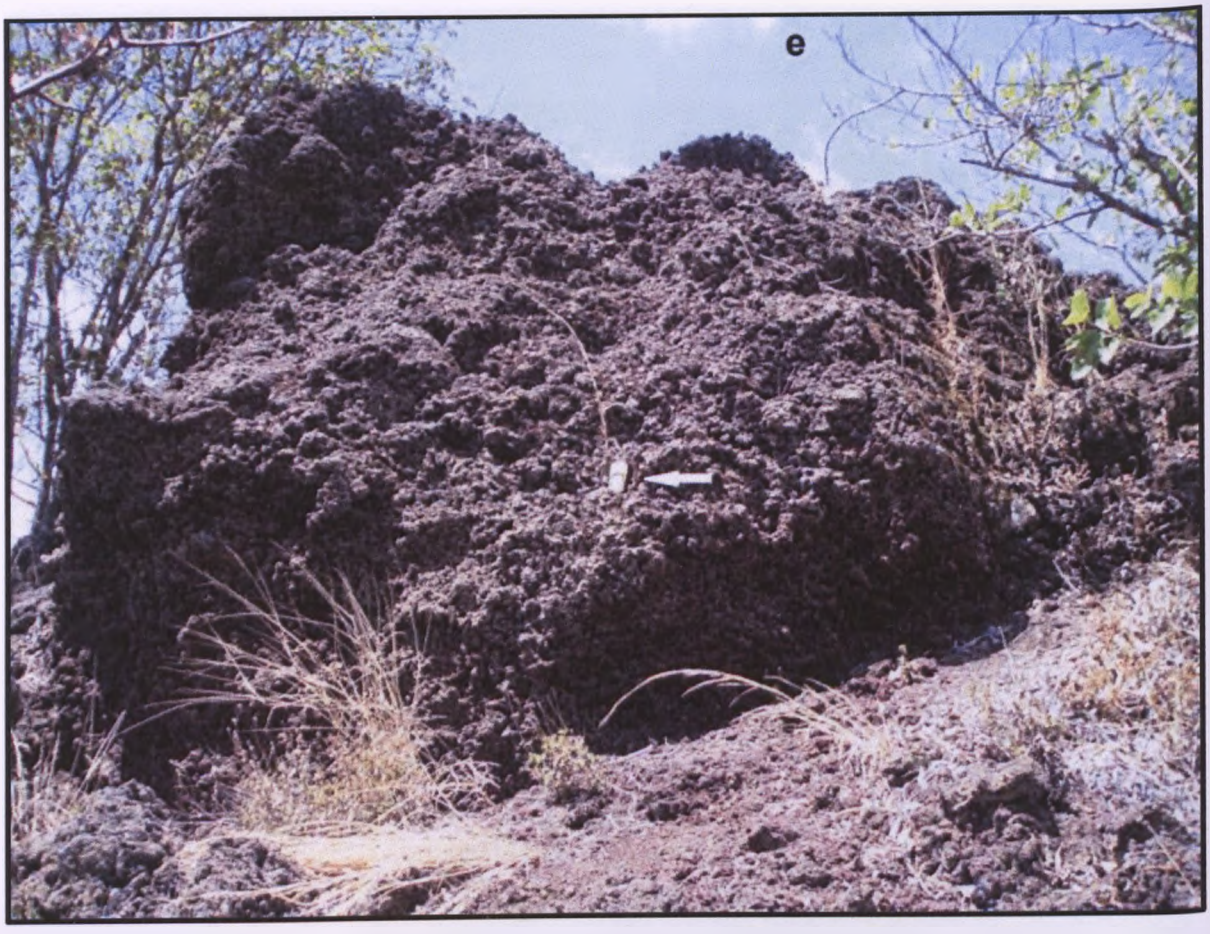
e

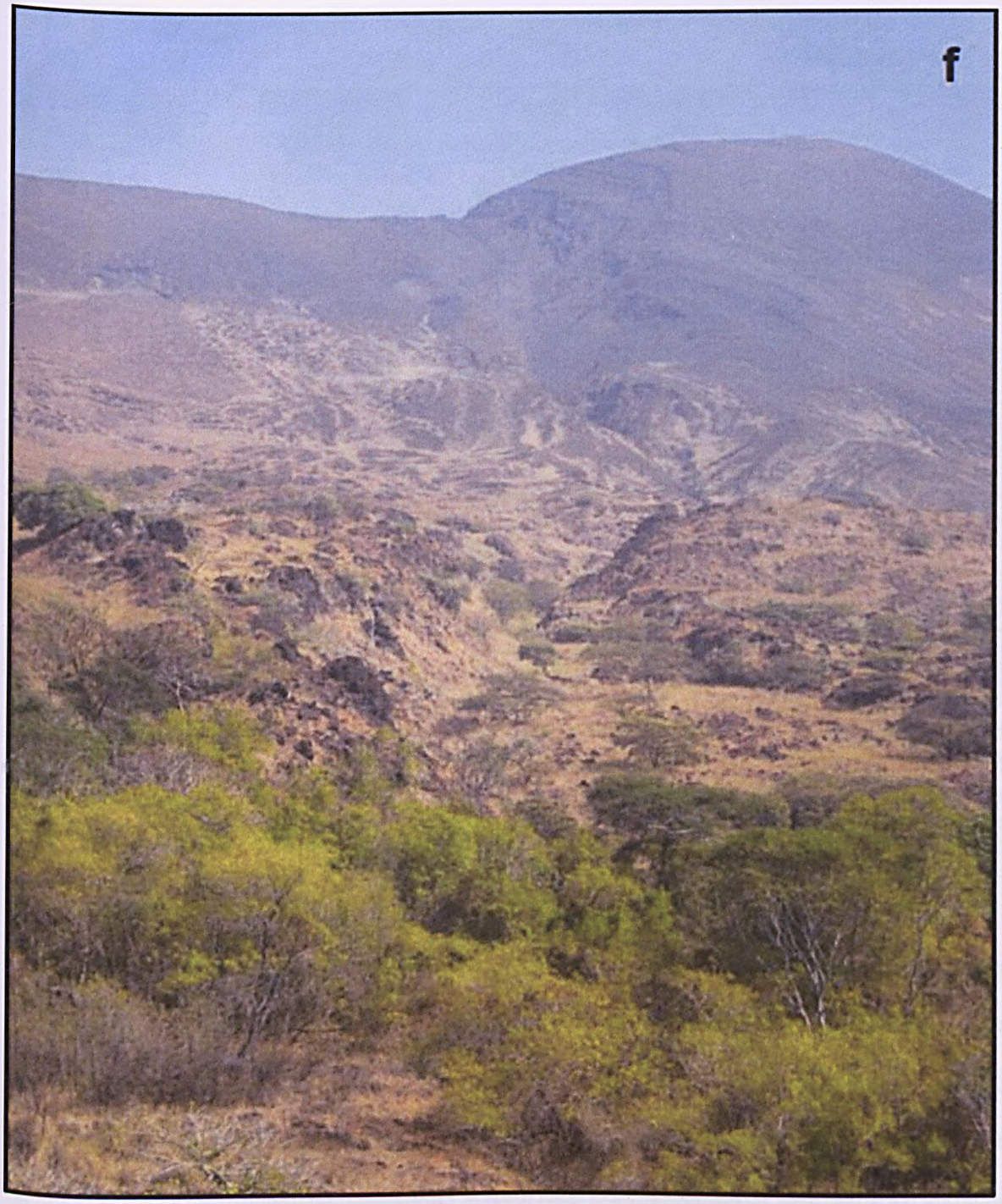
f

Figure 3-3: The photographs above show examples of a) recent opening or crack (O1), b) active vent, Santiago (MC3), c) fumarole in Comalito (F7), d) cinder cone in Cerro Montoso (MS3), e) spatter rampart (SC1), f) rift valley in San Pedro (RV1), g) fumarole in Nindiri covered by bees attracted by the moisture (F3).

3.4.2 Remote structural survey

The inherent characteristics of aa lava flows can hinder research efforts directed towards understanding the stress fields that affect them. The weak and easily collapsable nature of the terrain (due to the rapid cooling of the lavas, hydrothermal alteration and other factors), together with the profusion of lava tube structures underlying the superficial lava crust in certain areas of Masaya, make it difficult to access those locations on the caldera floor. Thus, the decision was taken to integrate the ground based survey data (also used as control points) with Google Earth imagery, in order to analyse in further detail certain areas, in particular the fracture field in the Northwest part of the caldera. Any faults, fractures and collapses affecting this field will be an indication of modern processes, since the surface is covered by a recent (1772) lava flow.

Using this method, several sets of features with the potential of revealing information on the stress fields in this area have been identified (Figure 3-4). They are classified into three categories

that reflect their geometrical and geomorphological characteristics. A first set of fractures (Figure 3-4a) can be found sub-parallel to the edges of some lobes of the 1772 lava flow (emitted from San Fernando's Fissure, Figure 3-2, RV2). They tend to possess a high degree of lateral continuity, and normally appear in the field as sets of 5-10 meters deep braided fractures occupying 10-30 m wide paths that split apart areas of relatively thick and compact lava packages. The cumulative width of these openings can reach (depending on the section selected) up to 10 m. The formation of these fractures is probably related to inflation processes (for studies on inflation, see (Walker 1991; Chitwood 1994; Hon, Kauahikaua et al. 1994; Rossi and Gudmundsson 1996; Anderson, Stofan et al. 1999)) associated with the 1772 lava flow.

A second set of fractures (Figure 3-4b) next to several families of the first set has also developed within the area covered by the 1772 lava flow. These fractures run up to 200 m sometimes, and normally are 1-6 m deep. Small spatter cones (1-3 m high above surrounding terrain) can be found associated with this type of fracture. Finally, their orientation (NNE-SSW) and disposition on the caldera floor suggest they might share a structural link with San Fernando rift valley-fissure, and at a bigger scale, with the easternmost boundary of Managua Graben (Cofradías Fault).

The third set of fractures (Figure 3-4c), also locally associated with small (0.5-8 m) spatter cones and ramparts, occupy a position consistent with the expected location of the Northern section of a ring fault represented in the West, East and South sections by a W-E semi-circular alignment of cones and pit craters. Despite the relatively shallow depth of the collapses (2-5 m), the degree of continuity of this last set of fractures (~500-800 m) and the disposition in collapse areas parallel among themselves, can't be explained by random mechanisms. The lower depth of the fractures compared to the other sets has probably to do with the mechanism of generation of these features, which most likely involve slow and gradual collapse of a central block within the caldera limited by a boundary fault, which has kept moving after the 1772 eruption, deforming the new terrain generated in the eruption.

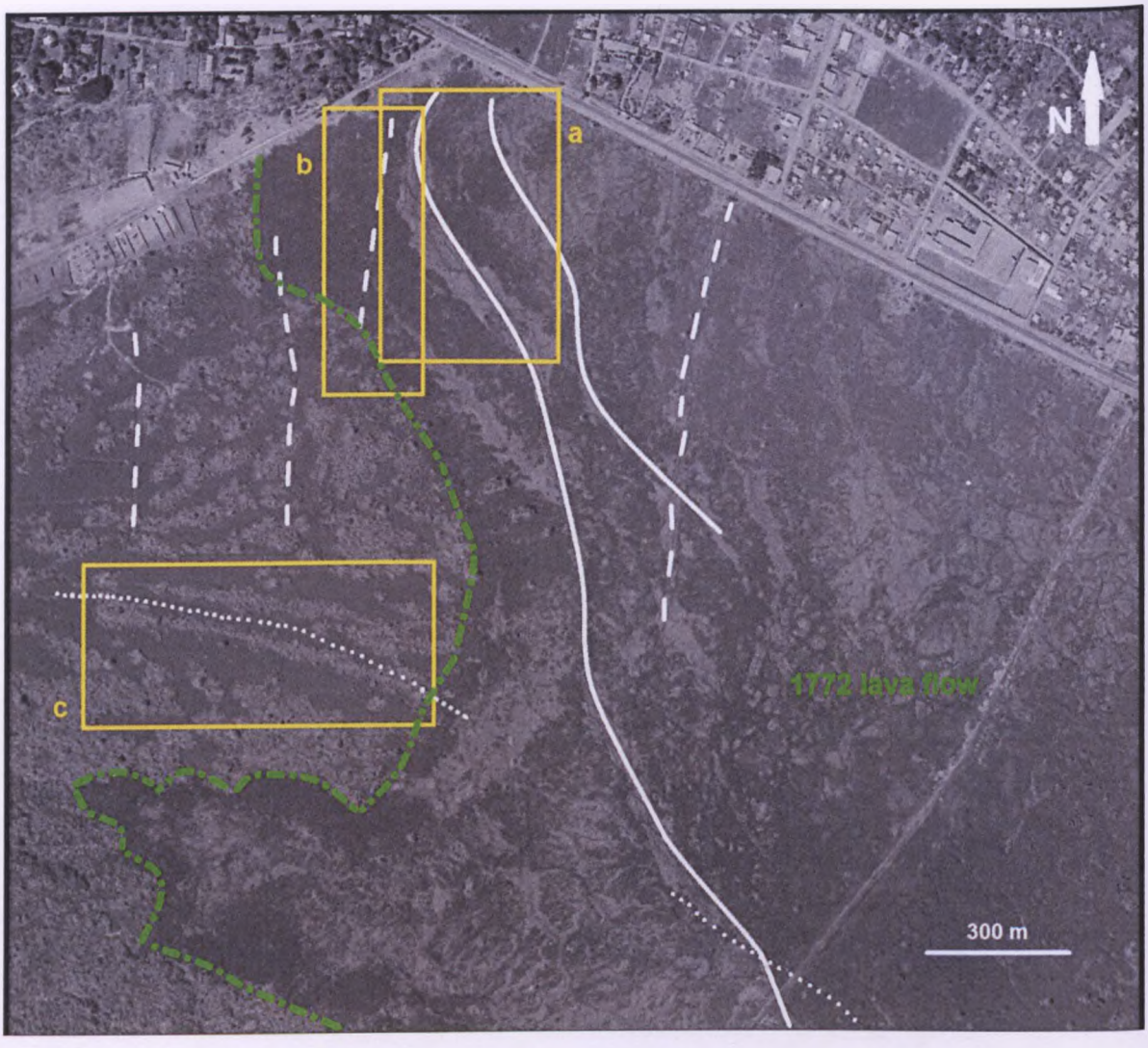
a
b
c
N
1772 lava flow
300 m

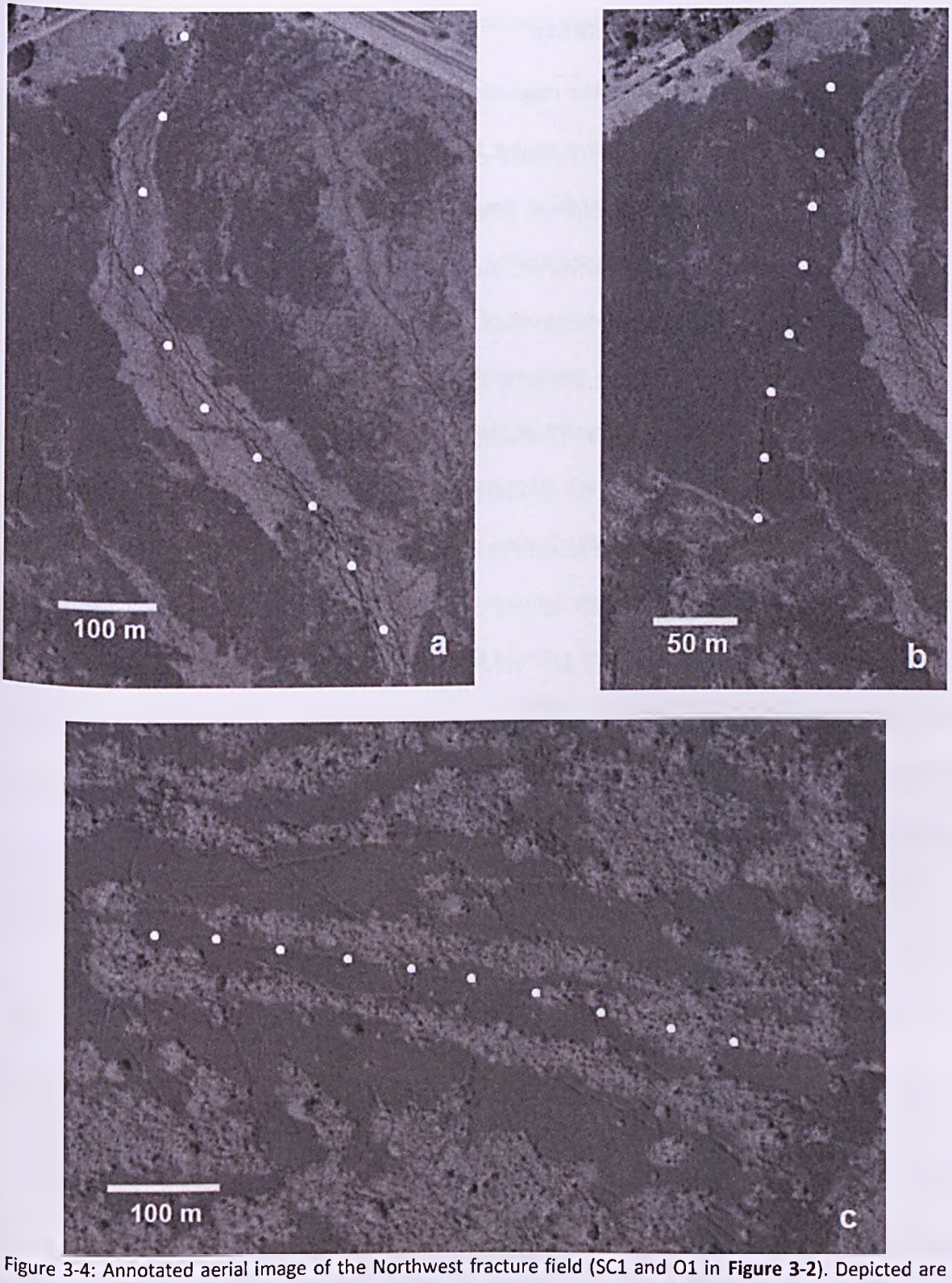

Figure 3-4: Annotated aerial image of the Northwest fracture field (SC1 and O1 in **Figure 3-2**). Depicted are inflation fractures (white continuous lines), fractures parallel to the Cofradías fault (white dashed lines), and ring fault fractures (white dotted lines). The maximum extent of the 1772 lava flow is shown in green, and in yellow boxes are the zoomed in areas (see below). The closer photographs show examples at a smaller scale of a) braided inflation fractures, b) Cofradías fractures, and c) double ring fault fracture (trees align along these subsided areas because of the accumulation of moisture).

3.5 Magnetic susceptibility study

The main source for variations in the magnetic field in volcanic terrains is the thermo-remnant magnetization of rocks after they have cooled below the Curie temperature (585°C). The high concentration of ferromagnetic minerals in basalts makes mafic volcanoes a good setting for magnetic studies. Thus, the lateral susceptibility contrast between the presence of basaltic dikes (indicators of deep fracturing) and successions of ashes and weathered lavas related to the cyclic emissions from the eruptive centres can generate important magnetic anomalies, and therefore become important from a structural point of view (Lopez-Loera, Urrutia-Fucugauchi et al. 2010). However, since most volcanic rocks are magnetic, with many of them having a strong remnant magnetization, the inhomogeneous distribution of rocks/sediments generates background noise which is normally very high on volcanic terrains. In order to interpret magnetic anomalies, those must be well above the signal-to-noise ratio. In this particular geographic location, buried bodies with higher remnant magnetization values tend to generate dipolar anomalies with a positive response south and a negative response north of the object.

A magnetic study covering the caldera floor has been completed (Figure **3-6**) using a Proton Precession Magnetometer (Appendix A: Magnetic data). Magnetic data from 2756 stations with a 25 m average spacing (69 line-kilometers) have been collected over a period of two years (3 months in 2009, 3 months in 2010). A continuously recording magnetometer with a 0.2 Hz sampling frequency was deployed for two days for each fieldwork campaign (four days in total) in order to help characterize the magnetic diurnal variation in the site of investigation (Figure **3-5**). The short term variations are negligible compared with the scale of the variations encountered along the survey lines. In days where no base station was available, measurements were repeated typically every 4-5 stations in order to discard the possible occurrence of magnetic storms, and only once the magnetic measurement was off by more than 50 nT, probably due to instrument malfunction since a value

similar to the one recorded originally was obtained again after another measurement was performed.

The magnetic data collected on the caldera floor show different characteristics for different parts of the caldera (map in Figure 3-6). The profile along the shoreline of Masaya Lake shows a high degree of variability, coinciding with an area where the water flow towards the lake (Mauri 2009; Mauri, Williams-Jones et al. 2010; Mauri, Williams-Jones et al. 2012) has been suggested to be close to the surface (MacNeil 2006; MacNeil, Sanford et al. 2007). Strongly variable data (shown by two bodies in intense red) in the intersection between the Northernmost tip of the lake and the caldera boundary (with values oscillating between 32000 and 38000 nT) are probably related to Nindiri's sewage system infrastructures that transport the city's waste waters into the lake. The profile along the SW boundary of the caldera shows the least variable data on the caldera floor, indicating a relatively homogenous lithology/structural framework. The central and NW region of the caldera shows a high degree of variability. To provide more detail on this area, where the existence of a ring fault has been suggested (Crenshaw, Williams et al. 1982), 6 magnetic profiles are shown in Figure 3-6a-f. There is good correlation between the expected location of the ring fault and magnetic dipoles found in the data.

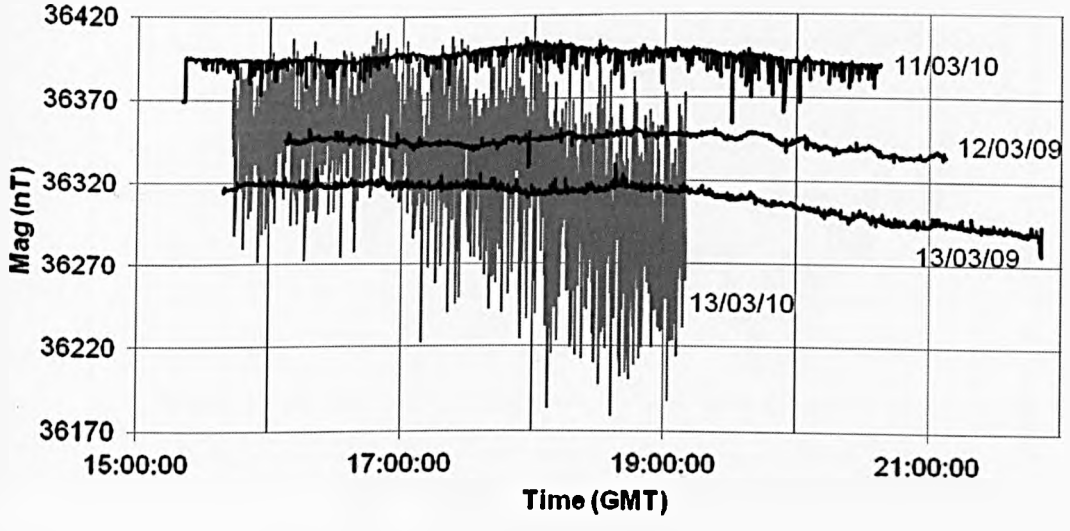

Figure 3-5: Record of magnetic diurnal variation on 4 different days (12°00'02.65"N, 86°09'03.63"W).

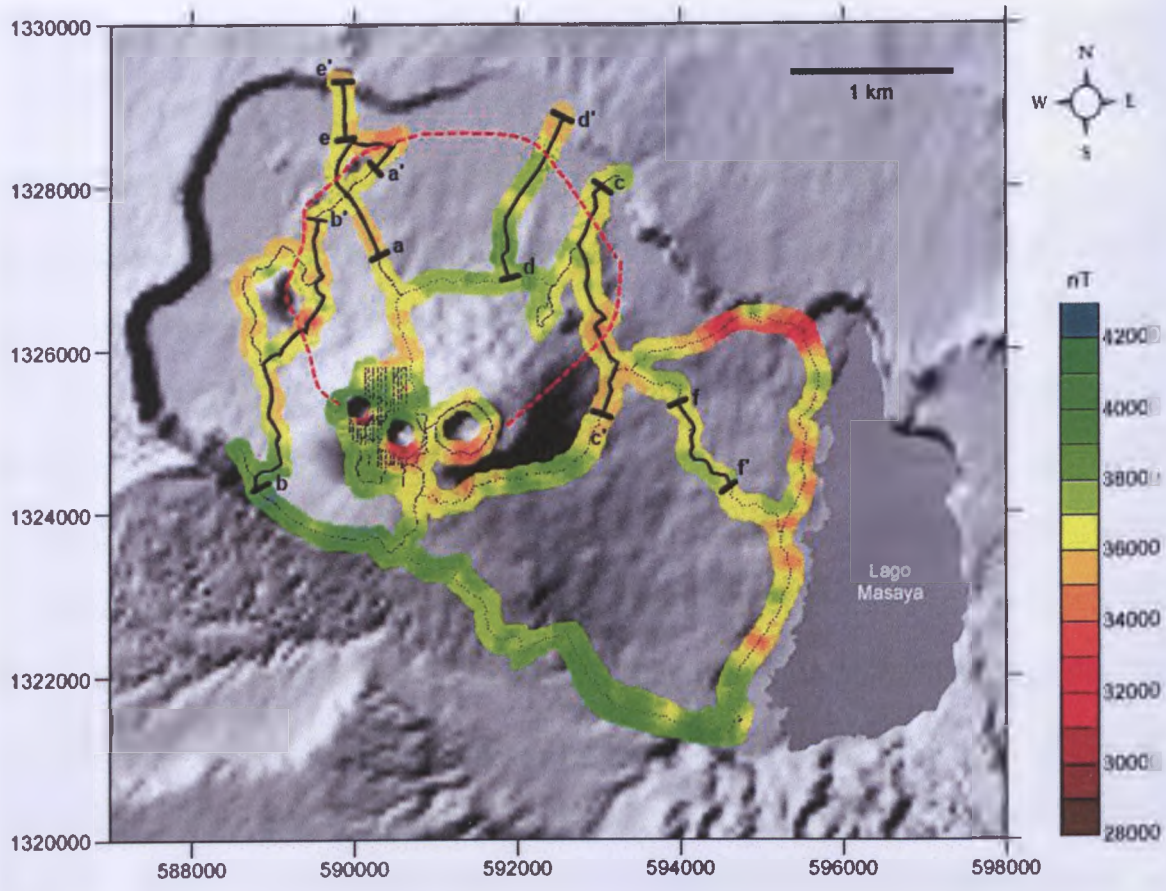
1330000
1328000
1326000
1324000
1322000
1320000
588000
590000
592000
594000
596000
598000
1 km
N
W
E
S
nT
42000
40000
38000
36000
34000
32000
30000
28000
Lago
Masaya
a
a'
b
b'
c
c'
d
d'
e
e'
f
f'

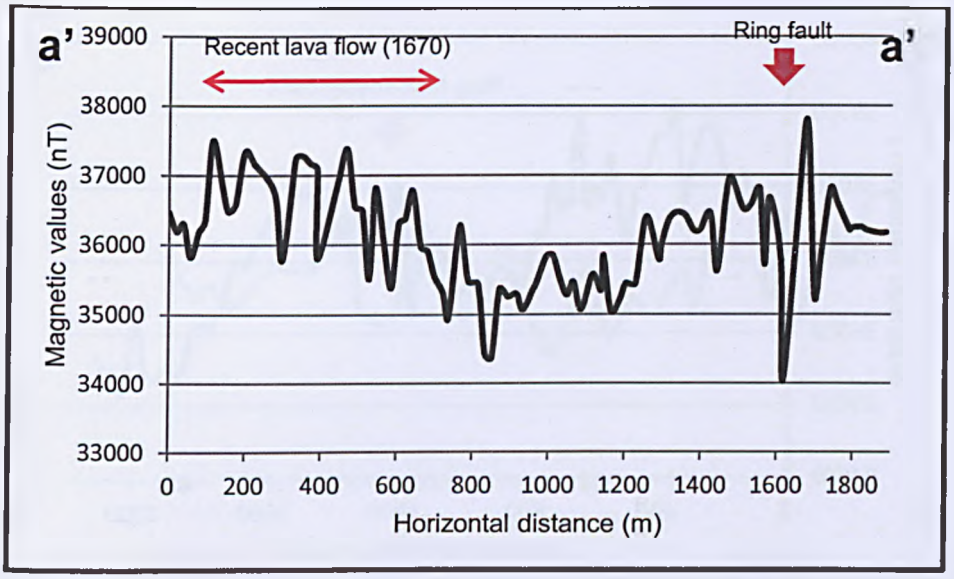
a'
a'
Recent lava flow (1670)
Ring fault
Magnetic values (nT)
39000
38000
37000
36000
35000
34000
33000
0
200
400
600
800
1000
1200
1400
1600
1800
Horizontal distance (m)

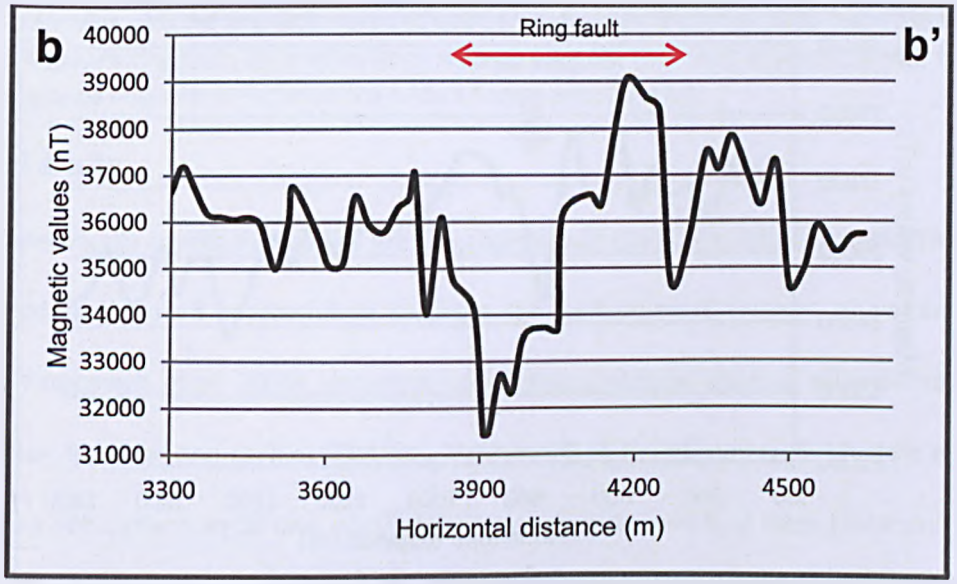
b
b'
Ring fault
Magnetic values (nT)
40000
39000
38000
37000
36000
35000
34000
33000
32000
31000
3300
3600
3900
4200
4500
Horizontal distance (m)

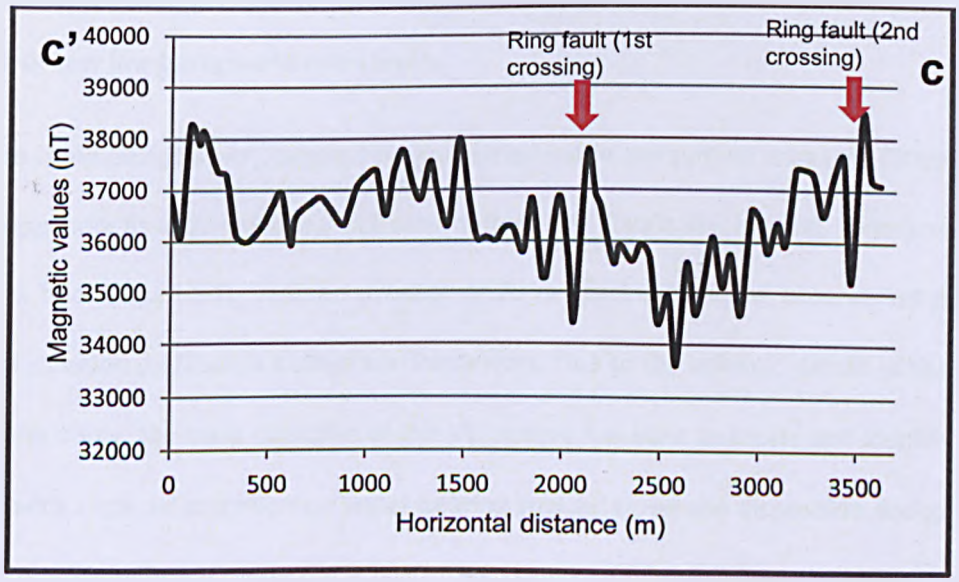
c'
c
Ring fault (1st crossing)
Ring fault (2nd crossing)
Magnetic values (nT)
40000
39000
38000
37000
36000
35000
34000
33000
32000
0
500
1000
1500
2000
2500
3000
3500
Horizontal distance (m)

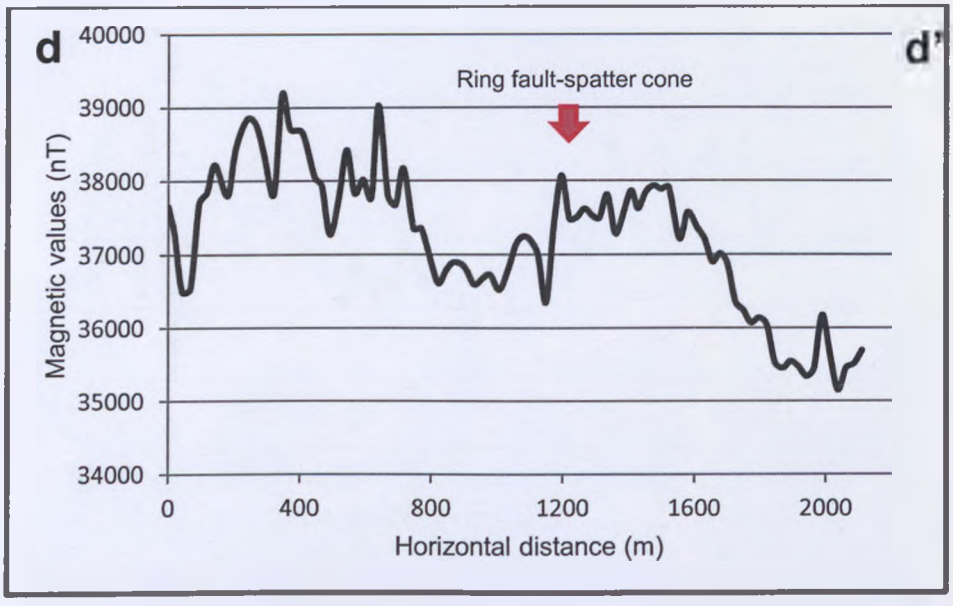
d
d'
Ring fault-spatter cone
Magnetic values (nT)
40000
39000
38000
37000
36000
35000
34000
0
400
800
1200
1600
2000
Horizontal distance (m)

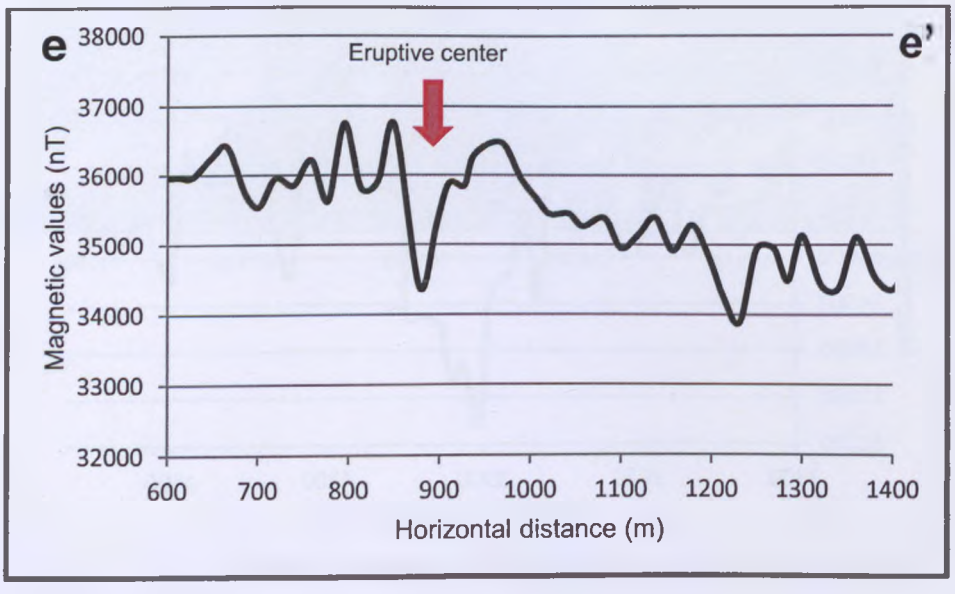
e
e'
Eruptive center
Magnetic values (nT)
38000
37000
36000
35000
34000
33000
32000
600
700
800
900
1000
1100
1200
1300
1400
Horizontal distance (m)

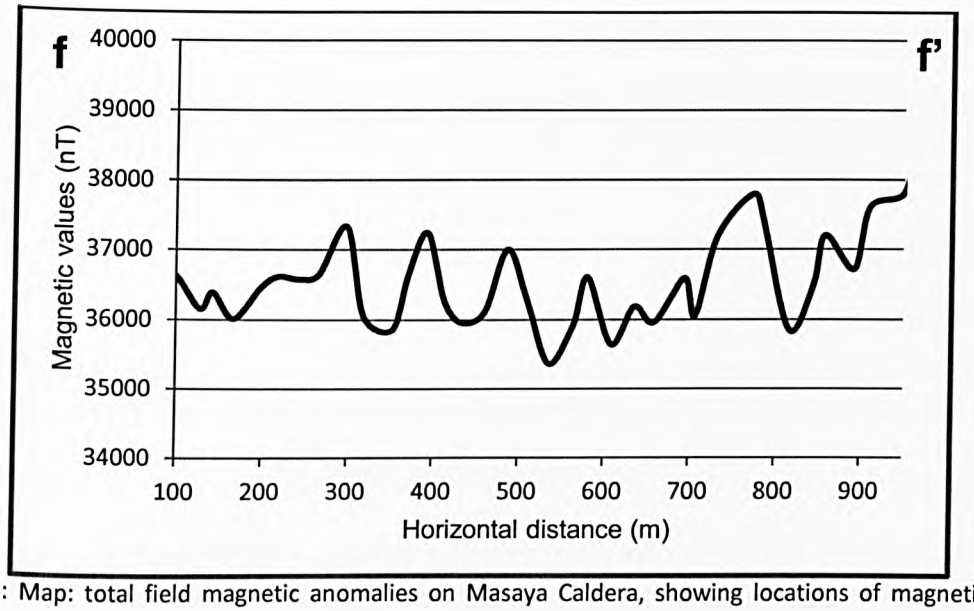

Figure 3-6: Map: total field magnetic anomalies on Masaya Caldera, showing locations of magnetic dipole anomalies coinciding with the ring fault expected outline. Dashed red line in the map shows the approximate location of Masaya's ring fault. All profiles from a) to e) cross the ring fault structure, profile f) shows the normal background magnetic variation on the caldera floor (control profile).

3.6 VLF study

Highly electrically conductive bodies are the objective of the VLF electromagnetic (EM) method. This method has proved successful in studying the hydrothermal system of volcanic edifices (Zlotnicki, Vargemezis et al. 2006), detecting conductive structures such as mineralized or water-bearing dikes, fractures and cavities (Zlotnicki, Vargemezis et al. 2006; Al-Oufi, Mustafa et al. 2008); and studying sub surface liquid lava within lava tubes, fissures and lava lakes (Zablocki 1978). The high resistivity of basaltic volcanic successions allows relatively high (~100 m) depths of penetration as a result of very low background noise levels.

Thus, to complement a very detailed survey carried out in the summit area (see Chapter 4) 3 VLF profiles (Appendix B) acquired using VLF transmitter NPM (Lualualei, Hawaii), were completed on the caldera floor (Figure 3-7). With an average of 20 m spacing between observation points, they provide information on Masaya's structural framework. Due to the volcanic nature of the geological setting under study, the main objective of this VLF survey has been to locate and identify dikes and fractures, with a special attention on water bearing structures, whose disposition and geometry at depth can provide information on the effect of the structural framework on the shallow part of the

volcanic construct. We present the data as a series of Karous-Hjelt filtered profiles (Karous and Hjelt 1977), where the values correspond to apparent current densities at different depths which would cause a magnetic field equal to the measurements. Areas of current densities with values far from 0 correspond to good conductors, providing in some cases information on the dip angle and dip direction of faults.

From the data we observe (Figure **3-7**) that water bearing structures, such as the metallic water pipe of profile 1-1' have a strong effect on the VLF values. In addition to this, where uniform lithologies are found, the VLF profiles show very little variation, confirming the low levels of noise that are expected in this area where no evidence for fault structures has been found, on the surface or at depth. Both profiles 2-2' and 3-3' cross areas where the ring fault is known to be present, and the VLF profiles show it by displaying strong anomalies with a very well defined dipping direction (in profile 3-3', even a double parallel fault has been detected). The orientation of the ring fault for both profiles corroborates observations on the surface, confirming that the ring fault very probably dips towards the centre of the area.

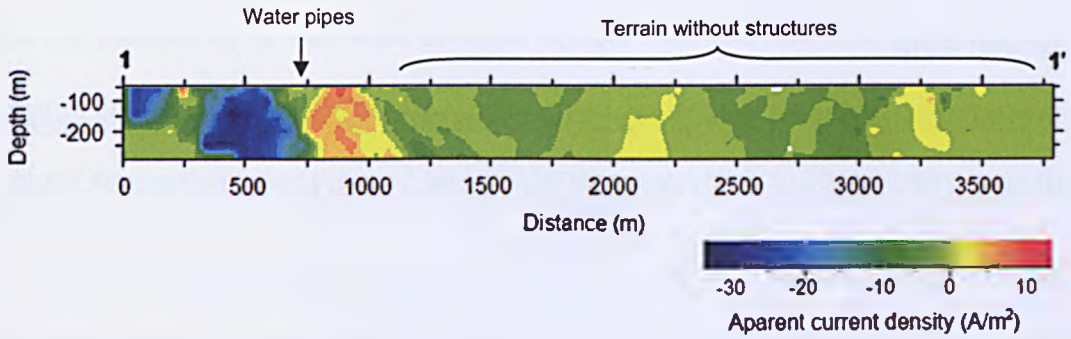

1-1': control profile showing effect of man-made water pipes buried at 2 m depth (dipole centred at 750 m) and terrain without evidence of structures on Masaya Caldera's floor

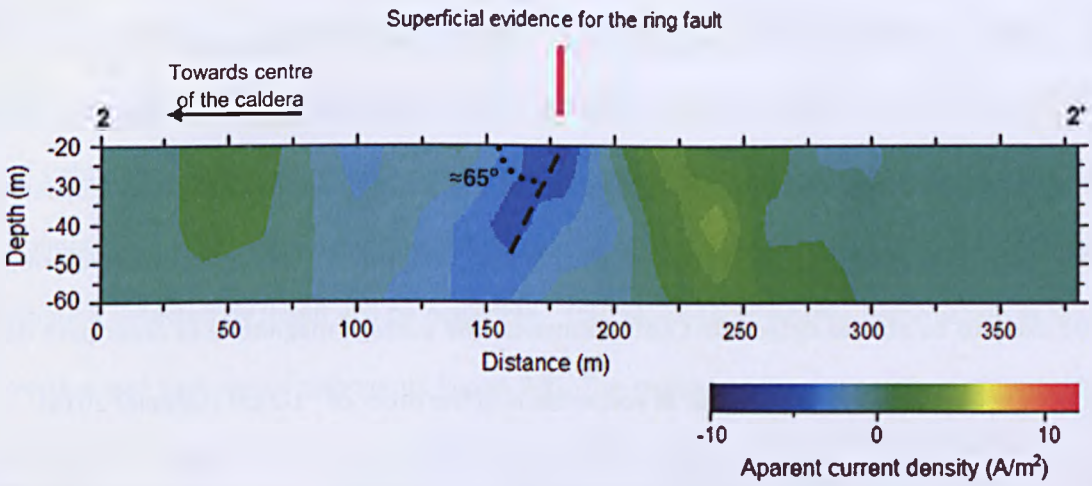

2-2': evidence for the ring fault, dipping towards the central point of the caldera lid (apparent dip: ≈65°)

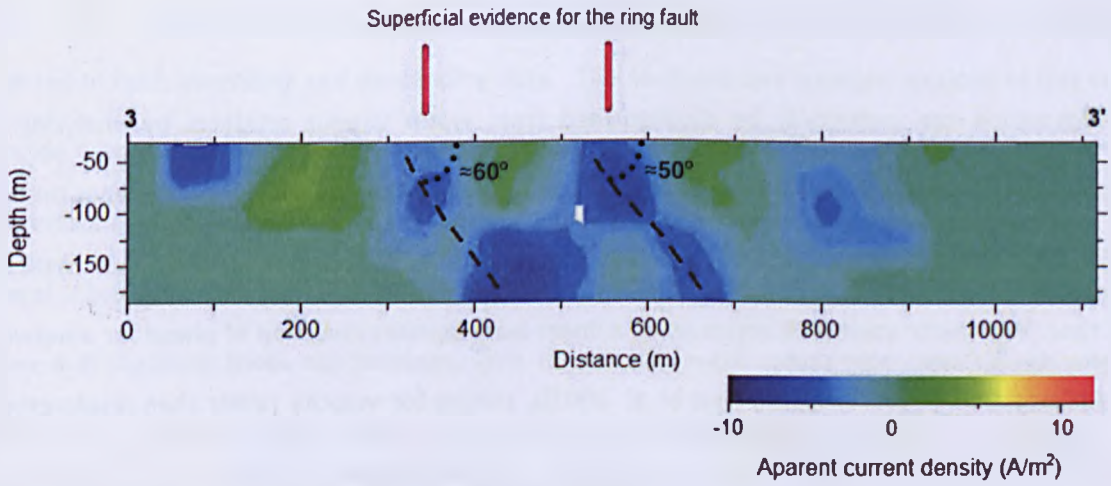

3-3': double ring fault dipping inwards (apparent dip: ≈50-60°)

Figure 3-7: VLF profiles showing several artificial and natural features on the floor of Masaya Caldera. A Karous-Hjelt filter was applied to the data. Red lines mark location of faults on the surface, and probable orientations at depth are shown with dashed black lines. The depth of penetration for each profile has been limited to the depth where the Signal to Noise Ratio remains acceptable for geological interpretations to be performed.

3.7 InSAR data

An interferometric synthetic aperture radar (InSAR) study of data from 2007-2009 (Appendix B) shows evidence of subsidence within the ring-fault identified using the ground based geophysical and geological methods described above.

Repeat pass InSAR uses time-separated radar images acquired from the same position in orbit to measure deformation of the Earth's surface with a precision of millimeters to centimeters (Massonnet and Feigl 1995; Massonnet and Feigl 1998). In addition to the movement of the ground, interferograms capture phase shifts caused by changes to satellite viewing geometry, instrument thermal noise, scattering and dielectric properties of the ground, and the effects of tropospheric water vapour. The magnitude of these 'nuisance factors' determine the magnitude of deformation we are likely to be able to detect. In Central America, the average magnitude of radar path delays associated with stratified water vapour at volcanoes is of the order of ~1-2 cm (Ebmeier 2013).

We constructed interferograms covering Masaya using the Repeat Orbit Processing software (ROI PAC) (Rosen, Hensley et al. 2004) and used NASA's Shuttle Radar Topography Mission 90 m Digital Elevation Model (DEM) to make topographic corrections (Rosen, Hensley et al. 2001).

Deformation can commonly be distinguished from water vapour artefacts by analyzing its temporal development. Atmospheric phase artefacts typically either a) lack any dependence on time or b) exhibit a seasonal dependence, whereas deformation is expected to develop systematically over time. We constructed time series using a linear least squares inversion of phase for a network of interferograms (e.g. (Lundgren, Usai et al. 2001)), solving for velocity rather than displacement using a generalized inverse matrix and singular value decomposition (e.g. (Berardino, Fornaro et al. 2002)). We explicitly assume that the volcano was not deforming on the first acquisition date.

Time series analysis reveals a region of steady subsidence in the southern half of the area bounded by the ring fault, and bordered by Nindiri and Santiago craters to the South (Figure 3-8). This

region has subsided by at least 4 cm between October 2007 and July 2010. Although there are cumulative displacements of similar magnitude in other parts of Masaya Caldera, they do not show a systematic development over time and we consider them most likely to be atmospheric in origin.

As InSAR measures displacement along satellite line of sight, multiple measurements from different look angles would be required to retrieve a full 3D deformation field. At Masaya we have 11 coherent ascending interferograms, and 5 coherent descending interferograms (Appendix K: InSAR data), providing only two independent constraints on a three dimensional problem. We therefore require an independent constraint or assumption to resolve components of motion from line-of sight deformation (e.g. (Fialko and Simons 2001)). Both ascending and descending data look from almost due east and west respectively, so we make the assumption that any north-south deformation detected by InSAR will be negligible. This allows us to resolve deformation at Masaya into vertical and east-west components (Figure 3-8). The motion of the region of steady subsidence described above is almost entirely vertical.

It is remarkable that the relative subsidence (~2 cm/yr) is centered just in the southern half of the ring fault. This displacement reaches maximum values close to the main edifice area, and is clearly reflected in both ascending and descending data. The southern and western sections of this signal coincide with the edge of the ring fault as inferred from our other geophysical observations. The differences in deformation within the lid limited by the ring fault might indicate its division into several sub-blocks, thus preventing the coherent subsidence of the lid as a single unit. The profiles (Figure 3-9) illustrate these observations, with the displacement values also showing the relative subsidence of the southern half of the terrain encircled by the ring fault, the differential displacement between terrain inside and outside the ring fault, and the peak of relative positive displacement in the middle of the inner caldera lid.

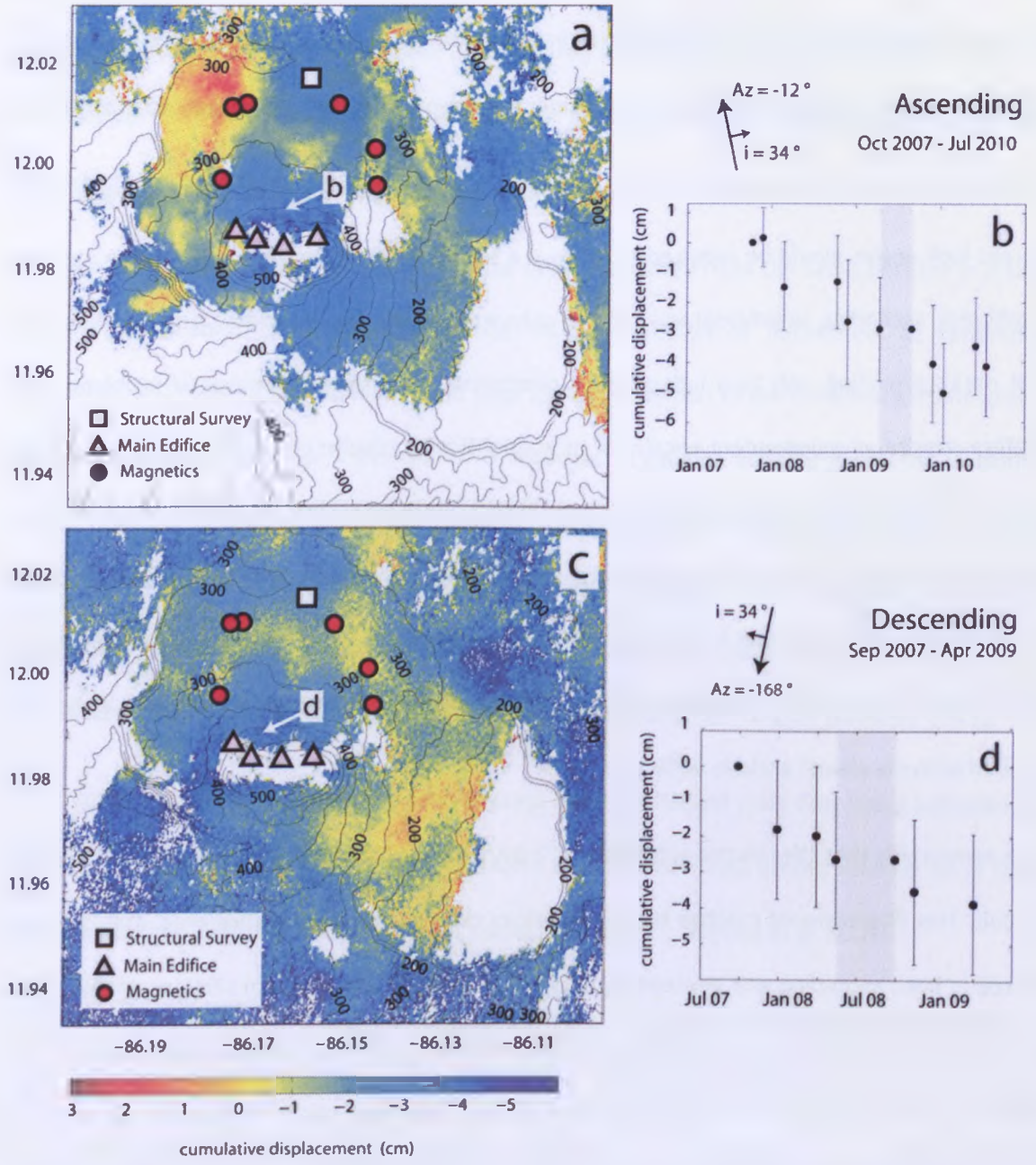

Figure 3-8: a) Cumulative displacement between October 2007 and July 2010 found from time series analysis of ascending interferograms over Masaya (grid in geographical coordinates). Some of the markers of the main ring fault described in the structural and magnetic sections are indicated by coloured shapes: white squares for structural survey, red circles for magnetics and purple triangles for the main edifice. Contours show topographic height above sea level. b) Time series constructed from ascending data for the point indicated in part a). Random noise of mean magnitude 1 cm was added to every pixel before inversion, neglecting the effects of spatial correlation. Error bars show the standard deviations for 100 Monte Carlo repititions. c) Cumulative displacement between September 2007 and April 2009 found from time series analysis of descending interferograms over Masaya. d) Time series of cumulative displacement for the point shown in part c. Az= satellite azimuth direction, and i=incidence angle. NOTE: These cumulative displacement maps show displacements relative to the average of path delay for an area surrounding Masaya Caldera.

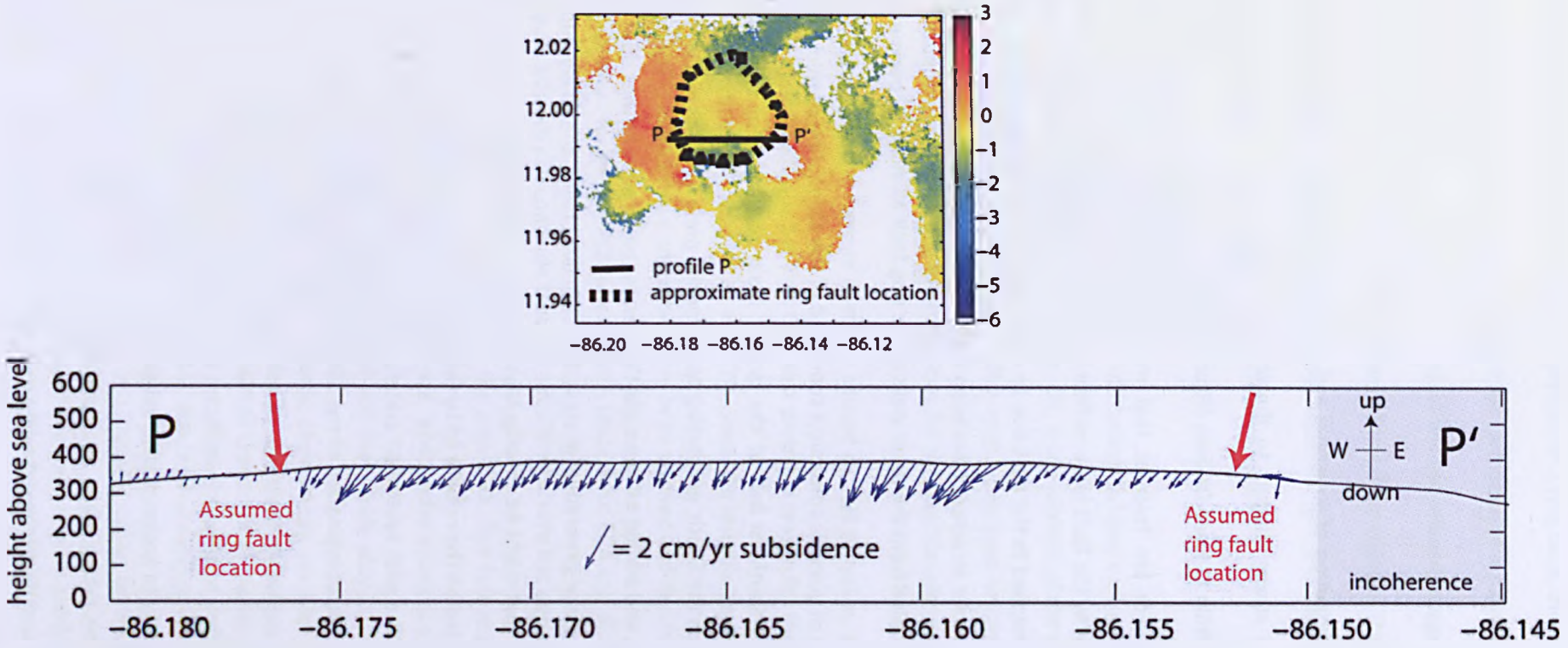

Figure 3-9: Profile across ring fault (location shown on inset) with cumulative displacements from the complete set of ascending interferograms shown as vectors. Arrow size shows total cumulative displacement, while directions indicate the direction of motion found from inversion of a pair of ascending and descending interferograms, assuming that North-south motion captured in interferograms is negligible. Uncertainties in displacement magnitude are of the order of ~1 cm, while uncertainties in direction of deformation are expected to be of the order of ~20 degrees.

3.8 Discussion

3.8.1 RING FAULT

3.8.1.1 Geometry

The non-random spatial distribution of structural and geophysical evidence accumulated in this study is enough to provide a strong support to the theories that suggest the existence of an approximately circular fault within Masaya Caldera (Figure 3-2). This 3.5 km diameter fault can be considered complete, since there are features that mark its presence all along its proposed perimeter. The terrain encircled by the fault has a surface of 10 km^2. In the northern edge of the ring fault, which had been poorly mapped in the past due to difficult terrain, several spatter cones and fractures oriented along the circular structure have been found. This probably means that the inner lid floor is almost entirely decoupled from the outer walls of the ring fault all along its perimeter.

The accumulation over time of volcanic constructs composed of the alternation of thick packages of lava flows and ashes in the Southern half of the circular fault, suggests also that the strata delimited by it are tilted towards the South; generating space for the preferential ascent of magmas through that particular section, and adding extra weight that forces the lid even further downwards. InSAR data suggest that this space-generating process is still active, being the likely superficial expression of two mechanisms that might be shaping Masaya Caldera's structural framework today: a) the downward pressure exerted on the caldera lid by the overlying part of a 300m high (above the surrounding plane) volcanic edifice with several pit craters; and/or b) a magma chamber that might have been partially emptied by the combination of the 1800 ybp Plinian eruption (Pérez, Freundt et al. 2009), effusive and minor explosive emissions of ash and lava (present as part of the main volcanic edifices within the caldera today) and significant degassing since 1852 (Stoiber, Williams et al. 1986), conferring it the capacity to accommodate subsidence. The deformation data also suggest that this collapse might not be taking place as a perfectly coherent single unit, and that the difference in the rate of downward displacement might be inducing the fracturing of the lid into 2 or

more blocks. Characteristics such as the presence of a ring fault, the asymmetry in the subsidence of the floor of the caldera (up to 4 cm/yr), and the formation of fractures and openings in the section of the ring fault opposite to the area of maximum subsidence, suggests an incipient caldera floor collapse resembling the end-member model of trapdoor collapse (Lipman 1997; Cole, Milner et al. 2005). The evidence provided by VLF data, suggests that this fault system is an inward dipping structure; defining an inner caldera within Masaya Caldera.

3.8.1.2 Relation to activity in time

The present shape and characteristics of Masaya Caldera's morphology, including the structural framework and the existing volcanic constructs, is the product of the evolution of the caldera system after the last Plinian eruption (10 km^3). This major explosive eruption took place 1800 years ago (Pérez Fernández 2007), setting the conditions for the later development of the caldera.

The emptying of the magma chamber caused by this eruption, and the subsequent additional subsidence associated with it is thus the most probable reason for the generation of the ring fault in the first place (Kutterolf, Freundt et al. 2007). Since the last Plinian eruption, an estimated 14.2 km^3 (Williams 1983) of lava flows and ashes have been erupted and deposited on the caldera floor. Since the source vents for most of these eruptions (except for SC3 and SC4) can be found along the ring fault (Figure 3-2), we can conclude that this circular structure has determined the nature and location of eruptive activity within the caldera for the past 2 ka. The fact that most active fumarolic fields, sources of recent lava emissions, subsidence, and cinder cones are located around the ring fault suggest that this structure still plays, and will very likely play in the future, a fundamental role controlling and concentrating most volcanic phenomena on the caldera floor. This feature is positioned in a relatively central location within the caldera, meaning that low energy explosive or effusive activity will very rarely affect areas outside the caldera boundaries. However, larger lava flows with volumes similar to the ones in 1772 and 1670; or smaller flows erupted along the Northern edge of the ring fault, have a significant potential of reaching nearby populated centres.

Given the presence of several densely populated communities (Masaya, Nindiri, Ticuantepe, La Concepción, Masatepe) with ~500,000 inhabitants around these boundaries (which coincide with the administrative limits of Masaya Volcano National Park), this has obvious implications for hazard assessment studies in the area. However, there is a high probability that the most important threat that local communities in the area will continue to face in the short term is the persistent degassing coming from Santiago vent. Continuous release of pressure and energy through degassing and minor explosive activity at Masaya's open vents may decrease the likelihood of major explosive activity resuming.

It is also important to note that the rate of juvenile magma emission since the last Plinian eruption has dropped considerably. After the major explosive eruption 1800 years ago, lava flows have been erupted and covered the caldera floor entirely, building all the major volcanic centres existing today. However, of the 14.2 km^3 estimated erupted volume (Williams 1983) only a small portion has been erupted in recent times. For the last ~350 years, several lava lakes have formed on the bottom of the pit craters, and five gas emission crises responsible for the degassing of approximately 10 km^3 of basaltic magma have taken place since 1852 (Stoiber, Williams et al. 1986); but only two lava flows have been emitted over that period: one in 1670 with a surface of 2.12 km^2 and an estimated volume of $10.6x10^6$ m^3, and another in 1772 with a surface of 7.51 km^2 and an estimated volume of $22.5x10^6$ m^3 by Williams (1983). Possible reasons for this include the effective emptying of the magma chamber through the emission of lava flows during the first few centuries subsequent to the Plinian eruption, or continuous release of gas through Masaya's open vent (Santiago Crater). However, a combination of these phenomena is the most likely explanation. Longer observation periods will be required to determine if the downward movement of the inner lid is an important factor in keeping the cyclicity of eruptive periods active.

3.8.2 COFRADIAS FAULT AND RELATED STRUCTURES

3.8.2.1 Geometry

Being part of the Managua Graben, this deep seated fault is probably one of the primary factors for the development of the caldera. The expression of this fault on the caldera floor is noticeable in two different locations:

1) A NNE-SSW eruptive fissure that runs Northwards from San Fernando Crater and which seems to continue South of it (Figure 3-2, RV2), in the form of a similar rift valley with a considerable width (8-10 m) and several volcanic centres (spatter cones) distributed along it. However, the orientation of the section South of San Fernando (N-S) is almost parallel to the first section of the fracture described here, suggesting a correlation with a different branch of the rhomboidal pull-apart basin suggested by (Girard and van Wyk de Vries 2005).

2) The second family of fractures within the fissure field in the North part of the Caldera. The chaotic and young nature of the terrain complicates identification of fracture families here; however, the N-S running set is one of the clearest sets of fractures. From its orientation and position compared with the other sets, it is likely to be related to the graben-limiting Cofradias Fault (Williams 1983).

3.8.2.2 Relation to activity in time

The graben fracture is the source for the last recorded lava flow on the caldera floor (1772). Thus, we suggest that present volcanic activity in the caldera is favoured by the continued development of the pull-apart basin, and, in particular, with the extensional activity generated by the sinistral Cofradías Fault. At least two of the active fumarolic centres on the caldera floor (F4 and F5) are found along this fracture, suggesting its character as one of the main centres of activity within the caldera.

3.8.3 HYDROTHERMAL SYSTEM

Masaya's hydrothermal system has been well studied (MacNeil, Sanford et al. 2007; Mauri 2009; Mauri, Williams-Jones et al. 2010). It is probably structurally-controlled since all the active degassing manifestations can be found in places where important underground discontinuities are evident on the surface (F2-F3) or can be inferred from the structural survey (either being coincident with the ring fault, or with the rift valley that is the expression of the graben within the caldera, F1-F4-F5-F6-F7). The high degree of stability over more than 20 years of the fumarolic emissions in at least three of those sites (F1-F4-F7), supports the existence of a stable hydrothermal system on Masaya Caldera that exploits the lateral discontinuities provided by structures such as the ring fault. This results in the structural framework being a major factor in dissipating the excess heat and pressure generated by successive injections of magma to the shallower plumbing system of the caldera, which has kept the caldera in a steady state free of major eruptive activity for the last 240 years. This long term stability suggests also that the circulation of fluids themselves can be an important factor to keep this communication path open. The intermittent appearance of the other 4 emission sites (F2-F3-F5-F6) is a response to fluctuations in the hydrothermal system caused by rain fall and heat flux variations.

3.9 Conclusions

There are two main structural features controlling the stress regime in the area of Masaya Volcano: the inner caldera collapse, limited by the ring fault and a consequence of the emptying of the magma chamber after the last Plinian eruption (2 ka); and the extensional regime represented by the Cofradias fault, the Eastern limiting fault of the Managua graben.

The morphology and characteristics of the ring fault define it as a caldera-limiting fault in itself, so that Las Sierras-Masaya volcanic complex is composed of a series of nested calderas the smallest of which would be delimited by the ring fault within Masaya Caldera.

After all the evidence collected, we agree with (Crenshaw, Williams et al. 1982) in that no geophysical or geological evidence supports the hypothesis suggested by some researchers (J. Garayar, in Crenshaw et al. (1982)) of the caldera being generated by two overlapping circular collapses, cited as an explanation for the elongated shape of the caldera. However, it cannot be discarded since thick lava flows accumulated on that particular section of the caldera might have masked the evidence and made it undetectable by geophysical methods.

4 Combination of VLF and gravity techniques to study the shallow structural framework of Masaya volcano (Nicaragua)

NOTE: this Chapter is a manuscript about to be submitted to Geophysical Research Letters.Authors contributions:

- Guillermo Caravantes González is the main author, conceived the idea for the paper, carried out most of the acquisition, processing and interpretation work included in it, and prepared the manuscript.
- Jeffrey Zurek acquired and processed the gravity data, and built the Bouguer gravity map.

4.1 Abstract

A Bouguer anomaly map has been constructed for Masaya volcano summit area using 115 gravity stations. A strong positive anomaly centred on the Nindiri plateau suggests that after being degassed under Santiago Crater's presently active vent, magma may migrate towards the NE before being recycled at depth. A VLF tilt angle map has also been compiled in the area to provide information on the volcano's shallow structural framework. VLF tilt anomalies have been found associated with known fractures presently being used by the hydrothermal system as a path for fluids. The ability to observe the geometrical characteristics of these faults at depth provides some confidence that a correlation between VLF tilt response and fault geometry can be established.

The same two techniques have been employed together in order to study a lava tube system that can be accessed in the Southern slopes of Masaya pit crater area, and extends as far as Masaya Caldera's southern bounding fault. This lava tube system has similar characteristics to those found on Etna (Calvari and Pinkerton 1999). Both the gravity and VLF methods show strong anomalies associated with the suspected location of the lava tube system, revealing some of its characteristics. The strong negative gravity anomaly is interpreted in terms of the presence of void spaces within an

enclosing lava unit. The strong VLF anomaly is interpreted in terms of the lava tube system being used by the hydrothermal/groundwater systems as a path for fluids.

The use of the VLF and gravity geophysical techniques has proved suitable to study the structural framework of active volcanic areas. The combination of these two methodologies has shown strong potential for detecting and characterizing buried features with influence on the hydrothermal and eruptive activity, including incipient collapse structures, faults, rift valleys and lava tubes.

4.2 Introduction

Masaya Volcano (Figure 4-1), 635 meters above sea level, is a basaltic shield volcano located in Western Nicaragua composed of a nested group of calderas and volcanic cones (McBirney 1956; Rymer, van Wyk de Vries et al. 1998; Girard and van Wyk de Vries 2005; Harris 2009). Several pit craters (see Figure 4-1) crown the highest basaltic cones, including Masaya, Nindiri, San Pedro, and Santiago (currently active) craters. The term *Masaya Volcano* is often employed in the literature to define exclusively this summit and pit crater area.

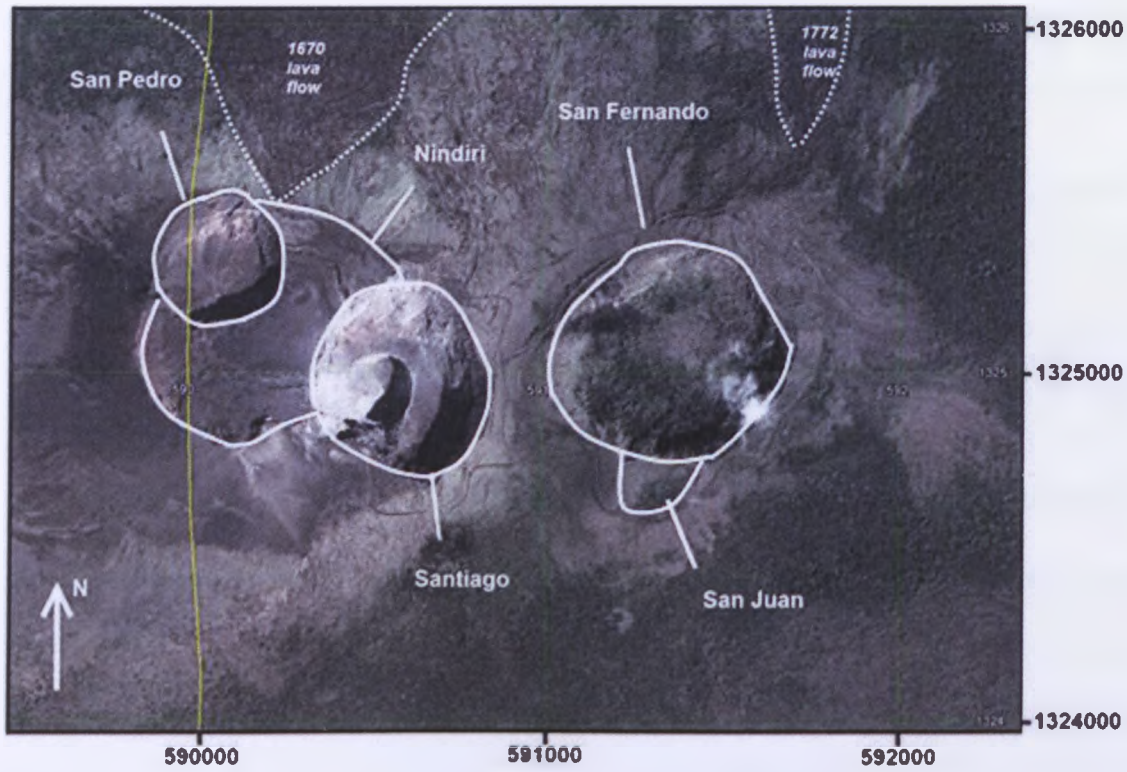

Figure 4-1: Pit craters and recent lava flows in Masaya summit area, Google Earth (2013).

The volcano emits an average of several hundred metric tonnes/day (t/d) of SO_2 (Rymer, van Wyk de Vries et al. 1998; Delmelle, Baxter et al. 1999; Nadeau and Williams-Jones 2009). The complex hosts a very active hydrothermal system (Duffell, Oppenheimer et al. 2003) with the highest quiescent water vapour output reported for a single volcano (Burton, Oppenheimer et al. 2000). At least 7 areas present gas emissions within the caldera floor. One of them, the active open vent (Santiago Crater) has emitted an estimated equivalent of the gas contained in ~10 km^3 of magma in the past 160 years (Stoiber, Williams et al. 1986), and is also the location for occasional strombolian eruptions. All these gas emissions combined pose a serious health hazard to local population living downwind of the active vent.

In addition to this, Masaya Volcano has been designated as a National Park by the Nicaraguan Government, attracting many visitors every year (including tourists, scientists and local media) and hosting a permanent team of 20-30 Park Rangers. The steadily increasing number of visitors has turned the otherwise low risk minor explosive and degassing activity into a volcanic hazard that has

to be analysed and understood, in order to provide valuable risk assessment information to local authorities and Masaya Volcano National Park Directors.

Masaya is a relatively well known volcano compared to others in Central America thanks to its conditions as a natural laboratory, easily accessible by road and with a relatively smooth terrain. Several morphological, geological and analogue modelling studies have provided very valuable information leading to a relatively well known eruptive history (especially for the summit area); and sketch models for the structures governing activity on the shallow region of the pit crater area have been developed based on that information (Rymer, van Wyk de Vries et al. 1998; Roche, van Wyk de Vries et al. 2001; Harris 2009). However, a geophysical study specifically aimed at uncovering the characteristics of the structural framework and its interaction with the magma plumbing and hydrothermal systems is still lacking for Masaya summit area.

The combination of the need for an improved knowledge of Masaya's structural framework influence on activity and the well-known local geology, make Masaya a perfect candidate to test and implement multi-technique geophysical studies capable of addressing unknown aspects of the shallow structure of the volcano, while assessing its validity as a method using some of the already well known geological structures as a Quality Control mechanism. In this article we employ a combination of Very Low Frequency (VLF), gravity and traditional geological techniques in order to test their combined potential as a methodology capable of detecting key structures in the upper part of volcanic edifices.

4.3 Methods

Two different geophysical methods have been used to acquire information on different physical parameters of the volcano.

[1] The gravity method relies on the difference in bulk density between different lithologies that cause variations in the measured gravitational field. This method is one of the most common in

volcano geophysics, due to its suitability to understand the subsuperficial structure of volcanic environments. Thus, the results of a gravity study are presented as contrasting subsurface density zones (Rymer and Brown 1986; Gudmundsson and Milsom 1997; Gottsmann, Camacho et al. 2008).

A Bouguer Anomaly gravimetric map was compiled using a Lacoste and Romberg relative gravity meter. Data from 115 gravity stations spaced an average of 50 m that cover most of the summit area of the volcano with a grid were collected, including several areas of difficult access restricted to the visitors of the National Park. A gravity profile with 26 more stations was collected on the caldera floor, south of the summit area until the caldera edge was reached, and then following that boundary towards the NW. Differential GPS was used to precisely define the position of the gravity readings collected, which is crucial to ensure low levels of error induced by incorrect height estimations, and other topographic effects when measuring gravity.

In the processing stage, 6 different corrections were applied to the data to avoid unwanted effects (see section 2.4.4). A latitude correction was applied to account for the non-spherical form of the Earth. A tidal correction removes the effect on gravity caused by celestial bodies, mainly the Sun and the Moon. A terrain correction is applied to remove the effect of different topographic configurations of the terrain around a gravity station on the gravity measurements. A drift correction solves the problem of gravimeter springs deforming over time. A free air correction accounts for the changes in elevation, and their effect on gravity, between the different gravity stations. A final correction called Bouguer correction generates an infinite horizontal slab of a given density to remove the effect of an increase or decrease of material at different elevations. The reduction density used for the Terrain and Bouguer corrections was 2.4 g/cm^3 (see Section 5.3.2. for further details) A unique value of correction density was used given the small dimensions of the survey area (less than 1x1 km).

[2] The VLF (EM) method is a relatively old technique e.g. (Collett and Becker 1968; Hoekstra, Sellmann et al. 1975; Klein and Lajoie 1980) that can be used to determine the location of sub-

vertical conductive zones in which the primary EM wave induces current flow. In this type of volcanic setting, water bearing structures are normally the main source of VLF anomalies over fractures filled with mineralization or clay. VLF transmitters asmilitary radio stations to communicate with submarines are the main source of EM waves. The waves propagate following the curvature of the Earth within a layer limited by the conductive surface of the Earth and the ionosphere D layer. These waves are reflected back and forth between both surfaces, travelling great distances this way with very little attenuation (Hunsucker and Hargreaves 2002). Due to their large wavelengths, VLF waves can travel through obstacles such as mountain ranges. The field radiated from a VLF transmitter over a uniform or horizontally layered Earth consists of a vertical electric field component and a horizontal magnetic field component, each perpendicular to the direction of propagation (McNeill and Labson 1991). Although the primary magnetic field is oriented horizontally and perpendicularly to its source, induced current flowing in fracture zones produces a secondary magnetic field that is out-of-phase with the primary magnetic field and is oriented in any direction (McNeill and Labson 1991). When this secondary magnetic field is added to the primary one, the resultant field becomes elliptically polarized, and a measurable (with a VLF detector) tilt anomaly is generated. The main factors controlling the VLF response to a buried conductive body are depth and conductivity. With increasing conductivity, the maximum amplitudes of the VLF response increase, and the same occurs with a reduction in depth (Paterson and Ronka 1971; Ward, Ryu et al. 1974).

The VLF method, scarcely used on volcanic locations to detect active lava tubes and cavities (Zablocki 1978; Zlotnicki, Vargemezis et al. 2006; Al-Oufi, Mustafa et al. 2008), is mainly used in mineral exploration to detect long, straight electrical conductors, such as faults or fractured systems filled with water or mineralized. The depth of exploration is limited by the conductivity of the medium, which means that in very conductive environments, the effective exploration depth is reduced. Given the comparable nature of the rocks close to the surface in Kilauea and Masaya volcanoes, relatively high resistivity values in the order of 10^4 Ωm are to be expected (Zablocki 1978). As a result, for a wave with a 18.6 kHz frequency (comparable to the frequencies emitted by

the transmitters employed in this study), the skin effect (or rate of attenuation in depth) would be approximately 370 m. The rate of attenuation with depth can be calculated from the square root of the ratio of the resistivity of the medium to the frequency of the incoming wave (Zablocki 1978). Since the effective depth of exploration is approximately one third of the skin depth (Zablocki 1978), a minimum depth of penetration of 100 m can be expected from the VLF data in this study.

A VLF-2 receiver manufactured by Phoenix Geophysics was employed for the acquisition of data. No important sources of noise were identified at the study site, mainly due to Masaya's status as a National Park, which makes industrial or other electrical activity almost non-existent in the area. Between March 2009 and January 2010 we collected 1552 measurements of tilt anomaly with 25 meters spacing (>38.8 line-kilometres). This resulted in a complete VLF anomaly map of Masaya's pit crater area. We also collected measurements to generate a profile of the Southern slopes of the edifice. Exploiting the characteristics of the device, we have tuned it to two sources of EM waves to collect data at every station. We have chosen transmitters (Table 1) that generate source fields approximately perpendicular to each other at the field site (~94.3°), what allows us to detect conductive bodies with different geometries and bearings. This is because the measured field decreases with increasing difference in orientation between the strike of conductors and the azimuth of the station until a maximum of 90 degrees is reached (Paterson and Ronka 1971). Another reason to do so is to ensure maximum coverage, since military stations may stop transmitting unexpectedly for maintenance or other purposes.

Code	Location	UTM Coordinates	Frequency	Distance	Heading	Channel
NPM	Lualualei, Hawaii	4Q, 587679, 2368910	21.4kHz	~7680km	~288.5°	F1
NAA	Cutler, Maine	19T, 639545, 4948170	17.8 kHz	~4044km	~22.87°	F2

Table 4-1: VLF transmitters employed in the study. Distance and heading are measured at Masaya volcano. F1, F2 are the two channels available in the Phoenix receiver.

4.4 Results

4.4.1 Summit area

A key area to understand Masaya's short and long-term behaviour, the summit area has been the source for most of the activity displayed by the volcano in the past 400 years.

4.4.1.1 Structure of the summit area

The summit area of Masaya Volcano is a complex one. It is pierced by several fractures that have been instrumental in accommodating the deformation undergone by this part of the volcano after the formation of 4 pit craters, several lava lakes, and a continuous history of deflation and inflation consequence of a very shallow magma chamber (Rymer, van Wyk de Vries et al. 1998; Harris 2009). The most prominent structural features noticeable today are the three main pit craters, namely San Pedro, the active Santiago, and San Fernando (Figure 4-1). The bottom of San Pedro and Santiago was deemed inaccessible due to the high instability of crater walls and risk of explosions in Santiago, and was therefore excluded from the study. Also prominent are the walls of the old Nindiri crater, which connect San Pedro (NW) and Santiago (SE) craters through two elevated ridges that constitute some of the highest elevations of the volcanic edifice (Figure 4-2). Inside these walls we find an inner circumferential crack about 100m inside the crater rim caused by subsidence of materials from Nindiri lava lake, mostly emitted in 1670 (Rymer, van Wyk de Vries et al. 1998; Harris 2009). Both the Nindiri Crater Walls and the inner circumferential crack are suspected to have acted as host to the hydrothermal system, with fumarolic emissions detected intermittently (but infrequently) along their outline (see Chapter 3, this thesis). West of San Pedro crater, there is also a major feature in the form of a rift valley (up to 15m deep) coincident with the outline of a ring fault that crosses the

caldera floor (see Chapter 3). San Pedro Rift Valley has been the source for fissural eruptions in the past and has also been host of hydrothermal manifestations until recently (see Chapter 3).

All these features share three important characteristics: a) they are structurally meaningful for the geological history of the volcano, b) they host or have hosted manifestations of the hydrothermal system, and c) all of them are highly visible and recognizable on the walls of San Pedro or Santiago craters, which means that we have precise information on their geometry in depth. These make them ideal candidates to test the response of VLF and gravity methods that have the capability to detect or provide information of such features in depth.

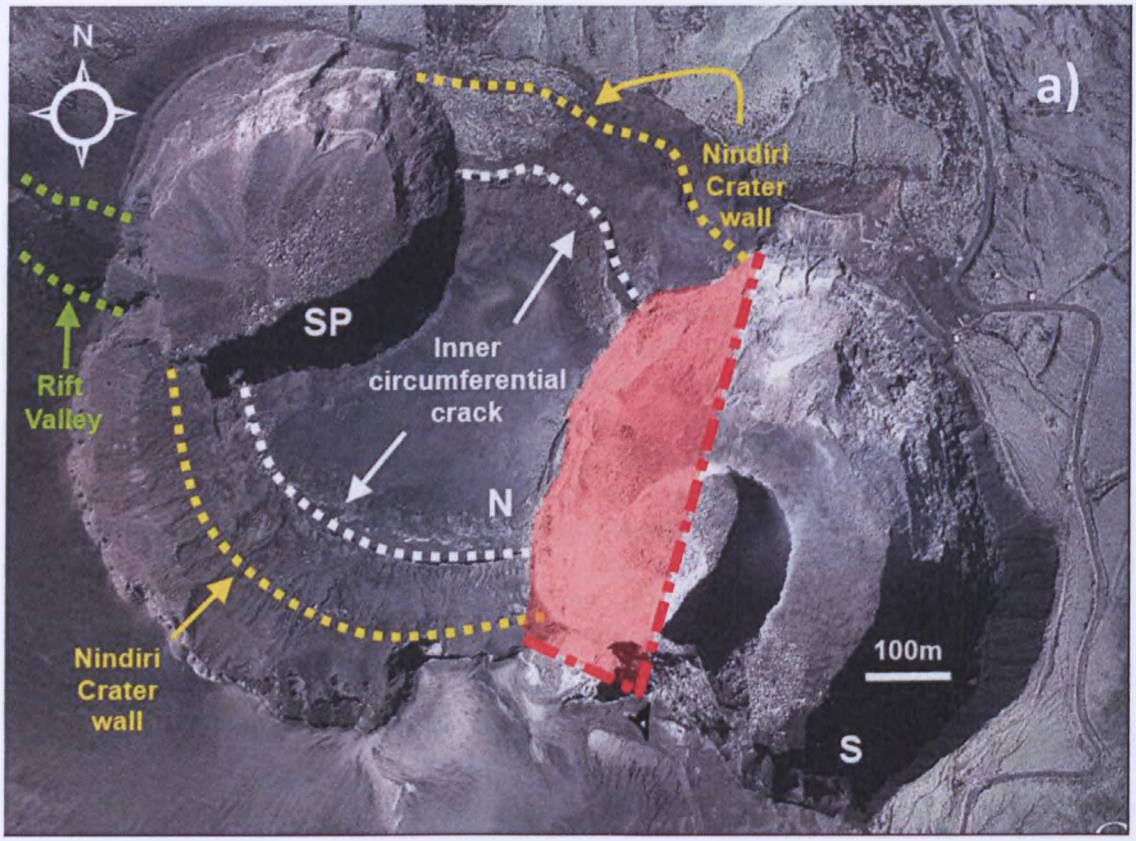

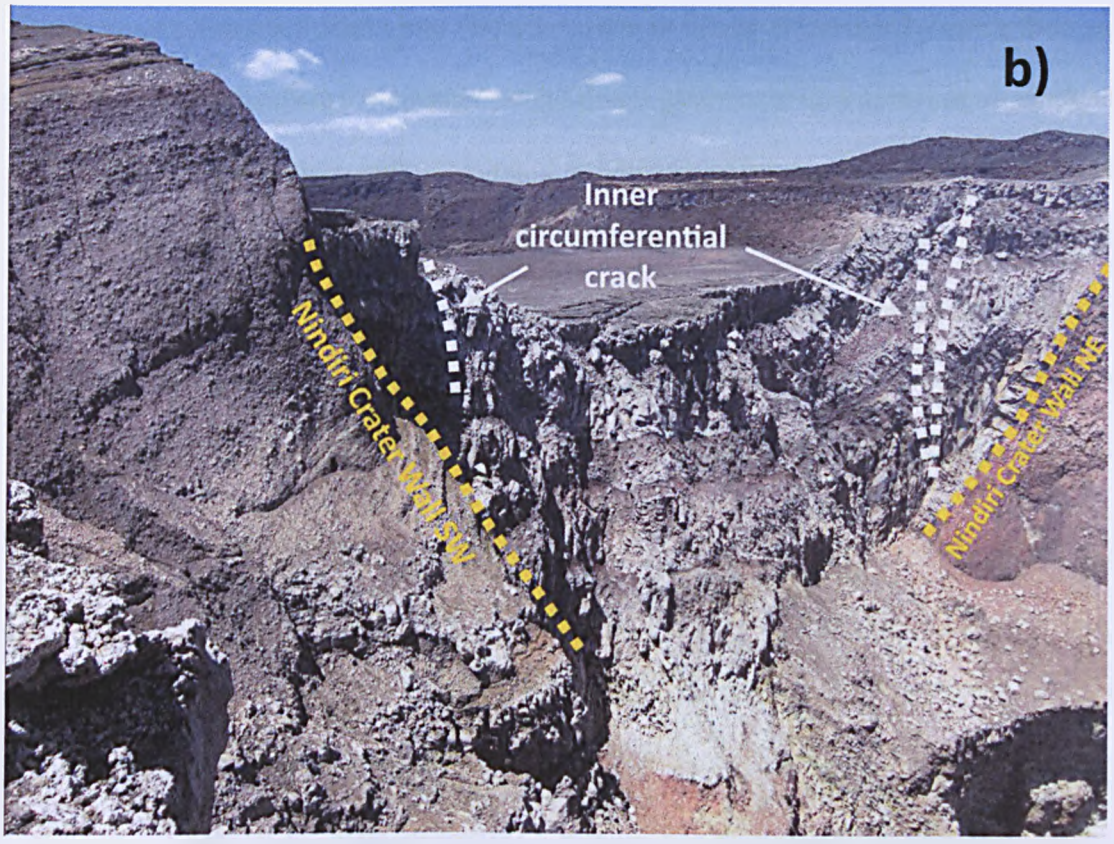

Figure 4-2: a) From Northwest to Southeast, Masaya Volcano's San Pedro (SP), Nindiri (N) and Santiago (S) pit craters (Google Earth). Dotted lines (white, yellow, green) represent the main structures intersecting the surface in the area, and discontinuous red lines indicate the field of vision seen in Figure 4-2b with an eye symbol at the observation point (old car park, South of Santiago crater). b) Lateral view of the fractures on the northwestern wall of Santiago. The inner circumferential crack and the Nindiri Crater wall are the main structural weaknesses visible on the crater wall, but their role as an effective host for the hydrothermal system has not been discussed before.

4.4.1.2 Gravity survey of the summit area

A Bouguer anomaly map has been generated (Figure 4-3) using data collected in January-March 2009 (Appendix D). The overall error for each data point is always less than 0.1 mGal (Zurek 2010). A relative gravity high centered in Nindiri Plateau dominates the signal in the area, with every other gravity feature in the map significantly subordinated to it. Several of the stations south of the map are located at similar elevations to some of the stations at Nindiri crater's bottom, yielding much lower gravity values consistent with the general trend in the area. This supports the existence of a geologically-generated gravity anomaly in the area unrelated to topography, and dissociates its existence from the presence of faulting and other structural features, or the sharp drops in altitude associated with the inner circumferential crack (whose shape would seem related to the gravity

contours on the map). The trend of decrease in gravity values away from the positive anomaly and the little general correlation with topography is also a good indication of the gravity anomalies being caused by real geological features. The size of the anomaly is also constrained by some of the stations to the NW and SE of it (located also on Nindiri floor, same altitude as the stations over the positive anomaly). Those closest to Santiago Crater (SE of the Nindiri anomaly) indicate that the gravity values decrease in that direction, suggesting lower values on and around Santiago Vent, which are consistent with the stations recorded across the crater (on the SE side of Santiago Crater).

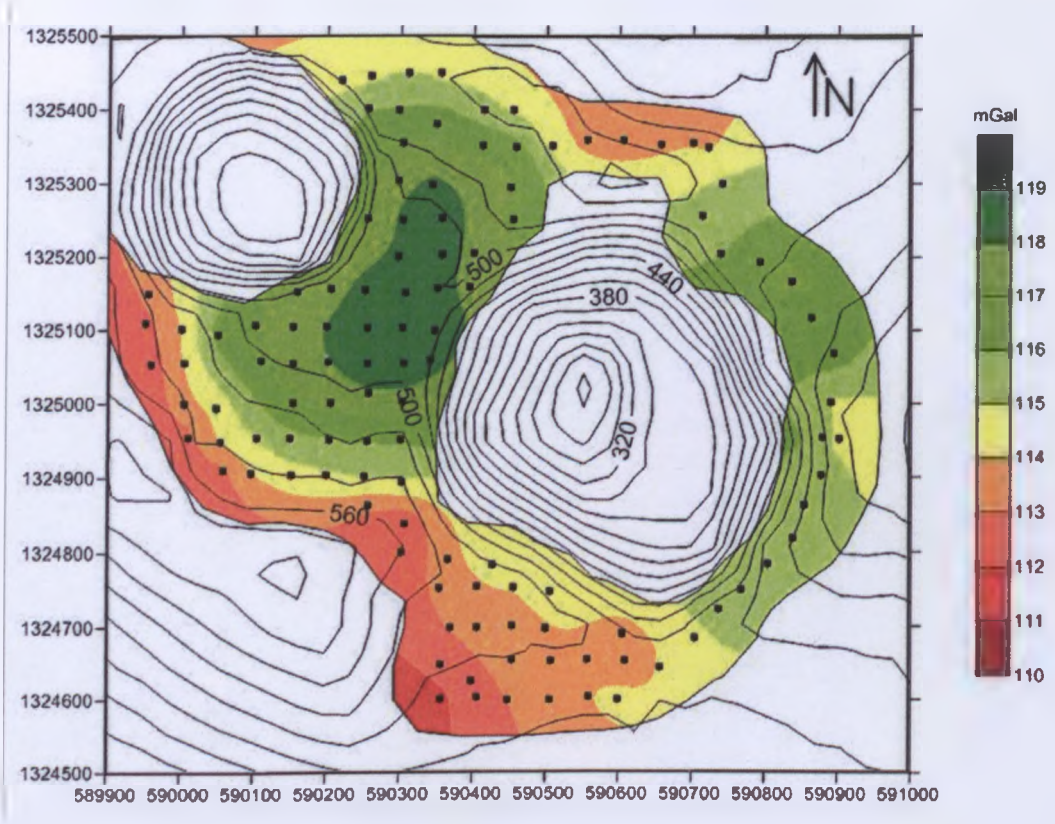

Figure 4-3: Bouguer anomaly map. The contours (black lines) correspond to topography and represent 20 m intervals. The software used to perform the gridding was Surfer 10.1.561., which uses a bilinear interpolation method to calculate Z values at points that do not coincide with grid nodes.

4.4.1.3 VLF survey of the summit area

Two maps have been generated using the VLF data collected on Masaya (Figure **4-4b**) in January-March 2009 (Appendix E). The first map corresponds to the data gathered with channel F1 (that was tuned to detect VLF waves produced by the NPM VLF transmitter in Lualualei, Hawaii, USA), and the second to data generated with channel F2 (NAA VLF transmitter in Cutler, Maine, USA). For more

details on the VLF transmitters, see Table 4-1. Due to the geometry of the conductive bodies in depth, the map generated using the tilt angle values of channel F1 (Hawaii) seems to have been more effective in providing information of the inner structure of the volcanic edifice, while F2 (Maine) has had more success in revealing structures outside the pit crater area). Positive or negative values in tilt angle (far from 0) both have a similar geophysical meaning, indicating higher values of conductivity underneath for higher absolute values in tilt angle. However, different signs can provide information on geometry of conductors at depth.

a) F1: At least 4 major conductive anomalous areas have been singled out in the F1 map (Figure **4-4b-F1**), with opposite tilt angle values and a WNW-ESE direction. The values range from +30 to -22 degrees. A section of data could not be collected using this channel around Masaya crater, due to antenna maintenance operations conducted in the VLF transmitter located in Lualualei, Hawaii (USA).

b) F2: In the map generated using the F2 values (Figure **4-4b-F2**); two main features are worth mentioning. In the West part of the map, a strong negative anomaly is associated with the San Pedro Rift Valley (Figure **4-2a**). The other one, a positive anomaly located in the South part of Figure 4-4b-F2 is located in the intersection between the adjacent (to the West) slope and the plain directly south of Santiago crater. The values range from +25 to -22 degrees.

c) F1 and F2: Both channels (F1 and F2) show very small amplitudes in the VLF response (values near 0) on the crater rim around Masaya cone (easternmost crater on Figure 4-4b). Given the characteristics of the terrain in this area, with sharp changes in topography of up to 180 m in a horizontal space of less than 50 m and in all possible spatial orientations, it seems that the topographic effect has very little influence on the VLF response of both channels, with conductivity being the main reason for the generation of anomalies.

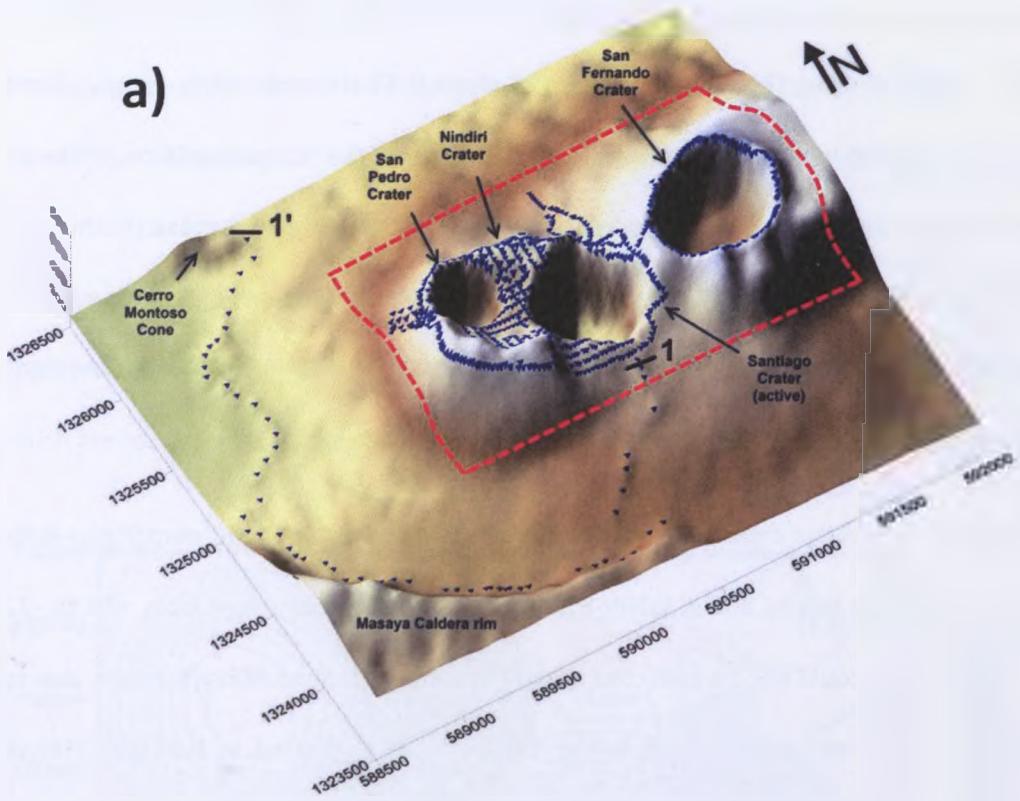
a)
N
San Fernando Crater
Nindiri Crater
San Pedro Crater
1'
1
Cerro Montoso Cone
Santiago Crater (active)
Masaya Caldera rim
1326500
1326000
1325500
1325000
1324500
1324000
1323500
588500
589000
589500
590000
590500
591000

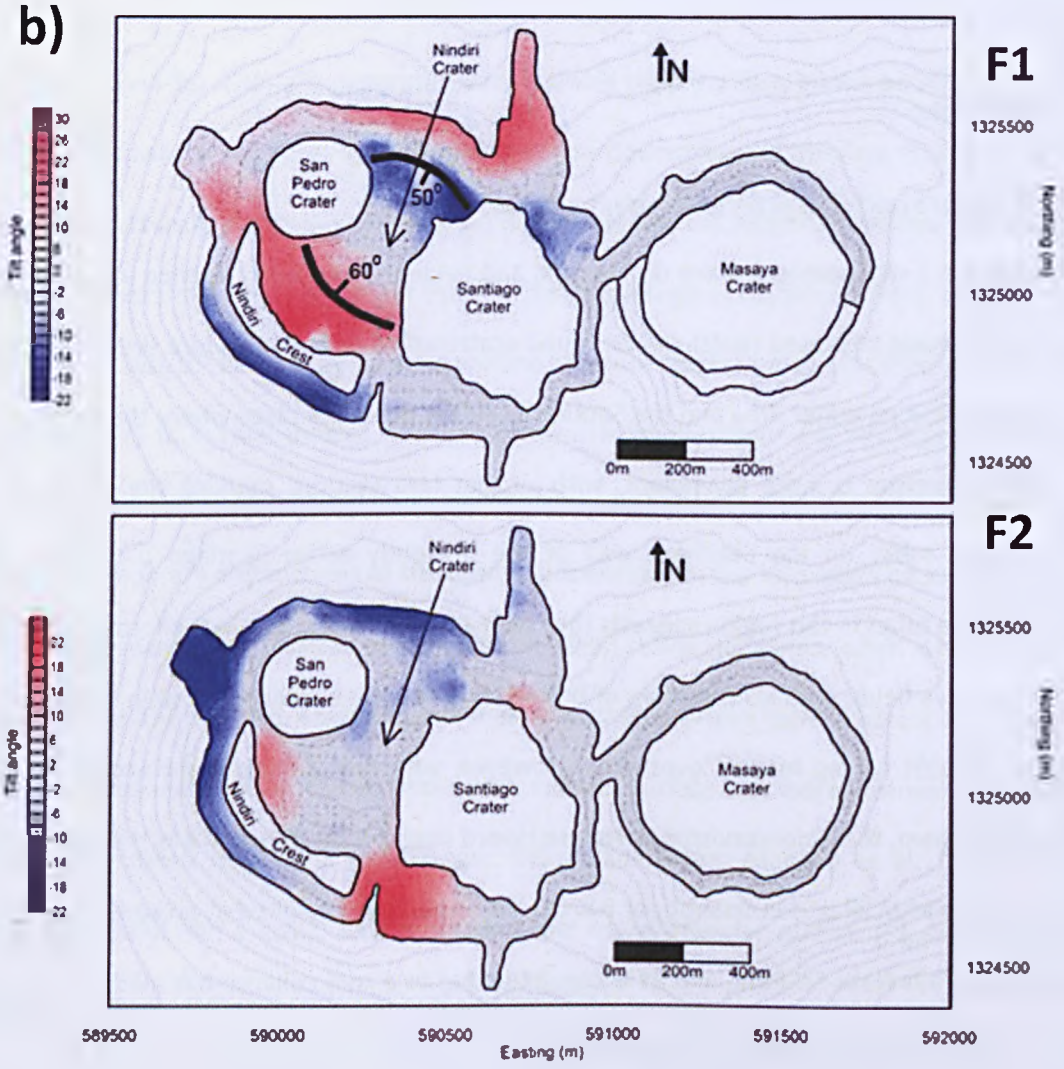

Figure 4-4: a) location of VLF stations measured for this study. The summit area is shown by a red dashed line and 1-1' marks the location of the VLF profile discussed in 3.2.c) (note: not all VLF stations collected for the profile are shown here). b) The maps show the VLF response in tilt angle mode for two perpendicular VLF channels (F1 and F2) that reveal different aspects of Masaya's summit structural framework.

GEOLOGY	**Nindiri Crater Wall SW**	**Nindiri Crater Wall NE**
Fault orientation (strike)	115°	120°
Dip angle (maximum)	≈60°NE	≈50°SW
VLF RESPONSE	**VLF Anomaly SW**	**VLF Anomaly NE**
Longest axis orientation	115°	115°
VLF Tilt Angle (maximum)	+24°	-20°

Table 4-2: Correlation between VLF anomalies and geological structures. The amplitude (tilt angle) of the signal and its orientation are proportional and can be correlated to the geometry of the faults.

4.4.2 Lava tubes

4.4.2.1 Structure and characteristics of lava tubes

Lava tubes are a widespread feature on Masaya, and evidence for their presence (mainly in the form of post-drainage collapsed roofs) can be found scattered all over the caldera floor. The slope located between the pit crater area and the Southern caldera rim is the place where the occurrence of this volcanic feature is more prominent, with circular lava sections marking the presence of several of those tubes on the Southern wall of the presently active Santiago pit crater. The abundance of lava tubes in this region suggests they have played a major role in the formation of the South and East lava fields, with 3D networks of braided lava tunnels similar to those in Etna (Calvari and Pinkerton 1999) having formed over time. However, very few tunnels grant access to their interior. One of them, the *Xinancanostoc* (a Nahuatl word that can be translated as the also locally used Cueva de los Murciélagos in Spanish, or Bat Cave in English), is exploited at present as a tourist attraction by Masaya National Park, and its accessibility due to a roof collapse has made it possible to improve our understanding of the features and characteristics of basaltic lava tunnels at Masaya.

There are several structures of interest that can provide information on the formation and processes undergone within a lava tube. This lava tunnel, just over two hundred metres long (202 m) of practicable exploratory length (Figure 4-5a) is a compound tunnel with 2 noticeable intersections with other lava tubes/flows. From these, one converges with the cave from the NE at the 50 metres mark from the entrance, and the other one coalesces also from the NE 5 meters north of the vent located near the midpoint of the tunnel. The size of the tunnel ranges from the 2x1.7 m width and height (respectively) of the entrance (even less in the last section at the end of the tunnel), to the 7/8 m high and 10 m wide of the area below the midpoint vent. Lateral benches (Figure 4-5b) are a common feature in the first 90 m of the tunnel, before reaching the first vent, indicating a stable lava level for a period of time (Calvari and Pinkerton 1999). Temporary vents are a characteristic

feature of lava tunnels, and sometimes can be recognized inside the tunnel (Figure 4-5c) and on the surface (Figure 4-5e). They are generated after a stable supply of lava allows an inflation front to be developed; finally resulting in a secondary eruption downstream if the lava flow is continuous in time. If a structurally stable roof (Figure 4-5e) is generated by the eruption, the lava flow can progress downslope and drain the space under the vent, leaving a large cavity (Figure 4-5e). The roof collapses that allow access to the lava tunnel are a common feature and take place at different scales, from <1 m (Figure 4-5d) to several metres. Multiple concentric layers (Figure 4-5f and Figure 4-5g) mark the occurrence of cycles of infilling/emptying of the tunnel that can be caused by several reasons, including temporary obstructions of the tunnel, fluctuations in the lava emission rate from the vent, tunnel coalescence, etc. (Calvari and Pinkerton 1999). Lava stalactites, often with native sulphur deposition at the tip, are a widespread feature within the lava tube (Figure 4-5h). Their shapes alternate between a group of stalactites with smooth surface and edges formed by remelting by gases accumulated below the roof (Jaggar 1931; Kauahikaua, Mangan et al. 1996; Calvari and Pinkerton 1999), and a group with a rougher and more irregular surface (Figure 4-5h) caused by dripping of crystal-rich lava from the roof (Jaggar 1931).

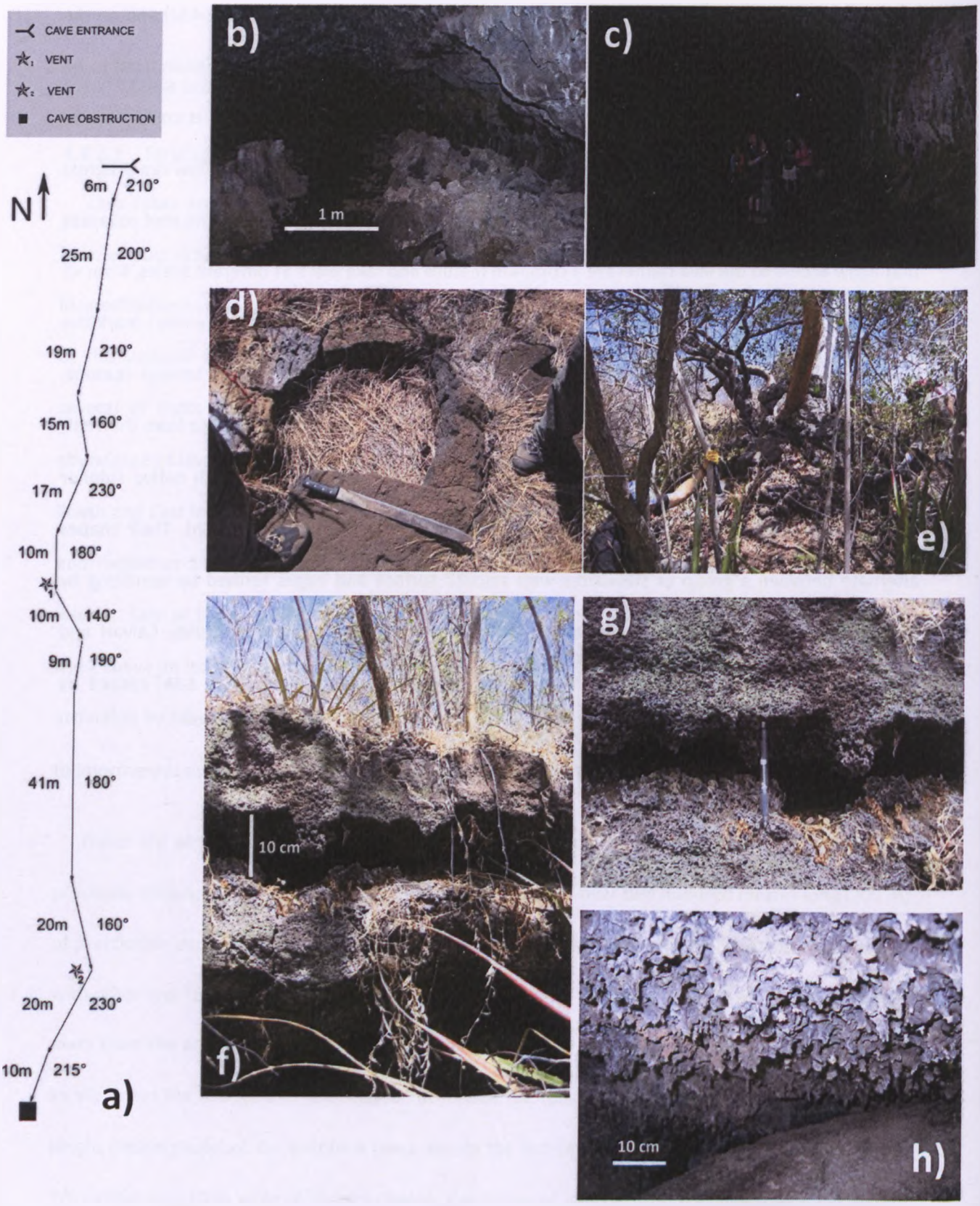

Figure 4-5: a) Lava tube outline. GPS position for Cave entrance (16P 0590616/1324363, 480masl) and Vent 1 (16P 0590580/1324293, 458masl) was recorded using a handheld GPS, b) example of the lava tube section showing signs of thermal erosion c) cave opening corresponding to Vent 1, d) Mini-collapse morphologically analogous to bigger scale cave openings, e) superficial expression of cave

opening/vent, f) double roof formed after cooling, acting as an effective insulator for the running lava underneath, g) porous structure of basaltic rock near a cooling surface, h) stalactites formed by dripping of crystal-rich lava.

4.4.2.2 Gravity profile on the South slope

Gravity data from 26 stations (Appendix F) spaced an average of 82m were collected in February-March 2010 on the South slope of the volcanic edifice (within caldera boundaries) using one of Masaya National Park trails that runs sub-parallel and to the East of the Xinancanostoc (see Figure 4-6). The values of gravity (data points displayed in the upper part of Figure 4-7 and labelled *Observed*) are relative to a base station located near Masaya's visitor centre (12°00'02.64706"N, 86°09'03.62968"W) within Masaya Caldera. The superficial evidence for the presence of lava tubes in the Southern slopes (including lava roof collapses and presence of mini-vents) are not limited to the surroundings of the Xinancanostoc, but extend further South until the caldera boundary is reached. At that particular point, the trail used to collect gravity data intersects these inferred lava tube sections, and a strong negative gravity anomaly is observed. To understand the cause of this negative gravity anomaly, a 2D model (Figure 4-7) that includes all the geological constraints known has been generated using Geosoft GM-SYS gravity modelling software and density values from Metaxian (1994). The thickness of the units has been assigned using approximate values from superficial units visible in cross section in other locations within the caldera.

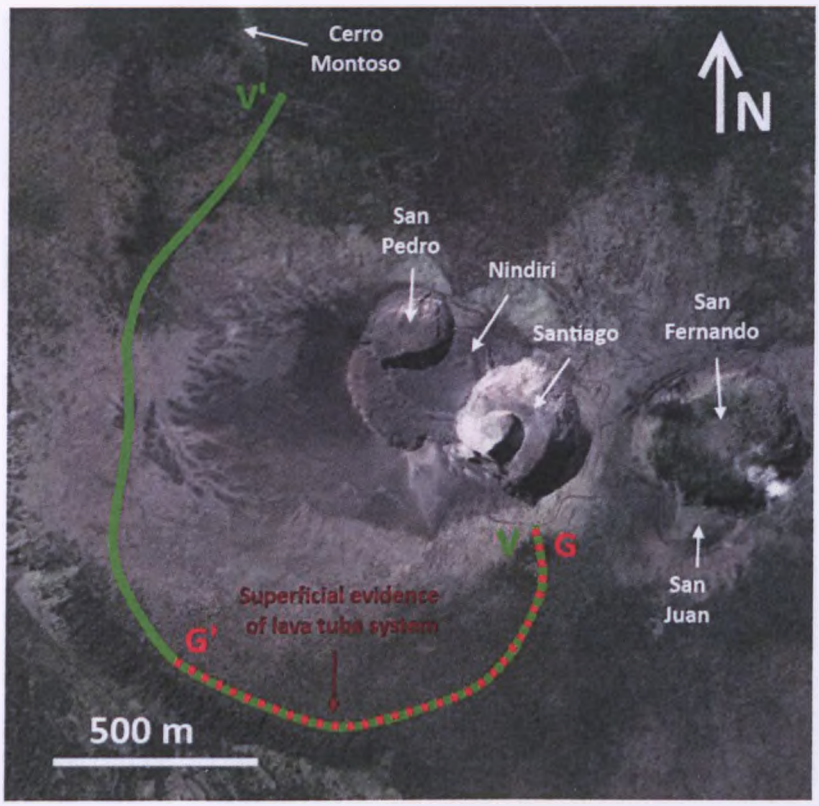

Figure 4-6: Location of gravity (G-G') and VLF (V-V') profiles on the caldera floor. The profiles are non-straight because they were collected along an established path part of Masaya National Park's trail network. This network was used to collect multiple Bouguer gravity profiles and generate a Bouguer Anomaly map (see Section 5.3.2).

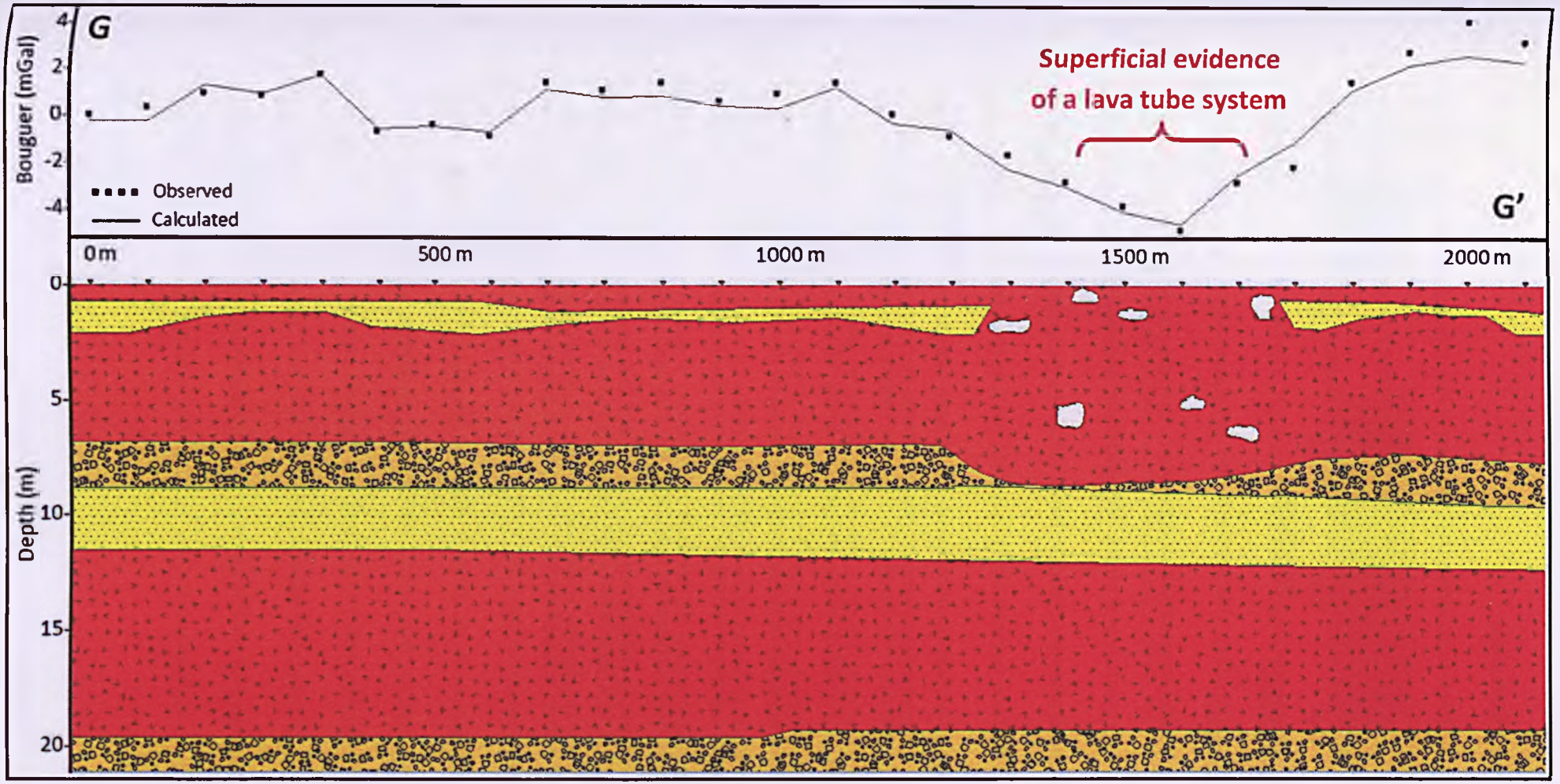

Figure 4-7: Observed gravity matches calculated gravity for a 2D geological model that includes a thick lava package with void spaces. The relative negative Bouguer gravity anomaly coincides in space with superficial evidence for the presence of a lava tube system. Parameters used: Fine pyroclastics (light yellow) = 2.1 kg/m^3, coarse pyroclastics (dark yellow) = 2.2 g/cm^3, basaltic lava flow (red) = 2.6 g/cm^3.

4.4.2.3 VLF profile on the South slope

A VLF profile originally designed to establish the influence of the topographic effect on the VLF values has been collected (Figure 4-6). A total of 112 stations spaced an average of 50 m were collected in January 2011. The data were gathered using the F1 channel (Hawaii transmitter, USA, Table 4-1) also used to compile the VLF map shown in section 3.1.3., and then processed using Khffilt software version 1.1A (Pirttijarvi 2004). This software uses the Karous-Hjelt method (Karous and Hjelt 1977; Karous and Hjelt 1983) to generate an apparent current density section (Figure 4-8). The most noticeable feature in the section is a strong pseudocurrent anomaly zone located near the 1000 m mark. The rest of the profile runs through similar terrain to the gravity profile shown in the previous section. To the left of the anomaly in Figure 4-8 we see a section that corresponds to the South slope, where relatively constant pseudocurrent values have been found. To the right of the anomaly in Figure 4-8 the profile runs NW parallel to the outer caldera bounding fault for 2km, and then separates from it and runs in NE direction towards the center of the caldera. The changes in pseudocurrent for this section are again obscured by the strong signal displayed in the anomaly area, but more contrasts appear as we move further NE, where a ring fault structure has been defined (see Chapter 3). The anomaly area corresponds again with the intersection between the VLF profile and the lava tube system that runs downslope from the summit area. It shows a sharp anomaly of tilt angle values (that translate in a pseudocurrent anomaly) in a short section near the southern edge of the caldera.

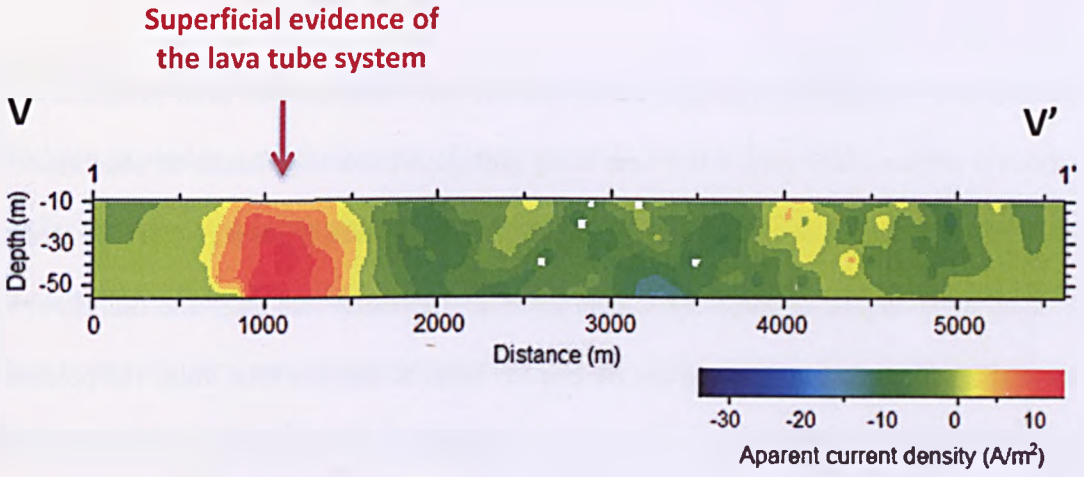

Figure 4-8: Karous-Hjelt filtered current density pseudo-section shows. For the location of the profile, see profile V-V' in Figure 4-6 or profile 1-1' in Figure 4-4a.

4.5 Discussion

4.5.1 Summit area

A possible explanation for the positive gravity anomaly centred on Nindiri Plateau (Figure 4-3) can be inferred from the nearby presence of Santiago Vent (SE of Nindiri, Figure 4-1), which hosts a periodically visible lava lake that is the superficial expression of a gas-rich magma conduit in depth (Rymer, van Wyk de Vries et al. 1998). The magma, after having ascended through the conduit and degassed close to the surface, is compelled to abandon the lava-atmosphere interphase zone due to its relative loss of buoyancy and has to find accommodation within or underneath the volcanic edifice. This positive gravity anomaly suggests that below the Nindiri frozen lava lake there might be an accumulation zone for material derived from the vent, or an evacuation area where degassed magma heads first prior to sinking in depth towards an accumulation zone. No sharp gravity anomalies were found associated with Nindiri Crater wall or the inner circumferential crack, confirming (as can be seen on Santiago and San Pedro crater walls) that these faults do not mark sharp changes in lithology; and that the 1670 intrusive dikes that according to Harris (2009) are emplaced along Nindiri Crater walls do not possess a sufficient density contrast with the surrounding materials to be singled out in a gravity map, and are completely obscured by Nindiri's positive gravity anomaly.

Regarding VLF, the opposite values in tilt for the two internal anomalies seen using channel F1 (Figure **4-4b-F1**) can be interpreted in this case using geological knowledge based on observations of Santiago crater walls. In Figure **4-2b** we can see that Nindiri crater wall forms a graben-type structure with limiting faults dipping towards the middle point of the frozen lava lake, and therefore, with opposite dip directions for the fault on the NE and SW sides of the lava lake. Thus, the positive vs. negative tilt angle values in the inner 2 anomalies are a consequence of the geometry of these faults in depth. In Table **4-2** there is a direct comparison between the geometry of these faults and the characteristics of the VLF response. This comparison shows that the longest axis of faults and associated VLF anomalies show a similar orientation; and the dip angles of the faults are proportional to the VLF tilt angle values of the associated VLF anomalies, with opposite signs that can be correlated with opposite dip directions in the faults. The fact that the anomalies yield strong conductivity values (proportional to tilt angle) also suggests that fluids and therefore the hydrothermal system actively use these opposite dipping faults as a path. The strong negative anomaly associated with the San Pedro Rift Valley using channel F2 (easternmost point of Figure **4-2b-F2**) confirms that this structure is an active host of the hydrothermal system, which has also been confirmed by recent findings of anomalous temperatures and native sulfur on its walls (Chapter 3). The other anomaly using channel F2, a positive anomaly located South of Santiago Crater and East of Nindiri Crest in Figure **4-2b-F2,** indicates a possible buried structure in the area occupied by the hydrothermal system, with an orientation close to N-S (as indicated by the orientation of NAA transmitter from Nicaragua).

4.5.2 Lava tube system

The presence of a short wavelength negative gravity anomaly in the upper part of Figure 4-7 suggests an important change in subsuperficial density at this point. From a geological standpoint, a significant lithological contrast caused by the presence of Masaya caldera's external fault, acting as a boundary between the external materials and the internal ones (that also include all the lava flows generated after the last Plinian eruption, see Chapter 3) is possible and might have an effect on

gravity values. However, the fact that all the gravity stations to the NW (end part of the gravity profile) are located in a similar geological context (i.e. in the vicinities of the caldera boundary, and at similar altitudes as the stations that show the gravity low) and yield gravity values similar to those to the left of the anomaly, indicate that neither a density contrast derived from the presence of the caldera boundary nor a topographic effect are accountable for the drop in gravity values. The most feasible explanation, given the close match between the presence of superficial evidence for the lava tube structures and the negative gravity anomaly can be found in the 2D model built as part of Figure 4-7. The existence of a thicker lava unit with cavities significantly lowering the mean density of the geological package in the area (and probably a well-developed network of collapse-related fractures connecting the voids) generates a calculated gravity signal that matches the observed data in the area. The presence of the voids and probable fractures creates a permeable geological unit with the potential to act as a path for the hydrothermal/groundwater systems. This is also supported by the fact that in the same location of the negative gravity anomaly, a strong pseudocurrent area has been found in the VLF profile (Figure 4-8), reinforcing the idea that the subsuperficial fractures and voids in this section of the profile are filled by the hydrothermal/groundwater systems.

4.6 Conclusions

4.6.1 Masaya cone structural framework

A very active hydrothermal system occupies the upper zone of Masaya cone. In this part of the volcano, the most conspicuous fractures are being used by the hydrothermal system to release energy, as evidenced by the high VLF tilt angle values over the faults in the area. The close proximity of the energy source (incandescence visible within Santiago crater, a mere 200m below) and intermittent sightings over the last 20 years of fumaroles emerging from the fractures in Nindiri crater (Rymer H., personal communication) means it is likely that this system to release energy has been sustained in time. In addition to these faults related to Nindiri crater wall, a strong VLF anomaly indicative of a highly active hydrothermal system has been found in the proximity of San

Pedro Rift Valley (source of fissural eruptions in the past); and a VLF anomaly South of Santiago crater marks the presence of a previously unknown fault in the summit area. The main feature highlighted by the gravity study in the summit area is a strong positive gravity anomaly centered in Nindiri Plateau (Figure 4-3). Given its location, this anomaly is almost certainly related to the magma plumbing system, with degassed and therefore denser magma probably migrating under Nindiri frozen lava lake after being displaced from the lava-atmosphere interface by more buoyant gas-rich magma fed by the conduit. Rymer et al. (1998) suggested values of 2700 kg m^{-3} for denser, degassed magma bodies and 100 to 600 kg m^{-3} less for vesiculated magma bodies underneath Santiago. This is consistent with the trends observed in our gravity data, which show a gradual decrease in the gravity values towards Santiago's crater.

Regarding the lava tube system, the lack of mass pointed out by the gravity profile suggests that several lava tubes have coalesced in a particular section of the Southern slope, building a complex structure in which some tubes are superimposed on others, and some are independent for some part but then coalesce with others through roof collapse or wall melting, as can be seen in the Xinancanostoc.

Geological evidence suggests that there is a well-developed lava tube system on the Southern slope of Masaya volcanic cone. This system runs S-SW from Santiago crater for approximately 900 meters, and then turns left towards the lake (E-SE) after having encountered the Caldera wall. Roof collapses can still be seen to the SE of the intersection between this postulated lava tube system and the caldera wall. Their track is then lost or buried by sediments and/or other lava flows after a few tens of meters.

The fact that the lava tube system shows such high pseudocurrent values is surprising, since voids theoretically have infinite resistivity and should therefore produce very low values in pseudocurrent. Since the water table is reportedly >200 m below the surface in this area (MacNeil 2006; MacNeil, Sanford et al. 2007; Mauri, Williams-Jones et al. 2010), the most likely explanation for the values we

see here is a lava tube system partially filled by the hydrothermal system, which actively uses it as a path for fluids. The lava caves may also contain some mineralization in part responsible for the VLF response. Secondary mineral assemblages such as silica, sulfate, and hematite have been found in basaltic lava tubes on Earth and are being analyzed as potential Martian analogues (Ruffini 2011). However, the dynamics of this hydrothermally occupied zone are yet to be determined. The hydrothermal fluids could have emerged from depth powered by the volcano's heat and ascend using the caldera wall as a connection to the surface, or this could also reflect the upper part of a hydrothermal cell that transfers heat upwards (Mauri, Williams-Jones et al. 2010; Mauri, Williams-Jones et al. 2012).

4.6.2 Gravity/VLF method

The positive tilt angle areas recorded by VLF channel F1 seem to match well the superficial expression of the Nindiri wall (Rymer, van Wyk de Vries et al. 1998), later used by the 1670 dike (Harris 2009) as a path. A comparison of electrically conductive zones revealed by VLF and the structural features underlying detected has allowed us to correlate and correctly interpret the cause for the generation of the aforementioned electromagnetic anomalies, and also to understand the relationship between VLF tilt angle and sub-superficial geometrical characteristics of faults (mainly strike, dip direction and dip angle). After firmly establishing a correlation between these two elements, extrapolations of geometry of conductive bodies in depth to other parts of the volcano can be assumed. From the map we can also see that in this case the topographic effects are negligible, since the VLF tilt angle is completely uninfluenced by the presence of the craters (Nissen 1986), which possess infinite resistivity. Therefore, the VLF method has the potential to become a key tool to understand active volcanoes' structural frameworks when the areas of interest are accessible and the level of risk is acceptable.

In combination with gravity, important structures as the lava tube system on the Southern slope can also be revealed. The almost perfect coincidence of the gravity and VLF anomalies with the

section of the trail that crosses the lava tube system is remarkable. Another argument to support the validity of a combined VLF/gravity method as a powerful tool to study structural framework of active volcanoes is the fact that the wave characteristics of both the gravity and VLF anomalies when they cross the lava tube system are comparable. The wavelength is in the range of 0.5km using both methods, and the relative amplitude is also comparable. This suggests a comparable depth for the source of the VLF and Bouguer gravity anomalies. These arguments show how different characteristics of geological constructs as lava tubes used by the hydrothermal system are detectable by both methods and that combining them can be very effective to resolve ambiguities. The use of this geophysical technique can provide very accurate information on size, depth, shape and geometry (inclination, tilt direction) of buried geological structures that generate both density and conductivity contrasts with the surrounding materials. For developing countries rich in geothermal resources like Nicaragua, this fast and cost effective technique has the potential to become an important exploration tool for local authorities/exploration companies.

5 Gravity study of Masaya Caldera

NOTE: this Chapter is a manuscript about to be submitted to Journal of Volcanology and Geothermal Research.

Authors contributions:

- Guillermo Caravantes González is the main author, conceived the idea for the paper, carried out most of the acquisition, processing and interpretation work included in it, and prepared the manuscript.
- Hazel Rymer helped conceived the idea and acquired all microgravity data.

5.1 Abstract

A gravity study involving Bouguer anomaly and microgravity techniques has been completed for Masaya Caldera and its surroundings. A Bouguer anomaly map has been compiled using data from 477 stations collected on the caldera floor and on areas adjacent to the caldera. Satellite gravity data have also been analysed to check the validity of the gravity models developed for the land survey. Bouguer anomaly data confirm a large positive anomaly already discovered by Connor and Williams (1989) and Metaxian (1994), corresponding to a large intrusion to the NE of the caldera. The location of the intrusion has been refined using more precise data positioning techniques, and 2D models have been built to test the validity of the physical characteristics of the intrusion proposed by Metaxian (1994). The results suggest a smaller or deeper intrusion as the source for the positive gravity anomaly than proposed by Metaxian(1994). Bandpass filters have been applied to remove the signal generated by this intrusion, revealing the presence of another intrusion, an elongated magma chamber coincident with the SW section of the ring fault within Masaya Caldera. Microgravity data have also been collected in Masaya's summit area providing information on the dynamics and evolution of the magma plumbing system. Three main types of processes have been identified for the summit area using the analysis of the spatial and temporal variations of gravity.

Short-term temporal changes are identified as annual variations in the gravity values at individual stations that can be caused by relatively shallow processes such as cavern filling, magma withdrawal, roof collapse, variations in the layer of vesiculated gas-rich magma, etc. Mid-term changes are 2-5 year coherent increases or decreases of gravity values throughout the summit area probably caused by magma injections-withdrawals or progressive degassing of vesiculated layers injected periodically. Long-term variations of the gravity signal occur with >10 year periodicity. These might be caused by overturns at depth of recharged gas-rich magma that rises buoyantly, generating new temperature and density contrasts in the shallow part of the plumbing system, and favouring the renovation or generation of new small convection cells (Rymer, van Wyk de Vries et al. 1998; Williams-Jones, Rymer et al. 2003; Stix 2007).

5.2 Introduction

Gravity studies provide information on the density distribution in depth, which makes them a particularly useful tool for active volcanic environments where lateral changes of physical properties are common as a result of the co-existence of materials with different densities, thermal states, etc. (e.g. magma batches, cooling intrusions, old lava flows, tuff deposits, Quaternary sediments, etc.). A variety of research projects using gravity methods has been completed in the Masaya area, including Bouguer gravity surveys (Connor and Williams 1989; Metaxian 1994) and microgravity studies (Bonvalot and P. 1992; Bonvalot, Metaxian et al. 1995; Rymer, van Wyk de Vries et al. 1998; Williams-Jones 2001; Williams-Jones and Rymer 2002; Williams-Jones, Rymer et al. 2003).

Bouguer gravity studies show the density distribution in depth at any particular moment. The spatial resolution of such a survey may be good (depending on the distribution of stations), but the temporal resolution is nonexistent as the survey represents a snapshot in time. While these data can provide very detailed information on the presence of molten bodies and lithological changes in depth, the necessity to acquire a significant number of gravity data points means that Bouguer surveys are rarely repeated so no information on the rate of change of density contrasts is obtained.

This means that Bouguer gravity studies normally cannot provide information on the evolution of dynamic systems. Two Bouguer anomaly gravity studies have been completed previously in Masaya at caldera scale. Connor and Williams (1989) acquired 217 gravity stations in the area, but only 35 of those were located within the caldera boundaries, providing information on the density distribution of an area of more than 58 km^2 (extension of the caldera floor). The density of gravity stations in Metaxian's study (1994) is much higher, with the acquisition of more than 600 gravity stations in the course of two years. However, the technology available for determining the location of the gravity stations has greatly improved since then, allowing a more accurate horizontal and vertical positioning of the stations. Metaxian (1994) employed a barometric station to determine the height above mean sea level of the stations measured, estimating the average error in 3 m. For a density of 2.15 g/cm^3, the error in the Free Air Correction is ±0.65 mGal. A mGal is one thousandth of a Gal, a unit of acceleration used extensively in gravimetry studies and defined as 1 centimeter per second squared (1 cm/s^2). For horizontal positioning, two methods were employed; a handheld GPS receptor with a maximum precision of 50 m, and a combination of topographic maps and car odometers (when possible) that introduced an average error of 100 m. The theoretical error introduced in the latitude correction is ±0.011-0.022 mGal. The total error was estimated by Metaxian in ±1.2 mGal. Since the difference between maximum and minimum Bouguer gravity values obtained in this study is ≈20 mGal, the error in Metaxian study (≈6% of signal) can have important implications for modelling (especially for small geological features).

Microgravity studies make use of accurately re-locatable gravity stations (signaled by concrete blocks and metal pins for accurate location) that are reoccupied on a periodic basis (normally annually at Masaya). They address the evolution of volcanic environments, providing information on the changes in distribution of different elements (gas-rich melt, degassed magma, voids, host rock, etc.). In spite of the spatial resolution being poor (as there are fewer stations than in a Bouguer survey), the advantages of understanding the evolution of a particular system makes this method suitable for active environments, such as Masaya's summit and pit crater area. Several studies have

used this method on Masaya, from the first studies and installation of many concrete blocks and metal pins (Bonvalot and P. 1992; Bonvalot, Metaxian et al. 1995) to the studies that followed and significantly expanded the microgravity network in Masaya (Rymer, van Wyk de Vries et al. 1998; Williams-Jones 2001; Williams-Jones and Rymer 2002; Williams-Jones, Rymer et al. 2003).

In this study we have employed a variety of gravity methods in order to investigate subsurface structures and processes at Masaya on the caldera scale. Public domain satellite gravity data have been examined for the Masaya area to understand the density distribution at a regional scale. Combined with new Bouguer gravity data acquired in the course of this study they provide new insights into the density characteristics of the caldera and its geodynamical context. Bouguer gravity data (477 new gravity stations) were accurately positioned using Differential Global Positioning System (DGPS) techniques and have been used to generate the most accurate Bouguer anomaly map to date (total error of ±0.1 mGal, see Section 5.3.2.), providing very detailed information on different wavelength structures. Two Leica 500 GPS receivers were used as a base and rover stations, with more than 5 minutes of data collected at every point, ensuring accuracies better than 2 cm on the vertical scale (Leica 1999). Finally, the network of microgravity stations re-occupied since 1993 by Rymer et al. (1998) has been re-occupied to understand the evolution of the summit area. Changes in the location of these gravity stations is investigated using the same DGPS system employed for the Bouguer gravity study, removing unwanted effects such as volcano inflation or deflation, fault-related deformation, etc, relative to the gravity base station.

5.3 Results

5.3.1 Satellite gravity survey

Processed ERS-1 and Geosat/GM altimetry and gravity satellite data (Parasnis 1952; Smith and Sandwell 1997) have been compiled to produce a Free Air Gravity map (Figure 5-1). The total error has been calculated in ±3 mGal (Sandwell and Smith 2009). Subsequently, a Bouguer correction has been applied to the data, and a series of Bouguer anomaly maps has been generated using different

superficial density values to perform terrain corrections, and calculate the Bouguer anomaly. The average density values of Masaya Caldera range from 2.2 gm/cm^3 for the summit area to 2.6 gm/cm^3 for the NE part of the caldera, as calculated by Metaxian (1994) using the Parasnis (1952) method. Finally, a reduction density of 2.4 g/cm^3 has been selected as a representative value of average density at regional scale. This value also coincides with the density of the upper layer (10 km) calculated by Girard and van Wyk de Vries (2005) for their analogue modeling study of Las Sierras-Masaya volcanic complex.

The Bouguer anomaly map (**Figure 5-1**) shows a gravity signal dominated by a strong positive anomaly centered in the NE corner of the caldera. This positive anomaly was already postulated by Connor and Williams (1989) and Metaxian (1994) in their gravity studies, but the location differs substantially. According to satellite gravity data, the centre of this anomaly (regional maximum value of gravity) is within the caldera boundaries near the Northern tip of Masaya Lake, while the centre of the anomaly is located ≈3 km to the North (outside the caldera boundaries) according to Connor and Williams (1989), and ≈4 km to the NE according to Metaxian (1994), see Figure 5-10. The satellite based Bouguer anomaly map shows a relative difference of 17 mGal between the highest and lowest gravity values in the area. If we consider the gravity values outside the caldera boundaries, we find that the regional patterns described by Connor and Williams (1989) and Metaxian (1994) –with higher gravity values to the SW of the caldera and lower values to the NE– are comparable to the results obtained using satellite data.

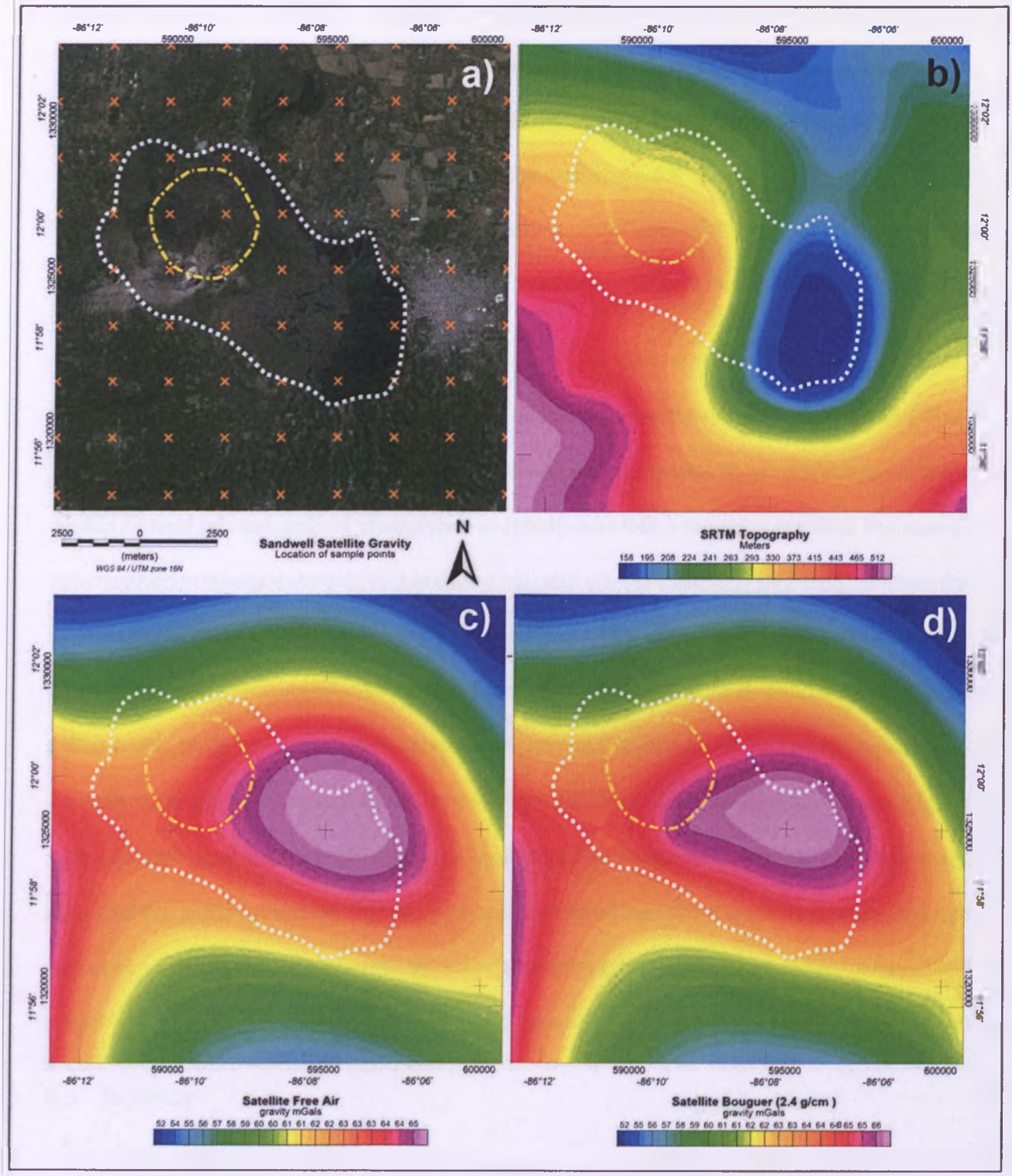

Figure 5-1: Topography and gravity data extracted from the Sandwell database: a) Satellite photograph of Masaya Caldera with the location of the sample measurements and the outline of the caldera and its inner ring fault. b) Topography map based on SRTM data. c) Free Air gravity map. d) Bouguer Anomaly map.

5.3.2 Land gravity survey

Some 477 new gravity stations have been measured within Masaya Caldera and its vicinities (Figure 5-2, Appendix I: Land Bouguer gravity data (caldera)). The spacing between stations ranges from 50 to 400 m depending on several factors (accessibility, distance to the caldera, etc.). Data have been collected in closed loops, with a permanent base station measured at least twice every day (at the beginning and end of the survey). All data were subsequently normalized to that base station (12°00'02.64706"N, 86°09'03.62968"W), adjacent to a weather station near the Visitor Centre. Six different corrections have been applied to the data, including latitude, tidal, terrain, drift, free air, and Bouguer corrections (for a detailed explanation on each of these corrections, see section 2.4.4). Four gravimeters have been used in the course of this study: Lacoste and Romberg models D-41, D-61, G-513 and G-403. The D-meters can record continuously but have a higher drift than G-meters. At least 5 minutes of data were acquired at every station to ensure stabilization of the gravity signal after commencement of recording. G-meters measure only a discrete value of gravity. Variability between both types of gravimeters has been minimized through periodic repetition of control profiles with different instruments to test differences, and averaging at least 3 measurements for every station of the profile. The variability between all the instruments (G-meters and D-meters) for this survey has been calculated to be less than 0.1%. Repeated measurements of local base stations (established for each specific survey day depending on its location) have allowed a precise calculation of daily instrumental drift for every gravimeter, with a maximum drift of -20 μGal per day (for D-61). For the Free Air correction, the elevation of each station has been determined using DGPS techniques. At least five minutes of 1 second interval recording has been done at every gravity station, with the accuracy of the position of each station estimated in 2 cm or less (equivalent to 4 μGal uncertainty). This represents a significant improvement from Metaxian's study (1994) in which the average vertical resolution was estimated in 3 m (900 μGal). To apply the Free Air correction, a constant value of -306.8 μGals m^{-1} (theoretical value) has been selected as free air gradient (FAG) due to the small anomaly values and relatively small elevation differences in the

survey area (<250 m), which make the error induced by using the theoretical FAG minimal. With the corrected data a Free Air Gravity map has been completed (Figure **5-2**). The total error has been estimated in ±120 µGal. The density used for the Bouguer correction applied has been 2.4 g/cm^3, in agreement with the Bouguer correction applied to the satellite gravity data. This allows for a more direct comparison between the two corrected data sets.

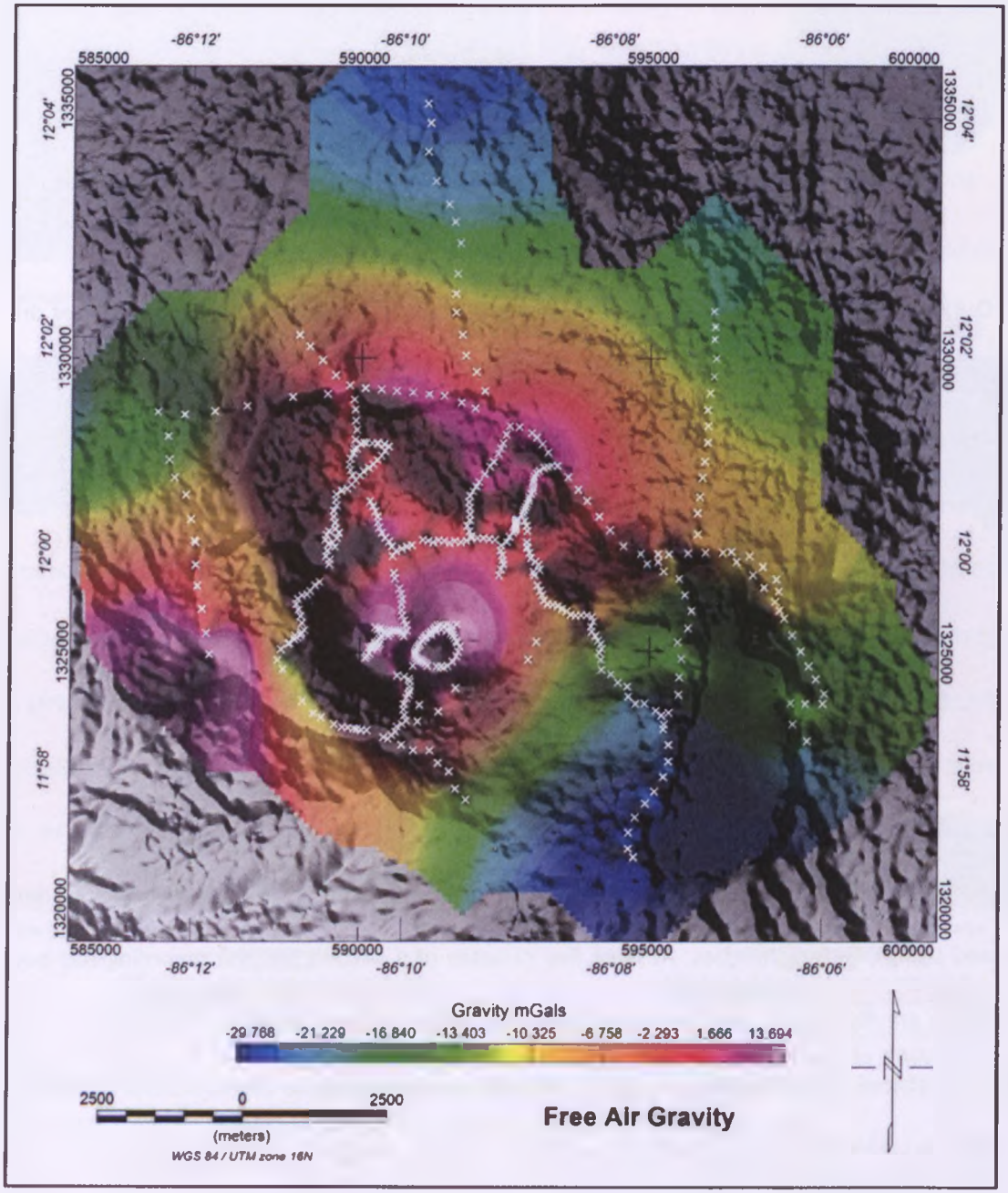

Figure 5-2: Free Air gravity map of Masaya Caldera overlaid on a 30 m resolution DEM of Masaya Caldera. White crosses represent the Bouguer gravity stations locations.

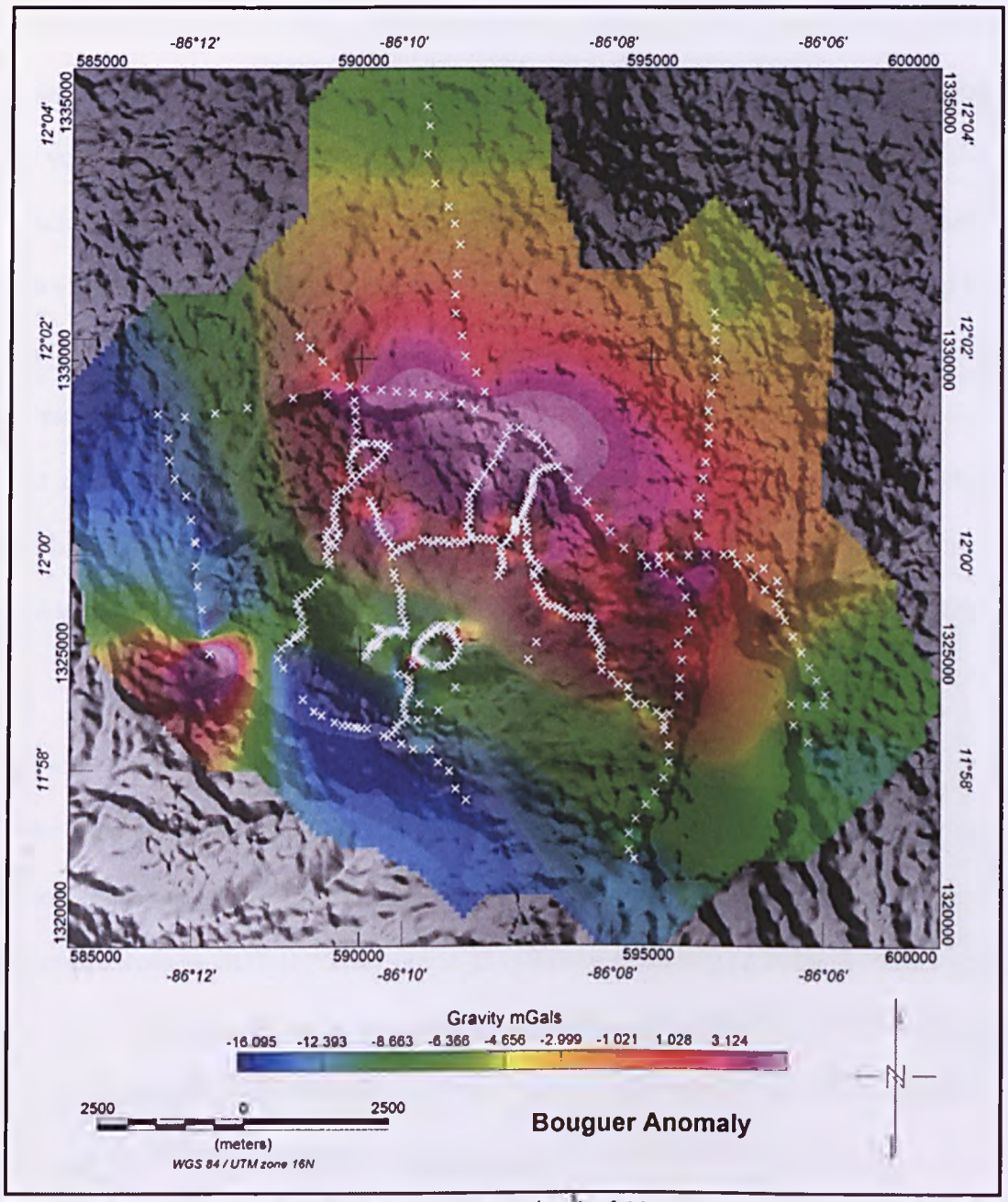

Figure 5-3: Bouguer Anomaly map (density = 2.4 g/cm^3) of Masaya Caldera overlaid on a 30 m resolution DEM of Masaya Caldera. White crosses represent the land Bouguer gravity stations locations.

The Bouguer Anomaly map (Figure **5-3**) is dominated by a large gravity anomaly (both in terms of wavelength and amplitude) centered in the NE part of the caldera, confirming the results obtained using public domain satellite gravity data. However, the location of the anomaly defined by this study is displaced to the NW compared to the satellite data (Figure 5-10), closer to the location postulated by Metaxian (1994). This difference is caused by the higher error values in satellite data (Sandwell and Smith 2009). The effect of this anomaly, also observed by Connor and Williams (1989) and Metaxian (1994), affects the gravity signal from the rest of the geological structures within the caldera, inducing a strong SW-NE gradient that acts to obscure the presence of other features. Only some local gravity highs in the summit area (related to accumulations of degassed magma but also to unwanted topographic effects, see Chapter 4) escape this pattern. To study the gravity signal from the rest of the caldera, the wavelength of this anomaly must be filtered and removed.

Using Metaxian (1994) estimations of the size and characteristics of the intrusion (see Table **5-1**); we have built two 2D sections (Figure 5-4) in GM-SYS software to calculate the gravity response of two geological models with specific density and dimensional characteristics. The geological models include a dense intrusion similar to the one described by Metaxian (1994). This will allow estimating the wavelength and amplitude of the gravity response to the intrusion and comparing it with the Bouguer Anomaly map in Figure **5-3**, providing information that will help to design appropriate filters to remove it and study the rest of structures. The two 2D models built have 10 and 15 km diameter, representing a long and short axis consistent with the elongated shape of the gravity anomaly seen in Figure **5-3**. A 40-50 km wavelength, 50-60 mGal gravity response results from the model built using Metaxian's estimations. These values are not consistent with the characteristics of the anomaly shown in Figure **5-3** (signal amplitude, ≈20 mGal), which must therefore be generated by a deeper or smaller intrusive body.

Las Sierras intrusion according to Metaxian (1994)	
Thickness	6 km
Depth	3–9 km
Diameter	10–15 km
Density	0.6 g/cm^3 denser than the surrounding rocks
Material	Gabbro

Table 5-1: Physical characteristics of intrusion in the NE corner of the caldera according to Girard and van Wyk de Vries (2005).

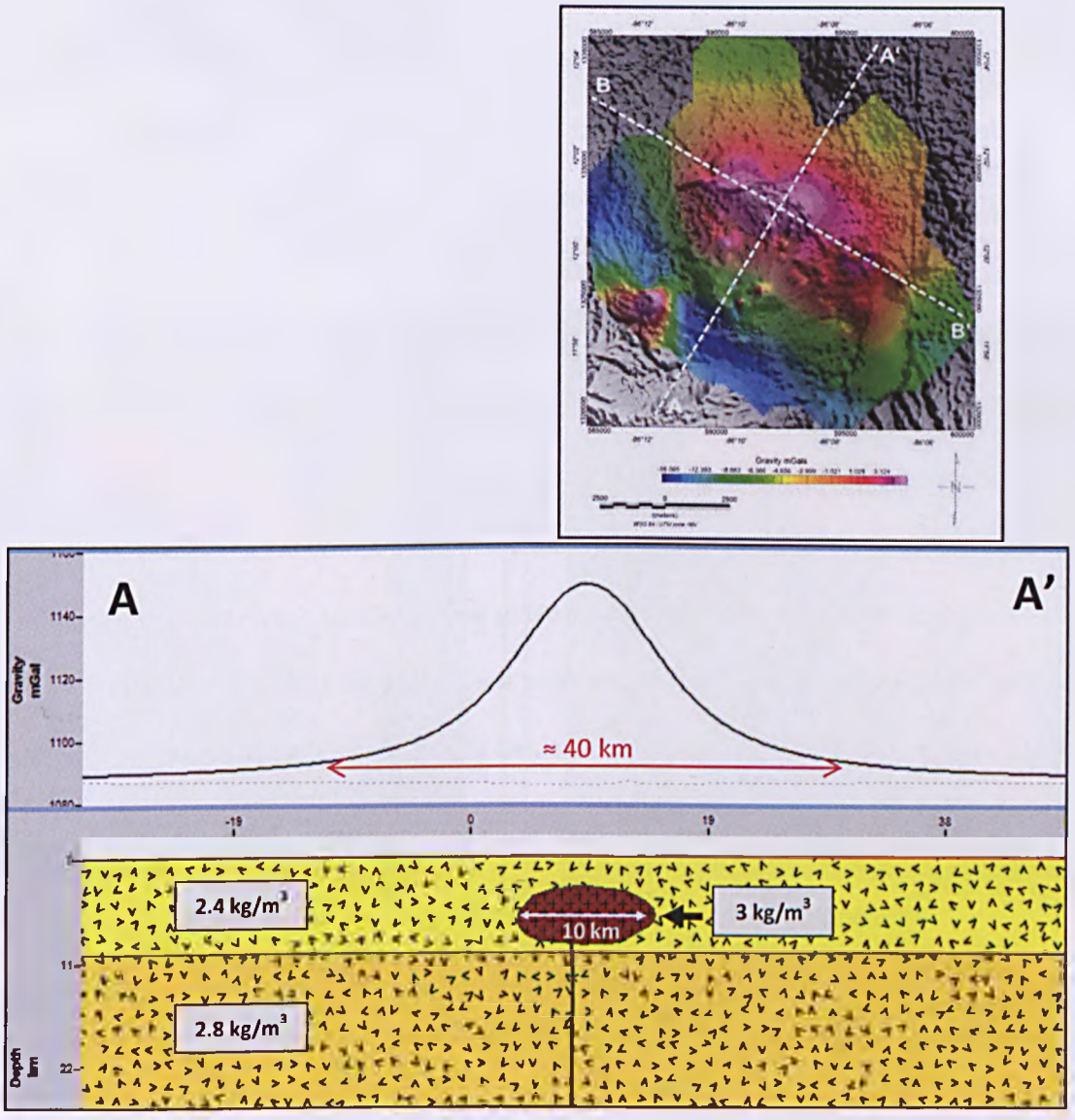

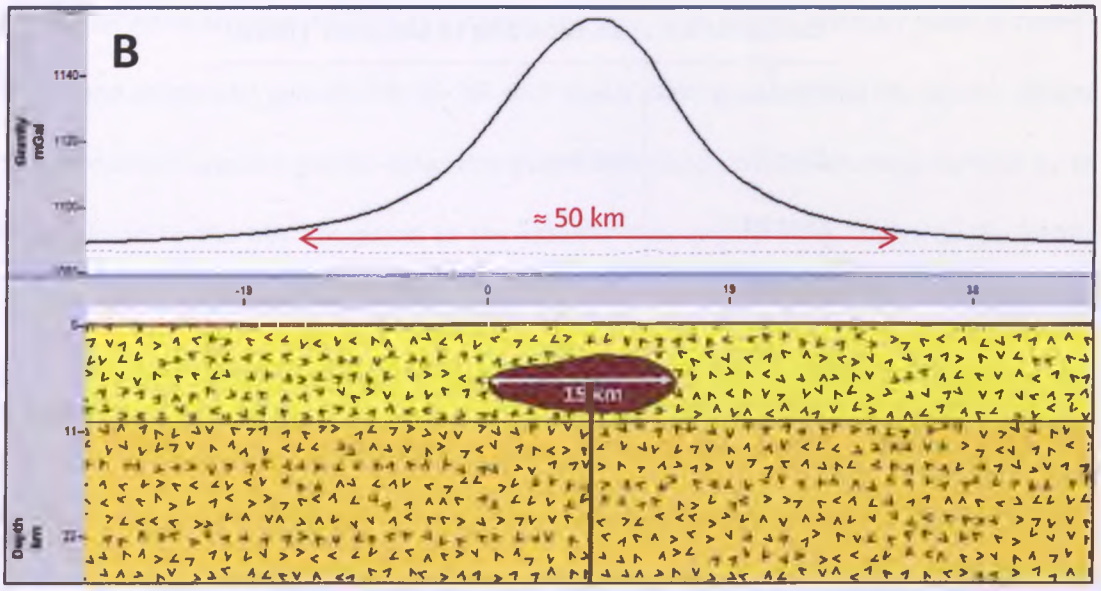

Figure 5-4: Gravity response (continuous line) of the dense intrusion (Table 1). The dotted line shows the gravity response of a 2.4 g/cm3 dense intrusive body (same as the surrounding geological materials). A 10 km diameter intrusion generates a 40 km wavelength gravity response, and a 15 km intrusion generates a 50 km response.

In order to study the structures of the rest of the caldera at different depths, we have tested the performance of different filters (high and low-pass) when applied to the Bouguer Anomaly grid. High-pass filters (Figure **5-5**) are used to remove the signal caused by large, deep, dense geological bodies. In this case, high-pass filters have been effective in removing the effects of the dense intrusion detected by Metaxian (1994) in the gravity field. For wavelengths shorter than 7 km, the internal coherence of the gravity anomaly disappears, but some residual signal can still be seen in the same location. For wavelengths shorter than 5 km, the majority of the signal generated by the intrusion is removed, and the signal left corresponds with mid-level and shallow geological features. Low-pass filters (Figure **5-6**) are applied to remove the signal from shallow lithological changes (lava tunnels, denser lava flows), and possible unwanted effects induced by sharp topography changes, the presence of pit craters, etc. For filters longer than 1 km, no spikes or low-frequency signal are left in the data.

High Pass Filtering

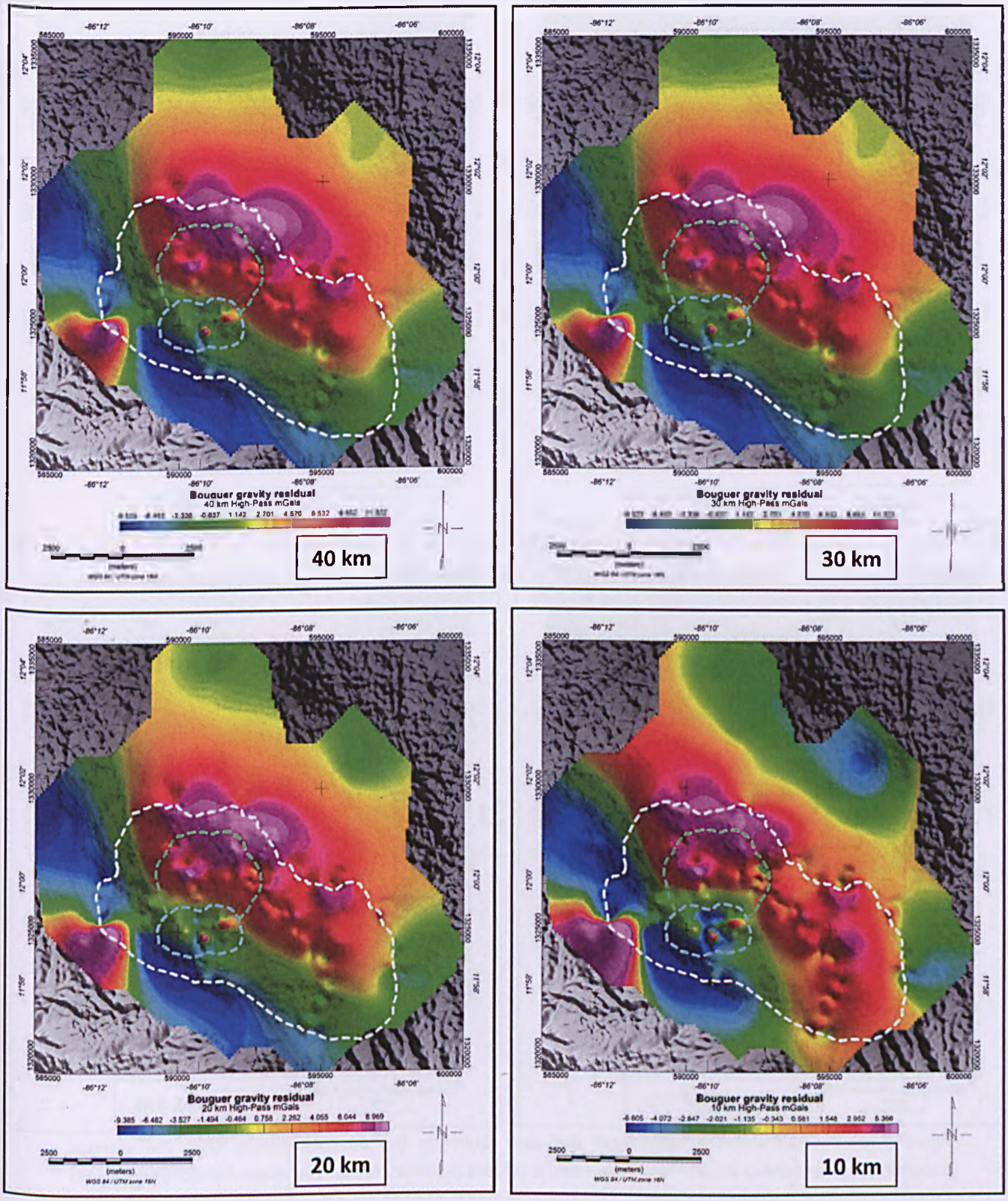

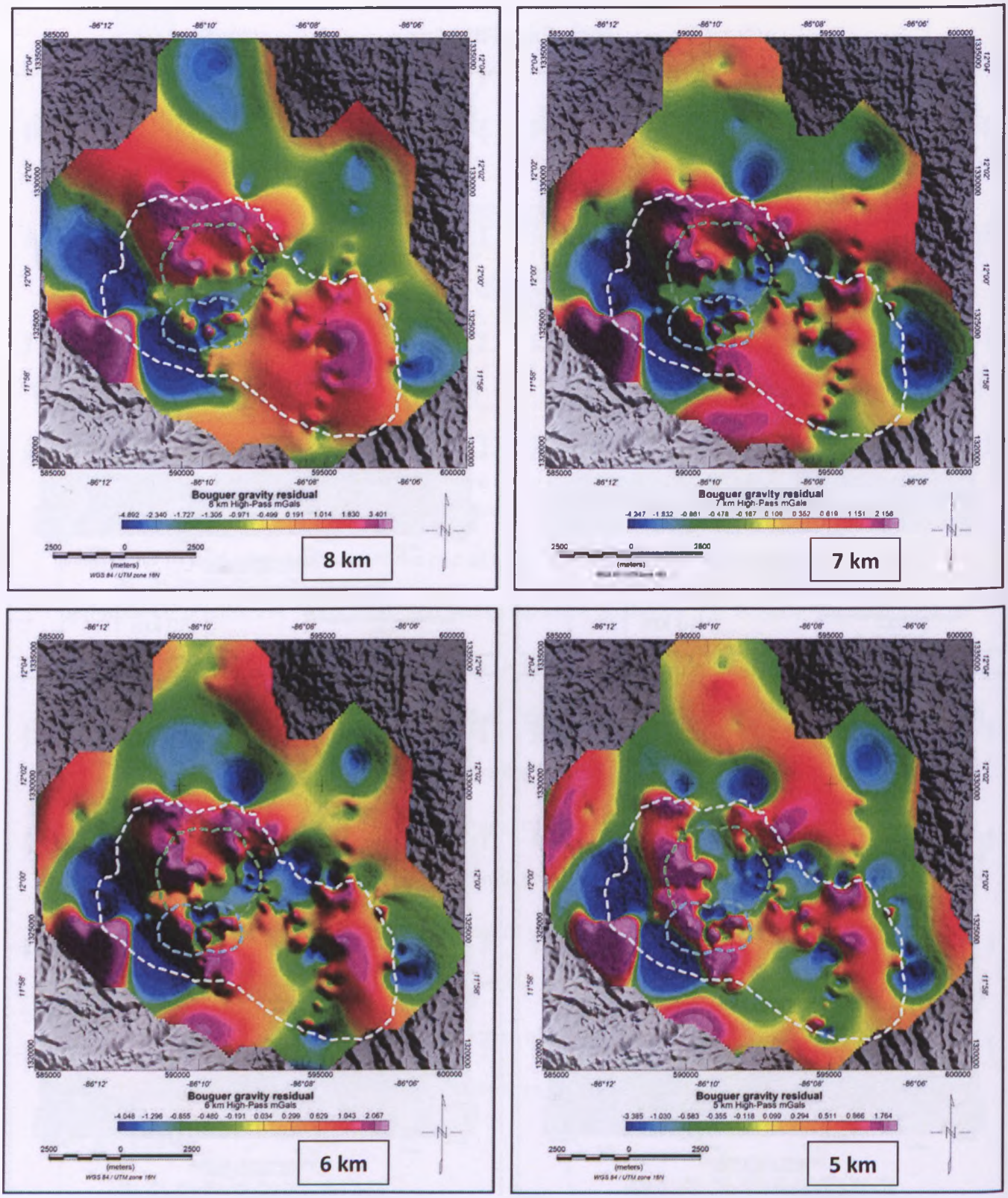

Figure 5-5: Effect of different wavelength high-pass filters on the Bouguer gravity data. The external discontinuous line (white) shows the location of the caldera boundary faults. The internal discontinuous lines show the ring fault described in Chapter 3 (North, light green) and the region occupied by the pit crater area (South, light blue). For the location of gravity stations, see Figure 5-3: Bouguer Anomaly map (density = 2.4 g/cm^3) of Masaya Caldera overlaid on a 30 m resolution DEM of Masaya Caldera. White crosses represent the land Bouguer gravity stations locations..

Low Pass Filtering

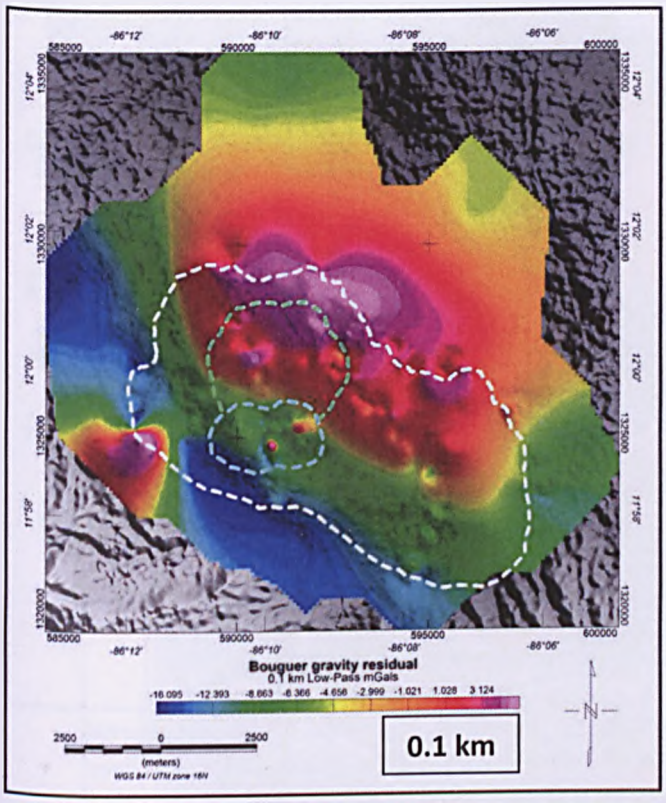

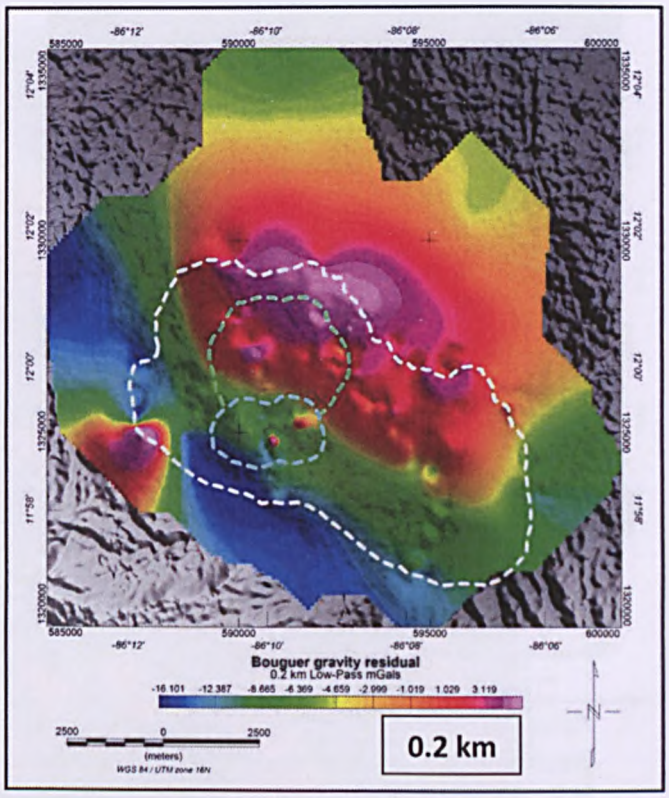

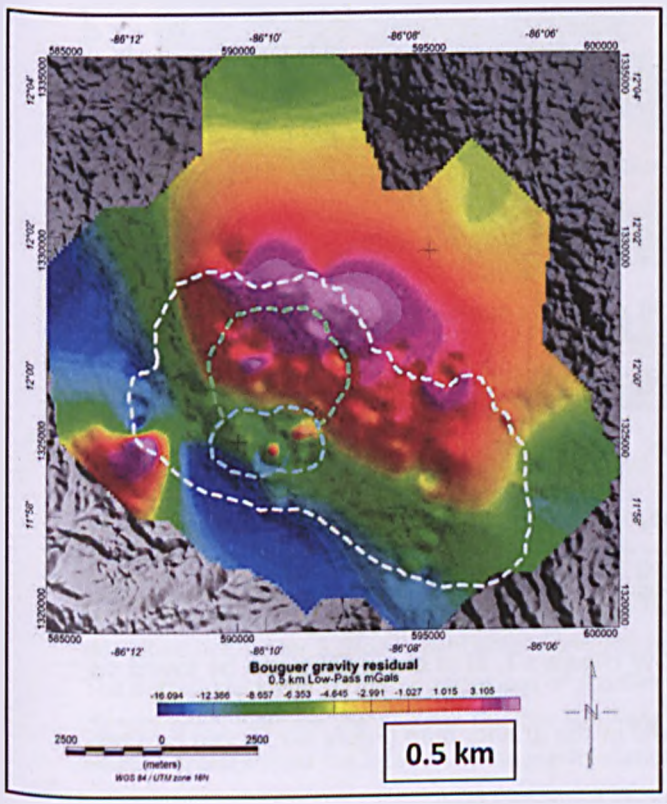

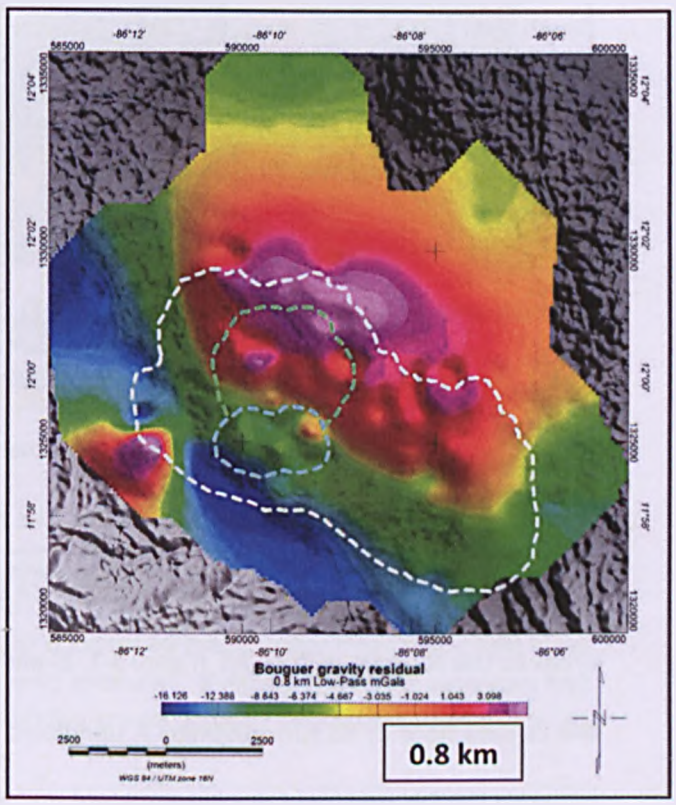

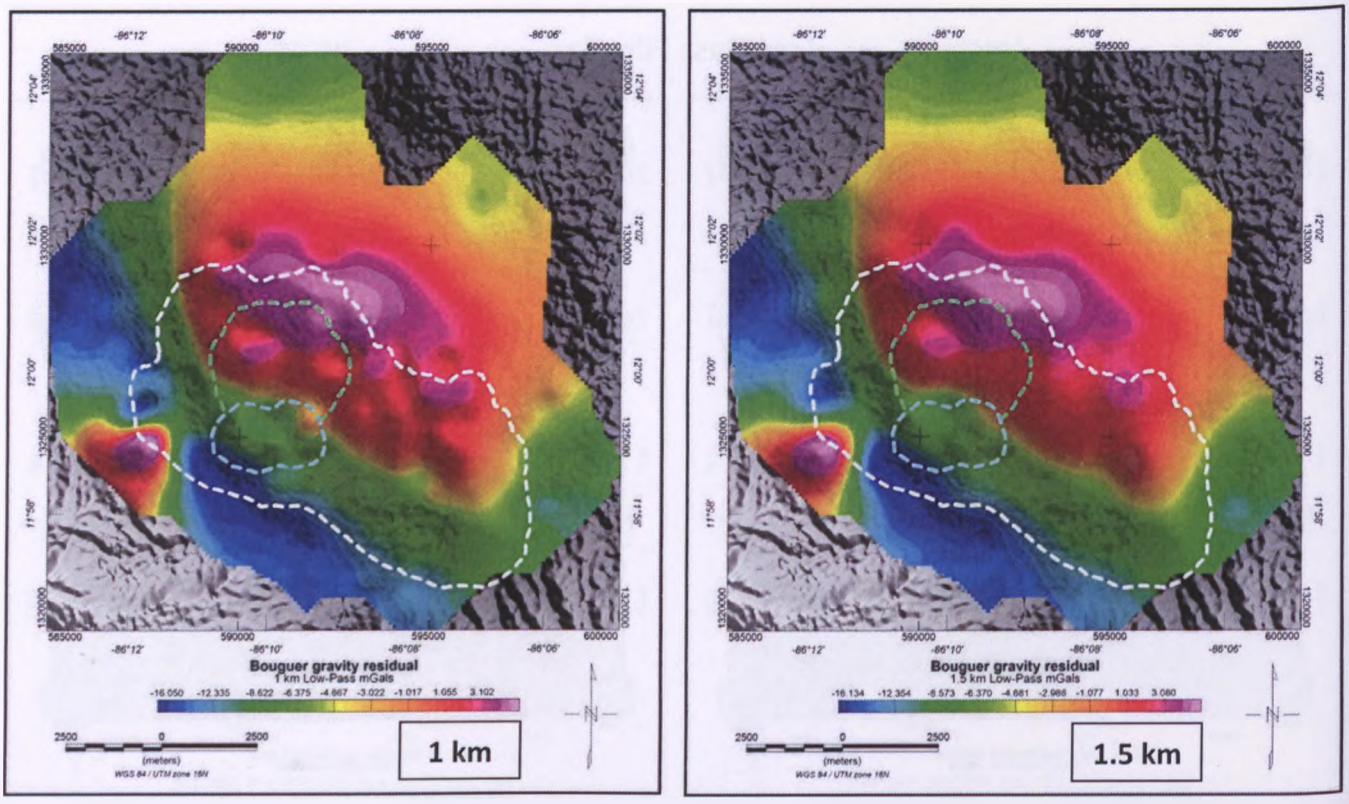

Figure 5-6: Effect of different wavelength low-pass filters on the Bouguer gravity data. The external discontinuous line (white) shows the location of the caldera boundary faults. The internal discontinuous lines show the ring fault described in Chapter 3 (North, light green) and the region occupied by the pit crater area (South, light blue). For the location of gravity stations, see Figure 5-3: Bouguer Anomaly map (density = 2.4 g/cm^3) of Masaya Caldera overlaid on a 30 m resolution DEM of Masaya Caldera. White crosses represent the land Bouguer gravity stations locations..

Using the information acquired through the evaluation of filters in the area, a 1-5 km band-pass filter has been selected as the most suitable to extract geological information from the Bouguer Anomaly grid. A residual gravity map (Figure **5-7**) built using the mentioned filter depicts the gravity signal generated by mid-level (<3 km deep) geological features, and excludes the gravity signal caused by deep structures like the dense intrusion, and also the effect of superficial lithological contrasts and unwanted topographic effects. The map shows a strong positive anomaly aligned with a NNW-SSE orientation that crosses the caldera (Figure **5-7**, dotted black line). Other high density areas to the N (Figure **5-7, 1**), NE (Figure **5-7, 2**) and SW (Figure **5-7, 3**) of the caldera can be found on the caldera floor or its surroundings. A significant low in the gravity map (Figure **5-7, 4**) can be seen between the SW section of the ring fault and the caldera bounding fault.

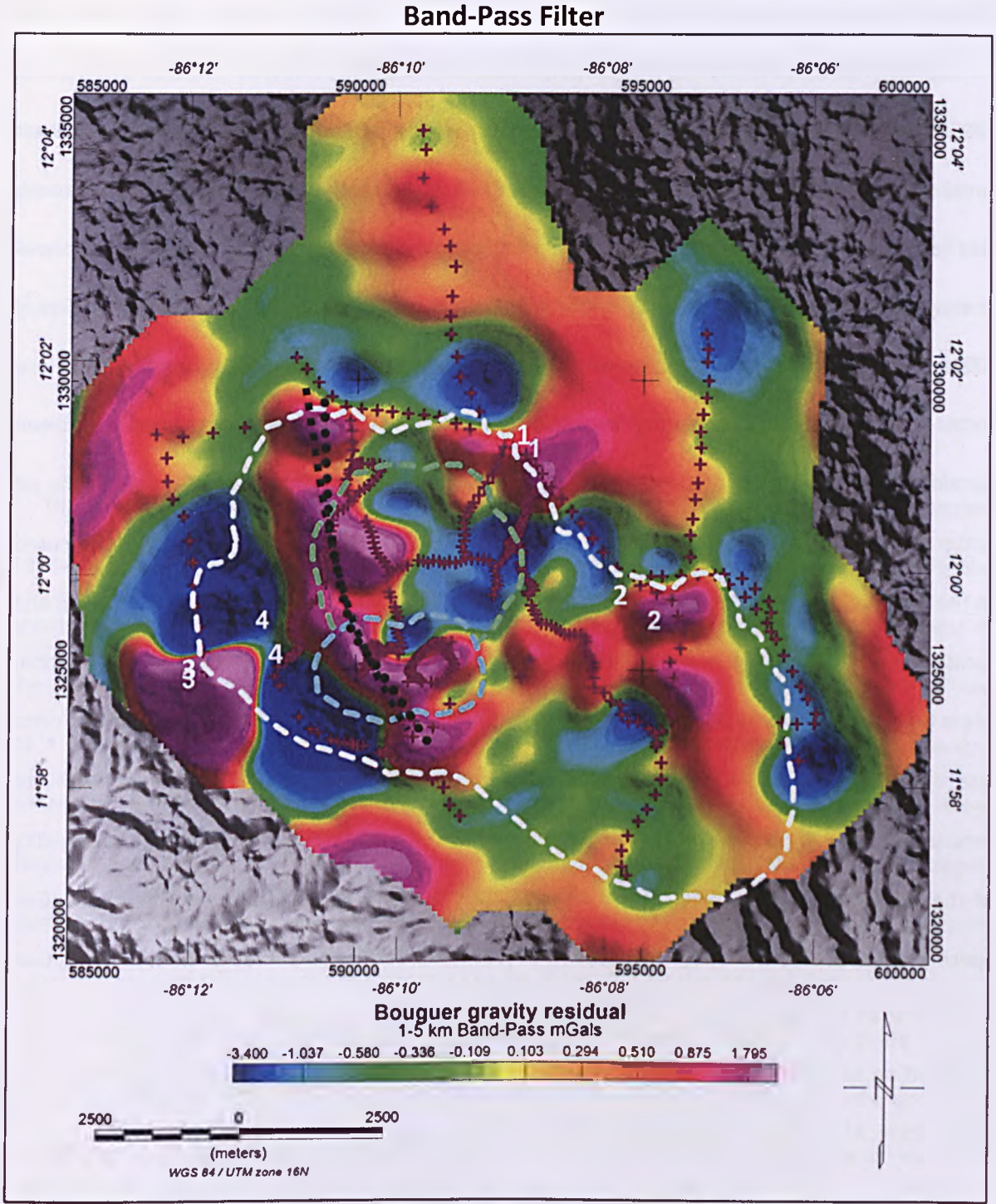

Figure 5-7: Effect of a 1-5 km band-pass filter on the Bouguer gravity data. The external discontinuous line (white) shows the location of the caldera boundary faults. The internal discontinuous lines show the ring fault described in Chapter 3 (North, light green) and the region occupied by the pit crater area (South, light blue). The dotted black line shows an alignment of positive gravity anomalies. Numbers 1, 2 and 3: secondary high density areas beneath the caldera; number 4: strong negative gravity anomaly beside the SW caldera edge. Maroon crosses show the location of the gravity stations.

5.3.3 Microgravity survey

The last microgravity study on Masaya summit area was published by Williams-Jones et al. (2003), comprising data from 32 different stations within the caldera boundaries (17 in the summit area) collected between October 1994 and March 2000. After March 2000, the microgravity network has been reoccupied five times. In the course of this investigation, up to 17 microgravity stations in the summit area of Masaya Volcano and 3 outside this region (Figure 5-8) have been reoccupied (2010 and 2011). Given the small changes in gravity values undergone by the microgravity stations located far from the active area of Masaya Volcano, only the stations near the summit have been considered for this study. This provides a good picture of the evolution of gravity data in the pit crater and summit area for the past 18 years. All data are normalized to the same base station used in the Bouguer Anomaly study (near the Visitor Centre, 12°00'02.64706"N, 86°09'03.62968"W), and located using a DGPS system that allows correction for position changes caused by deformation. More than 10 mins of data have been recorded by the GPS system at every station, ensuring an error less than ±1 cm. The data have been collected over 4-6 week periods performing repeated measurements, with values given as an average of at least 2 readings (Table 5-2). The repeatability of the measurements is subject to the instrumentation, which allows measurements of ±5 μGal. Specific survey procedures designed after Rymer (1996) were followed to reduce the total error, that is better than ±25 μGal (Rymer, van Wyk de Vries et al. 1998). The microgravity network has been occupied on an annual basis, with three exceptions; no data are available between April 1994 and March 1996, March 2000 and January 2004, and January 2004 and March 2008.

To calculate the values that populate Table 5-2, the first year a new gravity station is established; the difference between the value of gravity measured at that particular station and at base station A1 is calculated and recorded. Then the difference between the gravity at A1 and at the station is recalculated for any given year, and subtracted from the difference of the initial year. With this procedure, the evolution of gravity at a particular station relative to base station A1 can be tracked over time. The final values that populate the table (Δg_f) can be expressed as $\Delta g_f = \Delta g_x - \Delta g_0$;

where $\Delta g_x = A1_x - S_x$ and $\Delta g_0 = A1_0 - S_0$. The terms of these equations can be defined as: Δg_f: final gravity value; Δg_x: gravity difference between base station A1 and a particular microgravity station in a given year (x); Δg_0: gravity difference between base station A1 and a particular microgravity station the first year that station was established (x); $A1_x$: value of gravity measured at base station A1 in a given year (x); S_x: value of gravity measured at a microgravity station (S) in a given year (x); $A1_0$: value of gravity measured at base station A1 the first year the station in question was established (0); S_0: value of gravity measured at a microgravity station (S) the first year the station in question was established (0). Figure 5-8 is composed using the values of Table 5-2.

Three main types of gravity changes define the behaviour of Masaya summit area for the period 1994-2011 (Figure 5-9). Short term variations are common for individual stations, with changes in the gravity values typically less than 60 μGal per year. These short period changes account for most of the variability within the gravity dataset. In terms of distance, we can see that the anomalies defined by a certain interval of gravity values migrate with time. This is exemplified by the changes undergone by Station A9 (Figure 5-9) for the period February 1999/June 1999/March 2000. These displacements, typically less than 100 m in horizontal space, reflect subsurface structural changes. Medium term variations in Masaya are characterized by a general increase or decrease of gravity values for most of the stations. This process can be illustrated by the general decrease in gravity values that took place between March 1997 and March 2000, period during which there was an average decrease of ≈100 μGal for all the gravity stations (Figure 5-9). In addition to the short and medium term variations, longer term changes are also prominent in the dataset shown in this study. The main characteristic of this type of variations is not a general increase or decrease in the gravity values, but a distinction between periods with small gravity contrasts between stations (1994-2000) and periods with large gravity contrasts between stations (2004-2011).

Point_ID	Height_m	Easting (UTM 16P)	Northing (UTM 16P)	First reading	Feb-93	Apr-94	Oct-94	Mar-96	Mar-97	Feb-98	Sep-98	Feb-99	Jun-99	Mar-00	Jan-04	Mar-08	Mar-09	Jan-10	Mar-11
Delta_Nind	499.2921	590298.4	1325201	Mar-08	-	-	-	-	-	-	-	-	-	-	-	0	0.046	0.052	-0.031
Nindiri	498.585	590298.8	1325201	Feb-99	-	-	-	-	-	-	-	0	-0.044	-0.023	-	-	-	-	-
Zopilotes	539.7667	589970.2	1325146	Mar-08	-	-	-	-	-	-	-	-	-	-	-	0	0.0485	0.039	-0.002
Pecho_Viejo	540.4568	590050.1	1324995	Mar-08	-	-	-	-	-	-	-	-	-	-	-	0	0.031	0.008	-0.048
Teatro	538.8775	590235.3	1324912	Jan-04	-	-	-	-	-	-	-	-	-	-	0	-0.056	-0.06167	-0.065	-0.108
Bat1	508.1565	590646	1324602	Jan-10	-	-	-	-	-	-	-	-	-	-	-	-	-	0	-0.02
A9	525.9264	590785.9	1324703	Feb-93	-0	-0.08	-	-0.113	-0.064	-0.066	-0.083	-0.183	-0.15	-0.137	-0.171	-	-0.164	-0.172	-0.162
B4	538.5463	590758.1	1325172	Jan-04	-	-	-	-	-	-	-	-	-	-	-	0	-0.00936	0.004	-0.043
Guru	593.9622	591051.4	1325143	Mar-09	-	-	-	-	-	-	-	-	-	-	-	-	0	-0.005	0.014
Edge	526.5325	590451	1325227	Mar-97	-	-	-	-	0	0.004	-0.04	-0.056	-0.12	-0.114	-0.104	-0.0575	-0.09	-0.073	-0.13
E3	516.29	590633.4	1324680	Feb-93	0	0	-	-	-	-	-	-	-	-	-0.076	-	-0.006	-0.063	-0.102
A8	572.6873	590901.7	1324933	Feb-93	-0	-0.071	-	-0.052	-0.055	-0.068	-0.083	-0.085	-0.083	-0.076	-0.14	-0.14	-0.137	-0.142	-0.149
B2	538.1112	590728.4	1325208	Apr-94	-	-	0	0.029	-0.015	-0.023	-0.034	-0.035	-0.094	-0.081	-0.121	-0.1125	-	-	-
A11	516.5332	590484.4	1324615	Mar-97	-	-	-	-	-0	-0.036	-0.051	-0.063	-0.105	-0.107	0	-	0.061	0.007	-0.035
A10	522.4791	590400.2	1324629	Feb-93	0	-0.08	-	-0.065	-0.024	-0.053	-0.072	-0.074	-0.131	-0.127	-0.179	-	-0.1	-0.152	-0.009
A7	534.0615	590740.9	1325301	Feb-93	0	-0.078	-0.088	-0.051	-0.054	-0.056	-0.074	-0.082	-0.139	-0.135	-0.191	-0.1485	-	-	-0.013
Pedro	530.3625	590349.5	1325384	Mar-97	-	-	-	-	0	-0.012	-0.05	-0.052	-0.123	-0.111	-0.097	-0.0355	-0.066	-0.058	-0.102
Pedro2	533.4776	590220.8	1325443	Feb-99	-	-	-	-	-	-	-	0	-0.045	-0.053	-0.043	-0.015	0.004	0.045	-0.041

Table 5-2: evolution of microgravity data collected on the summit area of Masaya Volcano in the period February 1993/March 2011. Values are in mGal. For a detailed explanation on the procedure to calculate the values in this table, see section 5.3.3.

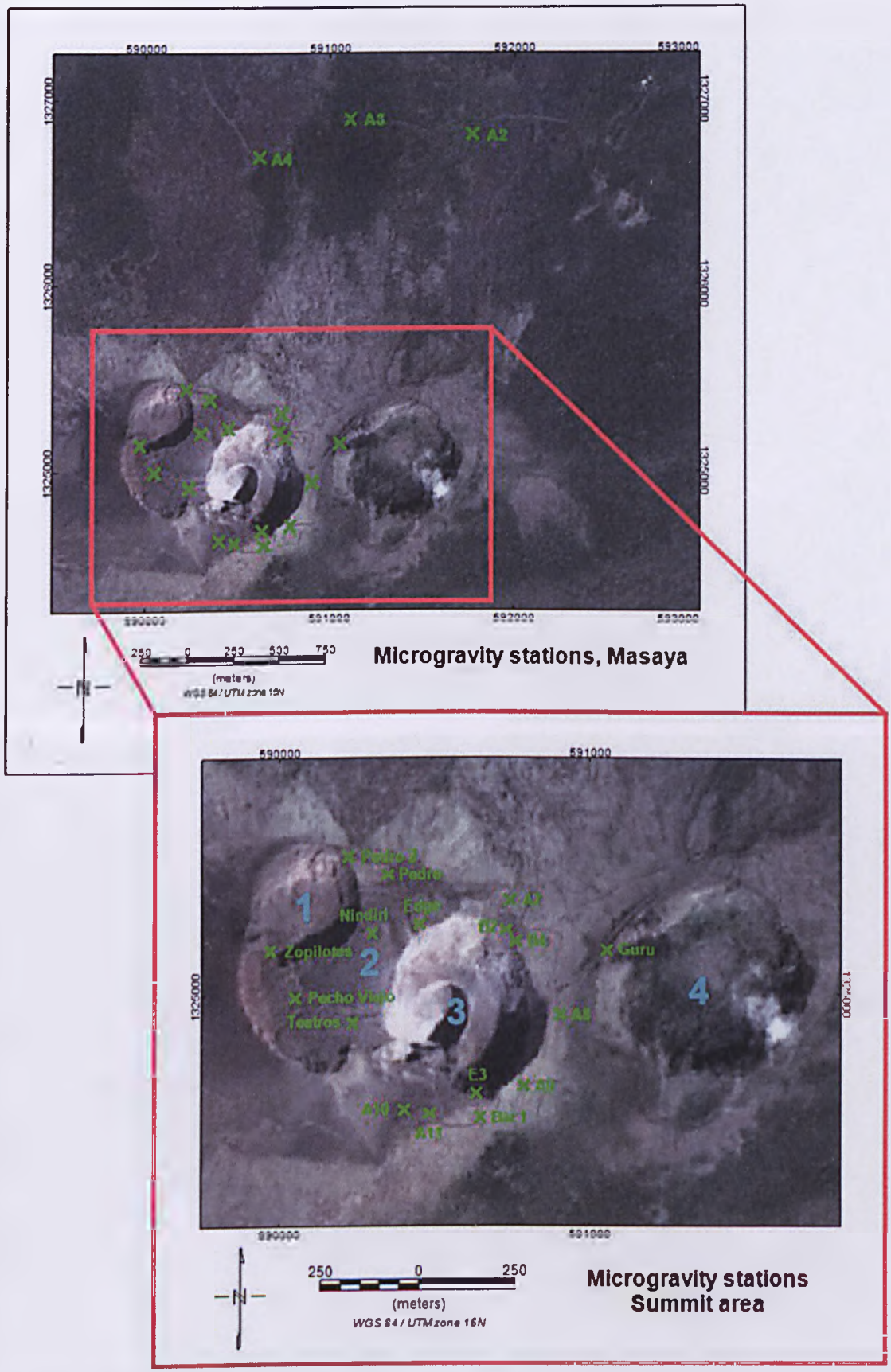

Figure 5-8: Location map of the summit microgravity stations.

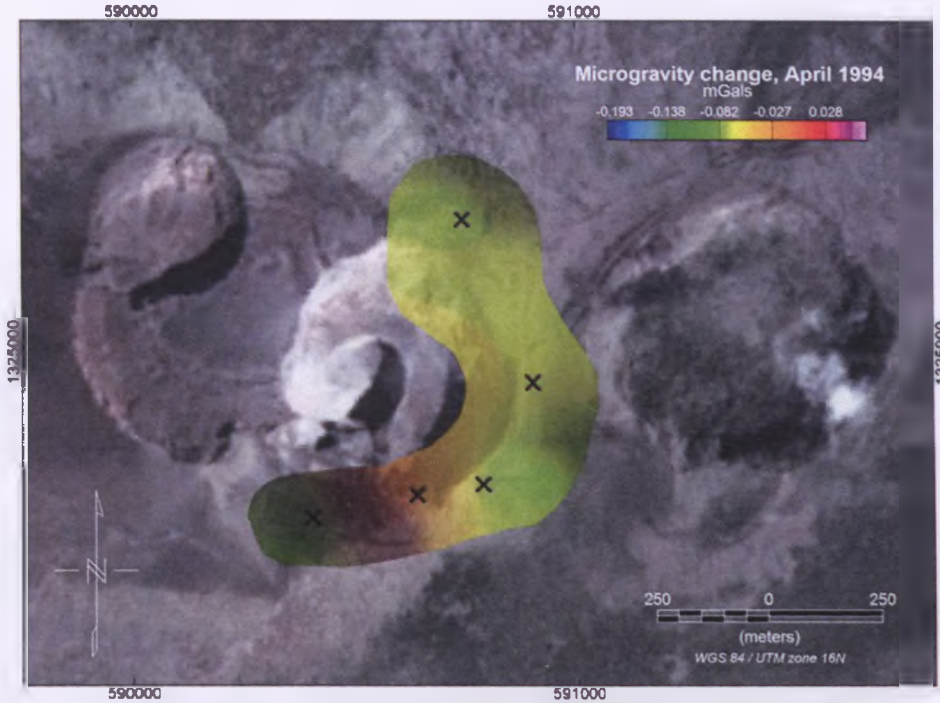
590000
591000
1325000
Microgravity change, April 1994
mGals
-0.193 -0.138 -0.082 -0.027 0.028
250 0 250
(meters)
WGS 84 / UTM zone 16N

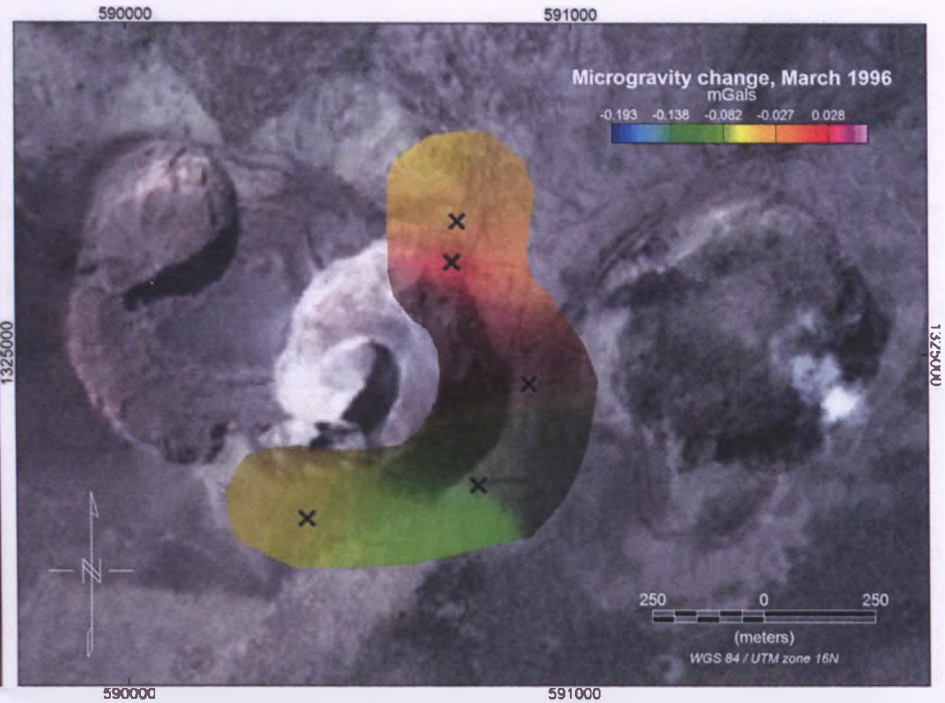
590000
591000
1325000
Microgravity change, March 1996
mGals
-0.193 -0.138 -0.082 -0.027 0.028
250 0 250
(meters)
WGS 84 / UTM zone 16N

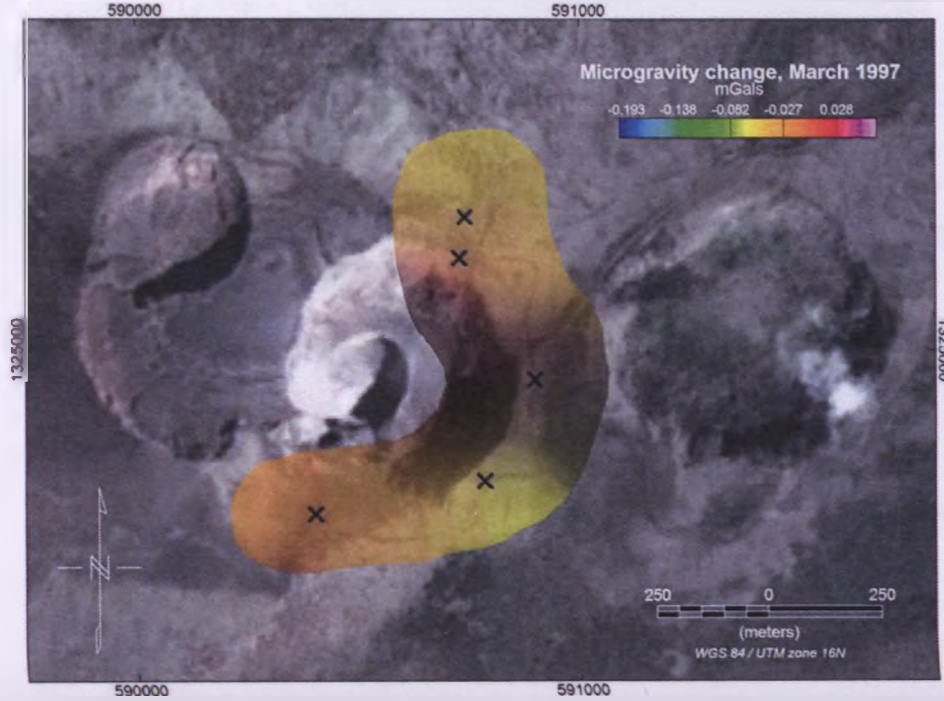
590000
591000
1325000
Microgravity change, March 1997
mGals
-0.193 -0.138 -0.082 -0.027 0.028
250 0 250
(meters)
WGS 84 / UTM zone 16N

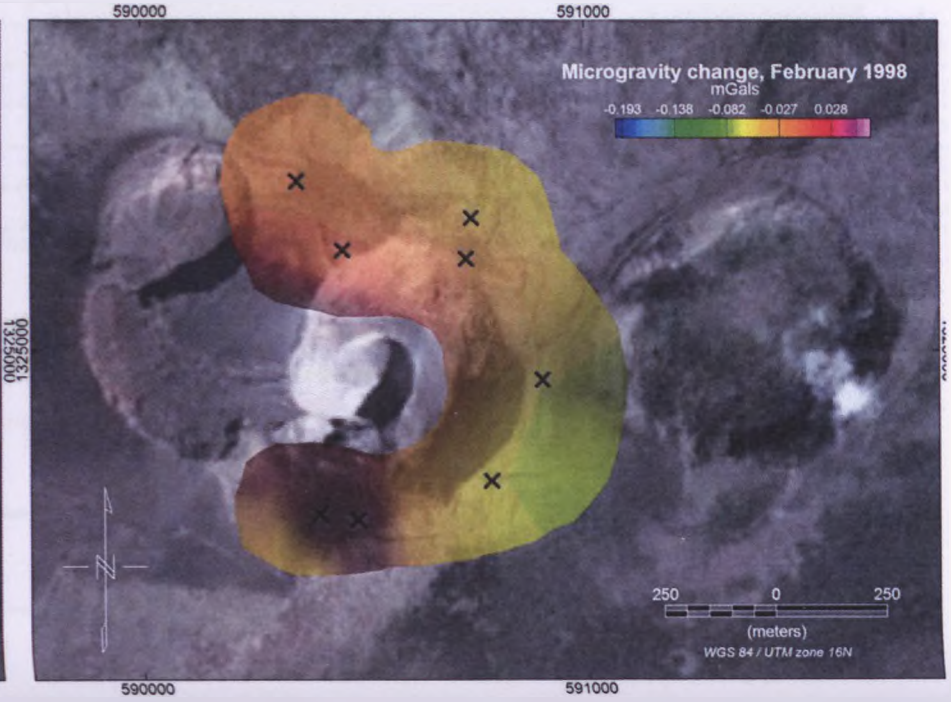
590000
591000
1325000
Microgravity change, February 1998
mGals
-0.193 -0.138 -0.082 -0.027 0.028
250 0 250
(meters)
WGS 84 / UTM zone 16N

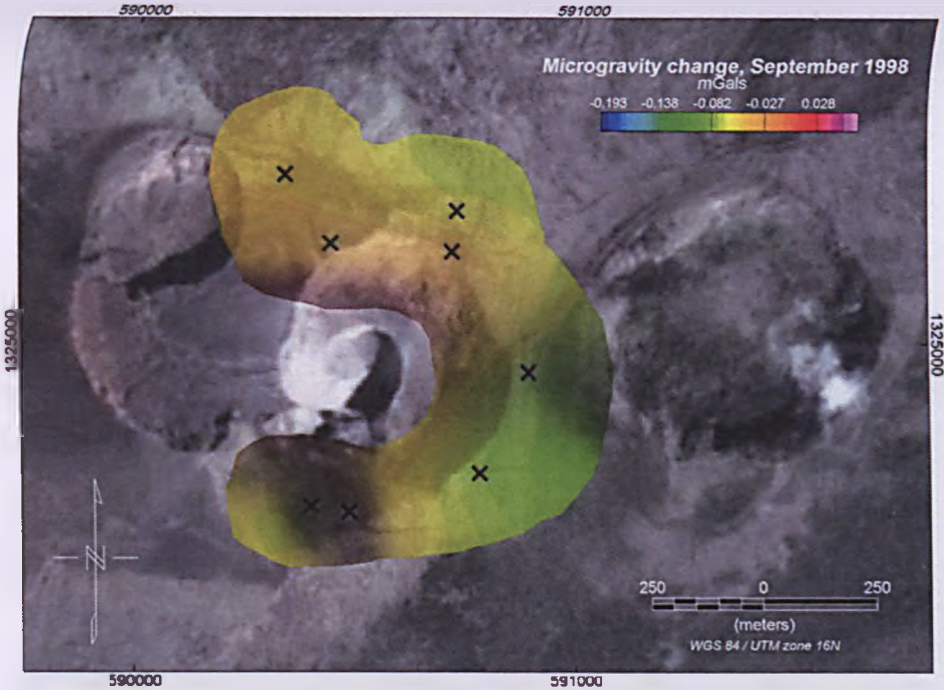
590000
591000
Microgravity change, September 1998
mGals
-0.193 -0.138 -0.082 -0.027 0.028
1325000
250 0 250
(meters)
WGS 84 / UTM zone 16N

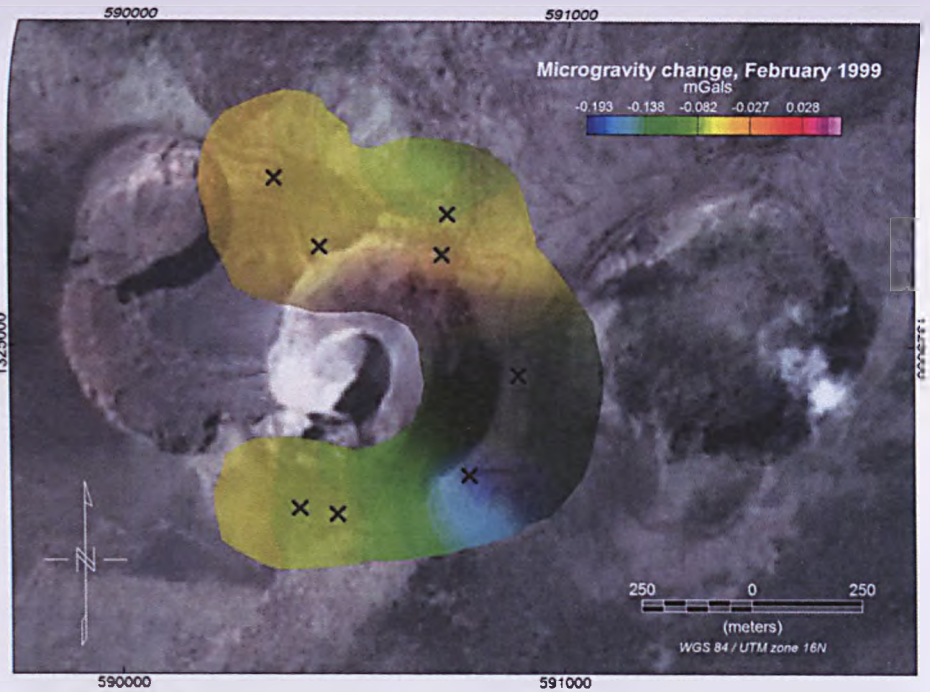
590000
591000
Microgravity change, February 1999
mGals
-0.193 -0.138 -0.082 -0.027 0.028
1325000
250 0 250
(meters)
WGS 84 / UTM zone 16N

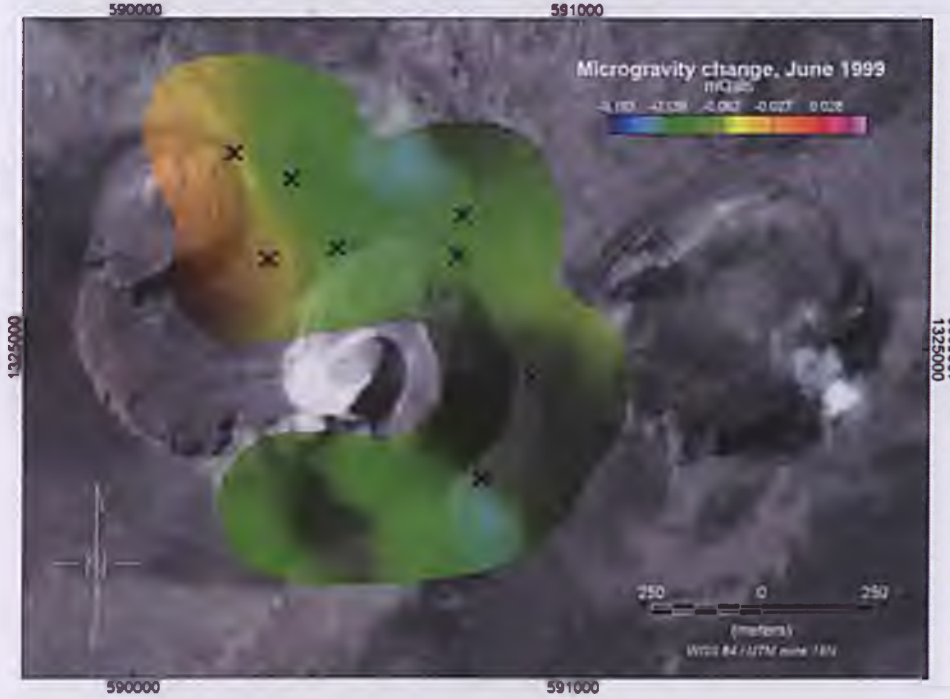
590000
591000
Microgravity change, June 1999
1325000
250 0 250
(meters)
590000
591000

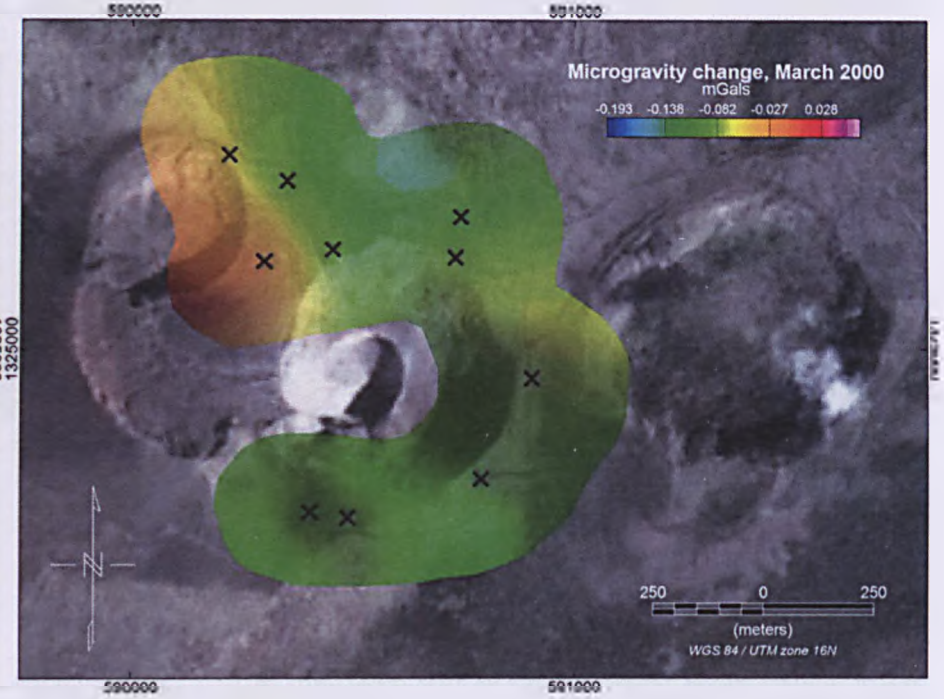
590000
591000
Microgravity change, March 2000
mGals
-0.193 -0.138 -0.082 -0.027 0.028
1325000
250 0 250
(meters)
WGS 84 / UTM zone 16N

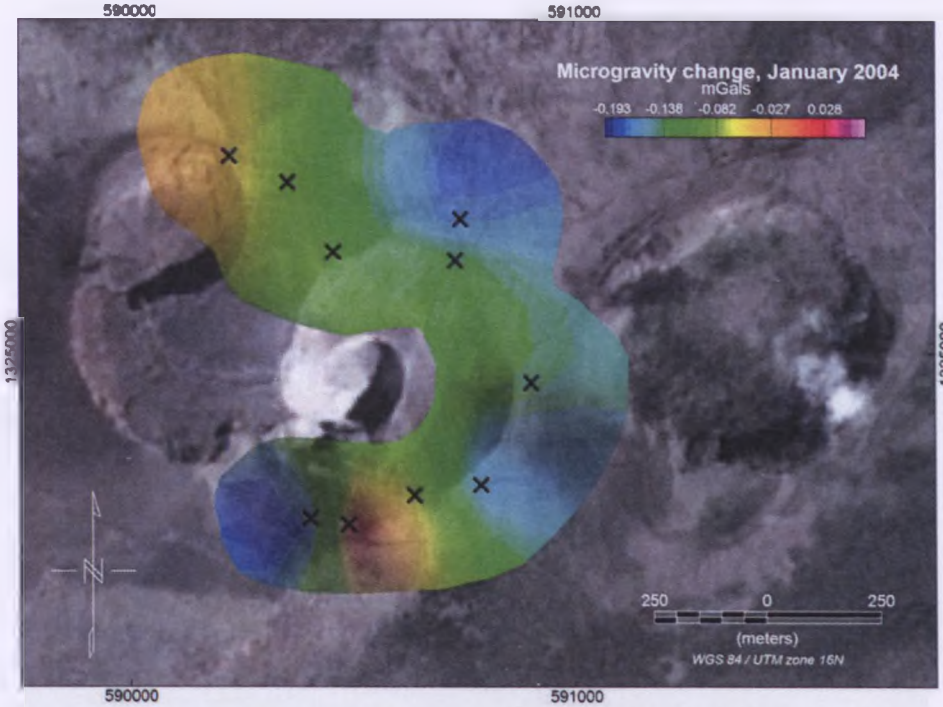
590000
591000
Microgravity change, January 2004
mGals
-0.193 -0.138 -0.082 -0.027 0.028
1325000
250 0 250
(meters)
WGS 84 / UTM zone 16N

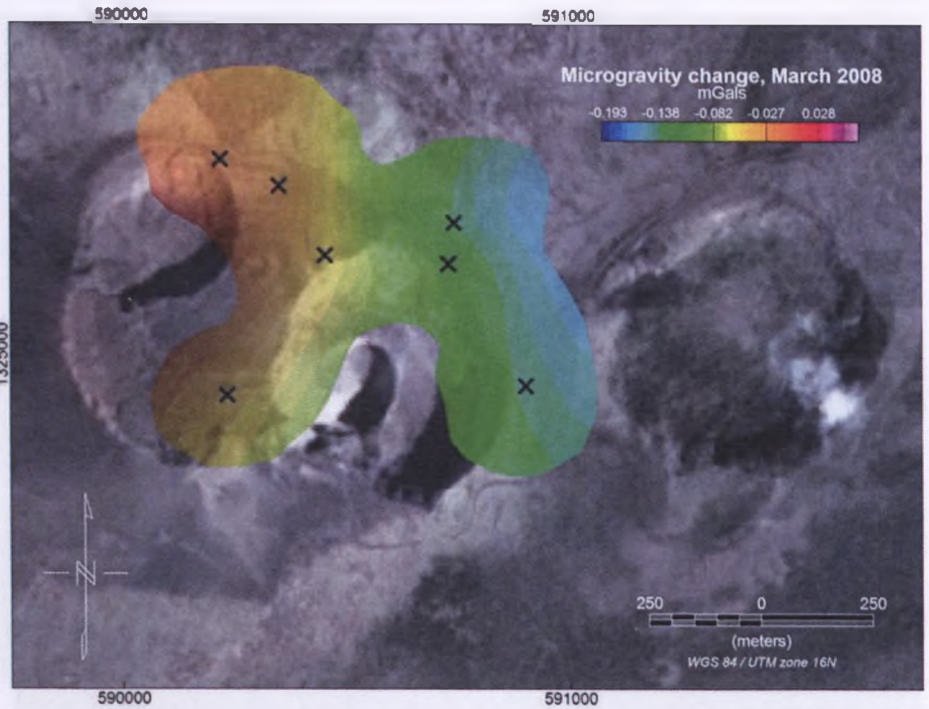
590000
591000
Microgravity change, March 2008
mGals
-0.193 -0.138 -0.082 -0.027 0.028
1325000
250 0 250
(meters)
WGS 84 / UTM zone 16N

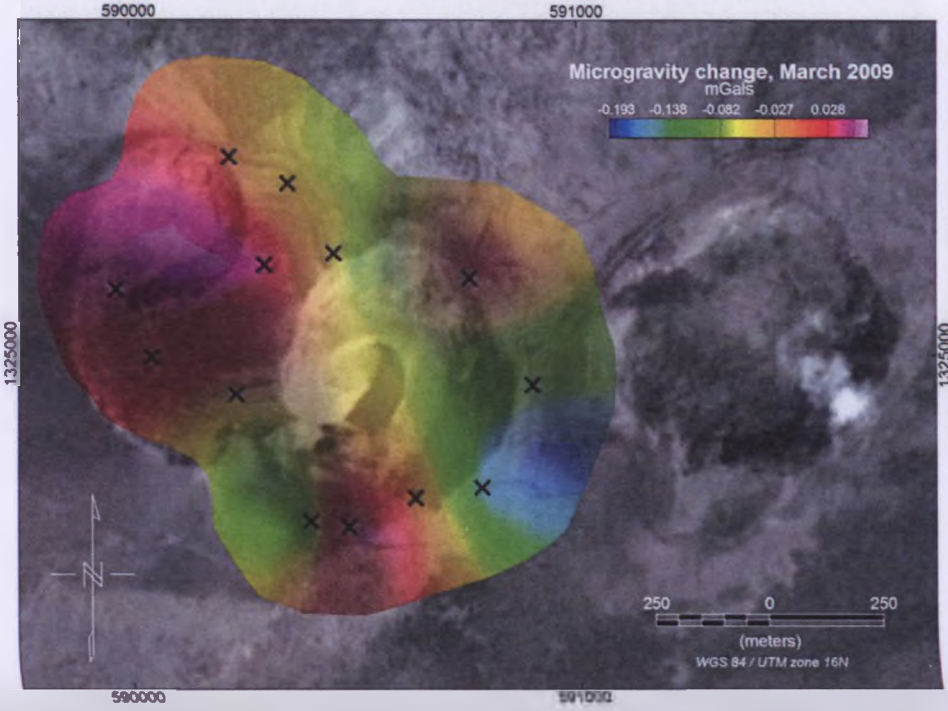
590000
591000
Microgravity change, March 2009
mGals
-0.193 -0.138 -0.082 -0.027 0.028
1325000
250 0 250
(meters)
WGS 84 / UTM zone 16N

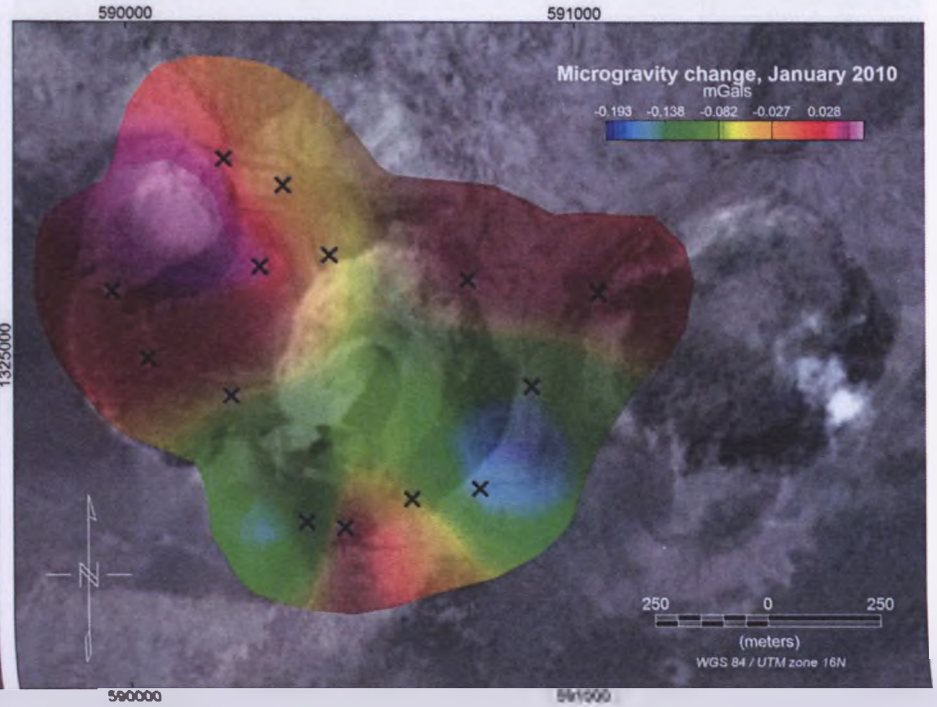
590000
591000
Microgravity change, January 2010
mGals
-0.193 -0.138 -0.082 -0.027 0.028
1325000
250 0 250
(meters)
WGS 84 / UTM zone 16N

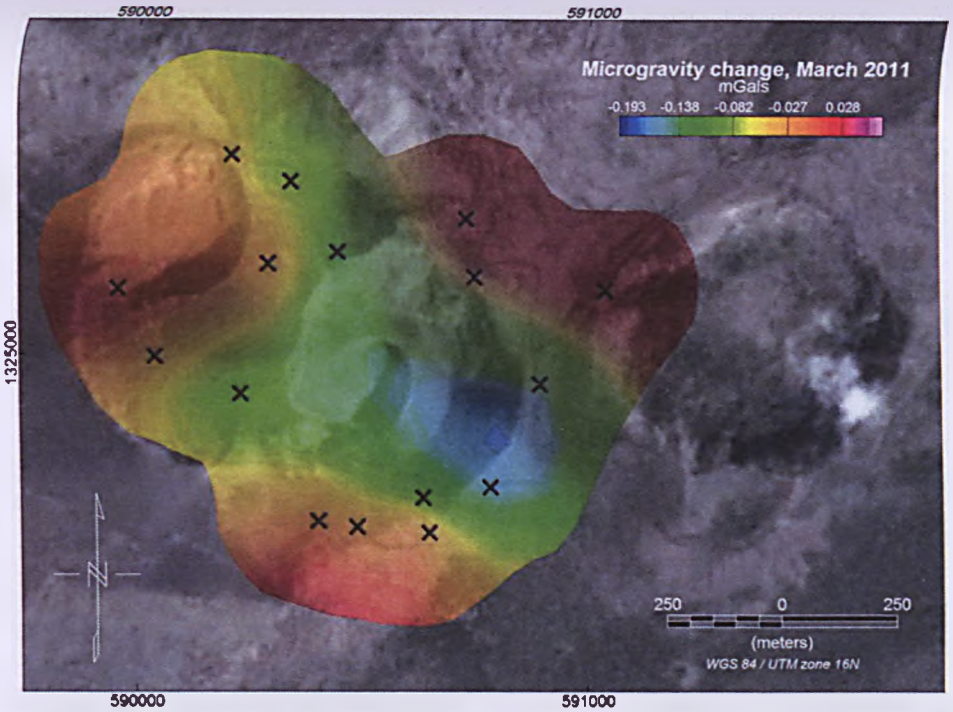

Figure 5-9: Time series of microgravity changes in the summit area of Masaya Volcano. The number of microgravity stations, marked by black crosses, has increased over time. The data were extracted from Table 5-2.

5.4 Discussion and conclusions

5.4.1 Caldera scale

Satellite gravity data are consistent with the presence of a large positive gravity anomaly to the NE of the Caldera (Connor and Williams 1989; Metaxian 1994), but its location is displaced to the SE compared with the anomaly found by Metaxian (1994) and section 5.3.2 (land gravity survey) of this study. The most probable explanation for this is the lack of detail provided by satellite gravity data.

Although the land gravity survey referred here (Figure **5-3**) has confirmed the presence of the anomaly, its location also differs (Figure 5-10) from the one proposed by Connor and Williams (1989) and Metaxian (1994), since its centre (maximum gravity value) partially underlies the NE part of the caldera (1 km to the SW of the centre of Metaxian's anomaly). This difference, probably caused by the smaller resolution of Satellite, Connor and Williams (1989) and Metaxian (1994) data, has important implications in terms of regional structural framework and caldera evolution. A dense intrusion located underneath the caldera itself might have an important effect on caldera processes such as subsidence of the ring fault (see Chapter 3), formation of magma chambers, etc. Regarding the characteristics of the intrusion, Metaxian (1994) suggested an elongated, 10-15 km diameter, 6 km thick gabbroic intrusion with a density 0.6 g/cm^3 higher than the surrounding rocks as the source of the anomaly (Table 1). The elongated shape has been confirmed by the Bouguer land gravity survey (Figure **5-3**). To compare the effect of an intrusion with the characteristics postulated by Metaxian with the Bouguer Anomaly map obtained after the land gravity survey, two 2D models have been built; but the gravity response of the models is not compatible with the characteristics of the pluton defined in this gravity study (the amplitude and wavelength of the calculated response would be significantly larger than the observed gravity in Figure **5-3**). The reason for the differences between the theoretical gravity response calculated in the 2D models and the Bouguer Anomaly map in this study is that the intrusive body has a smaller size, larger depth or smaller density contrast with the surrounding rocks, than previously believed.

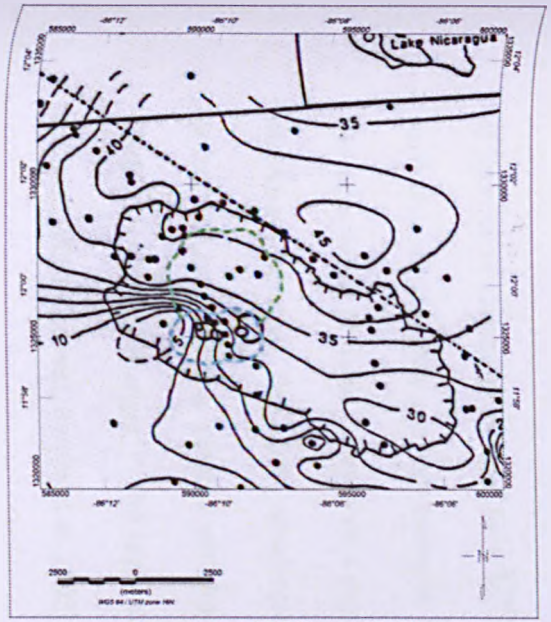

Connor and Williams, 1989

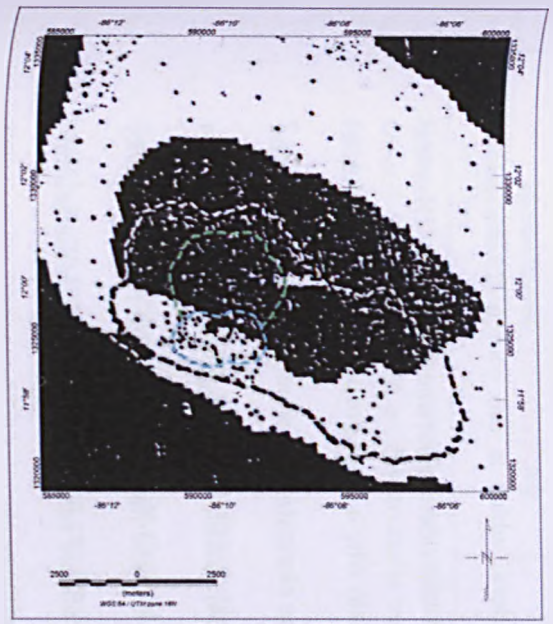

Metaxian, 1994

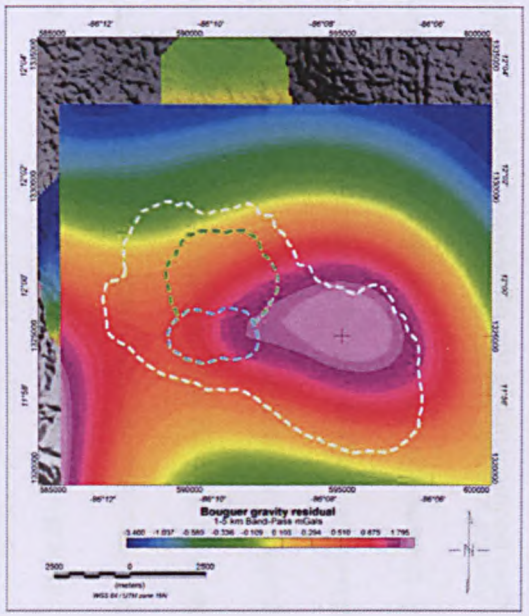

Satellite gravity, this study

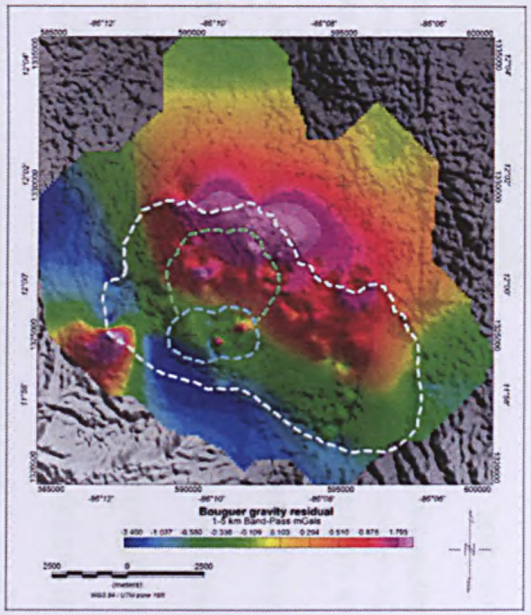

Bouguer gravity, this study

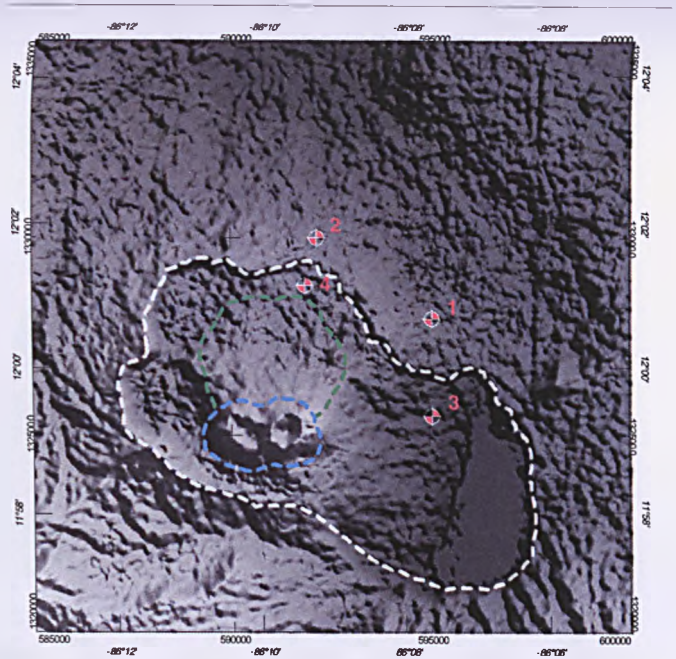

Location of the central point of the positive anomaly (defined as the intersection between the longest and shortest axis of the anomaly) for different authors.
1: Connor and Williams (1989).
2. Metaxian (1994).
3: Satellite gravity, this study.
4: Bouguer gravity, this study.

Figure 5-10: Location of the positive gravity anomaly NE of the Caldera according to different authors.

Different types of filters have been applied to the Bouguer gravity data in an effort to remove the signal induced by the large intrusion, and a 1-5 km band-pass filter has been selected as the most suitable for this scope. The residual gravity map produced after applying the filter shows a strong positive anomaly aligned with a NNW-SSE orientation that crosses the caldera (Figure **5-7**). If we compare the location of that gravity anomaly with the structural map compiled in Chapter 3 (Figure **5-11**), we can see that the gravity anomaly is located in the area where a substantial volume has been erupted since the last Plinian eruption 2100 years ago (Pérez, Freundt et al. 2009). The anomaly also includes two of the few volcanic centres that are not related to any of the major faults on the caldera floor (i.e. the ring fault, and the Cofradias fault, see Chapter 3). A possible explanation is that an elongated and partially depleted magma chamber with magma denser than the surrounding rocks has formed underneath Masaya caldera, which is the source for numerous eruptions since the formation of the caldera. The spatial coincidence between a magma chamber and a structural weakness such as a ring fault would explain why a large proportion of the material erupted in Masaya has been produced within this area. The elongated shape might be related to the presence of the large intrusion defined by Metaxian (1994). Smaller positive gravity anomalies can also be found in areas 1, 2 and 3 (Figure **5-7**). While area 1 is presumably a product of residual gravity signal from the intrusive body, areas 2 and 3 are the probable result of small and dense plutons intruded in earlier stages of the evolution of the caldera. Area 4 in Figure **5-7** marks the presence of a sharp negative gravity anomaly. The boundary between the NNW-SSE positive anomaly and area 4 negative anomaly marks the presence of a structural boundary.

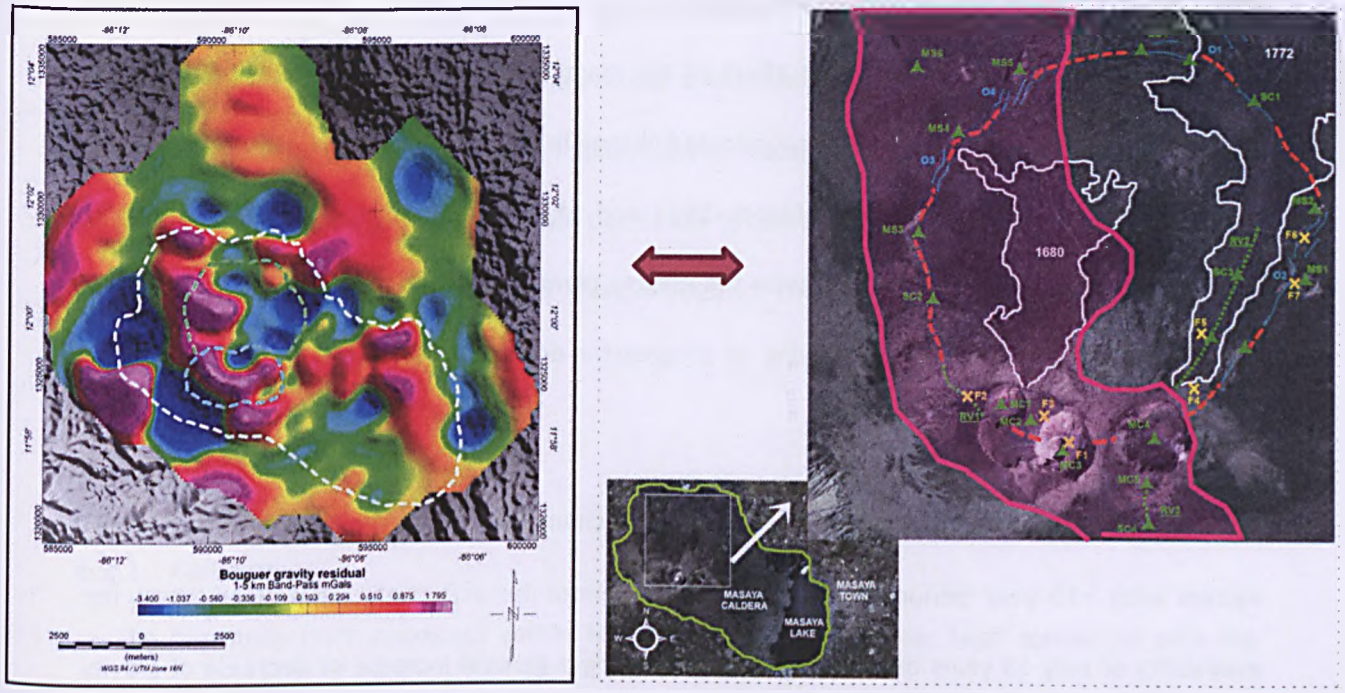

Figure 5-11: Comparison between the residual gravity map (left) and the structural map (right) compiled in Chapter 3. The pink area on the structural map represents the gravity high that crosses the caldera in the residual gravity map.

5.4.2 Summit area

The method used to study the evolution of the summit area in this study has been the microgravity technique. In spite of the still limited amount of data collected in Masaya (less than 20 years), some trends and patterns can be described. Using the data available we have defined three different processes, which take place with different periodicities and at different spatial scales (see Figure 5-9):

a) Short term variations: defined here as small (<60 μGal) annual changes in the value of gravity at a particular station; they are very common in Masaya and affect all the stations in the summit area. The occurrence of these changes on a regular basis testifies to the dynamism of the shallow region of Masaya volcano. The cyclic small-scale magma fluctuations are responsible for a repetitive process of cavern filling, magma withdrawal, roof collapse, etc. (Rymer, van Wyk de Vries et al. 1998). Short-term changes in the layer of vesiculated gas-rich magma that sits atop the magma column (Williams-Jones, Rymer et al. 2003) are responsible for the short term changes in gravity.

b) Mid-term variations: defined here as 2-5 years coherent descent or ascent of the gravity values (<100 μGal) measured in the summit area for all (or most) of the stations, are probably caused by magma injections or withdrawals that affect all the magma plumbing system underneath the pit crater region of Masaya Volcano. This coordinated change in the gravity values, clearly illustrated by the gravity drop occurred between March 1997 and March 2000, suggests a high degree of connectivity of all structures that comprise the magma plumbing system of Masaya Volcano. These changes can also be caused by thinning or progressive degassing of vesiculated layers injected periodically.

c) Long-term variations: proposed here as an internal change in the organization of the plumbing system with >10 year periodicity (the periodicity cannot be accurately determined given the availability of only 18 years of data). Instead of showing a general increase or decrease of gravity values that might be evidence for magma withdrawal or Injection processes for the area, the contrasts in gravity values sharpen, with a clearly defined positive anomaly areas beside negative anomaly areas. The difference between the maximum and minimum gravity values in the summit area goes then from <100 μGal in the less active phase of the cycles, to a difference of >200 μGal for the most active phases of the cycle. This might be evidence for an overturn at depth of recharged gas-rich magma that rises buoyantly, generating new temperature and density contrasts in the shallow part of the plumbing system, and favouring the renovation or generation of new small convection cells. Evidence for the presence of these convection cells can be found in the March 2009, January 2010, March 2011 maps of Figure 5-9, that show a clearly compartmentalised gravity signal where the gravity highs would correspond to denser, degassed magma in descent, and the lows would correspond to buoyant, gas-rich magma in ascent. The data from January 2004 probably show an intermediate stage between a steady state with not very active convective cells and a state of enhanced activity with density contrast-driven magma movement.

6 General conclusions

6.1 Introduction

The scope of this thesis was to improve our understanding of the characteristics of Masaya Volcano's structural framework, and its implications for hazard assessment. For this, a combination of geophysical and geological methods has been used to characterize the structural features present in the summit area and caldera floor of Masaya Volcano. The conclusions of the present work are summarized below.

6.2 Conclusions

6.2.1 Caldera

The two main fault structures within Masaya Caldera are a linear fault connected with the Cofradias Fault (Eastern limiting fault of the Managua graben, Figure 3-1) and a ring fault structure (Figure 3-2) generated after the last Plinian eruption (2.1 ka). The linear fault is the source of the last lava flow erupted from Masaya Volcano in 1772 (Figure 1-5). The ring fault defines a nested caldera within Masaya Caldera, with subsidence taking place in the SW part of the inner lid and numerous volcanic manifestations on its outline. Gravity studies reveal the presence of a dense body that crosses the SW corner of the caldera in a NNW-SSE direction (Figure 5-7) at a depth of 1-3 km. The spatial coincidence of this body (interpreted as a basaltic magma reservoir) below the ring fault is responsible for the concentration of erupted material in the SW section of the ring fault (Figure 5-11). The material erupted from this magma reservoir has built several volcanic cones (including the summit area of Masaya Volcano) that account for most of the volcanic material erupted in the last 2.1 ka in the caldera, thus contributing to partially emptying the reservoir. This has probably facilitated the subsidence observed in this region (Figure 3-8).

This investigation has also confirmed the presence of a previously known elongated intrusion (Connor and Williams 1989; Metaxian 1994) to the NE of Masaya Caldera. However, while in this thesis it is suggested that the intrusion is located partially underlying the NE part of the caldera, in

previous studies (Connor and Williams 1989; Metaxian 1994) the intrusion is more distant from the centre of the caldera (Figure 5-10). These differences in horizontal position are probably caused by the large levels of error present in previous datasets and improved in this thesis by the use of state-of-the-art instrumentation.

6.2.2 Summit area

The geometry at depth of a fault network that pierces the upper part of Masaya summit area has been characterized. VLF studies show that this network is occupied by an active hydrothermal system (Figure 4-4). Bouguer gravity studies have revealed the location of a degassed magma batch ≈300 m under Nindiri frozen lava lake denser than the gas-rich magma under Santiago active pit crater (Figure 4-3). Microgravity studies have revealed (Figure 5-9) that subsurface mass transfer in the summit area occurs on different timescales. Short-term changes (<1 year, <60 μGal) are caused by cyclic small-scale magma fluctuations like cavern filling, roof collapse, etc. Mid-term variations (2-5 years, <100 μGal) affect all the magma plumbing system and are the result of magma injections-withdrawals or changes in the vesiculated layer underneath the summit area. Long-term variations (>10 year, stable areas of minimum and maximum gravity values are defined) are caused by the ascent of gas-rich magma that creates density and temperature contrasts in the upper part of the magma column, generating active and relatively stable (several years period) convective cells. Mid-term and long-term cycles are responsible for the main changes in surface activity.

6.2.3 Methodology: combination of VLF and gravity techniques

A combination of VLF and Bouguer gravity techniques has been successful in characterizing the structural framework of Masaya Volcano's summit area, and also in identifying a water-bearing lava tube system in the Southern slopes of Masaya's cone. The combination of these geophysical techniques can provide very accurate information on size, depth, shape and geometry (inclination, tilt direction) of buried geological structures that generate both density and conductivity contrasts with the surrounding materials. This applies to a number of geological features in volcanic settings,

including lava tubes, dikes, faults and voids, and is especially effective for studying the hydrothermal system, making this fast and cost-effective technique advantageous for volcanology and geothermal research.

6.3 Future work

At present, insufficient mitigation strategies related to hazardous volcanic events have been designed or implemented for the Masaya region. INETER (Nicaraguan Institute of Territorial Studies) is responsible for Masaya Volcano's Early Warning System, which consists of one seismic station deployed within the caldera and two geochemistry stations near known fumaroles that store data (which are regularly retrieved by INETER). Only three documents exist that include references to evacuation plans or hazard maps for the Masaya area:

- A series of Volcanic Hazard Maps of Masaya (Delgado-Granados 2002a) with a representation of the areas subject to potential risks was completed in 2002. The associated report (Delgado-Granados 2002b) succinctly describes the volcanic hazards with the potential to affect the Masaya area, but no Evacuation Plans are described in this document.
- A Departmental Memorandum (SINAPRED 2004) states that a yellow or red alert will trigger the evacuation of local population. A yellow alert is defined as a hazardous volcanic event that will occur imminently, and a red alert is activated during and after the event takes place. According to this document, local authorities and the Commission of Special Operations are in charge in case of emergency. The Memorandum estimates that in the event of an evacuation only 30% of the population at risk can be effectively rescued.
- A publicly undisclosed generic plan for hazardous events (Plan contingente ante sismo y erupción volcánica de la Macro Región del Pacífico, or Contingency Plan: Earthquakes and Volcanic Eruptions in the Pacific Region) designed by the Nicaraguan Army provides guidelines for the implementation of mitigation measures in case of a volcanic eruption in Nicaraguan territory.

To palliate the deficiencies of current preparation plans and improve our knowledge of Masaya Volcano's characteristics, so that the areas threatened by certain types of volcanic activity can be more precisely defined, the evolution of volcanic processes can be effectively monitored and strategies to exploit its resources (e.g. geothermal energy) can be implemented; a variety of further studies could be undertaken:

- Acquisition of a dense Bouguer gravity dataset (currently limited to the open trails within the caldera) that includes the entire caldera floor with high station density (100 m grid spacing) would provide more detailed information on the geometry of the elongated (NNW-SSE) magma chamber discovered in this study and other magma batches under Masaya Caldera.
- Acquisition of a dense magnetic dataset (currently limited to the open trails) that includes the entire caldera floor with enough station density (20 m grid spacing) would provide more information on the location and geometry of dikes. An expansion of the total magnetic field survey beyond the edges of the caldera would also permit the depth to the Curie temperature isotherm to be mapped (complementary with the gravity study).
- Acquisition of a dense VLF dataset (currently limited to the open trails) in combination with Ground Penetrating Radar (GPR) techniques that includes the entire caldera floor with enough station density (20 m grid spacing) would provide more information on the location and geometry of faults and shallow manifestations of the hydrothermal system.
- Design and implementation of an effective Early Warning System tailored using the knowledge on Masaya Caldera's existing volcanic structures acquired in this thesis. In addition to the summit area, where most volcanic activity has occurred in historical times, the area where the SW section of the ring fault and the elongated (NNW-SSE) magma reservoir coincide spatially should be considered a high priority in terms of volcano monitoring.
- Continuous monitoring tools such as seismic networks combined with continuous gravimetry have the potential to characterize signs of activity prior to eruptions.

To improve our knowledge of the characteristics of society in the area and enhance the effectiveness of mitigation strategies, several measures could be undertaken in collaboration with local population:

- Semi-structured interviews addressed at representative samples of population affected by volcanic processes in the Masaya area that deal with general social aspects and knowledge of the volcano by locals, would improve our understanding of the characteristics, preparation and perception of volcanic threats of population in the area. Given the small penetration of English in Nicaraguan society, a native speaker of Spanish would be most effective in this project.
- Activities designed to raise the level of awareness of volcanic threats are essential for a successful implementation of mitigation strategies. Given the high primary school drop-out rate in the area, public outreach activities addressed at early levels of formal education would be most effective in accomplishing this task.
- As a third part of this project, preparation plans should be designed in collaboration with Nicaraguan government entities such as INETER, and a strategy for implementing those plans in the case of volcano-related emergencies should be prepared and tested.

To improve the VLF/gravity method applied in this thesis to a basaltic caldera, its effectiveness should be tested in different volcanic environments, including areas with active lava flows and lava tunnels (building on the work by Zablocki (1978) on VLF studies of Kilauea volcano) and volcanic environments with different lithologies and density/conductivity characteristics. Ground Penetrating Radar (GPR) methods used at the beginning of a gravity/VLF survey can help to identify the geometry at depth (tilt angle, tilt direction) of a conductive body source of a VLF anomaly in a specific area, thus characterizing the relationship between VLF response and geometry at depth for the entire survey.

7 References

Al-Oufi, A., H. Mustafa, et al. (2008). "Exploration of the extension of two lava tubes, faults and dikes using very low frequency-electromagnetic technique in NE Jordan." Acta Geophysica 56(2): 466-484.

Anderson, S., E. Stofan, et al. (1999). "Pulsed inflation of pahoehoe lava flows: implications for flood basalt emplacement." Earth and Planetary Science Letters 168(1): 7-18.

Andò, B. and D. Carbone (2001). "A methodology for reducing the effect of meteorological parameters on a continuously recording gravity meter." 50(5): 1248-1254.

Andò, B. and D. Carbone (2004). "A test on a Neuro-Fuzzy algorithm used to reduce continuous gravity records for the effect of meteorological parameters." Physics of the Earth and Planetary Interiors 142: 37-47.

Andò, B. and D. Carbone (2006). "A new computational approach to reduce the signal from continuously recording gravimeters for the effect of atmospheric temperature." Physics of the Earth and Planetary Interiors 159: 247-256.

Atlas, Z. D. (2008). "Volatiles in melt inclusions from Mexican and Nicaraguan volcanoes: implications for complex degassing processes", Ph.D. Thesis, University of Miami, Coral Gables, USA.

Barberi, F., E. Cassano, et al. (1991). "Structural evolution of Campi Flegrei caldera in light of volcanological and geophysical data." Journal of Volcanology and Geothermal Research 48(1): 33-49.

Barclay, J., K. Haynes, et al. (2008). "Framing volcanic risk communication within disaster risk reduction: finding ways for the social and physical sciences to work together." Geological Society, London, Special Publications 305(1): 163-177.

Baxter, P. J., R. E. Stoiber, et al. (1982). "Volcanic gases and health: Masaya Volcano, Nicaragua." The Lancet 320(8290): 150-151.

Berardino, P., G. Fornaro, et al. (2002). "A new algorithm for surface deformation monitoring based on small baseline differential SAR interferograms." Geoscience and Remote Sensing, IEEE Transactions on 40(11): 2375-2383.

Berrino, G., H. Rymer, et al. (1992). "Gravity-height correlations for unrest at calderas." Journal of Volcanology and Geothermal Research 53(1): 11-26.

Bice, D. C. (1980). "Tephra stratigraphy and physical aspects of recent volcanism near Managua, Nicaragua." Ph.D. Thesis, University of California, Berkeley, USA.

Bice, D. C. (1985). "Quaternary volcanic stratigraphy of Managua, Nicaragua: Correlation and source assignment for multiple overlapping plinian deposits." Geological Society of America Bulletin 93: 553-566.

Bonvalot, S., Albouy, Y., Remy, D., Metaxian, J.-P., Lesage, and P. P., O. (1992). "Geophysical survey of the Masaya Caldera (Nicaragua)." Eos 73 (43, suppl.): 348.

Bonvalot, S., J. P. Metaxian, et al. (1995). "Gravity and GPS studies at Masaya Volcano (Nicaragua): Structural modelling and monitoring volcanic activity." IUGG XIX meeting. Boulder, Colorado (USA).

Bonvalot, S., M. Diament, et al. (2002). "Continuous gravity recording with Scintrex CG-3M meters: a promising tool for monitoring active zones." Geophysical Journal International 135(2): 470-494.

Branan, Y. K. (2007). "Investigating short-term variation in volcanic plume and shallow subsurface dynamics using high temporal resolution gas emission rate data." Ph.D. Thesis, Michigan Technological University, Ann Arbor (USA).

Branan, Y. K., A. Harris, et al. (2008). "Investigation of at-vent dynamics and dilution using thermal infrared radiometers at Masaya volcano, Nicaragua." Journal of Volcanology and Geothermal Research 169(1-2): 34-47.

Broucke, R., W. Zürn, et al. (1972). "Lunar tidal acceleration on a rigid Earth", in Flow and Fracture of Rocks (eds H. C. Heard, I. Y. Borg, N. L. Carter and C. B. Raleigh), American Geophysical Union, Washington (USA): 319-324.

Brown, G., H. Rymer, et al. (1987). "The evolution of andesite volcano structures: new evidence from gravity studies in Costa Rica." Earth and Planetary Science Letters 82(3): 323-334.

Brown, R. D., P. L. Ward, et al. (1973). "Geologic and seismologic aspects of the Managua, Nicaragua, earthquakes of December 23, 1972." U.S. Geological Survey Professional Paper 838, 64(4): 1031.

Burton, M. R., C. Oppenheimer, et al. (2000). "Remote sensing of CO2 and H2O emission rates from Masaya volcano, Nicaragua." Geology 28(10): 915-918.

Burton, M., C. Oppenheimer, et al. (2001). "Diurnal changes in volcanic plume chemistry observed by lunar and solar occultation spectroscopy." Geophysical Research Letters 28(5): 843-846.

Calvari, S. and H. Pinkerton (1999). "Lava tube morphology on Etna and evidence for lava flow emplacement mechanisms." Journal of Volcanology and Geothermal Research 90(3-4): 263-280.

Camacho, A. G., J. C. Nunes, et al. (2007). "Gravimetric determination of an intrusive complex under the Island of Faial (Azores): some methodological improvements." Geophysical Journal International 171(1): 478-494.

Camacho, A., R. Vieira, et al. (1991). "Microgravimetric model of the Las Cañadas caldera (Tenerife)." Journal of Volcanology and Geothermal Research 47(1): 75-88.

Carbone, D., L. Zuccarello, et al. (2006). "Analysis of simultaneous gravity and tremor anomalies observed during the 2002-2003 Etna eruption." Earth and Planetary Science Letters 245(3-4): 616-629.

Carbone, D., L. Zuccarello, et al. (2008). "Geophysical indications of magma uprising at Mt Etna during the December 2005 to January 2006 non-eruptive period." Geophysical Research Letters 35(6): L06305.

Carr, M. J., I. Saginor, et al. (2007). "Element fluxes from the volcanic front of Nicaragua and Costa Rica." Geochemistry, Geophysics, Geosystems 8(6): 1–22.

Chiodini, G., Granieri, D., Avino, R., Caliro, S., Costa, A., and Werner, C. (2005). "Carbon dioxide diffuse degassing and estimation of heat release from volcanic and hydrothermal systems." Journal of Geophysical Research 110(B8): B08204.

Chitwood, L. (1994). "Inflated basaltic lava—Examples of processes and landforms from central and southeast Oregon." Oregon Geology 56(1): 11-21.

Cole, J. W., D. M. Milner, et al. (2005). "Calderas and caldera structures: a review." Earth-Science Reviews 69(1-2): 1-26.

Collett, L. and A. Becker (1968). "Radiohm method for earth resistivity mapping." Canadian Patent CA795919A.

Connor, C. and S. Williams (1989). Interpretation of gravity anomalies, Masaya Caldera Complex, Nicaragua. Preprint: Transaction of the 12th Caribbean Conference, St Croix, Virgin Islands.

Costantini, L., C. Bonadonna, et al. (2009). "New physical characterization of the Fontana Lapilli basaltic Plinian eruption, Nicaragua." Bulletin of Volcanology 71: 337–355.

Crenshaw, W. B., S. N. Williams, et al. (1982). "Fault location by radon and mercury detection at an active volcano in Nicaragua." Nature 300(5890): 345-346.

D'Angelo, A. G., Marbel (2009). "Explorando la ruta de la igualdad: trabajo, género y turismo en Nicaragua." UNIFEM, AGEM: 200.

Del Pezzo, E., F. Bianco, et al. (2001). "Separation of intrinsic and scattering Q for volcanic tremor: an application to Etna and Masaya Volcanoes." Geophysical Research Letters 28(16): 3083-3086.

Delgado-Granados, H., Navarro-Collado, M., Ferraz-Montes, I. (2002a). "Mapa de Amenaza Volcánica, Volcán Masaya." Managua, Geofisica UNAM / INETER / Japan International Cooperation Agency.

Delgado-Granados, H., Navarro-Collado, M., Ferraz-Montes, I. (2002b). "Report: Mapa de Amenaza Volcánica, Volcán Masaya." Managua, Geofisica UNAM / INETER / Japan International Cooperation Agency: 120.

Delmelle, P., J. Stix, et al. (2001). "Dry Deposition and Heavy Acid Loading in the Vicinity of Masaya Volcano, a Major Sulfur and Chlorine Source in Nicaragua." Environmental Science & Technology 35(7): 1289-1293.

Delmelle, P., P. Baxter, et al. (1999). "Origin, effects of Masaya volcano's continued unrest probed in Nicaragua." Eos, Transactions American Geophysical Union 80(48):575–581.

Deplus, C., S. Bonvalot, et al. (1995). "Inner structure of the Krakatau volcanic complex (Indonesia) from gravity and bathymetry data." Journal of Volcanology and Geothermal Research 64(1): 23-52.

Duffell, H. J., C. Oppenheimer, et al. (2003). "Changes in gas composition prior to a minor explosive eruption at Masaya volcano, Nicaragua." Journal of Volcanology and Geothermal Research 126(3-4): 327-339.

Ebmeier, S. K., Biggs, J., Mather, T. A. and Amelung, F. (2013). "On the lack of InSAR observations of magmatic deformation at Central American volcanoes." Journal of Geophysical Research: Solid Earth 118(5): 2571–2585.

Eggers, A. A. and D. Chavez (1979). "Temporal gravity variations at Pacaya volcano, Guatemala." Journal of Volcanology and Geothermal Research 6(3): 391-402.

Elston, W. (1994). "Evolution of Volcanic and Tectonic Features in Caldera Settings and Their Imporeance in the localization of Ore Deposits." Economic Geology 89:1662-1686.

Fernández, W. P. (2007). "Basaltic Plinian and Violent Surtseyan Eruptions from the Masaya Caldera Complex, Nicaragua." Ph.D. Thesis, Christian-Albrechts-Universität, Kiel, Germany.

Fialko, Y. and M. Simons (2001). "Evidence for on-going inflation of the Socorro magma body, New Mexico, from Interferometric Synthetic Aperture Radar imaging." Geophysical Research Letters 28(18): 3549-3552.

Fraser, D. (1969). "Contouring of VLF-EM data." Geophysics 34(6): 958-967.

Galle, B., C. Oppenheimer, et al. (2003). "A miniaturised ultraviolet spectrometer for remote sensing of SO2 fluxes: a new tool for volcano surveillance." Journal of Volcanology and Geothermal Research 119(1-4): 241-254.

Galle, B., M. Johansson, et al. (2010). "Network for Observation of Volcanic and Atmospheric Change (NOVAC)—A global network for volcanic gas monitoring: Network layout and instrument description." Journal of Geophysical Research 115(D5): D05304.

Gamboa, M. and H. López (2008). "Cada casa es un taller: Estudio sobre el sector artesanía con enfoque de género." UNIFEM, Managua (Nicaragua): 128.

García-Bresó, J. (1990). "Identidad y cultura en Nicaragua: estudio antropológico de Monimbó." Ph.D. Thesis, Universidad Complutense de Madrid, Madrid (Spain).

Girard, G. and B. van Wyk de Vries (2005). "The Managua Graben and Las Sierras-Masaya volcanic complex (Nicaragua); pull-apart localization by an intrusive complex: results from analogue modeling." Journal of Volcanology and Geothermal Research 144(1-4): 37-57.

Goepfert, K. and J. E. Gardner (2010). "Influence of pre-eruptive storage conditions and volatile contents on explosive Plinian style eruptions of basic magma." Bulletin of Volcanology 72: 511-521.

Goff, F. and J. N. Gardner (1988). "Valles caldera region, New Mexico, and the emerging continental scientific drilling program." Journal of Geophysical Research 93(B6): 5997-5999.

Goodkind, J. M. (1986). "Continuous measurement of nontidal variations of gravity." Journal of Geophysical Research 91(B9): 9125-9134.

Google-Inc. (2013). Google Earth. Version 7.1.1.1888.

Gottsmann, J., A. G. Camacho, et al. (2008). "Shallow structure beneath the Central Volcanic Complex of Tenerife from new gravity data: Implications for its evolution and recent reactivation." Physics of the Earth and Planetary Interiors 168(3-4): 212-230.

Gudmundsson, M. T. and J. Milsom (1997). "Gravity and magnetic studies of the subglacial Grímsvötn volcano, Iceland: Implications for crustal and thermal structure." Journal of Geophysical Research: Solid Earth 102(B4): 7691-7704.

Hammer, S. (1939). "Terrain corrections for gravimeter stations." Geophysics 4(3): 184-194.

Harris, A. (2009). "The pit-craters and pit-crater-filling lavas of Masaya volcano." Bulletin of Volcanology 71(5): 541-558.

Heiken, G. and F. Goff (1983). "Hot dry rock geothermal energy in the Jemez volcanic field, New Mexico." Journal of Volcanology and Geothermal Research 15(1-3): 223-246.

Henkel, H. and M. Guzman (1977). "Magnetic features of fracture zones." Geoexploration 15(3): 173-181.

Hoekstra, P., P. Sellmann, et al. (1975). "Ground and airborne resistivity surveys of permafrost near Fairbanks, Alaska." Geophysics 40(4): 641-656.

Hon, K., J. Kauahikaua, et al. (1994). "Emplacement and inflation of pahoehoe sheet flows: observations and measurements of active lava flows on Kilauea Volcano, Hawaii." Geological Society of America Bulletin 106(3): 351-370.

Horrocks, L. A. (2001). "Infrared spectroscopy of volcanic gases at Masaya, Nicaragua.", Ph.D. Thesis, The Open University, Milton Keynes (UK).

Horrocks, L., M. Burton, et al. (1999). "Stable gas plume composition measured by OP‐FTIR spectroscopy at Masaya Volcano, Nicaragua, 1998–1999." Geophysical Research Letters 26(23): 3497-3500.

Hunsucker, R. D. and J. K. Hargreaves (2002). "The high-latitude ionosphere and its effects on radio propagation." Cambridge University Press, Cambridge (UK): 20.

ILO. (1989). "International Labour Organization C169 - Indigenous and Tribal Peoples Convention." from http://www.ilo.org/dyn/normlex/en/f?p=NORMLEXPUB:12100:0::NO::P12100_ILO_CODE:C169.

INEC (1995). "VII Censo de Población y III de Vivienda. Resumen Censal." Managua, Instituto Nacional de Estadísticas y Censos: 87.

INEC (2006). "VIII Censo de Población y IV de Vivienda. Población por municipios." Managua, Instituto Nacional de Estadísticas y Censos. IV: 551.

Jaggar, T. (1931). "Lava stalactites, stalagmites, toes, and" squeeze-ups." The Volcano Letter 345: 1-3.

Johnson, G. V., A. Bjornsson, et al. (1980). "Gravity and elevation changes caused by magma movement beneath the Krafla caldera, northeast Iceland." Journal of Geophysics 47(1-3): 132-140.

Johnson, N. a. P. J., R. A. (1986). "Composition, distribution and neutralization of "acid rain" derived from Masaya volcano, Nicaragua." Tellus 38B: 106-117.

Jousset, P., S. Dwipa, et al. (2000). "Temporal gravity at Merapi during the 1993–1995 crisis: an insight into the dynamical behaviour of volcanoes." Journal of Volcanology and Geothermal Research 100(1): 289-320.

Karous, M. and S. Hjelt (1977). "Determination of apparent current density from VLF measurements", University of Oulu, Oulu (Sweden): 89.

Karous, M. and S. Hjelt (1983). "Linear filtering of VLF dip-angle measurements." Geophysical Prospecting 31: 782-794.

Kauahikaua, J., M. Mangan, et al. (1996). "A quantitative look at the demise of a basaltic vent: the death of Kupaianaha, Kilauea Volcano, Hawaii." Bulletin of Volcanology 57(8): 641-648.

Kern, C., H. Sihler, et al. (2009). "Halogen oxide measurements at Masaya Volcano, Nicaragua using active long path differential optical absorption spectroscopy." Bulletin of Volcanology 71: 659–670.

Klein, Jan, and J. Lajoie, 1980. "Electromagnetic Prospecting for Minerals." in Practical Geophysics for the Exploration Geologist, Northwest Mining Association, Spokane (USA): 239-290.

Kutterolf, S., A. Freundt, et al. (2007). "Late Pleistocene to Holocene temporal succession and magnitudes of highly-explosive volcanic eruptions in west-central Nicaragua." Journal of Volcanology and Geothermal Research 163(1-4): 55-82.

Kutterolf, S., A. Freundt, et al. (2008). "Pacific offshore record of plinian arc volcanism in Central America: 1. Along-arc correlations." Geochemistry Geophysics Geosystems 9(2): Q02S01.

La Femina, P., T. Dixon, et al. (2002). "Bookshelf faulting in Nicaragua." Geology 30(8): 751-754.

Lehto, H. L. (2007). "Self-Potential Anomalies and CO2 Flux on Active Volcanoes: Insights from Time and Spatial Series at Masaya, Telica, and Cerro Negro, Nicaragua." PhD Thesis, University of South Florida. Tampa (USA).

Leica. (1999). "Technical Reference Manual, GPS System 500. Leica." Retrieved 10th December 2013, from http://www.virginiadot.org/business/resources/locdes/survey-leica-gps-techref.pdf.

Lewicki, J. L., C. Connor, et al. (2003). "Self-potential, soil CO2 flux, and temperature on Masaya volcano, Nicaragua." Geophysical Research Letters 30(15).

Lewicki, J., D. Bergfeld, et al. (2005). "Comparative soil CO2 flux measurements and geostatistical estimation methods on Masaya volcano, Nicaragua." Bulletin of Volcanology 68(1): 76-90.

Lipman, P. W. (1984). "The roots of ash flow calderas in western North America: windows into the tops of granitic batholiths." Journal of Geophysical Research 89(B10): 8801-8841.

Lipman, P. W. (1997). "Subsidence of ash-flow calderas: relation to caldera size and magma-chamber geometry." Bulletin of Volcanology 59(3): 198-218.

Locke, C. A., H. Rymer, et al. (2003). "Magma transfer processes at persistently active volcanoes: insights from gravity observations." Journal of Volcanology and Geothermal Research 127(1-2): 73-86.

Lopez-Loera, H., J. Urrutia-Fucugauchi, et al. (2010). "Magnetic characteristics of fracture zones and constraints on the subsurface structure of the Colima Volcanic Complex, western Mexico." Geosphere 6(1): 35-46.

Lundgren, P., S. Usai, et al. (2001). "Modeling surface deformation observed with synthetic aperture radar interferometry at Campi Flegrei caldera." Journal of Geophysical Research 106(B9): 19.

Maciejewski, A. J. H. (1998). "Remote measurements of volcanic gases: Applications of open-path Fourier transform infrared spectroscopy (OP-FTIR) and Correlation spectroscopy (COSPEC)." PhD Thesis, The Open University, Milton Keynes (UK).

MacNeil, R. E. (2006). "Geophysical Investigations and Groundwater Modeling of the Hydrologic Conditions at Masaya Caldera, Nicaragua." MSc Thesis, University of South Florida, Tampa (USA).

MacNeil, R. E., W. E. Sanford, et al. (2007). "Investigation of the groundwater system at Masaya Caldera, Nicaragua, using transient electromagnetics and numerical simulation." Journal of Volcanology and Geothermal Research 166(3-4): 217-232.

Martin, E. and O. Sigmarsson (2007). "Low-pressure differentiation of tholeiitic lavas as recorded in segregation veins from Reykjanes (Iceland), Lanzarote (Canary Islands) and Masaya (Nicaragua)." Contributions to Mineralogy and Petrology 154(5): 559-573.

Martin, R. S., G. M. Sawyer, et al. (2012). "High-resolution size distributions and emission fluxes of trace elements from Masaya volcano, Nicaragua." Journal of Geophysical Research 117(B8): B08206.

Martin, R. S., Sawyer, G.M., Spampinato, L., Salerno, G.G., Ramirez, C., Ilyinskaya, E., Witt, M.L.I., Mather, T.A., Watson, I.M., Phillips, J.C., and Oppenheimer, C. (2010). "A total volatile inventory for Masaya Volcano, Nicaragua." Journal of Geophysical Research 115(9): B09215.

Martin, R. S., T. A. Mather, et al. (2010). "Major and trace element distributions around active volcanic vents determined by analyses of grasses: implications for element cycling and bio-monitoring." Bulletin of Volcanology 72: 1009-1020.

Martin, R., E. Ilyinskaya, et al. (2011). "A re-assessment of aerosol size distributions from Masaya volcano (Nicaragua)." Atmospheric Environment 45(3): 547-560.

Martin, R., T. Mather, et al. (2009). "Size distributions of fine silicate and other particles in Masaya's volcanic plume." Journal of Geophysical Research 114(D9): D09217.

Massonnet, D. and K. Feigl (1995). "Discrimination of geophysical phenomena in satellite radar interferograms." Geophysycal Research Letters 22(12): 1537–1540.

Massonnet, D. and K. Feigl (1998). "Radar interferometry and its application to changes in earth's surface." Revue Geophysics 36(4): 441-500.

Mather, T. A., A. G. Allen, et al. (2003). "Size-Resolved Characterisation of Soluble Ions in the Particles in the Tropospheric Plume of Masaya Volcano, Nicaragua: Origins and Plume Processing." Journal of Atmospheric Chemistry 46(3): 207-237.

Mather, T. A., A. G. Allen, et al. (2004). "Nitric acid from volcanoes." Earth and Planetary Science Letters 218: 17-30.

Mather, T. A., D. M. Pyle, et al. (2004). "Volcanic source for fixed nitrogen in the early Earth's atmosphere." Geology 32(10): 905-908.

Mather, T. A., D. M. Pyle, et al. (2006). "A reassessment of current volcanic emissions from the Central American arc with specific examples from Nicaragua." Journal of Volcanology and Geothermal Research 149(3-4): 297-311.

Mauri, G. (2009). "Multi-scale analysis of multiparameter geophysical and geochemical data from active volcanic systems." PhD Thesis, Simon Fraser University, Burnaby (Canada).

Mauri, G., G. Williams-Jones, et al. (2010). "Depth determinations of shallow hydrothermal systems by self-potential and multi-scale wavelet tomography." Journal of Volcanology and Geothermal Research 191(3-4): 233-244.

Mauri, G., G. Williams-Jones, et al. (2012). "A geochemical and geophysical investigation of the hydrothermal complex of Masaya volcano, Nicaragua." Journal of Volcanology and Geothermal Research.

McBirney, A. (1956). "The Nicaragua Volcano Masaya and Its Caldera." Eos Transactions, American Geophysical Union 37: 83-96.

McGonigle, A. J. S., C. Oppenheimer, et al. (2002). "Walking traverse and scanning DOAS measurements of volcanic gas emission rates." Geophysical Research Letters 29(20): 1985.

McGonigle, A., D. Hilton, et al. (2005). "Plume velocity determination for volcanic SO2 flux measurements." Geophysical Research Letters 32(11): L11302.

McGonigle, A., P. Delmelle, et al. (2004). "SO_2 depletion in tropospheric volcanic plumes." Geophysical Research Letters 31(13): L13201.

McNeill, J. and V. Labson (1991). "Geological mapping using VLF radio waves." Electromagnetic Methods in Applied Geophysics 2: 521-640.

Metaxian, J. (1994). "Etude sismologique et gravimetrique d'un volcan actif: Dynamisme interne et structure de la Caldeira Masaya, Nicaragua." PhD Thesis, Universite de Savoie, Chambéry (France): 200.

Métaxian, J. P., Lesage, P. and Dorel, J. (1997). "Permanent tremor of Masaya Volcano, Nicaragua: Wave field analysis and source location." Journal of Geophysical Research 102(B10): 22529-22545.

Molero, M. (1988). "Nicaragua sandinista: del sueño a la realidad (1979-1988)." IEPALA Editorial, Madrid (Spain): 299.

Montessus de Ballore, F. (1888). "Tremblements de terre et eruptions volcaniques au Centre Amérique." Dijon (France): 293.

Moune, S., F. Faure, et al. (2007). "Pele's hairs and tears: Natural probe of volcanic plume." Journal of Volcanology and Geothermal Research 164(4): 244-253.

Moune, S., P.-J. Gauthier, et al. (2010). "Trace elements in the particulate phase of the plume of Masaya Volcano, Nicaragua." Journal of Volcanology and Geothermal Research 193: 232–244.

Nadeau, P. (2004). "A multi-parameter investigation of volcanic plume behavior and resultant environmental impact at a persistently degassing volcano, Masaya, Nicaragua." MSc Thesis, Simon Fraser University, Burnaby (Canada).

Nadeau, P. and G. Williams-Jones (2009). "Apparent downwind depletion of volcanic SO2 flux—lessons from Masaya Volcano, Nicaragua." Bulletin of Volcanology 71(4): 389-400.

Nissen, J. (1986). "A versatile electromagnetic modeling program for 2-D structures." Geophysical Prospecting 34(7): 1099-1110.

Ogilvy, R. (1980). "An appraisal of the VLF ground resistivity technique as an aid to mineral exploration." (Unpublished). Institute of Geological Sciences, United Kingdom: 27pp.

Oviedo y Valdez, F. G. (1851). "Historia general y natural de las Indias, Islas y Tierra Firme del Mar Océano." Real Academia de la Historia, Madrid (Spain): 511.

Ozima, M. and H. Kinoshita (1964). "Magnetic anisotropy of andesites in a fault zone." Journal of geomagnetism and geoelectricity 16(3): 194-200.

Pantoja, A. (2012). "Iglesia Católica pierde adeptos". El Nuevo Diario. 28th July, 2012, Managua.

Parasnis, D. (1952). "A study of rock densities in the English Midlands." Geophysical Supplements to the Monthly Notices of the Royal Astronomical Society 6(5): 252-271.

Parasnis, D. S., Ed. (1995). "Principles of Applied Geophysics." Chapman and Hall, London (UK and New York (USA): 429.

Paterson, N. R. and V. Ronka (1971). "Five years of surveying with the Very Low Frequency—Electro magnetics method." Geoexploration 9(1): 7-26.

Pearson, S. C. P. (2010). "Diffuse degassing and the hydrothermal system at Masaya volcano, Nicaragua." PhD Thesis, University of South Florida, Tampa USA): 148.

Pearson, S. C. P., C. B. Connor, et al. (2008). "Rapid response of a hydrologic system to volcanic activity: Masaya volcano, Nicaragua." Geology 36(12): 951-954.

Pearson, S. C. P., K. Kiyosugi, et al. (2012). "Integrated geophysical and hydrothermal models of flank degassing and fluid flow at Masaya volcano, Nicaragua." Geochemistry Geophysics Geosystems 13: Q05011.

Peña-Hernández, E. (1968). "Folklore de Nicaragua." Editorial Unión, Masaya (Nicaragua): 410.

Pérez Fernández, W. (2007). "Basaltic Plinian and violent Surtseyan eruptions from the Masaya Caldera Complex, Nicaragua." PhD Thesis, Christian-Albrechts University, Kiel (Germany): 194.

Pérez, W. and A. Freundt (2006). "The youngest highly explosive basaltic eruptions from Masaya Caldera (Nicaragua): Stratigraphy and hazard assessment." Geological Society of America Special Papers 412: 189-207.

Pérez, W., A. Freundt, et al. (2009). "The Masaya Triple Layer: A 2100 year old basaltic multi-episodic Plinian eruption from the Masaya Caldera Complex (Nicaragua)." Journal of Volcanology and Geothermal Research 179(3-4): 191-205.

Pirttijarvi, M. (2004). "Karous–Hjelt and Fraser filtering of VLF measurements." Manual of the KHFFILT Program. University of Oulu, Finland.

Procuraduría de Derechos Humanos de Nicaragua, P. (2001). "Diagnóstico de la Situación de los Pueblos Indígenas y Comunidades Étnicas e Instalación de la Procuraduría Especial." Managua, Nicaragua.

Rathore, J. S. and M. Becke (1980). "Magnetic fabric analyses in the Gail Galley (Carinthia, Austria) for the determination of the sense of movements along this region of the Periadriatic Line." Tectonophysics 69(3–4): 349-368.

Richter, D. (2000). "Portable mid-infrared gas sensors: development and applications." PhD Thesis, Rice University, Houston (USA).

Richter, D., M. Erdelyi, et al. (2002). "Field measurements of volcanic gases using tunable diode laser based mid-infrared and Fourier transform infrared spectrometers." Optics and lasers in engineering 37(2): 171-186.

Roche, O., B. van Wyk de Vries, et al. (2001). "Sub-surface structures and collapse mechanisms of summit pit craters." Journal of Volcanology and Geothermal Research 105(1-2): 1-18.

Rodríguez-Pérez, J. R., M. Álvarez, et al. (2007). "Assessment of low-cost GPS receiver accuracy and precision in forest environments." Journal of Surveying Engineering 133(4): 159-167.

Rosen, P. A., S. Hensley, et al. (2001). "SRTM C-band topographic data: quality assessments and calibration activities." Geoscience and Remote Sensing Symposium, 2001. IGARSS'01. IEEE 2001 International, IEEE.

Rosen, P. A., S. Hensley, et al. (2004). "Updated repeat orbit interferometry package released." Eos, Transactions American Geophysical Union 85(5): 47.

Rossi, M. and A. Gudmundsson (1996). "The morphology and formation of flow-lobe tumuli on Icelandic shield volcanoes." Journal of Volcanology and Geothermal Research 72(3): 291-308.

Rousset, D., A. Lesquer, et al. (1989). "Complete gravity study of Piton de la Fournaise volcano, Réunion Island." Journal of Volcanology and Geothermal Research 36(1): 37-52.

Ruffini, J. J. (2011). "Hematite and Sulfate Minerals in Lava Tubes, Craters of the Moon, Idaho: An Analog for Diagenesis at Meridiani Planum, Mars." PhD Thesis, University of Wisconsin, Milwaukee (USA): 106.

Rymer, H. (1996). "Microgravity monitoring." Monitoring and mitigation of volcano hazards, Springer, Berlin, Heidelberg (Germany), New York (USA): 169-198.

Rymer, H. and G. Brown (1986). "Gravity fields and the interpretation of volcanic structures: geological discrimination and temporal evolution." Journal of Volcanology and Geothermal Research 27(3): 229-254.

Rymer, H. and G. Brown (1987). "Causes of microgravity change at Poás volcano, Costa Rica: an active but non-erupting system." Bulletin of Volcanology 49(1): 389-398.

Rymer, H., B. van Wyk de Vries, et al. (1998). "Pit crater structure and processes governing persistent activity at Masaya Volcano, Nicaragua." Bulletin of Volcanology 59(5): 345-355.

Rytuba, J. J. (1994). "Evolution of volcanic and tectonic features in caldera settings and their importance in localization of ore deposits." Economic Geology 89(8): 1687.

Sadofsky, S. J., M. Portnyagin, et al. (2008). "Subduction cycling of volatiles and trace elements through the Central American volcanic arc: evidence from melt inclusions." Contributions to Mineralogy and Petrology 155: 433-456.

Sandwell, D. T. and W. H. Smith (2009). "Global marine gravity from retracked Geosat and ERS-1 altimetry: Ridge segmentation versus spreading rate." Journal of Geophysical Research: Solid Earth (1978–2012) 114(B1).

Sapper, K. (1925). "El Infierno de Masaya." Verlax von Max Niemeyer, Halle (Germany): 65.

Schönberg, J. W. (1927). "Bericht uber die jungsten Ereignisse und Arbeiten am Masaya." Zs. Vul. 9: 128-134.

Sebesta, J. (1997). "Dynamic development of the relief in the Managua area, Nicaragua." Acta Univ Carol Geogr 2: 93-109.

Shah, P. S. and T. Balkhair (2011). "Air pollution and birth outcomes: A systematic review." Environment International 37(2): 498-516.

Shaw, A. M., D. R. Hilton, et al. (2003). "Contrasting He-C relationships in Nicaragua and Costa Rica: insights into C cycling through subduction zones." Earth and Planetary Science Letters 214(3-4): 499-513.

SINAPRED (2004). Plan de respuesta departamental con enfoque de gestión del riesgo. Departamento de Masaya, Región IV. Managua, Sistema Nacional para la Prevención, Mitigación y Atención de Desastres: 48.

Smith, W. H. and D. T. Sandwell (1997). "Global sea floor topography from satellite altimetry and ship depth soundings." Science 277(5334): 1956-1962.

Spampinato, L. and G. G. Salerno (2011). "Heat and SO2 Emission Rates at Active Volcanoes – The Case Study of Masaya, Nicaragua." in Geophysics, Kuala Lumpur (Malaysia): 24.

Squier, F. G. (1856). "Nicaragua; its people, scenery, monuments, and the proposed interoceanic canal." New York (USA): 424.

St-Amand, K. (1999). "The distribution and origin of Radon, CO2, and SO2 gases and Multifractal behaviour of SO2 at Masaya Volcano, Nicaragua, M.Sc. thesis." Université de Montreal, Montreal (Canada): 270.

Stephens, J. L., Ed. (1841). "Incidents of travel in Central America, Chiapas, and Yucatan." New York (USA).

Stix, J. (2007). "Stability and instability of quiescently active volcanoes: The case of Masaya, Nicaragua." Geology 35(6): 535-538.

Stoiber, R. E., S. N. Williams, et al. (1986). "Sulfur and halogen gases at Masaya caldera complex, Nicaragua: total flux and variations with time." Journal of Geophysical Research 91(B12): 12215-12212.

Stuart Almendárez, R. (2009). "Consejos del Poder Ciudadano y gestión pública en Nicaragua." Centro de Estudios y Análisis Político, Managua (Nicaragua).

The_World_Bank. (2012). "World Development Indicators." Retrieved 5th November, 2013, from http://data.worldbank.org/indicator/NY.GDP.MKTP.CD.

Tilling, R. I. (1989). "Measures of little gravity." Nature 342(6252): 862-863.

Ui, T. (1972). "Recent volcanism in Masaya-Granada Area, Nicaragua." Bulletin Volcanologique 36(1): 174-190.

UNDP (2011). "International Human Development Report." United Nations Development Program, New York (USA).

UNDP. (2013). "International Human Development Indicators.", United Nations Development Program, New York (USA). Retrieved 12th September 2013 from http://hdrstats.undp.org/en/tables/index.html.

UNDRO (1980). "Natural Disasters and Vulnerability Analysis: Report of Expert Group Meeting (9-12 July 1979)." Geneva (Switzerland).

USGS. (2010). "Volcanic ash - effects to buildings and mitigation strategies." Retrieved 21st September 2013, 2013, from http://volcanoes.usgs.gov/ash/build/.

Vallelonga, P. and T. Mather (2003). "Lead (Pb) fluxes and Pb isotopic compositions from Masaya volcano, Nicaragua." Atmospheric Environment 37(31): 4453-4460.

van Wyk de Vries, B. (1993). "Tectonics and magma evolution of Nicaraguan volcanic systems." PhD Thesis, The Open University, Milton Keynes (UK).

Viramonte, J. G. (1972). "Algunos volcanes Cuaternarios de la costa Pacífica de Nicaragua: Su composición, estructura, evolución y actividad." Universidad Nacional de Córdoba, Córdoba (Argentina).

Viramonte, J. G. and J. Incer-Barquero (2008). "Masaya, the "Mouth of Hell", Nicaragua: Volcanological interpretation of the myths, legends and anecdotes." Journal of Volcanology and Geothermal Research 176(3): 419-426.

von Seebach, K. (1892). "Über Vulkane Centralamerikas." Göttingen (Germany).

Walker, G. P. L. (1991). "Structure, and origin by injection of lava under surface crust, of tumuli,"lava rises","lava-rise pits", and "lava-inflation clefts" in Hawaii." Bulletin of Volcanology 53(7): 546-558.

Walker, J., S. Williams, et al. (1993). "Shallow open-system evolution of basaltic magma beneath a subduction zone volcano: the Masaya Caldera Complex, Nicaragua." Journal of Volcanology and Geothermal Research 56(4): 379-400.

Ward, S., J. Ryu, et al. (1974). "Electromagnetic methods in conductive terranes." Geoexploration 12(2): 121-183.

Wehrmann, H., C. Bonadonna, et al. (2006). "Fontana Tephra: a basaltic Plinian eruption in Nicaragua." GSA Special Papers 412: 209.

WHO (2006). "Air Quality Guidelines: Global Update 2005: Particulate Matter, Ozone, Nitrogen Dioxide and Sulfur Dioxide." World Health Organization. Regional Office for Europe: 484.

Williams, S. N. (1983). "Plinian airfall deposits of basaltic composition." Geology 11: 211-214.

Williams, S. N. (1983). "Geology and eruptive mechanisms of Masaya Caldera Complex, Nicaragua." PhD Thesis, Dartmouth College, Hanover (USA): 216 pages.

Williams-Jones, G. (2001). "Integrated Geophysical Studies at Masaya Volcano, Nicaragua." PhD Thesis, The Open University, Milton Keynes (UK).

Williams-Jones, G. and H. Rymer (2002). "Detecting volcanic eruption precursors: a new method using gravity and deformation measurements." Journal of Volcanology and Geothermal Research 113(3-4): 379-389.

Williams-Jones, G., H. Rymer, et al. (2003). "Gravity changes and passive SO2 degassing at the Masaya caldera complex, Nicaragua." Journal of Volcanology and Geothermal Research 123(1-2): 137-160.

Williams-Jones, G., K. A. Horton, et al. (2006). "Accurately measuring volcanic plume velocity with multiple UV spectrometers." Bulletin of Volcanology 68(4): 328-332.

Witt, M. L. I., T. A. Mather, et al. (2008). "Mercury and halogen emissions from Masaya and Telica volcanoes, Nicaragua." Journal of Geophysical Research 113: B06203.

Yokoyama, I. (1989). "Microgravity and height changes caused by volcanic activity: Four." Bulletin of Volcanology 51(5): 333-345.

Zablocki, C. J. (1978). "Applications of the VLF induction method for studying some volcanic processes of Kilauea volcano, Hawaii." Journal of Volcanology and Geothermal Research 3(1-2): 155-195.

Zlotnicki, J., G. Vargemezis, et al. (2006). "State of the hydrothermal activity of Soufrière of Guadeloupe volcano inferred by VLF surveys." Journal of Applied Geophysics 58(4): 265-279.

Zurek, J. M. (2010). "Characterizing the plumbing systems of active volcanoes through potential field studies." MSc Thesis, Simon Fraser University, Burnaby (Canada).

8 Appendices

8.1 Appendix A: Magnetic data (Chapter 3)

8.1.1 Base station data

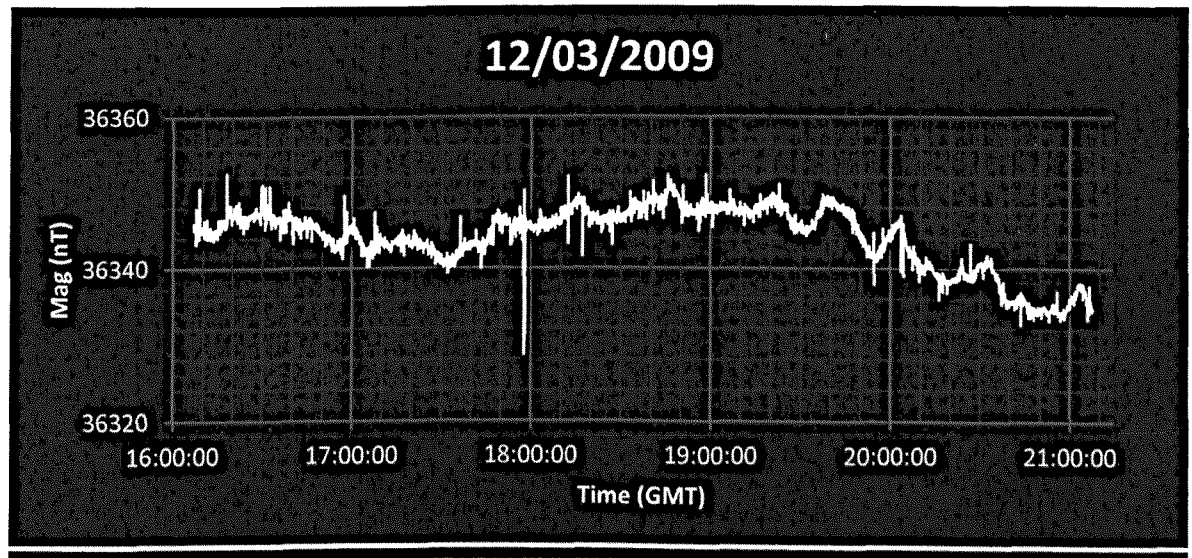

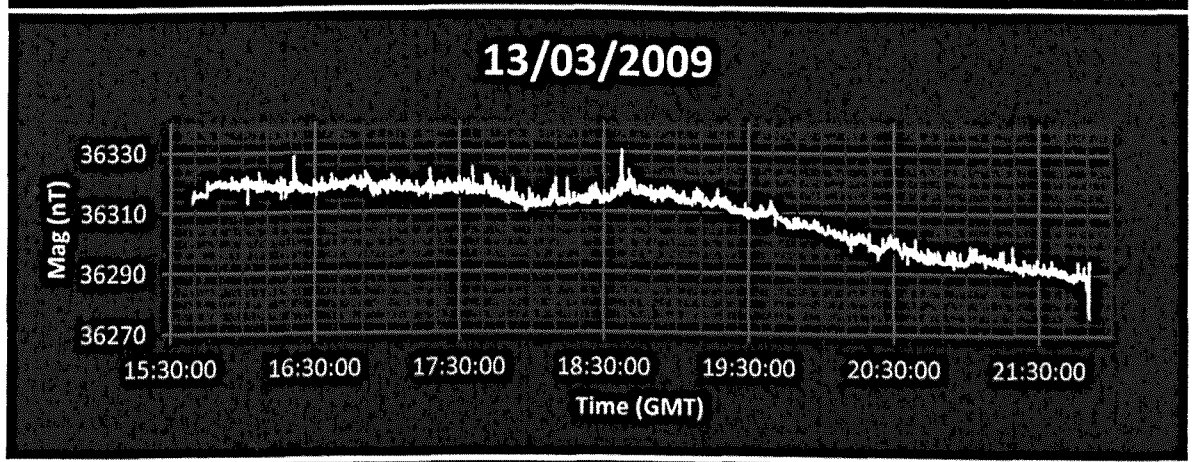

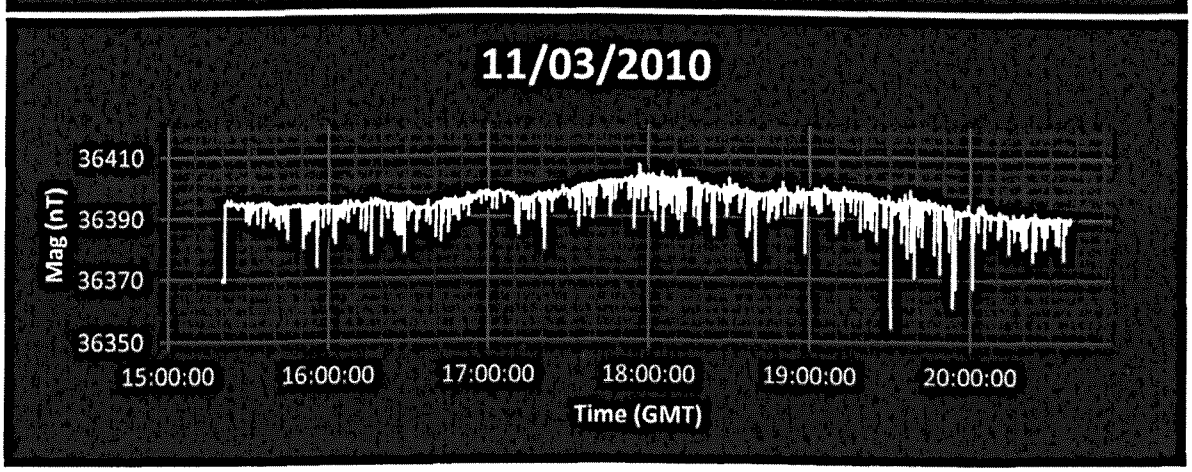

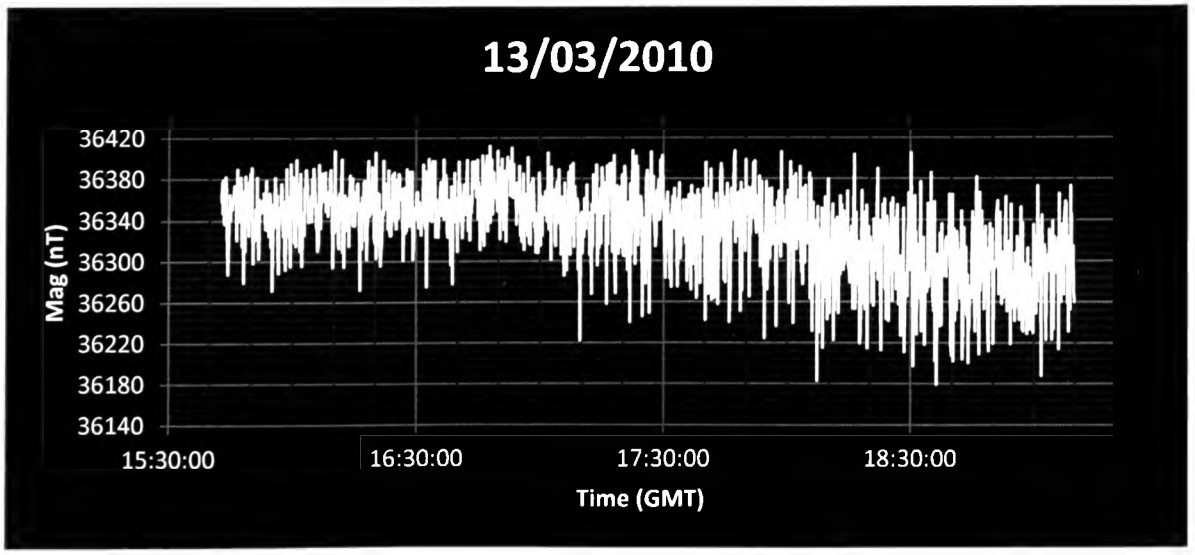

8.1.2 Total magnetic field profiles

Name	**Stations P1-P93**
Area description	**Las Pencas-Sastepe**
Ring fault crossed	**Yes**
Other structures	**Unknown**
Average spacing	**20.5**
Date	**03/03/2010**
Coordinate System	**UTM Zone 16P**

Point	Local time (hr:mn)	Eastings (m)	Northings (m)	Mag (nT)	Distance (m) to previous station	Accumulated spacing (m)
P1	11:09	590614	1326691	36471		0
P2	11:14	590594	1326692	36190.8	20.02498	20.02498
P3	11:15	590577	1326699	36304	18.38478	38.40976
P4	11:16	590568	1326715	35823.4	18.35756	56.76732
P5	11:17	590558	1326734	36185.4	21.47091	78.23823
P6	11:19	590550	1326749	36362	17	95.23823
P7	11:20	590541	1326765	37497	18.35756	113.5958
P8	11:22	590530	1326787	36898.4	24.59675	138.1925
P9	11:23	590520	1326800	36483.5	16.40122	154.5938
P10	11:24	590509	1326817	36594.1	20.24846	174.8422
P11	11:25	590499	1326838	37335	23.25941	198.1016
P12	11:27	590488	1326815	37166	25.4951	223.5967
P13	11:29	590476	1326867	36740	53.36666	276.9634
P14	11:30	590459	1326876	35772	19.23538	296.1988
P15	11:32	590442	1326895	36796.2	25.4951	321.6939
P16	11:33	590436	1326904	37256	10.81665	332.5105

P17	11:35	590424	1326918	37280	18.43909	350.9496
P18	11:37	590412	1326934	37169.8	20	370.9496
P19	11:39	590403	1326949	37090.2	17.49286	388.4425
P20	11:40	590403	1326949	35813.9	0	388.4425
P21	11:43	590380	1326976	36456.5	35.4683	423.9108
P22	11:45	590367	1326995	36987	23.02173	446.9325
P23	11:46	590356	1327013	37374	21.09502	468.0275
P24	11:48	590342	1327027	36559	19.79899	487.8265
P25	11:49	590336	1327046	36486	19.92486	507.7514
P26	11:50	590329	1327063	35519	18.38478	526.1361
P27	11:51	590321	1327076	36815	15.26434	541.4005
P28	11:53	590320	1327097	36114.9	21.0238	562.4243
P29	11:54	590311	1327117	35387	21.93171	584.356
P30	11:55	590306	1327135	36300	18.68154	603.0375
P31	11:56	590302	1327153	36383	18.43909	621.4766
P32	12:01	590296	1327171	36778.5	18.97367	640.4503
P33	12:03	590289	1327191	35975	21.18962	661.6399
P34	12:04	590288	1327209	35914.8	18.02776	679.6676
P35	12:06	590287	1327227	35560	18.02776	697.6954
P36	12:09	590286	1327251	35311.2	24.02082	721.7162
P37	12:10	590287	1327265	34940	14.03567	735.7519
P38	12:12	590287	1327285	35965.9	20	755.7519
P39	12:13	590278	1327292	36276	11.40175	767.1537
P40	12:17	590271	1327311	35486.4	20.24846	787.4021
P41	12:19	590260	1327336	35434.4	27.313	814.7151
P42	12:20	590256	1327353	34431	17.46425	832.1794
P43	12:23	590249	1327370	34372	18.38478	850.5641
P44	12:24	590244	1327389	35368.5	19.64688	870.211
P45	13:22	590234	1327408	35259	21.47091	891.6819
P46	13:23	590223	1327429	35297.9	23.70654	915.3885
P47	13:25	590215	1327443	35068	16.12452	931.513
P48	13:26	590200	1327464	35349.8	25.80698	957.32
P49	13:27	590194	1327473	35467	10.81665	968.1366
P50	13:29	590179	1327493	35831.7	25	993.1366
P51	13:30	590176	1327510	35841	17.26268	1010.399
P52	13:31	590166	1327527	35493.4	19.72308	1030.122
P53	13:32	590158	1327543	35281.5	17.88854	1048.011
P54	13:34	590148	1327556	35468.3	16.40122	1064.412
P55	13:35	590136	1327573	35069.5	20.80865	1085.221
P56	13:36	590121	1327599	35573	30.01666	1115.237
P57	13:37	590108	1327618	35344.9	23.02173	1138.259
P58	13:38	590107	1327623	35844.3	5.09902	1143.358
P59	13:39	590096	1327640	35048.5	20.24846	1163.607
P60	13:41	590084	1327660	35205.1	23.32381	1186.93
P61	13:41	590073	1327672	35446.4	16.27882	1203.209
P62	13:42	590065	1327696	35450.3	25.29822	1228.508
P63	13:43	590052	1327719	36402.9	26.41969	1254.927
P64	13:45	590039	1327750	35794.3	33.61547	1288.543
P65	13:46	590033	1327753	36011.1	6.708204	1295.251
P66	13:47	590022	1327770	36371.4	20.24846	1315.499
P67	13:48	590010	1327786	36467.5	20	1335.499
P68	13:49	589997	1327805	36419.5	23.02173	1358.521

P69	13:49	589987	1327824	36210.7	21.47091	1379.992
P70	13:50	589975	1327836	36216	16.97056	1396.963
P71	13:52	589962	1327859	36457	26.41969	1423.382
P72	13:53	589949	1327872	35620.6	18.38478	1441.767
P73	13:54	589935	1327886	36553	19.79899	1461.566
P74	13:55	589928	1327899	36982	14.76482	1476.331
P75	14:01	589908	1327926	36519	33.6006	1509.931
P76	14:02	589894	1327943	36598	22.02272	1531.954
P77	14:03	589884	1327962	36805.6	21.47091	1553.425
P78	14:04	589873	1327971	35713	14.21267	1567.638
P79	14:05	589863	1327975	36688.3	10.77033	1578.408
P80	14:06	589843	1328000	35779.9	32.01562	1610.424
P81	14:07	589838	1328005	34026	7.071068	1617.495
P82	14:07	589822	1328035	36184	34	1651.495
P83	14:09	589822	1328062	37794	27	1678.495
P84	14:10	589818	1328082	35281.5	20.39608	1698.891
P85	14:12	589812	1328097	35835.4	16.15549	1715.046
P86	14:13	589809	1328122	36810.4	25.17936	1740.226
P87	14:15	589795	1328131	36620	16.64332	1756.869
P88	14:16	589793	1328165	36211.4	34.05877	1790.928
P89	14:17	589795	1328168	36243.6	3.605551	1794.533
P90	14:19	589799	1328193	36258	25.31798	1819.851
P91	14:20	589800	1328209	36208.4	16.03122	1835.882
P92	14:21	589807	1328238	36170.2	29.83287	1865.715
P93	14:22	589806	1328259	36175.8	21.0238	1886.739

Name	**Stations 01-85**
Area description	**Km. 21 trail**
Ring fault crossed	**Yes**
Other structures	**No**
Average spacing	**25.1369737**
Date	**10/03/2010**
Coordinate System	**UTM Zone 16P**

Point	Local time (hr:mn)	Eastings (m)	Northings (m)	Mag (nT)	Distance (m) to previous station	Accumulated spacing (m)
1	10:16	591914	1326951	37661.3		0
2	10:17	591904	1326968	37270.0	19.72308	19.72308
3	10:18	591895	1326989	36501.6	22.84732	42.5704
4	10:21	591882	1327012	36552.3	26.41969	68.99009
5	10:21	591871	1327034	37686.2	24.59675	93.58684
6	10:22	591860	1327056	37846.2	24.59675	118.1836
7	10:23	591849	1327077	38226.5	23.70654	141.8901

8	10:25	591837	1327114	37803.1	38.8973	180.7874
9	10:26	591845	1327137	38437.5	24.35159	205.139
10	10:27	591857	1327169	38842.0	34.17601	239.315
11	10:28	591869	1327196	38757.5	29.54657	268.8616
12	10:29	591882	1327215	38352.9	23.02173	291.8833
13	10:30	591890	1327244	37822.9	30.08322	321.9666
14	10:31	591886	1327268	39174.2	24.33105	346.2976
15	10:32	591888	1327292	38709.1	24.08319	370.3808
16	10:34	591890	1327330	38657.9	38.0526	408.4334
17	10:35	591889	1327367	38056.5	37.01351	445.4469
18	10:36	591886	1327389	37932.1	22.2036	467.6505
19	10:37	591883	1327413	37271.8	24.18677	491.8373
20	10:39	591879	1327439	37734.1	26.30589	518.1432
21	10:40	591876	1327463	38424.7	24.18677	542.3299
22	10:41	591872	1327487	37839.8	24.33105	566.661
23	10:43	591870	1327513	38021.5	26.07681	592.7378
24	10:44	591866	1327538	37778.0	25.31798	618.0558
25	10:45	591869	1327559	39028.0	21.2132	639.269
26	10:47	591873	1327587	37805.8	28.28427	667.5533
27	10:48	591877	1327611	37674.0	24.33105	691.8843
28	10:49	591888	1327632	38171.9	23.70654	715.5908
29	10:50	591905	1327658	37354.4	31.06445	746.6553
30	10:51	591918	1327677	37354.0	23.02173	769.677
31	10:52	591932	1327701	36942.5	27.78489	797.4619
32	10:53	591947	1327721	36616.9	25	822.4619
33	10:54	591960	1327741	36800.0	23.85372	846.3156
34	10:54	591972	1327761	36900.3	23.32381	869.6394
35	10:55	591989	1327788	36845.4	31.90611	901.5456
36	10:56	592005	1327813	36602.6	29.68164	931.2272
37	10:57	592019	1327833	36677.8	24.41311	955.6403
38	10:58	592033	1327853	36733.2	24.41311	980.0534
39	10:59	592048	1327876	36524.7	27.45906	1007.512
40	11:00	592062	1327898	36783.5	26.07681	1033.589
41	11:01	592075	1327917	37124.8	23.02173	1056.611
42	11:02	592090	1327936	37248.1	24.20744	1080.818
43	11:03	592104	1327955	37178.4	23.60085	1104.419
44	11:04	592117	1327973	36974.6	22.2036	1126.623
45	11:07	592132	1327992	36356.1	24.20744	1150.83
46	11:08	592146	1328011	37449.0	23.60085	1174.431
47	11:10	592159	1328029	38073.4	22.2036	1196.635
48	11:10	592173	1328048	37486.6	23.60085	1220.236
49	11:12	592185	1328067	37507.9	22.47221	1242.708
50	11:12	592197	1328087	37621.7	23.32381	1266.032
51	11:13	592210	1328106	37529.1	23.02173	1289.053
52	11:14	592223	1328125	37502.1	23.02173	1312.075
53	11:15	592236	1328144	37813.0	23.02173	1335.097
54	11:16	592251	1328163	37286.2	24.20744	1359.304
55	11:17	592263	1328181	37504.9	21.63331	1380.938
56	11:18	592279	1328202	37868.8	26.40076	1407.338
57	11:19	592290	1328220	37623.5	21.09502	1428.433
58	11:19	592304	1328240	37851.6	24.41311	1452.846
59	11:21	592316	1328260	37934.0	23.32381	1476.17

60	11:22	592328	1328280	37888.6	23.32381	1499.494
61	11:23	592340	1328300	37907.2	23.32381	1522.818
62	11:25	592357	1328327	37214.0	31.90611	1554.724
63	11:26	592371	1328348	37573.3	25.23886	1579.963
64	11:28	592382	1328373	37372.4	27.313	1607.276
65	11:28	592392	1328396	37200.7	25.07987	1632.356
66	11:29	592400	1328417	36906.0	22.47221	1654.828
67	11:30	592409	1328439	37013.5	23.76973	1678.598
68	11:31	592418	1328460	36877.2	22.84732	1701.445
69	11:32	592428	1328482	36366.2	24.16609	1725.611
70	11:33	592437	1328505	36241.4	24.69818	1750.309
71	11:33	592444	1328527	36075.4	23.08679	1773.396
72	11:34	592454	1328550	36141.1	25.07987	1798.476
73	11:35	592462	1328572	36042.8	23.4094	1821.885
74	11:35	592469	1328595	35536.0	24.04163	1845.927
75	11:36	592477	1328618	35453.9	24.35159	1870.279
76	11:37	592486	1328639	35548.9	22.84732	1893.126
77	11:38	592498	1328661	35471.6	25.05993	1918.186
78	11:38	592509	1328683	35338.6	24.59675	1942.783
79	11:39	592518	1328704	35458.8	22.84732	1965.63
80	11:40	592527	1328726	36177.0	23.76973	1989.4
81	11:41	592535	1328749	35637.8	24.35159	2013.751
82	11:41	592545	1328771	35150.1	24.16609	2037.917
83	11:42	592554	1328793	35448.9	23.76973	2061.687
84	11:43	592563	1328817	35516.0	25.63201	2087.319
85	11:44	592575	1328838	35699.4	24.18677	2111.506

Name	**A01-A18**
Area description	**Short profile to look for anomalies along the 21k trail**
Ring fault crossed	**Yes (seen on surface as collapse fissures with spatter cones)**
Other structures	**Unknown**
Average spacing	**10.1**
Date	**04/03/2010**
Coordinate System	**UTM Zone 16P**

Point	Local time (hr:mn)	Eastings (m)	Northings (m)	Mag (nT)	Distance (m) to previous station	Accumulated spacing (m)
A01	10:05	592098	1327945	37256.4		0
A02	10:06	592102	1327952	37182.4	8.062258	8.062258
A03	10:08	592109	1327962	36958.1	12.20656	20.26881
A04	10:09	592115	1327969	36954.3	9.219544	29.48836
A05	10:11	592121	1327976	37318	9.219544	38.7079
A06	10:12	592128	1327981	37636.2	8.602325	47.31023

A07	10:13	592134	1327989	37535.4	10	57.31023
A08	10:15	592138	1327998	37569.9	9.848858	67.15909
A09	10:16	592145	1328007	37695.2	11.40175	78.56084
A10	10:18	592151	1328008	37100.5	6.082763	84.6436
A11	10:19	592152	1328022	38263	14.03567	98.67927
A12	10:20	592160	1328029	37648	10.63015	109.3094
A13	10:22	592166	1328037	37243	10	119.3094
A14	10:24	592172	1328047	37470.7	11.6619	130.9713
A15	10:25	592180	1328052	37432.4	9.433981	140.4053
A16	10:26	592185	1328066	37574.7	14.86607	155.2714
A17	10:27	592190	1328073	37624.3	8.602325	163.8737
A18	10:29	592192	1328081	37631.3	8.246211	172.1199

Name	**290-340**
Area description	**Road. From Plaza de Oviedo to the beginning of the trail to Comalito**
Ring fault crossed	**?**
Other structures	**Unknown**
Average spacing	**48.01096479**
Date	**08/03/2010**
Coordinate System	**UTM Zone 16P**

Point	Local time (hr:mn)	Eastings (m)	Northings (m)	Mag (nT)	Distance (m) to previous station	Accumulated spacing (m)
290	13:48	590582	1326269	36787.3		0
291	13:49	590567	1326315	35519.0	48.38388	48.38388
292	13:50	590570	1326361	35524.6	46.09772	94.4816
293	13:51	590555	1326402	36007.9	43.65776	138.1394
294	13:51	590551	1326450	35408.0	48.16638	186.3057
295	13:52	590548	1326503	34968.0	53.08484	239.3906
296	13:55	590545	1326545	36306.0	42.10701	281.4976
297	13:56	590542	1326596	37007.9	51.08816	332.5857
298	13:57	590560	1326640	36297.3	47.53946	380.1252
299	13:58	590590	1326678	36668.0	48.41487	428.5401
300	14:00	590611	1326696	36451.3	27.65863	456.1987
301	14:01	590655	1326714	37514.0	47.53946	503.7382
302	14:02	590699	1326733	36682.3	47.92703	551.6652
303	14:02	590746	1326748	36670.7	49.33559	601.0008
304	14:03	590790	1326763	37033.0	46.48656	647.4873
305	14:04	590837	1326782	37956.0	50.69517	698.1825
306	14:05	590876	1326798	36661.4	42.15448	740.337
307	14:06	590926	1326823	37118.0	55.9017	796.2387
308	14:07	590966	1326845	37593.0	45.65085	841.8895

309	14:08	591014	1326863	37663.0	51.26402	893.1536
310	14:09	591046	1326878	37792.2	35.34119	928.4947
311	14:14	591106	1326892	37245.6	61.61169	990.1064
312	14:15	591151	1326876	37148.1	47.75982	1037.866
313	14:16	591189	1326850	37363.6	46.04346	1083.91
314	14:17	591237	1326836	37464.3	50	1133.91
315	14:18	591266	1326847	37709.3	31.01612	1164.926
316	14:19	591322	1326871	37734.8	60.92618	1225.852
317	14:20	591378	1326876	38250.0	56.22277	1282.075
318	14:21	591430	1326868	38059.2	52.61179	1334.687
319	14:22	591468	1326853	37975.0	40.8534	1375.54
320	14:23	591518	1326835	37739.0	53.14132	1428.681
321	14:25	591567	1326831	38024.4	49.16299	1477.844
322	14:26	591612	1326855	38079.1	51	1528.844
323	14:27	591661	1326857	37841.1	49.0408	1577.885
324	14:28	591708	1326846	38295.9	48.27007	1626.155
325	14:28	591756	1326839	37148.5	48.50773	1674.663
326	14:29	591804	1326856	37046.6	50.92151	1725.584
327	14:30	591849	1326877	37549.8	49.65884	1775.243
328	14:31	591892	1326894	36001.0	46.23851	1821.482
329	14:32	591940	1326906	37527.4	49.47727	1870.959
330	14:33	591988	1326902	37748.3	48.16638	1919.125
331	14:33	592037	1326906	38626.0	49.16299	1968.288
332	14:37	592085	1326907	39254.0	48.01042	2016.299
333	14:39	592133	1326905	38795.2	48.04165	2064.34
334	14:40	592182	1326898	37949.6	49.49747	2113.838
335	14:42	592229	1326890	38096.0	47.67599	2161.514
336	14:44	592278	1326882	37818.9	49.64877	2211.163
337	14:45	592324	1326875	37850.0	46.52956	2257.692
338	14:47	592362	1326843	37159.4	49.67897	2307.371
339	14:48	592394	1326809	37497.0	46.69047	2354.062
340	14:49	592438	1326794	37435.0	46.48656	2400.548

Name	**1-167**
Area description	**From the big tree (4 yellow ribbons, cows) down Chocoyos to Montoso**
Ring fault crossed	**No (near Montoso maybe - the end of the profile?)**
Other structures	**Unknown**
Average spacing	**27.97303838**
Date	**09/03/2010**
Coordinate System	**UTM Zone 16P**

Point	Local time (hr:mn)	Eastings (m)	Northings (m)	Mag (nT)	Distance (m) to previous station	Accumulated spacing (m)
1	10:46	589083	1324100	39186.2		0

2	10:49	589065	1324124	40188.8	30	30
3	10:50	589053	1324145	40046.9	24.18677324	54.18677324
4	10:51	589037	1324154	39781.4	18.35755975	72.544333
5	10:52	589017	1324168	40196.2	24.41311123	96.95744423
6	10:52	588996	1324184	43862.0	26.40075756	123.3582018
7	10:54	588970	1324195	44442.0	28.23118843	151.5893902
8	10:55	588950	1324206	43427.0	22.82542442	174.4148146
9	10:56	588927	1324215	43752.0	24.69817807	199.1129927
10	10:57	588904	1324223	42199.2	24.35159132	223.464584
11	10:58	588883	1324233	42243.4	23.2594067	246.7239907
12	10:59	588871	1324259	39609.4	28.63564213	275.3596329
13	11:00	588858	1324279	39827.4	23.85372088	299.2133537
14	11:01	588840	1324297	41060.0	25.45584412	324.6691979
15	11:02	588823	1324316	38698.1	25.49509757	350.1642954
16	11:03	588803	1324330	38640.0	24.41311123	374.5774067
17	11:03	588796	1324357	38123.5	27.89265136	402.470058
18	11:04	588797	1324382	38406.5	25.01999201	427.49005
19	11:05	588795	1324407	38198.4	25.07987241	452.5699224
20	11:06	588798	1324430	38403.0	23.19482701	475.7647495
21	11:10	588794	1324453	38518.7	23.34523506	499.1099845
22	11:11	588784	1324476	39128.0	25.07987241	524.1898569
23	11:12	588772	1324490	38754.5	18.43908891	542.6289458
24	11:13	588753	1324506	39347.0	24.8394847	567.4684305
25	11:14	588739	1324525	38595.7	23.60084744	591.069278
26	11:14	588722	1324541	39645.8	23.34523506	614.414513
27	11:15	588707	1324562	38386.0	25.8069758	640.2214888
28	11:16	588696	1324582	38358.2	22.82542442	663.0469133
29	11:17	588687	1324610	38890.5	29.41088234	692.4577956
30	11:18	588685	1324631	37870.2	21.09502311	713.5528187
31	11:19	588684	1324656	38088.9	25.01999201	738.5728107
32	11:20	588684	1324678	38406.9	22	760.5728107
33	11:21	588680	1324705	38432.6	27.29468813	787.8674988
34	11:22	588670	1324729	38875.8	26	813.8674988
35	11:23	588663	1324750	39556.7	22.13594362	836.0034425
36	11:24	588650	1324775	39364.8	28.17800561	864.1814481
37	11:26	588639	1324794	40065.4	21.9544984	886.1359465
38	11:27	588627	1324813	40504.0	22.47220505	908.6081515
39	11:43	588802	1324460	38982.0	393.9974619	1302.605613
40	11:44	588812	1324488	39551.3	29.73213749	1332.337751
41	11:45	588840	1324506	39008.7	33.28663395	1365.624385
42	11:46	588855	1324519	39617.8	19.84943324	1385.473818
43	11:47	588876	1324533	39159.1	25.23885893	1410.712677
44	11:48	588896	1324542	39237.8	21.9317122	1432.644389
45	11:52	588928	1324529	39041.8	34.53983208	1467.184221
46	11:52	588948	1324535	40782.0	20.88061302	1488.064834
47	11:53	588969	1324542	39995.0	22.13594362	1510.200778
48	11:54	588995	1324551	40066.0	27.51363298	1537.714411
49	11:55	589016	1324556	39237.0	21.58703314	1559.301444
50	13:26	589041	1324580	39961.0	34.6554469	1593.956891
51	13:27	589064	1324575	40359.0	23.53720459	1617.494096

52	13:28	589088	1324596	38968.5	31.89043744	1649.384533
53	13:29	589109	1324621	38133.0	32.64965543	1682.034188
54	13:30	589114	1324653	36162.4	32.38826948	1714.422458
55	13:31	589113	1324655	38385.4	2.236067977	1716.658526
56	13:32	589111	1324672	38114.1	17.11724277	1733.775769
57	13:32	589108	1324697	37881.2	25.17935662	1758.955125
58	13:33	589103	1324725	37793.8	28.44292531	1787.398051
59	13:34	589102	1324746	37708.2	21.02379604	1808.421847
60	13:35	589099	1324769	37694.4	23.19482701	1831.616674
61	13:36	589093	1324801	37504.6	32.55764119	1864.174315
62	13:37	589092	1324826	37494.9	25.01999201	1889.194307
63	13:38	589093	1324843	37391.7	17.02938637	1906.223693
64	13:39	589088	1324872	37272.8	29.42787794	1935.651571
65	13:40	589087	1324891	38006.0	19.02629759	1954.677869
66	13:41	589094	1324916	36841.1	25.96150997	1980.639379
67	13:42	589103	1324935	36720.9	21.02379604	2001.663175
68	13:43	589110	1324960	36353.2	25.96150997	2027.624685
69	13:44	589101	1324987	36341.0	28.46049894	2056.085184
70	13:45	589096	1325009	35845.7	22.56102835	2078.646212
71	13:46	589081	1325028	36100.2	24.20743687	2102.853649
72	13:46	589068	1325045	36145.7	21.40093456	2124.254583
73	13:47	589055	1325062	36184.5	21.40093456	2145.655518
74	13:48	589038	1325079	36470.3	24.04163056	2169.697149
75	13:49	589026	1325097	35946.4	21.63330765	2191.330456
76	13:49	589008	1325115	35558.2	25.45584412	2216.7863
77	13:50	588994	1325130	35692.5	20.51828453	2237.304585
78	13:51	588979	1325155	35899.2	29.15475947	2266.459344
79	13:52	588978	1325178	35611.9	23.02172887	2289.481073
80	13:53	588977	1325201	36313.3	23.02172887	2312.502802
81	13:55	588985	1325222	36039.0	22.47220505	2334.975007
82	13:56	588983	1325237	35725.9	15.13274595	2350.107753
83	13:57	588986	1325265	35857.1	28.16025568	2378.268009
84	13:59	588986	1325297	35218.0	32	2410.268009
85	14:00	588981	1325313	35837.9	16.76305461	2427.031063
86	14:01	588989	1325338	35770.2	26.2488095	2453.279873
87	14:02	588996	1325367	35360.0	29.83286778	2483.112741
88	14:03	588996	1325400	35881.3	33	2516.112741
89	14:04	588998	1325395	35418.8	5.385164807	2521.497905
90	14:05	589023	1325422	34645.0	36.79673899	2558.294644
91	14:06	589018	1325458	34831.0	36.34556369	2594.640208
92	14:07	589000	1325476	35633.0	25.45584412	2620.096052
93	14:08	589001	1325507	35993.7	31.01612484	2651.112177
94	14:09	589001	1325527	36142.0	20	2671.112177
95	14:10	589000	1325549	34564.0	22.02271555	2693.134893
96	14:11	588995	1325570	34978.6	21.58703314	2714.721926
97	14:12	588985	1325587	36273.8	19.72308292	2734.445009
98	14:13	588974	1325600	37624.0	17.02938637	2751.474395
99	14:14	588969	1325627	36016.7	27.45906044	2778.933456
100	14:15	588955	1325647	36240.0	24.41311123	2803.346567
101	14:15	588939	1325673	35289.0	30.52867504	2833.875242
102	14:16	588939	1325699	35199.5	26	2859.875242
103	14:17	588937	1325735	35975.9	36.05551275	2895.930755

104	14:18	588920	1325757	36400.0	27.80287755	2923.733632
105	14:19	588913	1325780	36245.3	24.04163056	2947.775263
106	14:21	588901	1325816	36135.7	37.94733192	2985.722595
107	14:22	588919	1325830	35797.0	22.8035085	3008.526103
108	14:23	588899	1325855	37533.0	32.01562119	3040.541724
109	14:24	588921	1325887	36929.0	38.83297568	3079.3747
110	14:25	588936	1325913	36473.1	30.01666204	3109.391362
111	14:28	588966	1325938	37067.0	39.05124838	3148.44261
112	14:29	588985	1325957	38705.0	26.87005769	3175.312668
113	14:30	588999	1325963	39858.0	15.23154621	3190.544214
114	14:32	589034	1325962	39662.0	35.0142828	3225.558497
115	14:33	589057	1325965	37414.0	23.19482701	3248.753324
116	14:34	589093	1325983	36530.0	40.24922359	3289.002548
117	14:35	589111	1326004	37155.0	27.65863337	3316.661181
118	14:36	589118	1326012	37171.0	10.63014581	3327.291327
119	14:37	589144	1326043	36205.0	40.45985665	3367.751184
120	14:38	589161	1326067	36110.6	29.41088234	3397.162066
121	14:39	589179	1326086	36053.9	26.17250466	3423.334571
122	14:40	589197	1326104	36103.0	25.45584412	3448.790415
123	14:41	589213	1326122	35942.0	24.08318916	3472.873604
124	14:42	589232	1326144	34994.0	29.06888371	3501.942488
125	14:44	589246	1326164	35979.0	24.41311123	3526.355599
126	14:45	589251	1326171	36765.1	8.602325267	3534.957924
127	14:47	589294	1326190	35753.0	47.01063709	3581.968561
128	14:48	589315	1326200	35047.1	23.2594067	3605.227968
129	14:49	589332	1326222	35122.7	27.80287755	3633.030845
130	14:49	589343	1326241	36543.0	21.9544984	3654.985344
131	14:50	589370	1326247	35935.2	27.65863337	3682.643977
132	14:51	589399	1326244	35787.0	29.15475947	3711.798737
133	14:52	589422	1326233	36291.0	25.49509757	3737.293834
134	14:55	589435	1326214	36519.4	23.02172887	3760.315563
135	14:56	589445	1326218	37025.0	10.77032961	3771.085893
136	14:57	589446	1326241	34029.0	23.02172887	3794.107622
137	14:58	589442	1326268	36089.0	27.29468813	3821.40231
138	14:59	589439	1326292	34756.0	24.18677324	3845.589083
139	15:01	589432	1326334	34087.0	42.57933771	3888.168421
140	15:02	589437	1326352	31445.0	18.68154169	3906.849962
141	15:07	589440	1326362	31451.0	10.44030651	3917.290269
142	15:08	589451	1326380	32704.0	21.09502311	3938.385292
143	15:09	589466	1326398	32328.0	23.43074903	3961.816041
144	15:10	589472	1326420	33543.0	22.8035085	3984.619549
145	15:11	589506	1326443	33730.0	41.0487515	4025.668301
146	15:13	589519	1326464	33695.0	24.69817807	4050.366479
147	15:14	589524	1326467	36113.0	5.830951895	4056.197431
148	15:15	589561	1326506	36593.2	53.75872022	4109.956151
149	15:16	589570	1326527	36357.0	22.84731932	4132.80347
150	15:17	589569	1326554	38133.4	27.01851217	4159.821983
151	15:17	589583	1326570	39085.9	21.26029163	4181.082274
152	15:18	589607	1326599	38652.0	37.64306045	4218.725335
153	15:19	589618	1326622	38386.0	25.49509757	4244.220432
154	15:20	589624	1326645	34694.0	23.76972865	4267.990161
155	15:20	589620	1326679	35588.0	34.23448554	4302.224646

156	15:21	589602	1326706	37508.7	32.44996148	4334.674608
157	15:22	589588	1326727	37126.9	25.23885893	4359.913467
158	15:23	589573	1326747	37868.0	25	4384.913467
159	15:24	589555	1326778	36893.8	35.84689666	4420.760364
160	15:24	589547	1326799	36363.2	22.47220505	4443.232569
161	15:25	589545	1326828	37296.0	29.06888371	4472.301452
162	15:26	589551	1326854	34594.0	26.68332813	4498.98478
163	15:27	589560	1326881	34994.0	28.46049894	4527.445279
164	15:27	589574	1326902	35921.3	25.23885893	4552.684138
165	15:28	589598	1326929	35357.0	36.12478374	4588.808922
166	15:29	589614	1326955	35687.1	30.52867504	4619.337597
167	15:30	589626	1326976	35726.1	24.18677324	4643.52437

Name	**ASC1-110**
Area description	**Loop around Sastepe Cone**
Ring fault crossed	**Yes, 3 times**
Other structures	**Spatter cone on the third time the ring fault is crossed**
Average spacing	**25.59885225**
Date	**06/03/2010**
Coordinate System	**UTM Zone 16P**

Point	Local time (hr:mn)	Eastings (m)	Northings (m)	Mag (nT)	Distance (m) to previous station	Accumulated spacing (m)
ASC1	10:38	589816	1328280	36475.5		0
ASC2	10:40	589830	1328300	36332.7	24.41311	24.41311
ASC3	10:42	589838	1328325	37007.1	26.24881	50.66192
ASC4	10:43	589835	1328345	36815.8	20.22375	70.88567
ASC5	10:44	589872	1328379	36523.1	50.24938	121.135
ASC6	10:46	589889	1328395	37678	23.34524	144.4803
ASC7	10:48	589913	1328441	36811.2	51.88449	196.3648
ASC8	10:50	589920	1328450	36700.6	11.40175	207.7665
ASC9	10:52	589936	1328469	36603.3	24.83948	232.606
ASC10	10:54	589954	1328485	36789	24.08319	256.6892
ASC11	10:55	589973	1328502	35680	25.4951	282.1843
ASC12	10:59	589986	1328527	34314	28.17801	310.3623
ASC13	11:03	590008	1328543	34441	27.20294	337.5652
ASC14	11:10	590033	1328548	35054.7	25.4951	363.0603
ASC15	11:12	590059	1328548	35304.8	26	389.0603
ASC16	11:15	590082	1328544	35499.4	23.34524	412.4056
ASC17	11:17	590110	1328538	35101	28.63564	441.0412
ASC18	11:18	590141	1328536	35141.1	31.06445	472.1057
ASC19	11:20	590158	1328536	34428	17	489.1057

ASC20	11:22	590184	1328531	33746	26.4764	515.5821
ASC21	11:24	590210	1328529	34983.6	26.07681	541.6589
ASC22	11:25	590236	1328524	34404.6	26.4764	568.1353
ASC23	11:32	590257	1328526	34744.5	21.09502	589.2303
ASC24	11:34	590280	1328526	34737.7	23	612.2303
ASC25	11:36	590306	1328520	34734	26.68333	638.9136
ASC26	11:37	590330	1328518	34485.4	24.08319	662.9968
ASC27	11:39	590361	1328517	34725.3	31.01612	694.0129
ASC28	11:41	590386	1328514	33898	25.17936	719.1923
ASC29	11:43	590406	1328514	34126	20	739.1923
ASC30	11:44	590440	1328503	34633.9	35.73514	774.9274
ASC31	11:46	590456	1328486	35180.3	23.34524	798.2727
ASC32	11:47	590475	1328478	36306.7	20.61553	818.8882
ASC33	11:51	590446	1328459	35618.2	34.66987	853.5581
ASC34	12:53	590438	1328441	35647	19.69772	873.2558
ASC35	12:55	590421	1328421	35613.4	26.24881	899.5046
ASC36	12:57	590402	1328393	35875.7	33.83785	933.3425
ASC37	12:58	590387	1328373	35575.9	25	958.3425
ASC38	13:00	590378	1328361	35917.1	15	973.3425
ASC39	13:02	590362	1328337	36101.3	28.84441	1002.187
ASC40	13:03	590341	1328309	36162.1	35	1037.187
ASC41	13:05	590329	1328300	36289.4	15	1052.187
ASC42	13:06	590313	1328282	36597.9	24.08319	1076.27
ASC43	13:09	590292	1328267	36323.9	25.80698	1102.077
ASC44	13:10	590276	1328251	36461.5	22.62742	1124.704
ASC45	13:12	590259	1328230	37455	27.01851	1151.723
ASC46	13:13	590242	1328209	37349	27.01851	1178.741
ASC47	13:15	590227	1328190	36823.5	24.20744	1202.949
ASC48	13:17	590212	1328172	36804.1	23.43075	1226.38
ASC49	13:19	590196	1328157	35702	21.93171	1248.311
ASC50	13:22	590174	1328138	37293	29.06888	1277.38
ASC51	13:23	590147	1328118	36629	33.6006	1310.981
ASC52	13:25	590124	1328106	36903	25.94224	1336.923
ASC53	13:26	590111	1328097	36583	15.81139	1352.734
ASC54	13:27	590098	1328086	37393.4	17.02939	1369.764
ASC55	13:30	590067	1328073	37412.5	33.61547	1403.379
ASC56	13:31	590042	1328064	37272.7	26.57066	1429.95
ASC57	13:32	590017	1328048	36032	29.68164	1459.632
ASC58	13:36	590000	1328027	38339.2	27.01851	1486.65
ASC59	13:38	589988	1328013	38010	18.43909	1505.089
ASC60	13:39	589978	1327986	35525	28.79236	1533.882
ASC61	13:41	589966	1327970	37302	20	1553.882
ASC62	13:43	589950	1327948	36846.3	27.20294	1581.085
ASC63	13:45	589936	1327922	36689.3	29.52965	1610.614
ASC64	13:46	589918	1327905	36710	24.75884	1635.373
ASC65	14:02	589906	1327899	36754.1	13.41641	1648.789
ASC66	14:04	589866	1327876	36294	46.14109	1694.931
ASC67	14:05	589860	1327859	36349	18.02776	1712.958
ASC68	14:08	589848	1327844	36603	19.20937	1732.168
ASC69	14:09	589833	1327826	36866.3	23.43075	1755.598
ASC70	14:10	589817	1327812	36569.9	21.26029	1776.859
ASC71	14:11	589799	1327785	36253.2	32.44996	1809.309

ASC72	14:12	589775	1327773	36180.8	26.83282	1836.141
ASC73	14:14	589758	1327754	36165	25.4951	1861.637
ASC74	14:16	589732	1327745	36461.9	27.51363	1889.15
ASC75	14:18	589711	1327736	36900	22.84732	1911.998
ASC76	14:20	589691	1327734	36261	20.09975	1932.097
ASC77	14:22	589662	1327720	35751	32.20248	1964.3
ASC78	14:23	589642	1327710	36792.8	22.36068	1986.66
ASC79	14:28	589624	1327698	36357.3	21.63331	2008.294
ASC80	14:29	589604	1327678	37186.4	28.28427	2036.578
ASC81	14:30	589580	1327667	36671.2	26.40076	2062.979
ASC82	14:32	589559	1327651	36228.8	26.40076	2089.38
ASC83	14:32	589539	1327619	36418	37.73592	2127.115
ASC84	14:34	589548	1327609	36544.6	13.45362	2140.569
ASC85	14:35	589557	1327591	36114	20.12461	2160.694
ASC86	14:37	589580	1327560	36243.7	38.60052	2199.294
ASC87	14:39	589575	1327533	35744	27.45906	2226.753
ASC88	14:40	589568	1327511	35730.3	23.08679	2249.84
ASC89	14:42	589575	1327485	36048.7	26.92582	2276.766
ASC90	14:43	589576	1327461	36040.2	24.02082	2300.787
ASC91	14:44	589563	1327438	35865	26.41969	2327.206
ASC92	14:46	589545	1327422	36228.7	24.08319	2351.29
ASC93	14:47	589533	1327384	34862.4	39.84972	2391.139
ASC94	14:48	589524	1327365	34586	21.0238	2412.163
ASC95	14:50	589525	1327357	35721.5	8.062258	2420.225
ASC96	14:51	589523	1327339	35951.4	18.11077	2438.336
ASC97	14:52	589525	1327320	35590.6	19.10497	2457.441
ASC98	14:53	589532	1327274	35763.5	46.52956	2503.971
ASC99	14:56	589545	1327246	35154.5	30.8707	2534.841
ASC100	15:07	589549	1327233	35371.9	13.60147	2548.443
ASC101	15:08	589554	1327204	35732.7	29.42788	2577.871
ASC102	15:09	589560	1327180	36415.4	24.73863	2602.609
ASC103	15:10	589555	1327149	36325.5	31.40064	2634.01
ASC104	15:11	589556	1327120	36294.7	29.01724	2663.027
ASC105	15:12	589559	1327108	36300.4	12.36932	2675.397
ASC106	15:14	589561	1327086	35888	22.09072	2697.487
ASC107	15:24	589574	1327066	36626	23.85372	2721.341
ASC108	15:25	589573	1327063	35614	3.162278	2724.503
ASC109	15:26	589603	1327033	35894.8	42.42641	2766.93
ASC110	15:27	589620	1327017	34565	23.34524	2790.275

Name	**A45-A70b**
Area description	**Sastepe with 5m spacing**
Ring fault crossed	**Yes**
Other structures	**Unknown**
Average spacing	**5.2**
Date	**04/03/2010**
Coordinate System	**UTM Zone 16P**

Point	Local time (hr:mn)	Eastings (m)	Northings (m)	Mag (nT)	Distance (m) to previous station	Accumulated spacing (m)
A45	13:50	589917	1327915	37093.0		0
A45b	13:51	589913.5	1327919	37041.0	5.315073	5.315073
A46	13:52	589910	1327923	37033.0	5.315073	10.63015
A46b	13:53	589907	1327926	36688.0	4.242641	14.87279
A47	13:54	589904	1327929	36392.0	4.242641	19.11543
A47b	13:55	589901	1327933	36165.0	5	24.11543
A48	13:56	589898	1327937	36425.0	5	29.11543
A48b	13:57	589894	1327942	36537.0	6.020797	35.13622
A49	13:58	589890	1327946	36617.0	6.020797	41.15702
A49b	13:58	589887	1327950	37196.0	5	46.15702
A50	13:59	589884	1327954	36789.0	5	51.15702
A50b	13:59	589882	1327959	37216.0	4.924429	56.08145
A51	14:01	589880	1327963	36736.2	4.924429	61.00588
A51b	14:01	589876	1327966	36305.2	5	66.00588
A52	14:02	589872	1327969	36274.1	5	71.00588
A52b	14:03	589870.5	1327972	35957.0	2.915476	73.92136
A53	14:03	589869	1327974	35742.0	2.915476	76.83683
A53b	14:04	589859	1327979	35598.0	10.96586	87.80269
A54	14:06	589849	1327983	36682.0	10.96586	98.76854
A54b	14:06	589851	1327986	37128.0	3.201562	101.9701
A55	14:07	589853	1327988	36664.4	3.201562	105.1717
A55b	14:08	589849.5	1327993	37182.0	6.103278	111.2749
A56	14:09	589846	1327998	37125.0	6.103278	117.3782
A56b	14:09	589842	1328001	36193.9	5	122.3782
A57	14:11	589838	1328004	35874.0	5	127.3782
A57b	14:12	589834.5	1328006	35816.9	3.807887	131.1861
A58	14:13	589831	1328007	35445.0	3.807887	134.994
A58b	14:13	589828	1328012	35241.0	5.830952	140.8249
A59	14:14	589825	1328017	34224.0	5.830952	146.6559
A59b	14:15	589823.5	1328023	34689.0	5.700877	152.3568
A60	14:16	589822	1328028	36072.0	5.700877	158.0577
A60b	14:16	589820.5	1328034	36997.0	6.184658	164.2423
A61	14:17	589819	1328040	36466.0	6.184658	170.427
A61b	14:18	589819.5	1328044	35191.0	4.031129	174.4581
A62	14:19	589820	1328048	34553.0	4.031129	178.4892
A62b	14:19	589819.5	1328053	35400.0	5.024938	183.5142
A63	14:20	589819	1328058	37826.0	5.024938	188.5391
A63b	14:21	589819	1328063	36533.0	4.5	193.0391
A64	14:22	589819	1328067	35500.0	4.5	197.5391
A64b	14:23	589817.5	1328074	35672.5	6.670832	204.2099
A65	14:24	589816	1328080	35471.1	6.670832	210.8808
A65b	14:25	589817.5	1328084	35030.0	3.807887	214.6887
A66	14:26	589819	1328087	34909.0	3.807887	218.4965
A66b	14:27	589816	1328093	34911.0	6.264982	224.7615

A67	14:28	589813	1328098	35578.1	6.264982	231.0265
A67b	14:28	589813	1328103	36312.8	5	236.0265
A68	14:29	589813	1328108	36629.7	5	241.0265
A68b	14:30	589811	1328113	36763.5	4.924429	245.9509
A69	14:31	589809	1328117	36796.1	4.924429	250.8754
A69b	14:33	589806	1328121	36829.4	5	255.8754
A70	14:34	589803	1328125	36833.0	5	260.8754
A70b	14:35	589800	1328129	36793.7	5	265.8754

Name	**A20-A43**
Area description	**Short profile to look for anomalies coming from the shooting range**
Ring fault crossed	**Yes**
Other structures	**Unknown**
Average spacing	**6.9**
Date	**?**
Coordinate System	**UTM Zone 16P**

Point	Local time (hr:mn)	Eastings (m)	Northings (m)	Mag (nT)	Distance (m) to previous station	Accumulated spacing (m)
A20	11:52	590556	1328564	34972		0
A21	11:54	590552	1328562	34916.5	4.472136	4.472136
A22	11:55	590549	1328560	35016.4	3.605551	8.077687
A23	11:56	590547	1328552	35133.8	8.246211	16.3239
A24	11:58	590539	1328545	35080	10.63015	26.95404
A25	11:59	590535	1328538	35009	8.062258	35.0163
A26	12:00	590529	1328534	35901	7.211103	42.2274
A27	12:02	590525	1328529	35652	6.403124	48.63053
A28	12:03	590523	1328528	35984	2.236068	50.8666
A29	12:05	590517	1328520	36572	10	60.8666
A30	12:06	590512	1328514	36529	7.81025	68.67685
A31	12:07	590509	1328510	36562	5	73.67685
A32	12:08	590503	1328505	36478	7.81025	81.4871
A33	12:09	590494	1328499	36594	10.81665	92.30375
A34	12:11	590495	1328499	36476	1	93.30375
A35	12:12	590492	1328496	36085	4.242641	97.54639
A36	12:13	590486	1328488	36111	10	107.5464
A37	12:15	590476	1328484	35942	10.77033	118.3167
A38	12:16	590477	1328482	36327	2.236068	120.5528
A39	12:17	590475	1328476	36230	6.324555	126.8773
A40	12:18	590466	1328474	35500	9.219544	136.0969
A41	12:21	590458	1328468	35382.2	10	146.0969
A42	12:22	590454	1328464	35768	5.656854	151.7537
A43	12:24	590451	1328458	35508	6.708204	158.4619

Name	**240-367**
Area description	**From lake to Chocoyos Trail**
Ring fault crossed	**No**
Other structures	**Unknown**
Average spacing	**46.0**

Date	12/03/2010
Coordinate System	UTM Zone 16P

Point	Local time (hr:mn)	Eastings (m)	Northings (m)	Mag (nT)	Distance (m) to previous station	Accumulated spacing (m)
240		594743	1321483	36024.0		0
241		594774	1321487	36024.0	31.257	31.257
242		594729	1321474	35634.0	46.84015	78.09715
243		594681	1321469	37257.0	48.25971	126.3569
244		594667	1321455	38991.0	19.79899	146.1559
245		594654	1321398	38680.1	58.46366	204.6195
246		594629	1321355	39271.0	49.73932	254.3588
247		594590	1321345	38449.0	40.26164	294.6205
248		594552	1321366	39080.0	43.41659	338.0371
249		594509	1321384	38826.0	46.61545	384.6525
250		594468	1321405	39096.0	46.06517	430.7177
251		594431	1321433	39493.4	46.40043	477.1181
252		594381	1321427	38247.0	50.35871	527.4768
253		594345	1321403	38764.2	43.26662	570.7435
254		594302	1321383	40723.0	47.42362	618.1671
255		594252	1321393	39961.0	50.9902	669.1573
256		594204	1321401	40454.0	48.6621	717.8194
257		594165	1321416	40042.1	41.78516	759.6045
258		594119	1321424	41009.0	46.69047	806.295
259		594078	1321437	39640.0	43.01163	849.3066
260		594037	1321448	38446.0	42.44997	891.7566
261		593988	1321452	38983.0	49.16299	940.9196
262		593940	1321477	35171.0	54.12024	995.0398
263		593893	1321496	36373.7	50.69517	1045.735
264		593852	1321525	36627.0	50.21952	1095.955
265		593804	1321531	36842.8	48.37355	1144.328
266		593765	1321536	37155.3	39.31921	1183.647
267		593711	1321542	37608.2	54.33231	1237.98
268		593666	1321553	37875.0	46.32494	1284.305
269		593622	1321563	38200.0	45.12206	1329.427
270		593580	1321575	38939.0	43.68066	1373.107
271		593531	1321584	39410.2	49.81967	1422.927
272		593488	1321602	39206.0	46.61545	1469.542
273		593444	1321618	40380.9	46.8188	1516.361
274		593397	1321609	41005.7	47.85394	1564.215
275		593344	1321621	39288.8	54.34151	1618.557
276		593318	1321650	39234.6	38.94868	1657.505
277		593279	1321671	38491.2	44.29447	1701.8
278		593226	1321686	38815.4	55.08176	1756.882
279		593179	1321714	39012.8	54.70832	1811.59

280		593144	1321751	39091.7	50.93133	1862.521
281		593111	1321785	38537.0	47.38143	1909.903
282		593072	1321805	39978.0	43.82921	1953.732
283		593041	1321794	39757.8	32.89377	1986.626
284		593026	1321867	39637.0	74.52516	2061.151
285		593001	1321911	39191.7	50.60632	2111.757
286		592972	1321955	38969.3	52.69725	2164.454
287		592914	1321973	39288.8	60.72891	2225.183
288		592908	1322014	39286.8	41.4367	2266.62
289		592875	1322057	40058.7	54.20332	2320.823
290		592845	1322095	40065.4	48.41487	2369.238
291		592839	1322123	39144.4	28.63564	2397.874
292		592805	1322174	39122.2	61.29437	2459.168
293		592784	1322218	38839.0	48.75449	2507.923
294		592749	1322277	39515.3	68.60029	2576.523
295		592727	1322313	39796.0	42.19005	2618.713
296		592713	1322355	38947.4	44.27189	2662.985
297		592698	1322395	39236.6	42.72002	2705.705
298		592679	1322435	38417.3	44.28318	2749.988
299		592658	1322476	38168.9	46.06517	2796.053
300		592640	1322521	38813.6	48.46648	2844.52
301		592607	1322547	38345.3	42.0119	2886.532
302		592569	1322515	38722.6	49.67897	2936.211
303		592524	1322513	38405.8	45.04442	2981.255
304		592499	1322493	38282.5	32.01562	3013.271
305		592457	1322484	37997.9	42.95346	3056.224
306		592409	1322477	38080.8	48.50773	3104.732
307		592373	1322482	37801.2	36.34556	3141.077
308		592335	1322460	37510.8	43.909	3184.986
309		592291	1322430	37701.2	53.25411	3238.24
310		592252	1322414	38328.6	42.15448	3280.395
311		592219	1322403	37410.0	34.78505	3315.18
312		592177	1322365	36621.0	56.63921	3371.819
313		592138	1322336	38514.0	48.60041	3420.42
314		592091	1322327	39940.0	47.85394	3468.274
315		592041	1322329	37629.5	50.03998	3518.314
316		592055	1322381	37262.5	53.85165	3572.165
317		592056	1322430	36965.0	49.0102	3621.175
318		592037	1322469	38347.0	43.38202	3664.557
319		591998	1322488	38054.0	43.38202	3707.939
320		591953	1322485	37765.5	45.09989	3753.039
321		591908	1322474	38441.0	46.32494	3799.364
322		591863	1322461	38104.1	46.84015	3846.204
323		591813	1322459	37718.6	50.03998	3896.244
324		591770	1322473	38358.0	45.22168	3941.466
325		591728	1322507	37791.5	54.03702	3995.503
326		591697	1322542	38168.0	46.75468	4042.258
327		591664	1322587	37327.0	55.80323	4098.061
328		591661	1322620	37265.9	33.13608	4131.197
329		591651	1322664	37126.0	45.12206	4176.319
330		591637	1322711	37325.9	49.0408	4225.36
331		591624	1322754	36754.6	44.92215	4270.282

332		591631	1322799	36956.7	45.54119	4315.823
333		591630	1322845	37314.9	46.01087	4361.834
334		591619	1322860	38428.0	18.60108	4380.435
335		591592	1322910	37129.4	56.82429	4437.26
336		591552	1322946	37984.5	53.8145	4491.074
337		591511	1322969	37753.5	47.01064	4538.085
338		591477	1322997	38282.2	44.04543	4582.13
339		591433	1323025	37407.0	52.15362	4634.284
340		591401	1323056	37430.0	44.55334	4678.837
341		591366	1323086	38521.0	46.09772	4724.935
342		591328	1323105	37871.6	42.48529	4767.42
343		591288	1323130	37176.0	47.16991	4814.59
344		591263	1323168	37922.0	45.48626	4860.076
345		591239	1323205	38055.0	44.10215	4904.178
346		591247	1323235	36382.0	31.04835	4935.227
347		591266	1323282	39744.2	50.69517	4985.922
348		591256	1323322	38887.9	41.23106	5027.153
349		591211	1323317	40516.0	45.27693	5072.43
350		591169	1323328	39196.2	43.41659	5115.846
351		591131	1323339	39799.2	39.56008	5155.407
352		591092	1323328	39590.7	40.5216	5195.928
353		591055	1323313	39136.0	39.92493	5235.853
354		591015	1323302	38721.0	41.48494	5277.338
355		590969	1323310	39552.9	46.69047	5324.029
356		590926	1323320	40237.0	44.14748	5368.176
357		590902	1323351	40341.0	39.20459	5407.381
358		590857	1323366	39149.6	47.43416	5454.815
359		590819	1323379	39716.0	40.16217	5494.977
360		590788	1323367	38882.0	33.24154	5528.218
361		590745	1323400	39485.0	54.20332	5582.422
362		590714	1323427	39513.1	41.10961	5623.531
363		590675	1323461	38495.7	51.73973	5675.271
364		590680	1323499	38185.1	38.32754	5713.599
365		590656	1323537	38667.0	44.94441	5758.543
366		590630	1323578	37823.1	48.54894	5807.092
367		590602	1323598	37723.1	34.4093	5841.501

Name	**1-116**
Area description	**Around Cerro Montoso**
Ring fault crossed	**Yes**
Other structures	**Unknown**
Average spacing	**22.6**
Date	**12/03/2010**
Coordinate System	**UTM Zone 16P**

Point	Local	Eastings (m)	Northings (m)	Mag (nT)	Distance (m) to	Accumulated spacing (m)

	time (hr:mn)				previous station	
1	?	589549	1326870	36318.0		0
2	?	589536	1326861	35551.2	15.81139	15.81139
3	?	589522	1326846	35204.0	20.51828	36.32967
4	?	589505	1326829	35930.0	24.04163	60.3713
5	?	589483	1326825	35458.0	22.36068	82.73198
6	?	589457	1326823	35686.7	26.07681	108.8088
7	?	589440	1326829	35915.0	18.02776	126.8365
8	?	589426	1326842	35972.5	19.10497	145.9415
9	?	589406	1326872	36264.0	36.05551	181.997
10	?	589395	1326889	36094.6	20.24846	202.2455
11	?	589387	1326912	35699.7	24.35159	226.5971
12	?	589386	1326932	35319.5	20.02498	246.6221
13	?	589388	1326955	35916.0	23.08679	269.7089
14	?	589397	1326963	35110.0	12.04159	281.7505
15	?	589412	1326977	34827.0	20.51828	302.2687
16	?	589424	1326996	36338.0	22.47221	324.7409
17	?	589426	1327016	36971.0	20.09975	344.8407
18	?	589418	1327034	36840.9	19.69772	364.5384
19	?	589404	1327059	36849.8	28.6531	393.1915
20	?	589385	1327083	37056.0	30.61046	423.802
21	?	589378	1327088	37206.0	8.602325	432.4043
22	?	589362	1327104	37306.0	22.62742	455.0317
23	?	589344	1327126	37336.0	28.42534	483.457
24	?	589322	1327139	37880.0	25.55386	509.0109
25	?	589315	1327147	38100.8	10.63015	519.6411
26	?	589295	1327173	36765.1	32.80244	552.4435
27	?	589289	1327184	36380.0	12.52996	564.9735
28	?	589281	1327212	35531.0	29.12044	594.0939
29	?	589274	1327224	35604.0	13.89244	607.9863
30	?	589258	1327245	35343.4	26.40076	634.3871
31	?	589239	1327256	36784.0	21.9545	656.3416
32	?	589217	1327266	34315.0	24.16609	680.5077
33	?	589198	1327276	34365.0	21.47091	701.9786
34	?	589175	1327285	35350.0	24.69818	726.6768
35	?	589158	1327296	35470.0	20.24846	746.9252
36	?	589133	1327297	35501.0	25.01999	771.9452
37	?	589121	1327277	35355.0	23.32381	795.269
38	?	589116	1327256	35878.0	21.58703	816.8561
39	?	589105	1327235	35698.9	23.70654	840.5626
40	?	589096	1327218	35772.0	19.23538	859.798
41	?	589081	1327198	35309.0	25	884.798
42	?	589063	1327181	35372.2	24.75884	909.5568
43	?	589052	1327168	35726.4	17.02939	926.5862
44	?	589037	1327146	36125.7	26.62705	953.2133
45	?	589020	1327121	36948.7	30.23243	983.4457
46	?	589006	1327103	36704.5	22.80351	1006.249
47	?	588996	1327087	37226.4	18.86796	1025.117

48	?	588979	1327069	37282.3	24.75884	1049.876
49	?	588961	1327055	37090.0	22.80351	1072.68
50	?	588938	1327047	37036.6	24.35159	1097.031
51	?	588917	1327041	37376.6	21.84033	1118.871
52	?	588895	1327035	37112.6	22.80351	1141.675
53	?	588873	1327028	38162.0	23.08679	1164.762
54	?	588850	1327032	36081.0	23.34524	1188.107
55	?	588834	1327036	36316.6	16.49242	1204.599
56	?	588824	1327020	38172.0	18.86796	1223.467
57	?	588802	1327001	36677.1	29.06888	1252.536
58	?	588791	1326985	36172.1	19.41649	1271.953
59	?	588782	1326970	35928.1	17.49286	1289.446
60	?	588782	1326954	35778.2	16	1305.446
61	?	588761	1326935	36239.0	28.3196	1333.765
62	?	588744	1326928	35727.0	18.38478	1352.15
63	?	588722	1326925	36448.8	22.2036	1374.354
64	?	588705	1326930	36045.4	17.72005	1392.074
65	?	588679	1326922	35581.0	27.20294	1419.277
66	?	588679	1326901	35367.4	21	1440.277
67	?	588673	1326881	35558.1	20.88061	1461.157
68	?	588659	1326861	35724.0	24.41311	1485.57
69	?	588650	1326839	35577.2	23.76973	1509.34
70	?	588656	1326814	35575.7	25.70992	1535.05
71	?	588664	1326793	35642.7	22.47221	1557.522
72	?	588664	1326775	35610.2	18	1575.522
73	?	588670	1326744	35868.8	31.57531	1607.097
74	?	588673	1326718	36099.6	26.1725	1633.27
75	?	588682	1326705	36493.8	15.81139	1649.081
76	?	588695	1326685	36719.5	23.85372	1672.935
77	?	588709	1326669	36119.7	21.26029	1694.195
78	?	588707	1326643	36144.0	26.07681	1720.272
79	?	588709	1326623	36268.5	20.09975	1740.372
80	?	588719	1326601	36020.0	24.16609	1764.538
81	?	588734	1326586	35719.0	21.2132	1785.751
82	?	588751	1326571	36300.5	22.67157	1808.423
83	?	588771	1326552	37218.0	27.58623	1836.009
84	?	588770	1326536	37351.3	16.03122	1852.04
85	?	588788	1326502	37131.0	38.47077	1890.511
86	?	588799	1326483	36397.4	21.9545	1912.465
87	?	588815	1326468	36458.0	21.93171	1934.397
88	?	588816	1326446	36114.0	22.02272	1956.42
89	?	588808	1326423	35435.0	24.35159	1980.772
90	?	588806	1326401	35610.9	22.09072	2002.862
91	?	588806	1326378	35080.0	23	2025.862
92	?	588806	1326355	35741.0	23	2048.862
93	?	588796	1326337	36441.9	20.59126	2069.453
94	?	588784	1326318	35619.0	22.47221	2091.926
95	?	588777	1326295	35425.9	24.04163	2115.967
96	?	588767	1326274	35016.0	23.25941	2139.227
97	?	588758	1326256	35413.8	20.12461	2159.351
98	?	588758	1326233	35641.2	23	2182.351
99	?	588760	1326209	35480.0	24.08319	2206.435

100	?	588769	1326187	36167.0	23.76973	2230.204
101	?	588774	1326165	36963.0	22.56103	2252.765
102	?	588778	1326141	36456.0	24.33105	2277.096
103	?	588780	1326118	36340.6	23.08679	2300.183
104	?	588781	1326096	35793.0	22.02272	2322.206
105	?	588796	1326078	37047.0	23.43075	2345.637
106	?	588814	1326061	36619.8	24.75884	2370.395
107	?	588832	1326045	37264.0	24.08319	2394.479
108	?	588849	1326028	36470.0	24.04163	2418.52
109	?	588862	1326008	36329.0	23.85372	2442.374
110	?	588864	1325986	36492.4	22.09072	2464.465
111	?	588864	1325963	36359.0	23	2487.465
112	?	588865	1325936	37422.0	27.01851	2514.483
113	?	588869	1325914	37178.0	22.36068	2536.844
114	?	588870	1325888	35909.0	26.01922	2562.863
115	?	588874	1325861	36883.4	27.29469	2590.158
116	?	588885	1325859	36711.9	11.18034	2601.338

Name	**114-239**
Area description	**Laguna de Masaya**
Ring fault crossed	**No**
Other structures	**Unknown**
Average spacing	**48.6**
Date	**12/03/2010**
Coordinate System	**UTM Zone 16P**

Point	Local time (hr:mn)	Eastings (m)	Northings (m)	Mag (nT)	Distance (m) to previous station	Accumulated spacing (m)
114	?	594975	1326389	36970.5		0
115	?	594941	1326411	37215.1	40.49691	40.49691
116	?	594920	1326433	37533.7	30.41381	70.91073
117	?	594882	1326432	37433.8	38.01316	108.9239
118	?	594895	1326393	36849.7	41.10961	150.0335
119	?	594921	1326367	34715.0	36.76955	186.803
120	?	594963	1326345	34723.0	47.41308	234.2161
121	?	594994	1326327	34193.0	35.8469	270.063
122	?	595125	1326374	33989.0	139.1761	409.2392
123	?	595160	1326358	33884.0	38.48376	447.7229
124	?	595216	1326344	33859.0	57.72348	505.4464
125	?	595254	1326342	34578.0	38.0526	543.499
126	?	595313	1326325	33349.0	61.40033	604.8993
127	?	595366	1326312	33073.0	54.57105	659.4704

128	?	595401	1326288	33362.0	42.43819	701.9086
129	?	595454	1326276	33284.0	54.34151	756.2501
130	?	595492	1326235	31277.0	55.9017	812.1518
131	?	595515	1326198	30048.0	43.56604	855.7178
132	?	595533	1326153	30734.0	48.46648	904.1843
133	?	595550	1326107	32151.0	49.0408	953.2251
134	?	595565	1326062	33585.0	47.43416	1000.659
135	?	595583	1326018	34526.0	47.53946	1048.199
136	?	595598	1325971	35249.0	49.33559	1097.534
137	?	595619	1325925	36234.0	50.56679	1148.101
138	?	595640	1325881	36282.3	48.75449	1196.856
139	?	595663	1325836	36916.4	50.53712	1247.393
140	?	595682	1325791	36566.7	48.8467	1296.239
141	?	595702	1325745	37242.7	50.15974	1346.399
142	?	595720	1325700	37121.7	48.46648	1394.866
143	?	595723	1325654	37723.8	46.09772	1440.963
144	?	595716	1325604	37330.0	50.48762	1491.451
145	?	595706	1325555	38072.4	50.01	1541.461
146	?	595693	1325508	36988.6	48.76474	1590.226
147	?	595680	1325459	36062.6	50.69517	1640.921
148	?	595668	1325412	35556.9	48.50773	1689.429
149	?	595655	1325366	35471.9	47.80167	1737.23
150	?	595636	1325324	35616.0	46.09772	1783.328
151	?	595623	1325287	37230.7	39.21734	1822.545
152	?	595580	1325243	38005.9	61.52235	1884.068
153	?	595545	1325210	36696.0	48.10405	1932.172
154	?	595512	1325179	36616.7	45.27693	1977.449
155	?	595481	1325138	36864.3	51.40039	2028.849
156	?	595483	1325090	33822.0	48.04165	2076.891
157	?	595486	1325074	36218.3	16.27882	2093.17
158	?	595523	1325024	33731.0	62.20129	2155.371
159	?	595560	1324976	36611.8	60.60528	2215.976
160	?	595563	1324925	36114.0	51.08816	2267.064
161	?	595558	1324886	35333.0	39.31921	2306.383
162	?	595547	1324840	34991.7	47.29693	2353.68
163	?	595540	1324785	34574.0	55.44367	2409.124
164	?	595535	1324749	32405.0	36.34556	2445.47
165	?	595528	1324688	33173.0	61.40033	2506.87
166	?	595522	1324637	34743.1	51.35173	2558.222
167	?	595522	1324594	34753.0	43	2601.222
168	?	595512	1324545	37417.9	50.01	2651.232
169	?	595524	1324502	37431.1	44.64303	2695.875
170	?	595543	1324453	36567.0	52.55473	2748.429
171	?	595547	1324407	36245.8	46.17359	2794.603
172	?	595544	1324357	34252.0	50.08992	2844.693
173	?	595527	1324318	34042.0	42.54409	2887.237
174	?	595508	1324273	34478.0	48.8467	2936.084
175	?	595489	1324228	35622.0	48.8467	2984.93
176	?	595465	1324186	36971.6	48.37355	3033.304
177	?	595443	1324139	36751.0	51.89412	3085.198
178	?	595417	1324099	37069.8	47.70744	3132.906
179	?	595394	1324054	38512.0	50.53712	3183.443

180	?	595370	1324013	36532.3	47.50789	3230.951
181	?	595347	1323978	34932.4	41.88078	3272.831
182	?	595328	1323924	34525.0	57.24509	3330.076
183	?	595304	1323878	33456.0	51.88449	3381.961
184	?	595288	1323840	32889.0	41.23106	3423.192
185	?	595271	1323800	34434.2	43.46263	3466.655
186	?	595260	1323755	37666.0	46.32494	3512.98
187	?	595250	1323710	37728.0	46.09772	3559.077
188	?	595247	1323662	36355.0	48.09366	3607.171
189	?	595245	1323617	36589.0	45.04442	3652.215
190	?	595262	1323570	36145.6	49.98	3702.195
191	?	595299	1323535	35276.5	50.93133	3753.127
192	?	595323	1323496	35769.7	45.79301	3798.92
193	?	595336	1323449	35296.0	48.76474	3847.684
194	?	595335	1323406	33640.0	43.01163	3890.696
195	?	595355	1323358	33573.0	52	3942.696
196	?	595361	1323309	34578.0	49.36598	3992.062
197	?	595361	1323259	37709.0	50	4042.062
198	?	595369	1323225	36554.6	34.9285	4076.991
199	?	595357	1323176	35613.0	50.44799	4127.439
200	?	595340	1323121	36606.0	57.56735	4185.006
201	?	595323	1323072	36887.6	51.86521	4236.871
202	?	595299	1323025	35790.0	52.7731	4289.644
203	?	595268	1322984	38458.0	51.40039	4341.045
204	?	595258	1322939	37965.0	46.09772	4387.142
205	?	595256	1322893	37366.0	46.04346	4433.186
206	?	595249	1322838	36906.7	55.44367	4488.629
207	?	595236	1322792	34618.0	47.80167	4536.431
208	?	595213	1322757	37500.2	41.88078	4578.312
209	?	595190	1322723	36626.9	41.04875	4619.361
210	?	595161	1322677	35734.2	54.3783	4673.739
211	?	595126	1322637	35547.3	53.15073	4726.89
212	?	595096	1322595	36073.1	51.61395	4778.504
213	?	595071	1322558	37613.6	44.65423	4823.158
214	?	595042	1322519	37430.0	48.60041	4871.758
215	?	595011	1322482	34707.0	48.27007	4920.028
216	?	594983	1322443	32448.0	48.01042	4968.039
217	?	594955	1322402	33325.0	49.64877	5017.688
218	?	594925	1322364	34128.0	48.41487	5066.102
219	?	594897	1322326	34961.0	47.20169	5113.304
220	?	594869	1322286	36988.8	48.82622	5162.13
221	?	594841	1322246	36585.0	48.82622	5210.957
222	?	594814	1322210	38332.1	45	5255.957
223	?	594785	1322168	36276.0	51.0392	5306.996
224	?	594757	1322132	35846.0	45.60702	5352.603
225	?	594738	1322090	38078.0	46.09772	5398.7
226	?	594721	1322037	39693.0	55.65968	5454.36
227	?	594697	1321994	38409.0	49.24429	5503.604
228	?	594691	1321945	37865.4	49.36598	5552.97
229	?	594675	1321908	39533.2	40.31129	5593.282
230	?	594647	1321866	41271.0	50.47772	5643.759
231	?	594624	1321822	37734.0	49.64877	5693.408

232	?	594610	1321784	34691.0	40.49691	5733.905
233	?	594619	1321731	38691.0	53.75872	5787.664
234	?	594629	1321686	40521.0	46.09772	5833.762
235	?	594640	1321638	38598.0	49.24429	5883.006
236	?	594662	1321602	37314.0	42.19005	5925.196
237	?	594704	1321575	37961.0	49.92995	5975.126
238	?	594727	1321531	37794.0	49.64877	6024.775
239	?	594743	1321485	36581.0	48.70318	6073.478

Name	**1-113**
Area description	**Casco Buey-Jinocuabos (behing San Fernando Cone, acrossCoyotes Trail, ending in Nindiri Town)**
Ring fault crossed	**No**
Other structures	**Unknown**
Average spacing	**45.57750123**
Date	**11/03/2010**
Coordinate System	**UTM Zone 16P**

Point	Local time (hr:mn)	Eastings (m)	Northings (m)	Mag (nT)	Distance (m) to previous station	Accumulated spacing (m)
1	?	594705	1326383	34328.0		0
2	?	594665	1326355	32980.0	48.82622	48.82622
3	?	594643	1326349	31121.0	22.80351	71.62973
4	?	594608	1326312	31067.0	50.93133	122.5611
5	?	594555	1326273	30458.0	65.80274	188.3638
6	?	594526	1326241	31501.0	43.18565	231.5494
7	?	594479	1326212	31888.0	55.22681	286.7762
8	?	594429	1326188	32999.0	55.4617	342.2379
9	?	594393	1326166	33853.0	42.19005	384.428
10	?	594348	1326146	34490.0	49.24429	433.6723
11	?	594307	1326125	34760.0	46.06517	479.7374
12	?	594265	1326108	34672.0	45.31004	525.0475
13	?	594225	1326105	35180.0	40.11234	565.1598
14	?	594180	1326094	35708.0	46.32494	611.4848
15	?	594130	1326078	35931.0	52.49762	663.9824
16	?	594074	1326054	36159.0	60.92618	724.9086
17	?	594040	1326036	35946.4	38.47077	763.3793
18	?	594000	1326021	35635.0	42.72002	806.0994
19	?	593957	1326030	35862.2	43.93177	850.0311
20	?	593915	1326032	36234.0	42.04759	892.0787
21	?	593864	1326005	37907.0	57.70615	949.7849
22	?	593827	1326002	36722.0	37.12142	986.9063
23	?	593777	1325997	36417.0	50.24938	1037.156

24	?	593716	1325989	36589.0	61.52235	1098.678
25	?	593680	1325986	36475.0	36.12478	1134.803
26	?	593631	1325976	36470.6	50.01	1184.813
27	?	593598	1325923	38717.0	62.43397	1247.247
28	?	593573	1325897	37198.6	36.06938	1283.316
29	?	593572	1325894	38147.0	3.162278	1286.478
30	?	593485	1325838	38262.0	103.465	1389.943
31	?	593456	1325812	36869.1	38.94868	1428.892
32	?	593445	1325805	36617.2	13.0384	1441.93
33	?	593251	1325750	34335.0	201.6457	1643.576
34	?	593221	1325713	36602.6	47.63402	1691.21
35	?	593192	1325681	35414.8	43.18565	1734.396
36	?	593166	1325642	35753.8	46.87217	1781.268
37	?	593156	1325591	35162.4	51.97115	1833.239
38	?	593164	1325547	34971.1	44.72136	1877.961
39	?	593181	1325509	36898.4	41.62932	1919.59
40	?	593161	1325460	36254.9	52.92447	1972.514
41	?	593139	1325433	35073.0	34.82815	2007.342
42	?	593161	1325389	35214.6	49.1935	2056.536
43	?	593123	1325357	36150.2	49.67897	2106.215
44	?	593115	1325330	35251.2	28.16026	2134.375
45	?	593093	1325297	35060.0	39.66106	2174.036
46	?	593071	1325269	35236.0	35.60899	2209.645
47	?	593033	1325188	36623.0	89.47067	2299.116
48	?	593028	1325144	36262.0	44.28318	2343.399
49	?	593018	1325094	35525.5	50.9902	2394.389
50	?	592992	1325073	35623.7	33.42155	2427.811
51	?	592965	1325015	35902.9	63.97656	2491.787
52	?	592939	1324993	36229.1	34.05877	2525.846
53	?	592928	1324939	35308.0	55.10898	2580.955
54	?	592908	1324892	35994.2	51.07837	2632.034
55	?	592906	1324858	36478.9	34.05877	2666.092
56	?	592886	1324799	37099.1	62.29767	2728.39
57	?	592871	1324760	37370.0	41.78516	2770.175
58	?	592855	1324743	36717.5	23.34524	2793.52
59	?	592844	1324733	35849.0	14.86607	2808.386
60	?	592811	1324708	37120.0	41.40048	2849.787
61	?	592752	1324676	37271.0	67.1193	2916.906
62	?	592733	1324652	39366.0	30.61046	2947.517
63	?	592720	1324637	38219.0	19.84943	2967.366
64	?	592659	1324598	38136.8	72.40166	3039.768
65	?	592605	1324553	38855.0	70.29225	3110.06
66	?	592586	1324535	39045.0	26.1725	3136.233
67	?	592550	1324527	39026.0	36.87818	3173.111
68	?	592503	1324502	36845.0	53.23533	3226.346
69	?	592466	1324482	37179.5	42.05948	3268.406
70	?	592434	1324510	38111.3	42.52058	3310.926
71	?	592413	1324510	38600.0	21	3331.926
72	?	592379	1324499	37922.3	35.73514	3367.661
73	?	592358	1324511	38291.0	24.18677	3391.848
74	?	592284	1324497	37955.7	75.31268	3467.161
75	?	592260	1324483	37747.0	27.78489	3494.946

76	?	592246	1324486	37871.0	14.31782	3509.263
77	?	592146	1324485	38395.7	100.005	3609.268
78	?	592141	1324482	38005.2	5.830952	3615.099
79	?	592128	1324478	37389.7	13.60147	3628.701
80	?	592059	1324435	38044.0	81.30191	3710.003
81	?	592051	1324418	39734.0	18.78829	3728.791
82	?	592005	1324427	40534.0	46.87217	3775.663
83	?	591921	1324423	37603.0	84.09518	3859.758
84	?	591895	1324433	38539.0	27.85678	3887.615
85	?	591856	1324439	37366.0	39.45884	3927.074
86	?	591809	1324426	35789.8	48.76474	3975.839
87	?	591743	1324403	34960.2	69.89278	4045.732
88	?	591698	1324404	36330.5	45.01111	4090.743
89	?	591683	1324387	37589.0	22.67157	4113.414
90	?	591654	1324370	37290.0	33.61547	4147.03
91	?	591603	1324350	38360.4	54.78138	4201.811
92	?	591577	1324354	37416.0	26.30589	4228.117
93	?	591516	1324333	37592.0	64.51356	4292.631
94	?	591487	1324328	36160.0	29.42788	4322.058
95	?	591467	1324307	34369.0	29	4351.058
96	?	591442	1324260	34029.0	53.23533	4404.294
97	?	591423	1324213	35210.0	50.69517	4454.989
98	?	591419	1324195	36490.0	18.43909	4473.428
99	?	591389	1324174	36257.6	36.61967	4510.048
100	?	591360	1324169	36297.0	29.42788	4539.476
101	?	591315	1324157	36381.0	46.57252	4586.048
102	?	591272	1324148	35869.6	43.93177	4629.98
103	?	591232	1324131	36565.0	43.46263	4673.442
104	?	591158	1324139	38719.0	74.43118	4747.874
105	?	591118	1324140	36513.3	40.0125	4787.886
106	?	591086	1324134	35418.0	32.55764	4820.444
107	?	591045	1324138	35797.8	41.19466	4861.638
108	?	591025	1324171	35349.0	38.58756	4900.226
109	?	591020	1324184	35868.0	13.92839	4914.154
110	?	590980	1324212	35317.8	48.82622	4962.981
111	?	590930	1324207	35482.0	50.24938	5013.23
112	?	590883	1324214	35409.0	47.51842	5060.748
113	?	590840	1324223	37925.0	43.93177	5104.68

Name	**CH1-121**
Area description	**Chocoyos trail (lava tube system included)**
Ring fault crossed	**No**
Other structures	**Lava tube system**
Average spacing	**26.50504035**
Date	**05/03/2010**
Coordinate System	**UTM Zone 16P**

Point	Local time (hr:mn)	Eastings (m)	Northings (m)	Mag (nT)	Distance (m) to previous station	Accumulated spacing (m)
CH1	10:05	590726	1324609	33258		0
CH2	10:09	590740	1324591	34003	22.80351	22.80351
CH3	10:12	590761	1324578	34927.9	24.69818	47.50169
CH4	10:16	590785	1324573	36379.9	24.5153	72.01699
CH5	10:18	590810	1324569	36650.8	25.31798	97.33497
CH6	10:20	590834	1324550	36159.2	30.61046	127.9454
CH7	10:21	590840	1324536	36392.1	15.23155	143.177
CH8	10:23	590858	1324520	36012.6	24.08319	167.2602
CH9	10:25	590869	1324490	36467.9	31.95309	199.2132
CH10	10:26	590869	1324470	36619.5	20	219.2132
CH11	10:28	590862	1324448	36581.8	23.08679	242.3
CH12	10:29	590859	1324424	36651	24.18677	266.4868
CH13	10:31	590868	1324393	37332	32.28002	298.7668
CH14	10:32	590870	1324373	36050.9	20.09975	318.8666
CH15	10:34	590869	1324339	35857.4	34.0147	352.8813
CH16	10:35	590858	1324325	36643	17.80449	370.6858
CH17	10:42	590851	1324304	37243	22.13594	392.8217
CH18	10:46	590843	1324285	36259	20.61553	413.4373
CH19	10:47	590836	1324266	35956.5	20.24846	433.6857
CH20	10:48	590824	1324242	36114.4	26.83282	460.5185
CH21	10:50	590812	1324219	37004	25.94224	486.4608
CH22	10:51	590798	1324200	36279.5	23.60085	510.0616
CH23	10:52	590778	1324184	35368	25.6125	535.6741
CH24	10:54	590769	1324157	35911.3	28.4605	564.1346
CH25	10:56	590762	1324142	36608	16.55295	580.6876
CH26	11:00	590759	1324114	35640	28.16026	608.8478
CH27	11:01	590768	1324089	36186	26.57066	635.4185
CH28	11:02	590755	1324069	35960	23.85372	659.2722
CH29	11:04	590753	1324034	36592	35.0571	694.3293
CH30	11:05	590750	1324022	36055	12.36932	706.6986
CH31	11:06	590766	1324002	37191.1	25.6125	732.3111
CH32	11:08	590777	1323961	37803.6	42.44997	774.7611
CH33	11:10	590780	1323949	37359.6	12.36932	787.1304
CH34	11:12	590783	1323919	35849	30.14963	817.28
CH35	11:14	590786	1323891	36509	28.16026	845.4403
CH36	11:16	590791	1323879	37206.2	13	858.4403
CH37	11:17	590796	1323845	36720.6	34.36568	892.806
CH38	11:21	590791	1323828	37609.3	17.72005	910.526
CH39	11:22	590762	1323801	37809	39.62323	950.1492
CH40	11:24	590748	1323792	38549	16.64332	966.7925
CH41	11:25	590728	1323777	38628	25	991.7925
CH42	11:27	590699	1323763	39822	32.20248	1023.995
CH43	11:28	590678	1323746	38158.7	27.01851	1051.014
CH44	11:32	590648	1323746	38098.9	30	1081.014
CH45	11:33	590634	1323720	38125.5	29.52965	1110.543
CH46	11:36	590630	1323699	37507.5	21.37756	1131.921

CH47	11:37	590633	1323663	37362.8	36.12478	1168.046
CH48	11:38	590619	1323653	37632.6	17.20465	1185.25
CH49	11:40	590604	1323634	37727.1	24.20744	1209.458
CH50	11:42	590578	1323617	37836.2	31.06445	1240.522
CH51	11:43	590563	1323599	38634	23.43075	1263.953
CH52	11:44	590546	1323576	37979.9	28.6007	1292.554
CH53	11:46	590527	1323560	37479.2	24.83948	1317.393
CH54	11:47	590501	1323548	38219.9	28.63564	1346.029
CH55	11:49	590487	1323527	37182	25.23886	1371.268
CH56	11:51	590472	1323516	38523.9	18.60108	1389.869
CH57	11:55	590451	1323524	39696	22.47221	1412.341
CH58	11:57	590433	1323533	38240.3	20.12461	1432.465
CH59	11:58	590413	1323558	39325.2	32.01562	1464.481
CH60	12:01	590387	1323582	39828	35.38361	1499.865
CH61	12:02	590352	1323616	37279.3	48.79549	1548.66
CH62	12:03	590362	1323626	37853.4	14.14214	1562.802
CH63	12:05	590346	1323644	37918.9	24.08319	1586.885
CH64	12:06	590343	1323667	37530	23.19483	1610.08
CH65	12:07	590337	1323686	41978	19.92486	1630.005
CH66	12:12	590313	1323709	40356	33.24154	1663.247
CH67	12:13	590284	1323709	42244	29	1692.247
CH68	12:14	590264	1323708	42658	20.02498	1712.272
CH69	12:18	590239	1323714	41382.1	25.70992	1737.982
CH70	12:20	590215	1323715	41566.6	24.02082	1762.002
CH71	12:22	590186	1323688	40936.8	39.62323	1801.626
CH72	12:22	590179	1323677	40954.1	13.0384	1814.664
CH73	12:24	590146	1323673	42025	33.24154	1847.906
CH74	12:25	590112	1323667	40174.7	34.52535	1882.431
CH75	12:27	590117	1323664	39570	5.830952	1888.262
CH76	12:28	590073	1323672	41489	44.72136	1932.983
CH77	12:29	590034	1323677	40072	39.31921	1972.302
CH78	12:30	590007	1323684	42265	27.89265	2000.195
CH79	13:32	590012	1323686	42314	5.385165	2005.58
CH80	13:33	589987	1323688	41456	25.07987	2030.66
CH81	13:34	589964	1323687	41558	23.02173	2053.682
CH82	13:36	589934	1323694	41549.7	30.80584	2084.488
CH83	13:37	589913	1323701	41113	22.13594	2106.624
CH84	13:38	589880	1323707	41312.9	33.54102	2140.165
CH85	13:39	589859	1323711	42130	21.37756	2161.542
CH86	13:41	589829	1323719	43002	31.04835	2192.591
CH90	13:42	589813	1323722	42009	16.27882	2208.869
CH91	13:43	589778	1323720	41992	35.0571	2243.926
CH92	13:45	589754	1323720	40466.6	24	2267.926
CH93	13:46	589732	1323727	40406.3	23.08679	2291.013
CH94	13:47	589695	1323732	40350.1	37.33631	2328.35
CH95	13:48	589675	1323746	39800.5	24.41311	2352.763
CH96	13:49	589649	1323755	39642.2	27.51363	2380.276
CH97	13:51	589635	1323763	38850.3	16.12452	2396.401
CH98	13:52	589539	1323773	38652.4	96.51943	2492.92
CH99	13:53	589571	1323779	39180	32.55764	2525.478
CH100	13:54	589545	1323785	38239	26.68333	2552.161
CH101	13:56	589532	1323791	36976	14.31782	2566.479

CH102	13:57	589501	1323798	37324.1	31.7805	2598.26
CH103	13:59	589485	1323816	37298.4	24.08319	2622.343
CH104	14:03	589453	1323828	37572.1	34.17601	2656.519
CH105	14:04	589409	1323856	37981.1	52.15362	2708.672
CH106	14:07	589403	1323861	38149.1	7.81025	2716.483
CH107	14:08	589374	1323874	38545	31.7805	2748.263
CH108	14:09	589361	1323889	38735.2	19.84943	2768.113
CH109	14:10	589342	1323900	38587.8	21.9545	2790.067
CH110	14:11	589310	1323914	37901	34.9285	2824.996
CH111	14:12	589295	1323922	39635.5	17	2841.996
CH112	14:13	589269	1323934	39306.5	28.63564	2870.631
CH113	14:14	589251	1323946	39833	21.63331	2892.265
CH114	14:16	589223	1323963	40220.6	32.75668	2925.021
CH115	14:18	589205	1323976	39348.9	22.2036	2947.225
CH116	14:20	589179	1324003	39274.4	37.48333	2984.708
CH117	14:21	589172	1324019	39074.7	17.46425	3002.172
CH118	14:23	589148	1324039	39031	31.241	3033.413
CH119	14:24	589134	1324050	40111	17.80449	3051.218
CH120	14:25	589106	1324076	39839.7	38.20995	3089.428
CH121	14:27	589096	1324082	38803.5	11.6619	3101.09

Name	**1.00-75.00**
Area description	**From Km. 19 (road to Managua) to Sastepe Cone**
Ring fault crossed	**Yes**
Other structures	**Part of the Northern Fissure System: Spatter rampart (eruptive center)**
Average spacing	**21.39375313**
Date	**16/02/2011**
Coordinate System	**UTM Zone 16P**

Point	Local time (hr:mn)	Eastings (m)	Northings (m)	Mag (nT)	Distance (m) to previous station	Accumulated spacing (m)
1.00	16:11	35768.62	589825	1329285		0
2.00	16:12	35709.26	589883	1329264	61.6846821	61.6846821
3.00	16:20	36046.98	589888	1329251	13.9283883	75.6130703
4.00	16:22	36521.39	589905	1329219	36.2353419	111.848412
5.00	16:24	36662.50	589911	1329195	24.7386338	136.587046
6.00	16:34	35585.49	589910	1329128	67.0074623	203.594508
7.00	16:36	36388.68	589900	1329162	35.4400903	239.034599
8.00	16:37	36439.02	589898	1329195	33.0605505	272.095149
9.00	16:38	36405.02	589895	1329131	64.0702739	336.165423
10.00	16:39	36427.75	589898	1329111	20.2237484	356.389171
11.00	16:40	36656.12	589888	1329095	18.8679623	375.257134
12.00	16:41	37197.92	589883	1329080	15.8113883	391.068522

13.00	16:43	37530.54	589886	1329060	20.2237484	411.29227
14.00	16:44	36995.98	589891	1329053	8.60232527	419.894596
15.00	16:46	36679.71	589896	1329021	32.3882695	452.282865
16.00	16:47	37828.57	589900	1329001	20.3960781	472.678943
17.00	16:48	36960.30	589903	1328987	14.3178211	486.996764
18.00	16:49	36080.05	589903	1328969	18	504.996764
19.00	16:50	36918.08	589903	1328951	18	522.996764
20.00	16:51	36401.64	589899	1328930	21.3775583	544.374323
21.00	16:52	35910.03	589902	1328917	13.3416641	557.715987
22.00	16:54	36894.29	589906	1328898	19.4164878	577.132474
23.00	16:55	36039.65	589903	1328882	16.2788206	593.411295
24.00	16:57	35968.67	589893	1328864	20.5912603	614.002555
25.00	16:58	35969.40	589888	1328851	13.9283883	627.930944
26.00	16:59	36263.20	589899	1328833	21.0950231	649.025967
27.00	17:00	36408.50	589909	1328819	17.2046505	666.230617
29.00	17:05	35740.18	589920	1328803	19.4164878	685.647105
30.00	17:06	35543.99	589923	1328788	15.2970585	700.944164
31.00	17:07	35955.24	589925	1328770	18.1107703	719.054934
32.00	17:08	35850.89	589924	1328750	20.0249844	739.079918
33.00	17:09	36219.64	589920	1328731	19.4164878	758.496406
34.00	17:10	35625.06	589916	1328713	18.4390889	776.935495
35.00	17:12	36757.86	589914	1328695	18.1107703	795.046265
36.00	17:13	35818.60	589915	1328677	18.0277564	813.074022
37.00	17:15	35911.51	589916	1328658	19.0262976	832.100319
38.00	17:17	36730.69	589903	1328645	18.3847763	850.485096
39.00	17:18	34391.92	589890	1328621	27.2946881	877.779784
40.00	17:20	35311.50	589881	1328604	19.2353841	897.015168
41.00	17:24	35883.52	589875	1328592	13.4164079	910.431576
42.00	17:25	35853.43	589880	1328576	16.7630546	927.19463
43.00	17:28	36303.05	589887	1328567	11.4017543	938.596385
44.00	17:35	36477.76	589916	1328560	29.8328678	968.429252
45.00	17:37	35965.34	589936	1328554	20.880613	989.309865
46.00	17:39	35663.24	589954	1328555	18.0277564	1007.33762
47.00	17:41	35445.24	589968	1328555	14	1021.33762
48.00	17:42	35451.45	589989	1328551	21.3775583	1042.71518
49.00	17:44	35267.63	590004	1328554	15.2970585	1058.01224
50.00	17:46	35390.05	590027	1328547	24.0416306	1082.05387
51.00	17:47	34949.99	590045	1328545	18.1107703	1100.16464
52.00	17:52	35157.17	590065	1328543	20.0997512	1120.26439
53.00	17:53	35401.22	590083	1328541	18.1107703	1138.37516
54.00	17:54	34918.46	590102	1328539	19.1049732	1157.48013
55.00	17:56	35288.88	590123	1328538	21.023796	1178.50393
56.00	17:58	34866.05	590141	1328536	18.1107703	1196.6147
57.00	17:59	34215.53	590159	1328534	18.1107703	1214.72547
58.00	18:00	33892.97	590176	1328531	17.2626765	1231.98815
59.00	18:02	34945.27	590194	1328528	18.2482876	1250.23643
60.00	18:04	34955.99	590213	1328527	19.0262976	1269.26273
62.00	18:46	34487.00	590228	1328523	15.5241747	1284.78691
63.00	18:47	35139.40	590243	1328527	15.5241747	1300.31108
64.00	18:48	34421.84	590264	1328525	21.0950231	1321.4061
65.00	18:50	34382.44	590284	1328525	20	1341.4061
66.00	18:52	35114.99	590303	1328523	19.1049732	1360.51108

67.00	18:54	34513.20	590324	1328521	21.0950231	1381.6061
68.00	18:55	34375.65	590345	1328516	21.5870331	1403.19313
69.00	18:57	34972.52	590364	1328518	19.1049732	1422.29811
70.00	19:00	34038.76	590363	1328519	1.41421356	1423.71232
71.00	19:02	33858.66	590400	1328515	37.2155881	1460.92791
72.00	19:03	34203.89	590425	1328511	25.3179778	1486.24589
73.00	19:04	34733.70	590440	1328501	18.0277564	1504.27364
74.00	19:07	34992.26	590452	1328488	17.691806	1521.96545
75.00	19:08	36234.61	590469	1328481	18.3847763	1540.35023

Area description	**Loop beside Comalito Cone**
Ring fault crossed	**?**
Other structures	**Fumarolic field passed**
Average spacing	**25.76904734**
Date	**08/03/2010**
Coordinate System	**UTM Zone 16P**

Point	Local time (hr:mn)	Eastings (m)	Northings (m)	Mag (nT)	Distance (m) to previous station	Accumulated spacing (m)
111	09:35	592796	1327294	36954.9		0
112	09:37	592727	1327244	37643.6	85.2115	85.2115
113	09:38	592707	1327230	38219	24.41311	109.6246
114	09:38	592687	1327215	37825.1	25	134.6246
115	09:39	592674	1327198	37614.1	21.40093	156.0255
116	09:40	592668	1327174	36628.1	24.73863	180.7642
117	09:41	592668	1327150	36856.4	24	204.7642
118	09:41	592670	1327128	36908	22.09072	226.8549
119	09:42	592678	1327106	36253.8	23.4094	250.2643
120	09:43	592679	1327082	36734	24.02082	274.2851
121	09:44	592674	1327062	37210	20.61553	294.9007
122	09:45	592659	1327036	36526.8	30.01666	324.9173
123	09:46	592633	1327010	36008	36.76955	361.6869
124	09:47	592614	1326992	36139.4	26.1725	387.8594
125	09:48	592595	1326975	36426.5	25.4951	413.3545
126	09:48	592581	1326956	36265.3	23.60085	436.9553
127	09:49	592567	1326937	36478.2	23.60085	460.5562
128	09:50	592555	1326914	36393.5	25.94224	486.4984
129	09:50	592542	1326894	36573.8	23.85372	510.3521
130	09:51	592528	1326872	37268.8	26.07681	536.4289
131	09:54	592515	1326851	37337.2	24.69818	561.1271
132	09:55	592509	1326822	36996.5	29.61419	590.7413
133	09:56	592491	1326804	35946.4	25.45584	616.1971
134	09:56	592467	1326795	35740	25.63201	641.8292

135	09:57	592443	1326783	36152	26.83282	668.662
136	09:58	592433	1326765	37099	20.59126	689.2532
137	09:58	592433	1326741	36997.6	24	713.2532
138	09:59	592427	1326717	36423.9	24.73863	737.9919
139	10:00	592413	1326693	37530.6	27.78489	765.7768
140	10:01	592405	1326678	37002	17	782.7768
141	10:01	592400	1326660	36906	18.68154	801.4583
142	10:02	592417	1326640	36635	26.24881	827.7071
143	10:03	592433	1326613	36365	31.38471	859.0918
144	10:03	592434	1326592	37526.3	21.0238	880.1156
145	10:04	592440	1326563	36709	29.61419	909.7298
146	10:05	592450	1326542	36557.7	23.25941	932.9892
147	10:05	592448	1326521	35438.2	21.09502	954.0842
148	10:06	592441	1326497	36487.8	25	979.0842
149	10:07	592461	1326487	38401.9	22.36068	1001.445
150	10:08	592467	1326463	37545	24.73863	1026.184
151	10:08	592453	1326441	37006.3	26.07681	1052.26
152	10:13	592433	1326430	36689.5	22.82542	1075.086
153	10:14	592411	1326415	36319.8	26.62705	1101.713
154	10:15	592388	1326403	36159.4	25.94224	1127.655
155	10:15	592368	1326389	36234	24.41311	1152.068
156	10:16	592347	1326377	35626.8	24.18677	1176.255
157	10:17	592337	1326353	35557.2	26	1202.255
158	10:17	592334	1326329	36432.3	24.18677	1226.442
159	10:18	592348	1326310	37483.3	23.60085	1250.043
160	10:19	592328	1326297	37584	23.85372	1273.896
161	10:19	592303	1326296	36350.1	25.01999	1298.916
162	10:20	592291	1326311	36239.7	19.20937	1318.126
163	10:21	592279	1326322	36397.3	16.27882	1334.404
164	10:22	592274	1326357	36142.9	35.35534	1369.76
165	10:22	592276	1326371	37134.6	14.14214	1383.902
166	10:23	592273	1326409	37150.8	38.11824	1422.02
167	10:23	592271	1326435	36617.4	26.07681	1448.097
168	10:24	592272	1326460	38849	25.01999	1473.117
169	10:25	592274	1326493	37079.7	33.06055	1506.178
170	10:25	592271	1326513	37400.3	20.22375	1526.401
171	10:26	592290	1326527	37528.7	23.60085	1550.002
172	10:27	592314	1326546	37069.3	30.61046	1580.613
173	10:29	592345	1326547	37308.5	31.01612	1611.629
174	10:30	592350	1326540	37441.2	8.602325	1620.231
175	10:30	592370	1326535	36849.7	20.61553	1640.847
176	10:31	592396	1326542	36657	26.92582	1667.772
177	10:32	592387	1326562	37024.5	21.93171	1689.704
178	10:32	592393	1326584	36994.4	22.80351	1712.508
179	10:33	592399	1326617	38637	33.54102	1746.049
180	10:34	592400	1326649	37923	32.01562	1778.064

Name	**181-289**
Area description	**San Fernando crater**
Ring fault crossed	**No (well, in depth yes, but...)**

Other structures	**Graben related N-S fault**
Average spacing	**24.95320608**
Date	**08/03/2010**
Coordinate System	**UTM Zone 16P**

Point	Local time (hr:mn)	Eastings (m)	Northings (m)	Mag (nT)	Distance (m) to previous station	Accumulated spacing (m)
181	11:10	590886	1325033	36348.5		0
182	11:11	590909	1325041	36314.2	24.35159	24.35159
183	11:11	590928	1325052	36401.7	21.9545	46.30609
184	11:12	590952	1325063	36531.2	26.40076	72.70685
185	11:12	590969	1325074	36681.2	20.24846	92.9553
186	11:13	590989	1325085	36726.0	22.82542	115.7807
187	11:14	591001	1325100	36730.5	19.20937	134.9901
188	11:14	591013	1325114	36665.3	18.43909	153.4292
189	11:15	591039	1325132	36763.3	31.62278	185.052
190	11:16	591058	1325156	36903.4	30.61046	215.6624
191	11:17	591069	1325173	36845.7	20.24846	235.9109
192	11:17	591086	1325192	36761.4	25.4951	261.406
193	11:18	591103	1325208	36342.0	23.34524	284.7512
194	11:19	591124	1325222	36875.8	25.23886	309.9901
195	11:19	591142	1325239	36625.0	24.75884	334.7489
196	11:20	591156	1325260	36740.2	25.23886	359.9878
197	11:21	591173	1325276	36982.5	23.34524	383.333
198	11:22	591194	1325278	37204.6	21.09502	404.428
199	11:23	591212	1325290	36815.7	21.63331	426.0613
200	11:23	591237	1325300	36376.0	26.92582	452.9872
201	11:24	591262	1325312	36431.0	27.73085	480.718
202	11:25	591283	1325328	36882.6	26.40076	507.1188
203	11:25	591305	1325340	37129.0	25.05993	532.1787
204	11:26	591327	1325350	35722.0	24.16609	556.3448
205	11:27	591350	1325360	38412.0	25.07987	581.4247
206	11:29	591376	1325367	33533.0	26.92582	608.3505
207	11:31	591395	1325373	34715.0	19.92486	628.2753
208	11:32	591420	1325371	35667.0	25.07987	653.3552
209	11:33	591437	1325371	35943.0	17	670.3552
210	11:33	591457	1325363	36563.0	21.54066	691.8959
211	11:34	591476	1325354	34775.0	21.0238	712.9197
212	11:35	591493	1325348	38023.0	18.02776	730.9474
213	11:36	591520	1325337	36407.0	29.15476	760.1022
214	11:36	591545	1325322	38796.0	29.15476	789.2569
215	11:37	591564	1325306	38147.5	24.83948	814.0964
216	11:38	591575	1325290	38173.8	19.41649	833.5129
217	11:39	591588	1325269	40384.0	24.69818	858.2111
218	11:40	591605	1325258	38435.9	20.24846	878.4595

219	11:40	591621	1325237	37903.4	26.40076	904.8603
220	11:41	591641	1325219	38137.0	26.90725	931.7676
221	11:42	591650	1325199	37955.0	21.93171	953.6993
222	11:43	591660	1325172	37096.5	28.79236	982.4916
223	11:50	591677	1325158	35913.0	22.02272	1004.514
224	11:51	591699	1325141	35918.7	27.80288	1032.317
225	11:52	591699	1325117	37159.0	24	1056.317
226	11:52	591706	1325093	35730.2	25	1081.317
227	11:53	591717	1325074	35415.2	21.9545	1103.272
228	11:54	591711	1325049	36939.0	25.70992	1128.982
229	11:55	591707	1325022	34352.0	27.29469	1156.276
230	11:55	591687	1324994	33431.0	34.4093	1190.686
231	11:57	591678	1324978	35685.0	18.35756	1209.043
232	11:57	591677	1324954	36944.0	24.02082	1233.064
233	11:58	591668	1324931	35274.0	24.69818	1257.762
234	11:59	591653	1324911	36573.0	25	1282.762
235	11:59	591640	1324889	35975.0	25.55386	1308.316
236	12:00	591628	1324870	35707.0	22.47221	1330.788
237	12:01	591613	1324847	34478.6	27.45906	1358.247
238	12:01	591596	1324829	34087.0	24.75884	1383.006
239	12:02	591584	1324813	33431.0	20	1403.006
240	12:03	591573	1324798	33554.0	18.60108	1421.607
241	12:04	591563	1324783	38928.0	18.02776	1439.635
242	12:06	591543	1324777	33670.0	20.88061	1460.516
243	12:07	591522	1324766	33688.0	23.70654	1484.222
244	12:08	591501	1324754	33155.0	24.18677	1508.409
245	12:08	591483	1324731	33639.0	29.20616	1537.615
246	12:09	591467	1324733	39229.0	16.12452	1553.74
247	12:11	591449	1324730	33677.0	18.24829	1571.988
248	12:16	591426	1324735	32624.0	23.5372	1595.525
249	12:17	591407	1324743	32696.0	20.61553	1616.141
250	12:19	591384	1324746	33137.0	23.19483	1639.335
251	12:20	591360	1324757	34248.0	26.40076	1665.736
252	12:20	591343	1324755	33929.0	17.11724	1682.853
253	12:21	591319	1324754	34567.0	24.02082	1706.874
254	12:22	591304	1324757	34239.0	15.29706	1722.171
255	12:22	591280	1324753	33751.0	24.33105	1746.502
256	12:23	591256	1324742	34017.0	26.40076	1772.903
257	12:24	591238	1324739	33729.0	18.24829	1791.151
258	12:25	591223	1324734	34933.0	15.81139	1806.963
259	12:26	591211	1324747	34347.4	17.69181	1824.655
260	12:26	591195	1324770	33377.0	28.01785	1852.672
261	12:27	591179	1324783	33670.0	20.61553	1873.288
262	12:28	591160	1324799	35016.0	24.83948	1898.127
263	12:29	591139	1324808	35859.7	22.84732	1920.975
264	12:30	591116	1324817	36388.6	24.69818	1945.673
265	12:31	591097	1324830	36773.2	23.02173	1968.695
266	12:32	591076	1324846	36950.6	26.40076	1995.095
267	12:33	591061	1324866	37013.1	25	2020.095
268	12:34	591046	1324885	37087.9	24.20744	2044.303
269	12:34	591028	1324903	37125.1	25.45584	2069.759
270	12:35	591016	1324925	37189.6	25.05993	2094.819

271	12:36	591012	1324949	37326.8	24.33105	2119.15
272	12:36	591012	1324974	37545.0	25	2144.15
273	12:38	591017	1324999	37049.2	25.4951	2169.645
274	12:39	591014	1325024	37061.5	25.17936	2194.824
275	12:39	591015	1325050	37067.8	26.01922	2220.843
276	12:40	591018	1325076	37038.3	26.1725	2247.016
277	12:40	591029	1325104	36938.9	30.08322	2277.099
278	13:22	590887	1325056	36274.7	149.8933	2426.992
279	13:22	590886	1325079	36574.9	23.02173	2450.014
280	13:23	590891	1325103	37029.5	24.5153	2474.529
281	13:24	590894	1325127	37210.8	24.18677	2498.716
282	13:25	590901	1325151	36771.3	25	2523.716
283	13:25	590907	1325173	36311.5	22.80351	2546.52
284	13:26	590909	1325198	36513.2	25.07987	2571.6
285	13:27	590891	1325214	36616.7	24.08319	2595.683
286	13:28	590868	1325216	36732.8	23.08679	2618.77
287	13:29	590843	1325218	37342.5	25.07987	2643.849
288	13:29	590817	1325216	37104.8	26.07681	2669.926
289	13:30	590792	1325215	37609.6	25.01999	2694.946

Name	**341-384**
Area description	**Coyotes to Park Entrance**
Ring fault crossed	**Yes**
Other structures	**Going down from the visitor centre (which is another eruptive centre)**
Average spacing	**24.3499586**
Date	**08/03/2010**
Coordinate System	**UTM Zone 16P**

Point	Local time (hr:mn)	Eastings (m)	Northings (m)	Mag (nT)	Distance (m) to previous station	Accumulated spacing (m)
341	15:18	592795	1327296	37134.1		0
342	15:19	592789	1327311	36267.0	16.1554944	16.1554944
343	15:20	592805	1327343	34803.0	35.7770876	51.9325821
344	15:21	592812	1327368	36223.0	25.96151	77.894092
345	15:22	592825	1327391	37112.2	26.4196896	104.313782
346	15:24	592836	1327413	36734.7	24.5967478	128.910529
347	15:24	592846	1327430	36038.8	19.7230829	148.633612
348	15:25	592852	1327450	36132.4	20.880613	169.514225
349	15:26	592861	1327471	35967.0	22.8473193	192.361545
350	15:27	592877	1327499	36491.6	32.249031	224.610576
351	15:29	592892	1327522	37441.4	27.4590604	252.069636
352	15:30	592899	1327545	36891.0	24.0416306	276.111267
353	15:31	592900	1327560	36724.0	15.0332964	291.144563

354	15:31	592901	1327593	36369.0	33.015148	324.159711
355	15:32	592910	1327614	36708.0	22.8473193	347.00703
356	15:33	592924	1327630	36844.0	21.2602916	368.267322
357	15:34	592944	1327651	36043.0	29	397.267322
358	15:34	592957	1327669	36491.0	22.2036033	419.470925
359	15:35	592964	1327693	35631.0	25	444.470925
360	15:36	592974	1327717	36489.4	26	470.470925
361	15:36	592983	1327737	36755.9	21.9317122	492.402638
362	15:40	592981	1327758	37341.3	21.0950231	513.497661
363	15:40	592973	1327784	36594.1	27.202941	540.700602
364	15:41	592970	1327807	36532.0	23.194827	563.895429
365	15:42	592970	1327831	36124.0	24	587.895429
366	15:43	592974	1327857	35956.0	26.3058929	614.201322
367	15:44	592978	1327880	36533.5	23.3452351	637.546557
368	15:46	592984	1327904	36847.4	24.7386338	662.28519
369	15:47	592992	1327927	37057.0	24.3515913	686.636782
370	15:49	593000	1327951	36451.0	25.2982213	711.935003
371	15:50	593009	1327972	36348.0	22.8473193	734.782322
372	15:52	593022	1327993	36084.0	24.6981781	759.4805
373	15:53	593035	1328013	36277.0	23.8537209	783.334221
374	15:55	593058	1328034	37353.0	31.144823	814.479044
375	15:57	593080	1328044	37299.0	24.1660919	838.645136
376	15:57	593100	1328054	37071.0	22.3606798	861.005816
377	15:58	593119	1328066	36750.5	22.4722051	883.478021
378	16:00	593141	1328080	37207.0	26.0768096	909.554831
379	16:01	593158	1328091	37380.0	20.2484567	929.803287
380	16:01	593180	1328103	36870.0	25.0599282	954.863216
381	16:02	593205	1328113	36933.6	26.925824	981.78904
382	16:04	593224	1328116	36926.6	19.2353841	1001.02442
383	16:04	593249	1328116	36550.8	25	1026.02442
384	16:05	593270	1328115	37808.0	21.023796	1047.04822

Name	**LAG01-32**
Area description	**Beginning of profile from the lake and up Coyotes. Followed by Laguna (2) profile**
Ring fault crossed	**No**
Other structures	**Only if caldera is formed by two collapses**
Average spacing	**45.89186294**
Date	**17/02/2010**
Coordinate System	**UTM Zone 16P**

Point	Local time (hr:mn)	Eastings (m)	Northings (m)	Mag (nT)	Distance (m) to previous station	Accumulated spacing (m)
LAG01	?	595263	1323762	38666.9		0
LAG02	?	595224	1323761	35516.0	39.0128184	39.0128184

LAG03	?	595206	1323819	34334.0	60.7289058	99.7417242
LAG04	?	595206	1323863	32844.0	44	143.741724
LAG05	?	595209	1323892	33264.9	29.1547595	172.896484
LAG06	?	595214	1323957	38963.9	65.1920241	238.088508
LAG07	?	595196	1323978	37696.0	27.6586334	265.747141
LAG08	?	595151	1323993	37788.7	47.4341649	313.181306
LAG09	?	595102	1323996	37883.0	49.0917508	362.273057
LAG10	?	595059	1324016	36821.0	47.4236228	409.69668
LAG11	?	595023	1324046	36831.0	46.8614981	456.558178
LAG12	?	594983	1324073	37180.0	48.259714	504.817892
LAG13	?	594945	1324098	36522.2	45.4862617	550.304153
LAG14	?	594901	1324106	35820.4	44.7213595	595.025513
LAG15	?	594861	1324093	37887.4	42.0594817	637.084995
LAG16	?	594812	1324078	36670.0	51.2445119	688.329507
LAG17	?	594774	1324095	36384.2	41.6293166	729.958823
LAG18	?	594744	1324131	36547.0	46.8614981	776.820321
LAG19	?	594706	1324156	37172.0	45.4862617	822.306583
LAG20	?	594665	1324183	35782.2	49.0917508	871.398334
LAG21	?	594642	1324214	36334.4	38.6005181	909.998852
LAG22	?	594650	1324257	36580.0	43.7378555	953.736707
LAG23	?	594653	1324302	37175.6	45.0998891	998.836596
LAG24	?	594641	1324350	36880.0	49.4772675	1048.31386
LAG25	?	594622	1324391	35996.9	45.1884941	1093.50236
LAG26	?	594594	1324425	38166.8	44.0454311	1137.54779
LAG27	?	594550	1324451	37102.4	51.1077294	1188.65552
LAG28	?	594502	1324458	36916.5	48.5077313	1237.16325
LAG29	?	594459	1324462	37244.0	43.1856458	1280.3489
LAG30	?	594409	1324493	36531.3	58.8302643	1339.17916
LAG31	?	594389	1324523	37625.2	36.0555128	1375.23467
LAG32	?	594367	1324565	37208.7	47.4130784	1422.64775

Name	**lag33-110**
Area description	**Upper part of Los Coyotes Trail. Preceded by Laguna (1) profile**
Ring fault crossed	**Yes. Where the water pipe is.**
Other structures	**No**
Average spacing	**47.05635662**
Date	**02/03/2010**
Coordinate System	**UTM Zone 16P**

Point	Local time (hr:mn)	Eastings (m)	Northings (m)	Mag (nT)	Distance (m) to previous station	Accumulated spacing (m)
lag33	?	594341	1324606	36899.0		0
lag34	?	594303	1324640	36097.0	50.9901951	50.9901951

lag35	?	594260	1324656	38257.0	45.880279	96.8704741
lag36	?	594213	1324662	37898.0	47.381431	144.251905
lag37	?	594195	1324675	38153.7	22.2036033	166.455508
lag38	?	594146	1324724	37379.9	69.2964646	235.751973
lag39	?	594162	1324767	37287.0	45.880279	281.632252
lag40	?	594175	1324813	36142.0	47.8016736	329.433926
lag41	?	594161	1324862	35976.1	50.9607692	380.394695
lag42	?	594161	1324909	36106.0	47	427.394695
lag43	?	594143	1324956	36373.0	50.3289181	477.723613
lag44	?	594133	1325000	36739.0	45.1220567	522.84567
lag45	?	594165	1325024	36940.4	40	562.84567
lag46	?	594181	1325070	35934.0	48.7031826	611.548852
lag47	?	594168	1325087	36458.8	21.4009346	632.949787
lag48	?	594125	1325155	36757.7	80.4549563	713.404743
lag49	?	594093	1325192	36866.0	48.9182992	762.323042
lag50	?	594074	1325232	36673.3	44.2831797	806.606222
lag51	?	594037	1325290	36313.2	68.7968023	875.403024
lag52	?	594011	1325311	36609.0	33.4215499	908.824574
lag53	?	593983	1325339	37074.0	39.5979797	948.422554
lag54	?	593978	1325390	37300.6	51.2445119	999.667066
lag55	?	594001	1325430	37378.0	46.141088	1045.80815
lag56	?	594023	1325473	36501.0	48.3011387	1094.10929
lag57	?	594023	1325515	37366.7	42	1136.10929
lag58	?	594017	1325562	37778.0	47.381431	1183.49072
lag59	?	593970	1325575	37112.0	48.7647414	1232.25546
lag60	?	593932	1325594	36821.0	42.4852916	1274.74076
lag61	?	593884	1325599	37567.0	48.259714	1323.00047
lag62	?	593845	1325601	36896.0	39.0512484	1362.05172
lag63	?	593796	1325572	36322.0	56.9385634	1418.99028
lag64	?	593749	1325594	37991.0	51.894123	1470.88441
lag65	?	593695	1325591	36781.3	54.0832691	1524.96767
lag66	?	593654	1325600	36034.6	41.9761837	1566.94386
lag67	?	593620	1325627	36080.6	43.4165867	1610.36044
lag68	?	593577	1325656	36012.0	51.8652099	1662.22565
lag69	?	593540	1325676	36255.4	42.0594817	1704.28514
lag70	?	593501	1325699	36247.2	45.2769257	1749.56206
lag71	?	593455	1325727	35792.0	53.8516481	1803.41371
lag72	?	593421	1325753	36825.6	42.8018691	1846.21558
lag73	?	593370	1325768	35280.0	53.1601354	1899.37571
lag74	?	593350	1325774	35288.4	20.880613	1920.25633
lag75	?	593287	1325778	36872.0	63.1268564	1983.38318
lag76	?	593238	1325787	35671.7	49.8196748	2033.20286
lag77	?	593228	1325817	34472.0	31.6227766	2064.82564
lag78	?	593175	1325848	37690.0	61.4003257	2126.22596
lag79	?	593158	1325887	36922.8	42.5440948	2168.77006
lag80	?	593138	1325907	36671.9	28.2842712	2197.05433
lag81	?	593131	1325973	35579.0	66.370174	2263.4245
lag82	?	593114	1325999	35928.4	31.0644491	2294.48895
lag83	?	593083	1326054	35615.2	63.1347765	2357.62373
lag84	?	593065	1326096	35955.6	45.6946386	2403.31837

lag85	?	593045	1326137	35693.0	45.6179789	2448.93634
lag86	?	593022	1326171	34398.0	41.0487515	2489.9851
lag87	?	593005	1326221	34954.0	52.8109837	2542.79608
lag88	?	593001	1326262	33615.0	41.1946598	2583.99074
lag89	?	592992	1326314	35574.7	52.7730992	2636.76384
lag90	?	593016	1326349	34580.0	42.4381903	2679.20203
lag91	?	593059	1326347	35133.0	43.0464865	2722.24852
lag92	?	593098	1326372	36098.1	46.3249393	2768.57345
lag93	?	593089	1326420	35104.2	48.8364618	2817.40992
lag94	?	593065	1326455	35756.0	42.4381903	2859.84811
lag95	?	593027	1326491	34584.0	52.3450093	2912.19312
lag96	?	592980	1326516	36603.0	53.2353266	2965.42844
lag97	?	592950	1326549	36427.0	44.5982062	3010.02665
lag98	?	592926	1326579	35780.0	38.4187454	3048.44539
lag99	?	592913	1326626	36360.1	48.7647414	3097.21014
lag100	?	592921	1326668	35945.7	42.7551167	3139.96525
lag101	?	592888	1326708	37392.8	51.8555686	3191.82082
lag102	?	592882	1326743	37406.7	35.5105618	3227.33138
lag103	?	592869	1326796	37288.0	54.5710546	3281.90244
lag104	?	592872	1326846	36496.0	50.0899191	3331.99236
lag105	?	592896	1326893	37254.1	52.7730992	3384.76546
lag106	?	592878	1326938	37631.0	48.4664833	3433.23194
lag107	?	592882	1326980	35215.0	42.1900462	3475.42199
lag108	?	592882	1327036	38452.0	56	3531.42199
lag109	?	592867	1327077	37221.3	43.6577599	3575.07975
lag110	?	592862	1327125	37103.1	48.259714	3623.33946

Name	**CM01-13**
Area description	**Upper part of Los Coyotes trail. Repetition from Coyotes 2**
Ring fault crossed	**?**
Other structures	**?**
Average spacing	**41.69064779**
Date	**16/02/2010**
Coordinate System	**UTM Zone 16P**

Point	Local time (hr:mn)	Eastings (m)	Northings (m)	Mag (nT)	Distance (m) to previous station	Accumulated spacing (m)
CM01	?	592836	1327193	36799.2		0
CM02	?	592848	1327152	37198.0	42.7200187	42.7200187
CM03	?	592864	1327114	36315.0	41.2310563	83.951075
CM04	?	592863	1327071	38222.2	43.0116263	126.962701
CM05	?	592870	1327029	38024.2	42.5793377	169.542039
CM06	?	592873	1327031	36126.0	3.60555128	173.14759
CM07	?	592883	1326938	37405.0	93.5360893	266.68368

CM08	?	592883	1326906	37241.0	32	298.68368
CM09	?	592872	1326856	37110.7	51.1957029	349.879383
CM10	?	592864	1326815	37169.4	41.7731971	391.65258
CM11	?	592867	1326769	37334.7	46.0977223	437.750302
CM12	?	592874	1326764	37637.2	8.60232527	446.352627
CM13	?	592884	1326711	36839.8	53.9351462	500.287773

Name	**ROAD001-024**
Area description	**Beginning of the road -uncertain-**
Ring fault crossed	**?**
Other structures	**?**
Average spacing	**45.15023468**
Date	**02/03/2010**
Coordinate System	**UTM Zone 16P**

Point	Local time (hr:mn)	Eastings (m)	Northings (m)	Mag (nT)	Distance (m) to previous station	Accumulated spacing (m)
ROAD001	?	590766	1325247	36748.0		0
ROAD002	?	590791	1325279	36792.0	40.607881	41
ROAD003	?	590808	1325325	39488.8	49.0407993	90
ROAD004	?	590811	1325368	40172.0	43.1045241	133
ROAD005	?	590805	1325407	39332.5	39.4588393	172
ROAD006	?	590794	1325440	38701.7	34.7850543	207
ROAD007	?	590779	1325482	39477.6	44.5982062	252
ROAD008	?	590761	1325524	37816.6	45.6946386	297
ROAD009	?	590747	1325565	37366.6	43.324358	341
ROAD010	?	590728	1325602	37683.0	41.5932687	382
ROAD011	?	590703	1325635	36883.7	41.4004831	424
ROAD012	?	590709	1325680	37812.9	45.3982379	469
ROAD013	?	590709	1325728	37956.0	48	517
ROAD014	?	590710	1325775	36188.2	47.0106371	564
ROAD015	?	590715	1325819	36038.5	44.2831797	608
ROAD016	?	590724	1325866	36123.6	47.8539445	656
ROAD017	?	590718	1325911	35598.1	45.3982379	702
ROAD018	?	590708	1325961	35998.0	50.9901951	753
ROAD019	?	590698	1326001	35490.2	41.2310563	794
ROAD020	?	590680	1326049	35233.3	51.2640225	845
ROAD021	?	590665	1326096	36436.0	49.3355855	894
ROAD022	?	590636	1326141	35688.1	53.5350353	948
ROAD023	?	590627	1326184	35757.7	43.9317653	992
ROAD024	?	590609	1326227	36547.0	46.6154481	1038

Name	**TLT1-4 and MW1-13**
Area description	**From the south end of Nindiri (arriba de la plataforma) to the North edge of the ledge**
Ring fault crossed	**No**
Other structures	**Nindiri lava lake south graben fault crossed**
Average spacing	**28.25078668**
Date	**19/02/2010**
Coordinate System	**UTM Zone 16P**

Point	Local time (hr:mn)	Eastings (m)	Northings (m)	Mag (nT)	Distance (m) to previous station	Accumulated spacing (m)
TLT1	?	590112	1324889	36929.7		0.0000
TLT2	?	590120	1324929	37121.0	40.7921561	40.7922
TLT3	?	590128	1324941	37644.2	14.4222051	55.2144
TLT4	?	590135	1324957	37572.5	17.4642492	72.6786
MOONWALK1	?	590142	1325055	36035.0	98.2496819	170.9283
MW2	?	590161	1325070	35794.0	24.2074369	195.1357
MW3	?	590173	1325084	35726.0	18.4390889	213.5748
MW4	?	590182	1325093	36255.0	12.7279221	226.3027
MW5	?	590196	1325120	36402.0	30.4138127	256.7166
MW6	?	590218	1325136	36487.2	27.202941	283.9195
MW7	?	590244	1325141	36728.0	26.4764046	310.3959
MW8	?	590249	1325157	36876.0	16.7630546	327.1590
MW9	?	590285	1325177	37774.0	41.1825206	368.3415
MW10	?	590299	1325192	38053.4	20.5182845	388.8598
MW11	?	590312	1325200	38540.2	15.2643375	404.1241
MW12	?	590343	1325218	38351.1	35.8468967	439.9710
MW13	?	590352	1325226	38359.8	12.0415946	452.0126

8.2 Appendix B: VLF data (caldera)

Point	Tilt F1 (degrees – tilt direction)	Signal Dir. F1	Maximum F1	Minimum F1	Tilt F2 (degrees – tilt direction)	Signal Dir. F2	Maximum F2	Minimum F2	Northing (UTM 16P)	Easting (UTM 16P)	Spacing (m)	Total Distance (m)
MONTOSO PROFILE												
15	0	112	6.4	0.5	0	32	4	0.2	1326824	589459	0	0
16	1N	304	3.7	0.1	2W	31	4.2	0.2	1326827	589449	10.44030651	10.44030651
17	4N	300	4.6	0.1	0	26	4.2	0.1	1326833	589436	14.31782106	24.75812757
18	6N	302	4.8	0.3	1W	25	4.2	0.1	1326849	589418	24.08318916	48.84131673
19	5N	298	0.5	0.1	0	30	4.2	0.2	1326865	589409	18.35755975	67.19887648
20	4N	296	0.4	0.2	4W	28	4.2	0.1	1326882	589400	19.23538406	86.43426054
21	4N	314	5.4	0.3	2W	29	4.3	0.1	1326904	589387	25.55386468	111.9881252
23	4N	296	5.7	0.2	0	32	4.2	0.2	1326926	589385	22.09072203	134.0788473
24	3N	300	6.2	0.2	0	40	4	0.1	1326947	589382	21.21320344	155.2920507
25	4N	300	6.3	0.2	0	34	4.2	0.2	1326962	589391	17.49285568	172.7849064
26	4N	300	6.4	0.2	0	34	4.2	0.4	1326973	589405	17.80449381	190.5894002
27	4N	308	6.6	0.2	4W	20	4.3	0.1	1326983	589416	14.86606875	205.4554689
28	4N	300	6.8	0.2	2W	35	4.2	0.1	1327007	589425	25.63201124	231.0874802
29	3N	120	7.2	0.2	0	20	4.5	0.1	1327018	589445	22.82542442	253.9129046
30	2N	296	7.2	0.2	0	220	4.4	0.2	1327045	589446	27.01851217	280.9314168
31	4N	300	7.8	0.2	2W	203	4.4	0.1	1327068	589462	28.01785145	308.9492682
32	5N	290	8.4	0.2	1W	207	4.2	0.1	1327044	589476	27.78488798	336.7341562
33	2N	300	8.3	0.2	0	36	4.2	0.2	1327058	589404	73.34848328	410.0826395
34	4N	290	0.6	0.2	0	29	4.3	0.1	1327081	589387	28.60069929	438.6833388
35	2N	300	8.2	0.2	2W	20	4.2	0.1	1327098	589370	24.04163056	462.7249693
36	0	290	8.6	0.2	0	40	4.2	0.1	1327117	589351	26.87005769	489.595027

Point	Tilt F1 (degrees – tilt direction)	Signal Dir. F1	Maximum F1	Minimum F1	Tilt F2 (degrees – tilt direction)	Signal Dir. F2	Maximum F2	Minimum F2	Northing (UTM 16P)	Easting (UTM 16P)	Spacing (m)	Total Distance (m)
37	2N	295	0.6	0.2	3W	30	4.4	0.1	1327139	589331	29.73213749	519.3271645
38	3N	300	9.2	0.2	0	30	4.4	0.2	1327150	589306	27.31300057	546.6401651
39	2N	296	8.8	0.3	1W	30	4.3	0.1	1327179	589294	31.38470965	578.0248747
KM. 21 PROFILE												
RIFA77?	3S	120	2.1	0.3	6W	110	11	0.2	1327899	592065	0	0
RIFA07?	5N?	302	2.1	0.25	3E	50	2.7	0.25	1327919	592083	26.90724809	26.90724809
RIFA01	5S	300	1.9	0.3	7W	218	8.2	0.4	1327945	592099	30.52867504	57.43592314
RIFA02	3S	125	6	0.3	2E	110	2.6	0.29	1327964	592112	23.02172887	80.45765201
RIFA03	0	290	3.2	0.4	0	51	11	0.3	1327998	592139	43.41658669	123.8742387
A01	14N	340	1.2	0.4	2W	26	2.8	0.4	-	-	-	-
A03	6N	332	1.1	0.3	1W	16	5	0.9	-	-	-	-
A05	10N	336	1.1	0.3	2E	16	4.6	0.4	-	-	-	-
A07	12N	330	3.8	0.9	1E	19	4.4	0.2	-	-	-	-
A09	8N	342	6	0.6	2E	27	4.2	0.2	-	-	-	-
A11	8N	330	3.2	1	0	17	2.9	0.2	-	-	-	-
A13	14N	338	2.8	0.9	2E	18	4.6	0.2	-	-	-	-
A15	12N	340	2.9	0.9	2E	24	4.2	0.1	-	-	-	-
A17	12N	339	3.2	0.8	2E	23	4.2	0.2	-	-	-	-
SAN PEDRO RIFT VALLEY PROFILE												
A01	12N	111	-	-	2W	200	-	-	1325288	589894	0	0
A02	10N	114	-	-	6W	202	-	-	1325275	589882	17.69180601	17.69180601
A03	16N	110	-	-	7W	217	-	-	1325269	589888	8.485281374	26.17708739
A04	19N	99	-	-	9W	214	-	-	1325241	589858	41.03656906	67.21365644
A05	16N	128	-	-	11W	206	-	-	1325238	589858	3	70.21365644

Point	Tilt F1 (degrees – tilt direction)	Signal Dir. F1	Maximum F1	Minimum F1	Tilt F2 (degrees – tilt direction)	Signal Dir. F2	Maximum F2	Minimum F2	Northing (UTM 16P)	Easting (UTM 16P)	Spacing (m)	Total Distance (m)
A06	17N	130	-	-	13W	204	-	-	1325238	589852	6	76.21365644
A07	17N	130	-	-	11W	188	-	-	1325254	589852	16	92.21365644
A08	13N	125	-	-	10W	182	-	-	1325281	589861	28.46049894	120.6741554
A09	13N	128	-	-	10W	208	-	-	1325278	589867	6.708203932	127.3823593
A10	11N	120	-	-	14W	214	-	-	1325324	589861	46.38965402	173.7720133
A11	13N	125	-	-	9W	200	-	-	1325294	589858	30.14962686	203.9216402
A12	14N	130	-	-	13W	200	-	-	1325272	589852	22.8035085	226.7251487
A13	20N	130	-	-	12W	196	-	-	1325241	589819	45.27692569	272.0020744
A14	16N	122	-	-	15W	210	-	-	1325266	589801	30.8058436	302.807918
A15	20N	126	-	-	13W	203	-	-	1325275	589810	12.72792206	315.5358401
A16	15N	128	-	-	14W	201	-	-	1325287	589822	16.97056275	332.5064028
A17	13N	128	-	-	17W	190	-	-	1325309	589846	32.55764119	365.064044
A18	12N	118	-	-	20W	198	-	-	1325364	589816	62.64982043	427.7138644
A19	13N	120	-	-	16W	212	-	-	1325352	589822	13.41640786	441.1302723
A20	16N	121	-	-	18W	198	-	-	1325312	589810	41.76122604	482.8914983
A21	17N	124	-	-	18W	191	-	-	1325299	589782	30.87069808	513.7621964
A22	14N	130	-	-	19W	199	-	-	1325309	589770	15.62049935	529.3826958
A23	13N	122	-	-	19W	194	-	-	1325327	589779	20.1246118	549.5073076
A24	11N	134	-	-	20W	199	-	-	1325336	589776	9.486832981	558.9941405
A25	7N	120	-	-	21W	201	-	-	1325361	589740	43.829214	602.8233545
A26	7N	110	-	-	21W	202	-	-	1325394	589713	42.63801121	645.4613658
A27	7N	88	-	-	19W	190	-	-	1325373	589695	27.65863337	673.1199991
A28	10N	122	-	-	20W	198	-	-	1325382	589710	17.49285568	690.6128548
A29	10N	117	-	-	21W	198	-	-	1325324	589737	63.97655821	754.589413
A30	8N	110	-	-	19W	190	-	-	1325376	589779	66.84309987	821.4325129

Point	Tilt F1 (degrees – tilt direction)	Signal Dir. F1	Maximum F1	Minimum F1	Tilt F2 (degrees – tilt direction)	Signal Dir. F2	Maximum F2	Minimum F2	Northing (UTM 16P)	Easting (UTM 16P)	Spacing (m)	Total Distance (m)
A31	6N	78	-	-	19W	190	-	-	1325398	589749	37.20215048	858.6346634
A32	5N	130	-	-	18W	192	-	-	1325425	589722	38.18376618	896.8184295
A33	7N	122	-	-	16W	202	-	-	1325456	589749	41.10960958	937.9280391
A34	8N	116	-	-	17W	190	-	-	1325432	589782	40.80441153	978.7324507
A35	7N	108	-	-	16W	190	-	-	1325404	589818	45.607017	1024.339468
A36	10N	121	-	-	13W	190	-	-	1325377	589864	53.33854141	1077.678009
A37	7N	120	-	-	4W	196	-	-	1325352	589894	39.05124838	1116.729257
VISITOR CENTRE FUMAROLE PROFILE												
15	3N	115	9	0.8	5W	40	5.1	0.2	1326784	592448	0	0
16	5N	300	9.4	0.8	7W	215	4.8	0.2	1326791	592462	15.65247584	15.65247584
17	5N	124	8.7	0.7	4W	40	5.2	0.2	1326801	592484	24.16609195	39.81856779
18	8N	294	9.2	0.7	5W	35	5	0.2	1326813	592504	23.32380758	63.14237537
19	8N	290	9.8	0.7	0	35	5.2	0.2	1326827	592522	22.8035085	85.94588387
20	5N	310	9.5	0.7	0	50	5	0.2	1326833	592533	12.52996409	98.47584796
21	5N	105	9	0.8	3E	40	5	0.1	1326837	592550	17.4642492	115.9400972
22	7N	300	9.2	0.7	0	40	5	0.2	1326846	592568	20.1246118	136.064709
23	10N	300	9	0.8	5E	40	4.8	0.1	1326851	592581	13.92838828	149.9930972
24	7N	290	9.2	0.8	7E	35	4.7	0.1	1326858	592611	30.8058436	180.7989408
25	8N	300	9	0.8	7E	50	4.6	0.1	1326864	592632	21.84032967	202.6392705
26	7N	305	9.5	0.9	7E	48	4.5	0.1	1326867	592652	20.22374842	222.8630189
27	8N	300	9.2	0.7	7E	63	4.4	0.2	1326861	592684	32.55764119	255.4206601
28	7N	290	9.3	0.9	7E	25	3.8	0.1	1326860	592713	29.01723626	284.4378964

Point	Tilt F1 (degrees – tilt direction)	Signal Dir. F1	Maximum F1	Minimum F1	Tilt F2 (degrees – tilt direction)	Signal Dir. F2	Maximum F2	Minimum F2	Northing (UTM 16P)	Easting (UTM 16P)	Spacing (m)	Total Distance (m)
COMALITO PROFILE												
COM 01	8N	120	4.2	0.6	4W	35	4.3	0.2	1326433	592401	0	0
COM 02	8N	127	5.1	0.6	2W	222	4.4	0.2	1326422	592413	16.2788206	16.2788206
COM 03	8N	117	5.2	0.6	3E	40	4.3	0.1	1326405	592428	22.6715681	38.95038869
COM 04	8N	113	7.4	0.7	9E	39	4.3	0.2	1326385	592445	26.2488095	65.19919819
COM 05	8N	117	7.6	0.8	9E	53	3.9	0.1	1326364	592463	27.65863337	92.85783156
COM 06	16N	297	7.6	0.8	4W	210	4.2	0.2	1326342	592342	122.9837388	215.8415703
COM 07	13N	297	7.6	0.8	8W	216	4.2	0.2	1326358	592365	28.01785145	243.8594218
COM 08	12N	290	7.5	0.1	5W	49	4.3	0.1	1326368	592388	25.07987241	268.9392942
COM 09	9N	293	7.6	0.8	1W	227	4.4	0.2	1326382	592411	26.92582404	295.8651182
COM 10	6N	292	7.9	0.9	6E	58	4.2	0.6	1326421	592439	48.01041554	343.8755338
COM 11	4N	127	7.8	0.8	3E	234	4.2	0.6	1326443	592454	26.62705391	370.5025877
SHOOTING RANGE PROFILE												
A20	5S	120	2.4	0.8	0	206	9	0.5	-	-	0	0
A23	6S	120	3	0.8	0	196	9.2	0.7	-	-	20	20
A26	4S	124	3.2	0.8	0	208	9.2	0.6	-	-	20	40
A29	8S	114	3	1	2E	203	9.2	0.6	-	-	20	60
A32	1N	120	3.6	1	2E	200	9.2	0.6	-	-	20	80
A35	2S	310	3.4	0.8	0	209	9.6	0.8	-	-	20	100
A38	2S	305	3.4	0.8	1E	210	9.4	0.8	-	-	20	120
A41	2N	315	3.4	0.8	1E	217	9.4	0.5	-	-	20	140

Point	Tilt F1 (degrees – tilt direction)	Signal Dir. F1	Maximum F1	Minimum F1	Tilt F2 (degrees – tilt direction)	Signal Dir. F2	Maximum F2	Minimum F2	Northing (UTM 16P)	Easting (UTM 16P)	Spacing (m)	Total Distance (m)
AROUND SASTEPE CONE PROFILE												
A45	3N	316	4.4	0.8	2W	198	7.8	0.6	-	-	0	0
A47	2S	308	3.8	0.8	2W	200	8	0.6	-	-	20	20
A49	0	310	3.8	0.8	0	200	8.4	0.8	-	-	20	40
A51	0	294	3.4	0.9	2W	194	8	0.8	-	-	20	60
A53	4N	300	3.4	0.7	2W	192	8.4	0.8	-	-	20	80
A55	0	290	3.4	0.9	4W	208	3.2	0.9	-	-	20	100
A57	0	298	3.3	0.7	4W	208	8.4	0.8	-	-	20	120
A59	0	300	3.2	0.8	0	204	8.4	0.9	-	-	20	140
A61	2N	294	4	0.7	4W	206	8.2	0.7	-	-	20	160
A63	5S	300	4.2	0.8	0	200	8	0.6	-	-	20	180
A65	8S	300	3.4	0.6	0	204	7.8	0.6	-	-	20	200
A67	4S	310	3.6	0.7	0	206	8.4	0.5	-	-	20	220
A69	0	308	3.8	0.9	2W	200	3.2	0.8	-	-	20	240
A71	1S	314	3.2	0.8	2W	208	8.2	0.8	-	-	20	260
A73	2N	297	3.4	0.8	2W	213	7.8	0.7	-	-	20	280
A75	2S	305	3.4	0.8	1E	206	8	0.8	-	-	20	300
A77	2N	325	3.4	0.8	0	218	8.3	0.8	-	-	20	320
A79	1S	316	3	0.8	2W	216	8	0.8	-	-	20	340
A81	3S	310	3	0.8	2E	200	8	0.6	-	-	20	360
A83	3S	310	3	0.7	0	209	8	1	-	-	20	380
ASC01	-	-	-	-	7W	206	2.6	0.1	-	-	25	405
ASC02	-	-	-	-	3W	206	2.45	0.1	-	-	25	430
ASC03	-	-	-	-	0	210	2.7	0.1	-	-	25	455

Point	Tilt F1 (degrees – tilt direction)	Signal Dir. F1	Maximum F1	Minimum F1	Tilt F2 (degrees – tilt direction)	Signal Dir. F2	Maximum F2	Minimum F2	Northing (UTM 16P)	Easting (UTM 16P)	Spacing (m)	Total Distance (m)
ASC04	-	-	-	-	1W	218	2.65	0.15	-	-	25	480
ASC05	-	-	-	-	0	206	2.8	0.1	-	-	25	505
ASC06	-	-	-	-	2W	215	2.7	0.1	-	-	25	530
ASC07	-	-	-	-	8W	208	2.6	0.1	-	-	25	555
ASC08	-	-	-	-	1W	209	2.8	0.1	-	-	25	580
ASC09	-	-	-	-	2E	206	2.8	0.1	-	-	25	605
ASC10	-	-	-	-	1W	205	2.8	0.1	-	-	25	630
ASC11	-	-	-	-	2W	211	2.9	0.15	-	-	25	655
ASC12	-	-	-	-	2W	212	2.8	0.15	-	-	25	680
ASC13	-	-	-	-	0	208	2.8	0.1	-	-	25	705
ASC14	-	-	-	-	7W	218	2.8	0.2	-	-	25	730
ASC15	-	-	-	-	3W	208	2.9	0.1	-	-	25	755
ASC16	-	-	-	-	3W	214	2.8	0.15	-	-	25	780
ASC17	-	-	-	-	4W	222	2.6	0.1	-	-	25	805
ASC18	-	-	-	-	1W	206	2.7	0.16	-	-	25	830
ASC19	-	-	-	-	2W	211	2.75	0.1	-	-	25	855
ASC20	-	-	-	-	3W	210	2.7	0.1	-	-	25	880
ASC21	-	-	-	-	3W	209	2.75	2	-	-	25	905
ASC22	-	-	-	-	2W	213	2.8	0.1	-	-	25	930
ASC23	-	-	-	-	0	201	2.3	0.2	-	-	25	955
ASC24	-	-	-	-	0	207	2.4	0.15	-	-	25	980
ASC25	-	-	-	-	1W	206	2.5	0.15	-	-	25	1005
ASC26	-	-	-	-	0	213	2.4	0.2	-	-	25	1030
ASC27	-	-	-	-	2E	207	2.5	0.15	-	-	25	1055

Point	Tilt F1 (degrees – tilt direction)	Signal Dir. F1	Maximum F1	Minimum F1	Tilt F2 (degrees – tilt direction)	Signal Dir. F2	Maximum F2	Minimum F2	Northing (UTM 16P)	Easting (UTM 16P)	Spacing (m)	Total Distance (m)
ASC28	-	-	-	-	0	210	2.5	0.2	-	-	25	1080
ASC29	-	-	-	-	1W	206	2.5	0.2	-	-	25	1105
ASC30	-	-	-	-	0	206	2.6	0.2	-	-	25	1130
ASC31	-	-	-	-	1W	204	2.5	0.15	-	-	25	1155
ASC32	-	-	-	-	2W	207	2.4	0.15	-	-	25	1180
ASC33	-	-	-	-	2W	206	2.3	0.2	-	-	25	1205
ASC34	-	-	-	-	3W	203	2.5	0.2	-	-	25	1230
ASC35	-	-	-	-	0	211	2.4	0.15	-	-	25	1255
ASC36	-	-	-	-	3E	203	2.3	0.2	-	-	25	1280
ASC37	-	-	-	-	1E	204	2.4	0.2	-	-	25	1305
ASC38	-	-	-	-	2W	210	2.5	0.2	-	-	25	1330
ASC39	-	-	-	-	2W	207	2.5	0.2	-	-	25	1355
ASC40	-	-	-	-	0	212	2.3	0.3	-	-	25	1380
ASC41	-	-	-	-	2E	213	2.3	0.2	-	-	25	1405
ASC42	-	-	-	-	2E	208	2.4	0.2	-	-	25	1430
ASC43	-	-	-	-	1W	210	2.4	0.2	-	-	25	1455
ASC44	-	-	-	-	1W	211	2.3	0.2	-	-	25	1480
ASC45	-	-	-	-	1E	207	2.3	0.2	-	-	25	1505
SASTEPE STRAIGHT LINE												
40	0	293	8.1	0.2	0	30	4.4	0.1	1327883	589885	0	1505
41	0	290	8.4	0.1	0	30	4.2	0.2	1327897	589904	23.60084744	1528.600847
42	2N	300	8.4	0.2	0	220	4.4	0.2	1327913	589919	21.9317122	1550.53256
42 bis	0	300	8.4	0.3	1W	210	4.3	0.1	1327927	589933	19.79898987	1570.33155
43	0	300	8.6	0.3	0	40	4.2	0.1	1327943	589949	22.627417	1592.958967

Point	Tilt F1 (degrees – tilt direction)	Signal Dir. F1	Maximum F1	Minimum F1	Tilt F2 (degrees – tilt direction)	Signal Dir. F2	Maximum F2	Minimum F2	Northing (UTM 16P)	Easting (UTM 16P)	Spacing (m)	Total Distance (m)
44	0	300	8.6	0.2	0	40	4.4	0.2	1327956	589959	16.40121947	1609.360186
45	0	300	8.4	0.2	0	30	4.5	0.2	1327981	589974	29.15475947	1638.514945
46	0	300	8.5	0.2	0	36	4.5	0.1	1328002	589985	23.70653918	1662.221485
47	0	300	8.7	0.2	0	40	4.6	0.2	1328024	589996	24.59674775	1686.818232
48	0	298	8.8	0.2	0	27	4.4	0.1	1328041	590009	21.40093456	1708.219167
49	0	298	8.8	0.3	0	36	4.5	0.1	1328058	590026	24.04163056	1732.260798
50	0	300	9	0.1	0	32	4.5	0.1	1328065	590047	22.13594362	1754.396741
51	0	113	8.6	0.3	0	215	4.6	0.1	1328073	590066	20.61552813	1775.012269
52	0	296	8.8	0.2	0	40	4.4	0.1	1328085	590088	25.05992817	1800.072197
53	0	112	8.8	0.2	0	40	4.8	0.2	1328099	590110	26.07680962	1826.149007

8.3 Appendix C: InSAR data

Master date	Slave date	Time Spanned (days)	Approximate B_{perp} (m)	Track	Frame	Orientation
10th Oct. 2007	25th Feb. 2008	138	339	165	230	Ascending
10th Oct. 2007	12th Oct. 2008	368	-987	165	230	Ascending
25th Nov. 2007	25th Feb. 2008	92	282	165	230	Ascending
25th Feb. 2008	12th Oct. 2008	230	-1406	165	230	Ascending
12th Oct. 2008	27th Nov. 2008	46	102	165	230	Ascending
27th Nov. 2008	14th Apr. 2009	138	736	165	230	Ascending
30th Aug. 2009	30th Nov. 2009	92	-183	165	230	Ascending
30th Nov. 2009	18th July 2010	230	302	165	230	Ascending
30th Nov. 2009	15th Jan 2010	46	-26	165	230	Ascending
2nd June 2010	18th July 2010	46	-45	165	230	Ascending
15th Jan 2010	2nd June 2010	138	373	165	230	Ascending
27th Sep. 2007	28th Dec. 2007	368	508	470	3380	Descending
28th Dec. 2007	29th Mar. 2008	92	74	470	3380	Descending
29th Mar. 2008	14th May 2008	46	-302	470	3380	Descending
29th Sep 2008	14th Nov. 2008	46	-114	470	3380	Descending
14th Nov. 2008	1st Apr. 2009	138	542	470	3380	Descending

8.4 Appendix D: Bouguer gravity data (summit area)

Station	Easting (UTM 16P)	Northing (UTM 16P)	Elevation (masl)	Bouguer gravity (mGal) normalized to B4
1	590722	1325350	534.638	113.8815
1	590299	1325201	496.03	118.2244
1	590299	1325201	496.03	118.3914
1	590299	1325201	496.03	118.4394
1	590705	1324687	516.837	114.5374
2	590741	1325302	530.649	115.1785
2	590305	1325252	495.685	118.2524
2	590737	1324724	524.657	115.9624
3	590714	1325258	531.395	115.4975
3	590298	1325305	500.617	117.6164
3	590768	1324751	531.964	115.4174
4	590739	1325206	533.186	115.9515
4	590804	1324785	540.883	115.5484
4	590305	1325356	527.509	117.086
5	590793	1325195	535.521	116.4865
5	590838	1324819	550.667	115.9214
5	590298	1325400	530.821	116.076
6	590837	1325168	541.9	117.4075
6	590854	1324864	561.493	115.3774
6	590312	1325451	538.391	115.035
7	590862	1325117	549.029	116.2645
7	590876	1324904	568.585	115.7014
8	590893	1325070	558.332	116.5705
8	590879	1324956	569.988	115.9184
9	590889	1325004	570.997	114.9675
10	590900	1324953	575.644	114.3725
12	590700	1325356	533.446	113.9583
14	590308	1325153	495.819	118.4384
15	590304	1325105	496.21	118.6534
16	590306	1325056	497.499	118.5084
17	590305	1325005	502.807	117.6974
18	590302	1324953	526.247	116.1044
19	590305	1324896	538.85	115.0284
20	590308	1324841	571.197	112.1774
21	590305	1324803	556.61	112.3254
26	590357	1325203	495.429	118.3584
27	590358	1325254	495.542	118.3134
28	590345	1325299	501.34	118.1694
30	590350	1325381	529.784	116.636
31	590356	1325451	538.657	114.742

39	590352	1325157	495.779	118.3334
40	590348	1325101	496.037	118.5594
41	590342	1325060	496.63	118.2824
46	590367	1324793	535.692	113.6574
47	590355	1324754	532.506	113.2875
48	590370	1324702	524.503	113.1275
49	590358	1324651	521.304	112.3305
50	590358	1324604	516.64	111.8555
50	590358	1324604	516.64	119.8434
51	590402	1325205	502.033	117.7064
54	590412	1325352	530.417	116.631
55	590414	1325401	538.946	115.404
64	590395	1325160	496.571	117.6644
71	590428	1324785	532.404	114.5125
72	590408	1324756	528.816	113.8805
73	590407	1324702	523.726	113.3555
74	590400	1324629	519.867	112.7555
74	590400	1324629	519.867	112.7555
75	590407	1324605	515.989	112.5675
77	590454	1325252	532.539	116.86
77	590454	1325252	532.539	116.841
78	590451	1325296	529.774	117.2
79	590458	1325350	530.778	116.377
80	590454	1325401	537.205	114.8223
97	590456	1324754	530.955	114.0465
98	590454	1324704	523.504	113.6855
99	590454	1324658	520.267	113.3405
100	590450	1324602	514.382	113.0505
104	590508	1325352	536.738	114.7673
122	590506	1324750	530.058	114.3545
123	590501	1324699	524.65	113.9645
124	590509	1324655	517.793	113.8195
125	590506	1324603	510.753	113.6665
129	590555	1325360	544.706	113.5683
129	590555	1325360	544.706	113.5113
149	590558	1324657	516.951	113.8894
150	590559	1324606	507.762	113.9754
154	590606	1325360	538.774	113.5613
173	590605	1324691	521.149	113.7094
174	590609	1324655	515.667	113.4964
175	590599	1324603	505.364	114.1674
179	590657	1325355	534.891	113.8173
199	590657	1324647	510.147	114.0494
202	590256	1325253	497.913	116.9174

205	590257	1325403	529.364	115.931
206	590260	1325447	538.604	114.772
214	590252	1325156	496.074	118.3544
215	590256	1325105	496.817	118.4834
216	590257	1325056	497.663	118.4174
217	590259	1325016	500.671	117.9474
218	590257	1324952	527.478	116.0314
219	590253	1324903	536.744	115.2454
220	590259	1324865	552.624	113.2824
231	590221	1325440	532.891	114.659
239	590207	1325158	497.248	117.6004
240	590202	1325106	497.871	118.0274
241	590204	1325059	499.657	117.9884
242	590206	1325004	508.637	117.3014
243	590205	1324953	527.141	115.9774
244	590202	1324906	537.37	114.9134
264	590162	1325154	499.336	117.2854
265	590156	1325106	499.336	117.7224
266	590156	1325056	501.067	117.4014
267	590156	1325004	510.554	116.9344
268	590152	1324956	527.736	115.7544
269	590153	1324905	537.958	114.6144
290	590104	1325108	500.021	117.0184
291	590111	1325060	502.917	116.9824
293	590105	1324956	531.874	115.1314
294	590099	1324907	540.347	114.0524
315	590052	1325095	504.411	116.4224
317	590051	1324995	537.197	114.3594
317	590051	1324995	537.197	114.3074
318	590057	1324949	537.728	114.2074
319	590060	1324911	545.161	112.8574
340	590002	1325103	533.845	114.0854
341	590007	1325057	534.226	114.1654
342	590007	1325002	538.012	113.7024
343	590012	1324956	542.885	112.8234
364	589957	1325151	537.449	113.2994
365	589954	1325111	540.358	112.8404
366	589961	1325054	543.698	112.5174

8.5 Appendix E: VLF data (summit area)

Easting (UTM 16P)	Northing (UTM 16P)	F1: Tilt direction (signs: negat.-W, posit.-E) and Tilt Angle (number)	Easting (UTM 16P)	Northing (UTM 16P)	F2: Tilt direction (signs: negat.-S, posit.-N) and Tilt Angle (number)
590760	1325173	-16	590760	1325173	6
590781	1325161	-11	590781	1325161	2
590784	1325152	-10	590784	1325152	3
590796	1325118	-11	590796	1325118	-4
590808	1325100	-5	590808	1325100	-2
590827	1325085	-9	590827	1325085	-3
590836	1325063	-5	590836	1325063	-3
590845	1325045	-4	590845	1325045	-8
590863	1325029	-4	590863	1325029	-4
590869	1325014	-2	590869	1325014	-2
590902	1325002	-1	590902	1325002	-2
590896	1325005	-5	590896	1325005	-1
590890	1325032	0	590890	1325032	-4
590887	1325063	-6	590887	1325063	-3
590890	1325097	-2	590890	1325097	-3
590902	1324968	-3	590902	1324968	-3
590906	1324953	-3	590906	1324953	-2
590903	1324937	-1	590903	1324937	-3
590903	1324922	-2	590903	1324922	-4
590894	1324882	-5	590894	1324882	-4
590894	1324854	-3	590894	1324854	-3
590891	1324836	-5	590891	1324836	-5
590897	1324811	-3	590897	1324811	-5
590897	1324796	-6	590897	1324796	-2
590909	1324781	-6	590909	1324781	-1
590912	1324753	-3	590912	1324753	-2
590891	1324747	-4	590891	1324747	-3
590864	1324744	-3	590864	1324744	-3
590843	1324744	-4	590843	1324744	1
590815	1324734	-3	590815	1324734	-1
590794	1324728	-3	590794	1324728	-1
590791	1324710	-3	590791	1324710	0
590791	1324679	-4	590791	1324679	-1
590785	1324654	-3	590785	1324654	-1
590767	1324636	-2	590767	1324636	-1
590749	1324617	-2	590749	1324617	2
590716	1324611	-2	590716	1324611	3
590701	1324611	-4	590701	1324611	3
590680	1324605	-6	590680	1324605	5

590647	1324605	-1	590647	1324605	3
590893	1325125	-7	590893	1325125	-4
590902	1325143	-10	590902	1325143	-3
590905	1325162	-4	590905	1325162	0
590908	1325189	-8	590908	1325189	1
590893	1325205	-7	590893	1325205	3
590859	1325207	-6	590859	1325207	4
590838	1325207	-7	590838	1325207	5
590817	1325210	-9	590817	1325210	5
590799	1325210	-4	590799	1325210	8
590778	1325207	-10	590778	1325207	8
590741	1325204	-12	590741	1325204	7
590869	1325125	-5	590869	1325125	0
590845	1325134	-5	590845	1325134	1
590835	1325155	-8	590835	1325155	-2
590826	1325171	-8	590826	1325171	1
590802	1325183	-10	590802	1325183	6
590775	1325201	-11	590775	1325201	4
590763	1325219	-7	590763	1325219	9
590744	1325235	-11	590744	1325235	8
590735	1325247	-7	590735	1325247	12
590744	1325229	-10	590744	1325229	8
590760	1325244	-13	590760	1325244	11
590778	1325266	-6	590778	1325266	9
590790	1325284	-5	590790	1325284	7
590799	1325303	-3	590799	1325303	4
590802	1325315	1	590802	1325315	3
590808	1325349	7	590808	1325349	2
590808	1325376	5	590808	1325376	2
590804	1325404	9	590804	1325404	-2
590801	1325425	11	590801	1325425	-4
590792	1325450	14	590792	1325450	0
590786	1325456	16	590786	1325456	-3
590771	1325493	18	590771	1325493	-3
590762	1325517	17	590762	1325517	-6
590750	1325539	17	590750	1325539	-6
590746	1325548	16	590746	1325548	-6
590743	1325560	17	590743	1325560	-6
590734	1325579	14	590734	1325579	-6
590710	1325609	16	590710	1325609	-6
590707	1325631	14	590707	1325631	-4
590707	1325652	16	590707	1325652	-7
590707	1325677	15	590707	1325677	-7
590704	1325695	13	590704	1325695	-6

590707	1325717	13	590707	1325717	-3
590710	1325745	12	590710	1325745	-6
590301	1325247	4	590301	1325247	-3
590307	1325302	-3	590307	1325302	-3
590356	1325305	-8	590356	1325305	-10
590353	1325258	-14	590353	1325258	-12
590358	1325204	8	590358	1325204	-5
590253	1325205	-8	590253	1325205	-9
590301	1325247	4	590258	1325258	-7
590258	1325258	4	590389	1325255	-7
590389	1325255	-2	590394	1325197	-4
590394	1325197	-13	590359	1325152	0
590359	1325152	-5	590300	1325201	3
590300	1325201	-1	590052	1325107	11
590052	1325107	16	590086	1325104	5
590086	1325104	17	590107	1325104	1
590107	1325104	17	590131	1325104	-1
590131	1325104	14	590158	1325104	-5
590158	1325104	8	590185	1325101	-3
590185	1325101	11	590210	1325101	-4
590210	1325101	10	590234	1325104	-3
590234	1325104	11	590261	1325101	-6
590261	1325101	6	590282	1325107	-2
590282	1325107	5	590309	1325104	1
590309	1325104	4	590337	1325105	4
590337	1325105	1	590306	1325049	2
590306	1325049	5	590279	1325052	-2
590279	1325052	4	590252	1325052	-5
590252	1325052	8	590231	1325052	0
590231	1325052	10	590204	1325052	-6
590204	1325052	13	590179	1325052	-3
590179	1325052	14	590152	1325052	-4
590152	1325052	17	590128	1325055	2
590128	1325055	17	590104	1325052	1
590104	1325052	16	590080	1325052	7
590080	1325052	17	590058	1325051	5
590058	1325051	18	590055	1325137	4
590055	1325137	15	590088	1325135	4
590088	1325135	14	590137	1325138	3
590137	1325138	13	590152	1325147	-2
590152	1325147	15	590182	1325150	-4
590182	1325150	8	590209	1325153	-5
590209	1325153	6	590234	1325160	-6
590234	1325160	4	590258	1325153	-7

590258	1325153	4	590282	1325157	-4
590282	1325157	2	590306	1325157	-1
590306	1325157	4	590333	1325154	-3
590333	1325154	2	590358	1325154	2
590358	1325154	1	590382	1325154	5
590382	1325154	-5	590397	1325182	-3
590397	1325182	-7	590406	1325197	2
590406	1325197	-7	590379	1325197	0
590379	1325197	-5	590351	1325203	-3
590351	1325203	-3	590327	1325203	-4
590327	1325203	-2	590282	1325203	-3
590282	1325203	2	590254	1325230	-7
590254	1325230	-2	590285	1325249	-8
590285	1325249	-3	590309	1325252	-2
590309	1325252	-2	590330	1325252	-5
590330	1325252	-3	590357	1325255	-4
590357	1325255	6	590369	1325252	-4
590369	1325252	-11	590406	1325258	-5
590406	1325258	-8	590403	1325277	-5
590403	1325277	-11	590399	1325298	-5
590399	1325298	-14	590409	1325292	-4
590409	1325292	-13	590354	1325301	-5
590354	1325301	-13	590321	1325286	-3
590321	1325286	-10	590303	1325301	-3
590303	1325301	-9	590272	1325283	-6
590272	1325283	-8	590278	1325322	-5
590278	1325322	-12	590294	1325332	-4
590294	1325332	-11	590306	1325338	-4
590306	1325338	-11	590330	1325335	-3
590330	1325335	-9	590357	1325341	-2
590357	1325341	-14	590303	1325227	-6
590303	1325227	-1	590303	1325175	-4
590303	1325175	1	590309	1325126	0
590309	1325126	2	590309	1325077	3
590309	1325077	4	590313	1325025	4
590313	1325025	8	590258	1325006	-3
590258	1325006	12	590252	1325027	-1
590252	1325027	10	590255	1325080	-3
590255	1325080	8	590352	1325129	4
590352	1325129	2	590348	1325181	2
590348	1325181	-4	590351	1325231	-5
590351	1325231	-6	590378	1325452	-8
590378	1325452	2	590399	1325443	-8
590399	1325443	0	590420	1325437	-7

590420	1325437	1	590441	1325430	-6
590441	1325430	4	590463	1325418	-4
590463	1325418	1	590487	1325406	-1
590487	1325406	1	590505	1325391	-7
590505	1325391	1	590517	1325375	-6
590517	1325375	-3	590535	1325363	-2
590535	1325363	4	590547	1325360	-1
590547	1325360	4	590554	1325345	-6
590554	1325345	4	590569	1325336	0
590569	1325336	6	590575	1325323	2
590575	1325323	1	590584	1325308	1
590584	1325308	-2	590608	1325305	3
590608	1325305	-1	590635	1325299	5
590635	1325299	-1	590678	1325305	6
590678	1325305	0	590684	1325284	11
590684	1325284	-2	590690	1325284	13
590690	1325284	-2	590717	1325275	7
590717	1325275	-6	590732	1325287	11
590732	1325287	-5	590714	1325315	11
590714	1325315	0	590717	1325330	10
590717	1325330	3	590717	1325345	4
590717	1325345	7	590702	1325351	4
590702	1325351	9	590572	1325363	2
590572	1325363	10	590596	1325360	3
590596	1325360	14	590623	1325357	3
590623	1325357	12	589906	1325343	-1
589906	1325343	9	589912	1325358	-2
589912	1325358	6	589915	1325398	0
589915	1325398	5	589948	1325426	1
589948	1325426	4	589994	1325466	-1
589994	1325466	4	590048	1325491	1
590048	1325491	8	590096	1325491	-4
590096	1325491	5	590136	1325482	-3
590136	1325482	6	590184	1325476	-4
590184	1325476	6	590205	1325467	-2
590205	1325467	-1	590316	1324794	16
590316	1324794	2	590307	1324806	11
590307	1324806	2	590301	1324816	11
590301	1324816	8	590289	1324831	8
590289	1324831	10	590277	1324813	12
590277	1324813	2	590265	1324800	11
590265	1324800	1	590259	1324776	16
590259	1324776	-4	590256	1324763	16
590256	1324763	-1	590250	1324745	18

590250	1324745	-5	590247	1324717	17
590247	1324717	-7	590238	1324696	14
590238	1324696	-9	590223	1324683	14
590223	1324683	-9	590214	1324653	14
590214	1324653	-9	590187	1324653	8
590187	1324653	-10	590172	1324656	6
590172	1324656	-13	590153	1324662	2
590153	1324662	-15	590129	1324671	1
590129	1324671	-17	590108	1324686	10
590108	1324686	-19	590090	1324698	-2
590090	1324698	-17	590062	1324711	-2
590062	1324711	-15	590044	1324723	-4
590044	1324723	-16	590059	1324735	-5
590059	1324735	-13	590008	1324747	-6
590008	1324747	-12	589990	1324766	-6
589990	1324766	-15	589969	1324772	-6
589969	1324772	-13	589953	1324781	-7
589953	1324781	-14	589932	1324793	-9
589932	1324793	-15	589917	1324808	-7
589917	1324808	-14	589899	1324821	-10
589899	1324821	-13	589881	1324833	-9
589881	1324833	-14	589869	1324842	-9
589869	1324842	-13	589856	1324863	-9
589856	1324863	-12	589844	1324876	-8
589844	1324876	-10	589829	1324897	-11
589829	1324897	-11	589817	1324913	-10
589817	1324913	-12	589808	1324931	-10
589808	1324931	-7	589796	1324943	-10
589796	1324943	-9	589787	1324965	-12
589787	1324965	-10	589780	1324986	-13
589780	1324986	-8	589777	1325014	-15
589777	1325014	-8	589780	1325029	-15
589780	1325029	-4	589786	1325048	-15
589786	1325048	-4	589795	1325078	-16
589795	1325078	2	589801	1325088	-14
589801	1325088	3	589813	1325112	-13
589813	1325112	7	589819	1325131	-11
589819	1325131	0	589831	1325152	-10
589831	1325152	6	589822	1325164	-15
589822	1325164	10	589810	1325180	-14
589810	1325180	8	589810	1325198	-16
589810	1325198	11	589810	1325223	-16
589810	1325223	6	589801	1325229	-14
589801	1325229	12	589786	1325247	-15

589786	1325247	9	589771	1325260	-16
589771	1325260	8	589792	1325269	-16
589792	1325269	14	589795	1325281	-19
589795	1325281	20	589807	1325296	-18
589807	1325296	12	589822	1325297	-16
589822	1325297	12	589822	1325327	-17
589822	1325327	10	589846	1325343	-18
589846	1325343	8	589852	1325352	-15
589852	1325352	5	589861	1325383	-15
589861	1325383	8	589876	1325404	-14
589876	1325404	5	589882	1325417	-13
589882	1325417	8	589894	1325441	-18
589894	1325441	6	589909	1325441	-9
589909	1325441	7	589933	1325460	-13
589933	1325460	11	589951	1325478	-6
589951	1325478	5	589972	1325484	-10
589972	1325484	9	589997	1325494	-2
589997	1325494	8	590015	1325509	-11
590015	1325509	10	590036	1325528	-9
590036	1325528	7	590060	1325537	-2
590060	1325537	7	590081	1325525	-3
590081	1325525	9	590096	1325519	-4
590096	1325519	8	590127	1325519	-13
590127	1325519	10	590139	1325516	-7
590139	1325516	7	590172	1325513	-13
590172	1325513	9	590190	1325507	-8
590190	1325507	11	590220	1325500	-12
590220	1325500	11	590248	1325504	-16
590248	1325504	10	590263	1325504	-14
590263	1325504	13	590287	1325501	-13
590287	1325501	12	590311	1325501	-14
590311	1325501	9	590320	1325498	-13
590320	1325498	12	590344	1325492	-15
590344	1325492	19	590369	1325489	-14
590369	1325489	10	590387	1325476	-12
590387	1325476	13	590408	1325483	-15
590408	1325483	12	590426	1325483	-13
590426	1325483	14	590444	1325480	-14
590444	1325480	16	590450	1325480	-12
590450	1325480	16	590493	1325471	-12
590493	1325471	11	590508	1325458	-9
590508	1325458	16	590526	1325437	-2
590526	1325437	12	590532	1325434	-7
590532	1325434	12	590547	1325394	-8

590547	1325394	11	590635	1324556	9
590300	1324100	2	590629	1324513	5
590228	1324008	-2	590617	1324460	3
590134	1323918	2	590575	1324294	5
590301	1323737	14	590342	1324161	3
590214	1323728	16	590300	1324100	2
590084	1323660	22	590228	1324008	2
590017	1323660	25	590134	1323918	-1
589942	1323699	28	590301	1323737	1
589887	1323705	24	590214	1323728	-9
589802	1323727	25	590084	1323660	-9
589548	1323784	21	590017	1323660	-7
589509	1323796	19	589942	1323699	-6
589463	1323827	16	589887	1323705	-6
589442	1323833	13	589802	1323727	-9
589418	1323848	13	589548	1323784	-3
589384	1323876	16	589509	1323796	4
589363	1323888	14	589463	1323827	5
589294	1323919	16	589442	1323833	2
589236	1323958	13	589418	1323848	4
589188	1323986	14	589384	1323876	2
589060	1324130	12	589363	1323888	-3
589003	1324179	17	589294	1323919	0
588945	1324206	17	589236	1323958	1
588894	1324219	16	589188	1323986	-2
588875	1324286	17	589060	1324130	2
588806	1324320	13	589003	1324179	0
588793	1324415	8	588945	1324206	-3
588781	1324473	5	588894	1324219	5
588705	1324562	11	588875	1324286	0
588684	1324602	10	588806	1324320	5
588681	1324660	-7	588793	1324415	5
588683	1324762	8	588781	1324473	6
588607	1324823	11	588705	1324562	6
588571	1324878	6	588684	1324602	3
588598	1324970	5	588681	1324660	2
588725	1325020	0	588683	1324762	2
588797	1325171	-4	588607	1324823	3
588878	1325220	-3	588571	1324878	3
588957	1325260	-1	588598	1324970	1
588999	1325328	7	588725	1325020	2
589011	1325429	4	588797	1325171	-1
589002	1325540	0	588878	1325220	-4
588953	1325635	6	588957	1325260	-2

588941	1325712	2	588999	1325328	0
588883	1325813	-2	589011	1325429	3
588904	1325868	7	589002	1325540	9
588943	1325927	7	588953	1325635	7
588985	1325954	-2	588941	1325712	3
589030	1325961	3	588883	1325813	2
589103	1326001	-1	588904	1325868	0
589160	1326066	-2	588943	1325927	2
589239	1326164	-4	588985	1325954	2
589323	1326229	3	589030	1325961	5
589426	1326269	-1	589103	1326001	-1
589453	1326383	-6	589160	1326066	1
589519	1326460	-5	589239	1326164	-5
591689	1325007	-2	589323	1326229	-10
591707	1325041	1	589426	1326269	-9
591719	1325063	-2	589453	1326383	-4
591710	1325084	2	591041	1325125	1
591707	1325106	-10	591035	1325113	0
591706	1325130	3	591026	1325085	-2
591694	1325146	-1	591017	1325070	-2
591676	1325158	-2	591014	1325045	-2
591658	1325173	-4	591020	1325014	-2
591652	1325195	-4	591017	1324993	-2
591643	1325213	-2	591017	1324965	-2
591628	1325234	2	591017	1324944	1
591612	1325250	-10	591020	1324965	-1
591597	1325268	2	591036	1324910	-3
591585	1325283	-6	591051	1324882	-3
591573	1325299	-6	591066	1324864	-4
591561	1325314	-2	591084	1324846	-5
591540	1325323	-6	591112	1324830	-1
591527	1325329	-6	591118	1324824	-4
591491	1325341	-2	591145	1324806	-3
591482	1325354	-3	591154	1324797	-4
591464	1325363	8	591172	1324791	-3
591452	1325375	0	591190	1324775	0
591434	1325372	0	591199	1324772	-1
591412	1325372	2	591212	1324763	-3
591388	1325372	-6	591236	1324732	-2
591367	1325366	1	591245	1324742	-4
591346	1325356	-3	591263	1324745	-2
591334	1325341	-8	591275	1324754	-2
591325	1325344	5	591296	1324754	-4
591298	1325335	3	591321	1324748	1

591273	1325322	0	591336	1324751	-3
591258	1325304	-4	591366	1324761	-2
591240	1325298	-5	591378	1324751	-2
591222	1325288	-3	591402	1324742	-3
591195	1325279	-1	591411	1324736	-1
591162	1325307	-1	591426	1324733	2
591159	1325270	-3	591451	1324736	-2
591147	1325254	1	591466	1324745	2
591138	1325236	-3	591481	1324752	-2
591122	1325224	-2	591496	1324752	0
591107	1325214	-3	591517	1324761	1
591092	1325199	-5	591535	1324776	0
591077	1325184	-3	591556	1324783	1
591059	1325156	-2	591568	1324795	0
591023	1325116	-3	591577	1324807	0
591008	1325100	-1	591589	1324820	1
590990	1325085	0	591602	1324838	-1
590972	1325076	-2	591605	1324832	-1
590942	1325054	3	591611	1324841	-2
590923	1325042	-4	591638	1324887	-3
590625	1324599	0	591644	1324897	-2
590604	1324598	-1	591659	1324918	-2
590574	1324598	-1	591674	1324943	-1
590553	1324604	-3	591680	1324961	-4
590523	1324607	-2	591680	1324983	-4
590504	1324604	-5	591692	1325001	-3
590474	1324601	-4	591689	1325007	1
590453	1324601	-2	591707	1325041	-1
590429	1324604	-1	591719	1325063	2
590405	1324604	-2	591710	1325084	-2
590380	1324604	1	591707	1325106	0
590356	1324604	1	591706	1325130	-5
590329	1324607	2	591694	1325146	0
590311	1324607	-4	591676	1325158	-2
590308	1324650	-4	591658	1325173	-5
590338	1324656	-7	591652	1325195	5
590353	1324653	-6	591643	1325213	0
590389	1324653	-6	591628	1325234	0
590410	1324653	-4	591612	1325250	6
590438	1324653	-4	591597	1325268	-3
590456	1324653	-6	591585	1325283	-2
590486	1324656	-4	591573	1325299	3
590510	1324653	-6	591561	1325314	-2
590537	1324657	-3	591540	1325323	-2

590556	1324654	-1	591527	1325329	-3
590580	1324657	0	591491	1325341	4
590604	1324654	0	591482	1325354	4
590631	1324657	-3	591464	1325363	2
590655	1324657	-3	591452	1325375	0
590559	1324697	2	591434	1325372	-5
590528	1324700	3	591412	1325372	0
590507	1324703	1	591388	1325372	2
590474	1324699	-5	591367	1325366	-2
590459	1324706	-1	591346	1325356	-4
590425	1324702	-3	591334	1325341	-4
590410	1324705	-1	591325	1325344	-2
590374	1324705	-2	591298	1325335	-2
590356	1324705	-1	591273	1325322	6
590329	1324702	-4	591258	1325304	-2
590311	1324705	-2	591240	1325298	1
590310	1324754	1	591222	1325288	3
590338	1324757	-3	591195	1325279	3
590356	1324748	0	591162	1325307	-1
590383	1324751	0	591159	1325270	8
590407	1324755	0	591147	1325254	6
590431	1324755	2	591138	1325236	5
590453	1324755	0	591122	1325224	3
590483	1324752	-1	591107	1325214	7
590454	1325378	-15	591092	1325199	3
590460	1325400	-6	591077	1325184	8
590484	1325246	-15	591059	1325156	2
590493	1325372	-8	591023	1325116	2
590511	1325253	-20	591008	1325100	0
590508	1325280	-20	590990	1325085	4
590511	1325302	-18	590972	1325076	1
590511	1325326	-18	590942	1325054	-2
590508	1325354	-11	590923	1325042	-1
590532	1325311	-19	590625	1324599	5
590539	1325271	-20	590604	1324598	4
590411	1325329	14	590574	1324598	6
590408	1325406	13	590553	1324604	7
590399	1325430	-5	590523	1324607	9
590429	1325397	-14	590504	1324604	8
590378	1325344	-15	590474	1324601	13
590360	1325353	-14	590453	1324601	11
590354	1325378	-13	590429	1324604	13
590357	1325403	-15	590405	1324604	15
590357	1325421	17	590380	1324604	17

590351	1325452	-3	590356	1324604	19
590354	1325461	6	590329	1324607	23
590321	1325369	-13	590311	1324607	18
590384	1325440	2	590308	1324650	22
590306	1325356	-15	590338	1324656	23
590305	1325381	-13	590353	1324653	22
590302	1325402	-10	590389	1324653	20
590299	1325430	-13	590410	1324653	18
590302	1325448	-10	590438	1324653	18
590305	1325467	2	590456	1324653	14
590272	1325433	-14	590486	1324656	11
590263	1325470	-4	590510	1324653	9
590254	1325445	-12	590537	1324657	11
590251	1325427	-14	590556	1324654	9
590254	1325402	-11	590580	1324657	9
590266	1325375	-9	590604	1324654	5
590239	1325427	-9	590631	1324657	6
590215	1325445	-7	590655	1324657	5
590205	1325476	-1	590559	1324697	6
590246	1324880	20	590528	1324700	8
590262	1324902	18	590507	1324703	10
590249	1324929	18	590474	1324699	11
590201	1324926	24	590459	1324706	15
590207	1324904	23	590425	1324702	16
590180	1324904	23	590410	1324705	15
590156	1324904	24	590374	1324705	22
590156	1324932	24	590356	1324705	21
590156	1324953	22	590329	1324702	20
590131	1324956	20	590311	1324705	23
590101	1324956	23	590310	1324754	18
590004	1325002	22	590338	1324757	18
590007	1325033	20	590356	1324748	20
590004	1325054	17	590383	1324751	20
590004	1325088	24	590407	1324755	18
590004	1325113	19	590431	1324755	15
590019	1325113	20	590453	1324755	14
590034	1325079	16	590483	1324752	14
590043	1325067	18	590457	1325252	1
590058	1325051	18	590460	1325274	-6
590049	1325024	21	590451	1325295	-6
590053	1324993	21	590460	1325326	-7
590050	1324975	25	590457	1325354	-9
590056	1324953	23	590454	1325378	-4
590059	1324929	26	590460	1325400	-7

590056	1324904	27	590484	1325246	-2
589952	1325159	20	590493	1325372	-5
589955	1325125	18	590511	1325253	-4
589955	1325103	18	590508	1325280	-8
589956	1325073	18	590511	1325302	-15
589962	1325027	20	590511	1325326	-6
589962	1325011	22	590508	1325354	-8
590007	1324971	24	590532	1325311	-16
590010	1324953	27	590539	1325271	-5
590010	1324925	29	590411	1325329	-5
590035	1324925	28	590408	1325351	-3
590068	1324876	28	590408	1325378	-5
590104	1324904	26	590408	1325406	-8
590104	1324935	25	590399	1325430	-8
590113	1324877	-26	590429	1325397	-7
590138	1324870	28	590378	1325344	-4
590153	1324877	26	590360	1325353	-4
590204	1324877	24	590354	1325378	-3
590280	1324908	15	590357	1325403	-4
590310	1324932	17	590357	1325421	-4
590307	1324905	21	590351	1325452	-6
590307	1324877	17	590354	1325461	-7
590304	1324862	14	590321	1325369	-6
590286	1324871	17	590384	1325440	-8
590274	1324856	17	590306	1325356	1
589894	1325288	12	590305	1325381	-2
589882	1325275	10	590302	1325402	-2
589888	1325269	16	590299	1325430	0
589858	1325241	19	590302	1325448	-2
589858	1325238	16	590305	1325467	-6
589852	1325238	17	590272	1325433	0
589852	1325254	17	590263	1325470	-4
589861	1325281	13	590254	1325445	2
589867	1325278	13	590251	1325427	1
589861	1325324	11	590254	1325402	-1
589858	1325294	13	590266	1325375	-1
589852	1325272	14	590239	1325427	-2
589819	1325241	20	590215	1325445	1
589801	1325266	16	590205	1325476	-2
589810	1325275	20	590246	1324880	-3
589822	1325287	15	590262	1324902	-2
589846	1325309	13	590249	1324929	-1
589816	1325364	12	590201	1324926	-3
589822	1325352	13	590207	1324904	-4

589810	1325312	16	590180	1324904	-6
589782	1325299	17	590156	1324904	-4
589770	1325309	14	590156	1324932	-3
589779	1325327	13	590156	1324953	-4
589776	1325336	11	590131	1324956	-2
589740	1325361	7	590101	1324956	4
589713	1325394	7	590004	1325002	11
589695	1325373	7	590007	1325033	12
589710	1325382	10	590004	1325054	11
589737	1325324	10	590004	1325088	13
589779	1325376	8	590004	1325113	12
589749	1325398	6	590019	1325113	10
589722	1325425	5	590034	1325079	10
589749	1325456	7	590043	1325067	10
589782	1325432	8	590058	1325051	8
589818	1325404	7	590049	1325024	6
589864	1325377	10	590053	1324993	8
589894	1325352	7	590050	1324975	10
590653	1325354	12	590056	1324953	8
590653	1325379	14	590059	1324929	5
590659	1325400	20	590056	1324904	3
590656	1325428	23	589952	1325159	13
590659	1325462	23	589955	1325125	17
590665	1325471	19	589955	1325103	15
590692	1325490	20	589956	1325073	14
590701	1325505	22	589962	1325027	13
590713	1325527	22	589962	1325011	15
590698	1325551	22	590007	1324971	11
-	-	-	590010	1324953	8
-	-	-	590010	1324925	10
-	-	-	590035	1324925	7
-	-	-	590068	1324876	2
-	-	-	590104	1324904	-2
-	-	-	590104	1324935	2
-	-	-	590113	1324877	-1
-	-	-	590138	1324870	-2
-	-	-	590153	1324877	-5
-	-	-	590204	1324877	-4
-	-	-	590280	1324908	0
-	-	-	590310	1324932	5
-	-	-	590307	1324905	5
-	-	-	590307	1324877	3
-	-	-	590304	1324862	4
-	-	-	590286	1324871	2

-	-	-	590274	1324856	3
-	-	-	589894	1325288	-2
-	-	-	589882	1325275	-6
-	-	-	589888	1325269	-7
-	-	-	589858	1325241	-9
-	-	-	589858	1325238	-11
-	-	-	589852	1325238	-13
-	-	-	589852	1325254	-11
-	-	-	589861	1325281	-10
-	-	-	589867	1325278	-10
-	-	-	589861	1325324	-14
-	-	-	589858	1325294	-9
-	-	-	589852	1325272	-13
-	-	-	589819	1325241	-12
-	-	-	589801	1325266	-15
-	-	-	589810	1325275	-13
-	-	-	589822	1325287	-14
-	-	-	589846	1325309	-17
-	-	-	589816	1325364	-20
-	-	-	589822	1325352	-16
-	-	-	589810	1325312	-18
-	-	-	589782	1325299	-18
-	-	-	589770	1325309	-19
-	-	-	589779	1325327	-19
-	-	-	589776	1325336	-20
-	-	-	589740	1325361	-21
-	-	-	589713	1325394	-21
-	-	-	589695	1325373	-19
-	-	-	589710	1325382	-20
-	-	-	589737	1325324	-21
-	-	-	589779	1325376	-19
-	-	-	589749	1325398	-19
-	-	-	589722	1325425	-18
-	-	-	589749	1325456	-16
-	-	-	589782	1325432	-17
-	-	-	589818	1325404	-16
-	-	-	589864	1325377	-13
-	-	-	589894	1325352	-4
-	-	-	590653	1325354	-1
-	-	-	590653	1325379	-1
-	-	-	590659	1325400	-4
-	-	-	590656	1325428	-9
-	-	-	590659	1325462	-5
-	-	-	590665	1325471	-7

-	-	-	590692	1325490	6
-	-	-	590701	1325505	-4
-	-	-	590713	1325527	-5
-	-	-	590698	1325551	-7

8.6 Appendix F: Bouguer gravity data (lava tube profile)

Station Name	Date	Time (GMT)	Easting (UTM 16P)	Northing (UTM 16P)	Elevation (masl)	Distance to previous station (m)	Bouguer gravity (mGal) normalized to first station Bat_1)
Bat_1	15/01/2010	17:15	590648.81	1324602	500.1603	0	0
Choc_3	15/01/2010	17:58	590761.96	1324578.7	494.7702	115.52613	0.361551
Choc_7	15/01/2010	18:24	590841.95	1324537.6	495.6473	89.928177	0.9368203
Choc_9	15/01/2010	18:43	590866.98	1324499.8	496.4377	45.361277	0.8517476
Choc_12a	15/01/2010	19:13	590861.96	1324410.6	487.3903	89.354796	1.7378531
Choc_16	15/01/2010	20:50	590862.08	1324338.1	476.8501	72.468042	-0.6808738
Choc_18	15/01/2010	21:14	590840.28	1324284.3	465.1581	58.039192	-0.3921131
Choc_18	20/01/2010	16:34	590845.92	1324277.6	465.6224	8.7652885	-0.8539847
Choc_22	20/01/2010	16:50	590810.54	1324215.3	464.3752	71.623362	1.4295681
Choc_26	20/01/2010	17:07	590761.98	1324113.1	469.0974	113.13972	1.0887479
Choc_30	20/01/2010	17:18	590757.64	1324027.8	464.2057	85.448781	1.4330447
Choc_34	20/01/2010	17:35	590777.51	1323933.3	456.9619	96.587871	0.6222112
Choc_38	20/01/2010	18:02	590804.59	1323835.4	440.542	101.50811	0.9631555
Choc_42	20/01/2010	18:26	590733.6	1323779.1	436.7788	90.648903	1.4052776
Choc_46	20/01/2010	19:20	590642.49	1323737	436.2849	100.34819	0.0527647
Choc_50	20/01/2010	19:27	590620.37	1323649.8	431.7985	89.970065	-0.8527727
Choc_54	20/01/2010	19:34	590552.5	1323590	430.5323	90.447512	-1.6544737
Choc_58	20/01/2010	20:00	590492.34	1323524.7	431.3063	88.830389	-2.8049074
Choc_59	10/02/2010	17:26	590416.53	1323555.8	428.9188	81.974261	-3.8282682
Crescent_2b	09/03/2010	17:30	590026.85	1323681.1	424.6216	409.31897	-4.8876963
Crescent_5	09/03/2010	19:52	588674.65	1324719	361.2493	1704.6269	-2.8410908
Crescent_6	09/03/2010	20:00	588578.03	1324876.5	347.1663	184.7103	-2.1665923
Crescent_7	09/03/2010	20:12	588638.9	1325058	336.9666	191.4763	1.446135
Crescent_8	09/03/2010	20:22	588766.35	1325150.8	333.0162	157.63596	2.76554
Crescent_9	09/03/2010	20:39	588877.84	1325285.6	325.4769	174.95965	4.1277648
Crescent_10	09/03/2010	20:51	588990.74	1325341.5	325.353	125.95733	3.1599

8.7 Appendix G: VLF data (lava tube profile)

[illegible]	KILL ZONE PROFILE
[illegible]	From the corner of Chocoyos, before the lava tubes
[illegible]	No
[illegible]	Lava tubes
[illegible]	93.56951
[illegible]	20/03/2009

Point	Tilt F1	Tilt Direction F1	Signal Dir. F1	Northing (UTM)	Easting (UTM)	Spacing (m)	Acc. Spac (m)	Elevation	Date	Time (GMT)
KZ 6	2	34	124	1324100	590300	74.061	611.337	445	3/20/2009	16:15
KZ 7	2	210	120	1324008	590228	116.825	728.162	437	3/20/2009	16:18
KZ 8	2	48	138	1323918	590134	130.138	858.300	432	3/20/2009	16:21
KZ 9	14	22	112	1323737	590301	246.272	1104.572	438	3/20/2009	16:28
KZ 10	16	28	118	1323728	590214	87.464	1192.036	432	3/20/2009	16:31
KZ 11	22	20	110	1323660	590084	146.711	1338.747	441	3/20/2009	16:53
KZ 12	25	18	108	1323660	590017	67.000	1405.747	429	3/20/2009	16:57
KZ 13	28	32	122	1323699	589942	84.534	1490.281	431	3/20/2009	16:59
KZ 14	24	20	110	1323705	589887	55.326	1545.607	423	3/20/2009	17:01
KZ 15	25	30	120	1323727	589802	87.801	1633.408	424	3/20/2009	17:04
KZ 16	21	33	123	1323784	589548	260.317	1893.725	413	3/20/2009	17:09
KZ 17	19	21	111	1323796	589509	40.804	1934.530	410	3/20/2009	17:14
KZ 18	16	16	106	1323827	589463	55.471	1990.000	409	3/20/2009	17:16
KZ 19	13	19	109	1323833	589442	21.840	2011.841	409	3/20/2009	17:18
KZ 20	13	356	86	1323848	589418	28.302	2040.143	411	3/20/2009	17:23
KZ 21	16	30	120	1323876	589384	44.045	2084.188	412	3/20/2009	17:26
KZ 22	14	8	98	1323888	589363	24.187	2108.375	405	3/20/2009	17:28
KZ 23	16	22	112	1323919	589294	75.644	2184.019	406	3/20/2009	17:32
KZ 24	13	24	114	1323958	589236	69.893	2253.912	405	3/20/2009	17:34
KZ 25	14	6	96	1323986	589188	55.570	2309.481	405	3/20/2009	17:37
KZ 26	12	2	92	1324130	589060	192.666	2502.147	401	3/20/2009	17:43
KZ 27	17	22	112	1324179	589003	75.166	2577.313	396	3/20/2009	17:50
KZ 28	17	6	96	1324206	588945	63.977	2641.290	391	3/20/2009	17:59
KZ 29	16	356	86	1324219	588894	52.631	2693.921	389	3/20/2009	18:02
KZ 30	17	23	113	1324286	588875	69.642	2763.563	385	3/20/2009	18:06
KZ 31	13	10	100	1324320	588806	76.922	2840.485	380	3/20/2009	18:15
KZ 32	8	35	125	1324415	588793	95.885	2936.370	378	3/20/2009	18:19
KZ 33	5	8	98	1324473	588781	59.228	2995.598	372	3/20/2009	18:22

KZ 34	11	14	104	1324562	588705	117.034	3112.633	364	3/20/2009	18:24
KZ 35	10	355	85	1324602	588684	45.177	3157.810	361	3/20/2009	18:27
KZ 36	7	172	82	1324660	588681	58.078	3215.888	359	3/20/2009	18:31
KZ 37	8	342	72	1324762	588683	102.020	3317.907	359	3/20/2009	18:36
KZ 38	11	10	100	1324823	588607	97.453	3415.360	351	3/20/2009	18:38
KZ 39	6	355	85	1324878	588571	65.734	3481.094	339	3/20/2009	19:16
KZ 40	5	15	105	1324970	588598	95.880	3576.974	339	3/20/2009	19:19
KZ 41	0	19	109	1325020	588725	136.488	3713.462	332	3/20/2009	19:24
KZ 42	4	183	93	1325171	588797	167.287	3880.749	328	3/20/2009	19:28
KZ 43	3	185	95	1325220	588878	94.668	3975.417	327	3/20/2009	19:31
KZ 44	1	160	70	1325260	588957	88.549	4063.967	329	3/20/2009	19:34
KZ 45	7	34	124	1325328	588999	79.925	4143.892	328	3/20/2009	19:37
KZ 46	4	40	130	1325429	589011	101.710	4245.602	328	3/20/2009	19:40
KZ 47	0	190	100	1325540	589002	111.364	4356.966	325	3/20/2009	19:41
KZ 48	6	32	122	1325635	588953	106.892	4463.859	323	3/20/2009	19:43
KZ 49	2	7	97	1325712	588941	77.929	4541.788	327	3/20/2009	19:45
KZ 50	2	190	100	1325813	588883	116.469	4658.257	320	3/20/2009	19:48
KZ 51	7	40	130	1325868	588904	58.873	4717.130	318	3/20/2009	19:50
KZ 52	7	24	114	1325927	588943	70.725	4787.855	319	3/20/2009	19:52
KZ 53	2	189	99	1325954	588985	49.930	4837.785	322	3/20/2009	19:53
KZ 54	3	10	100	1325961	589030	45.541	4883.326	330	3/20/2009	19:55
KZ 55	1	165	75	1326001	589103	83.241	4966.566	330	3/20/2009	19:57
KZ 56	2	180	90	1326066	589160	86.452	5053.019	332	3/20/2009	20:00
KZ 57	4	195	105	1326164	589239	125.877	5178.896	340	3/20/2009	20:02
KZ 58	3	14	104	1326229	589323	106.212	5285.108	340	3/20/2009	20:04
KZ 59	1	200	110	1326269	589426	110.494	5395.602	346	3/20/2009	20:07
KZ 60	6	192	102	1326383	589453	117.154	5512.756	345	3/20/2009	20:09
KZ 61	5	190	100	1326460	589519	101.415	5614.171	346	3/20/2009	20:11

8.8 Appendix H: Sandwell satellite gravity data (caldera)

Easting (UTM 16P)	Northing (UTM 16P)	Elevation (masl)	Free Air Gravity (mGal)	Terrain Correction (mGal)	Bouguer Gravity (mGal)
586164.5	1334220	215.844	45.8	0.768	46.568
587971.3	1334225	182.386	46.4	0.675	47.075
589789	1334230	151.886	47.4	0.630	48.030
591595.7	1334236	134.512	48.4	0.580	48.980
593413.4	1334241	134.361	48.9	0.527	49.427
595231.1	1334247	179.749	48.5	0.467	48.967
597048.8	1334253	195.392	46.8	0.432	47.232
598855.6	1334259	188.912	43.8	0.416	44.216
600673.3	1334265	168.477	39.7	0.406	40.106
586169.7	1332417	228.226	51.5	0.929	52.429
587976.6	1332422	211.072	51.8	0.748	52.548
589794.4	1332428	193.297	52.7	0.693	53.393
591601.3	1332433	177.989	53.7	0.632	54.332
593419.1	1332439	167.735	54.4	0.547	54.947
595236.8	1332444	180.852	54.1	0.464	54.564
597054.6	1332450	204.115	52.5	0.436	52.936
598861.6	1332456	205.363	49.4	0.424	49.824
600679.4	1332462	191.676	45	0.422	45.422
586174.9	1330614	268.659	56.3	0.994	57.294
587981.9	1330620	264.653	56.4	0.797	57.197
589799.8	1330625	260.992	57.2	0.718	57.918
591606.8	1330631	244.602	58.3	0.661	58.961
593424.7	1330636	212.105	59.1	0.585	59.685
595242.6	1330642	193.763	59	0.495	59.495
597060.5	1330648	196.136	57.5	0.444	57.944
598867.5	1330654	217.355	54.5	0.438	54.938
600685.4	1330660	215.269	50	0.446	50.446
586180.1	1328812	317.263	60.2	0.964	61.164
587987.2	1328817	321.790	60	0.831	60.831
589805.2	1328822	295.497	60.6	0.761	61.361
591612.3	1328828	283.604	61.7	0.709	62.409
593430.3	1328834	261.829	62.6	0.646	63.246
595248.3	1328839	214.213	62.7	0.536	63.236
597066.3	1328845	204.487	61.6	0.469	62.069
598873.5	1328851	226.732	58.8	0.458	59.258
600691.5	1328857	238.640	54.5	0.482	54.982
586185.3	1327009	379.611	62.7	1.012	63.712
587992.5	1327014	340.299	62.2	1.000	63.200
589810.6	1327020	345.772	62.6	0.935	63.535

591617.8	1327025	340.205	63.6	0.943	64.543
593435.9	1327031	271.577	64.5	0.786	65.286
595254.1	1327037	208.880	64.9	0.623	65.523
597072.2	1327042	215.865	64.1	0.530	64.630
598879.4	1327048	244.024	61.7	0.504	62.204
600697.6	1327054	240.991	57.9	0.478	58.378
586190.5	1325207	445.726	64	1.094	65.094
587997.8	1325212	439.667	63.2	1.012	64.212
589816	1325217	442.593	63.2	1.074	64.274
591623.3	1325223	462.584	64	1.780	65.780
593441.5	1325228	263.121	64.8	1.115	65.915
595259.8	1325234	159.612	65.4	0.871	66.271
597078	1325240	179.269	65	0.643	65.643
598885.4	1325246	238.614	63.3	0.543	63.843
600703.6	1325252	248.229	60.1	0.505	60.605
584377.4	1323399	541.760	66.7	1.558	68.258
586195.7	1323404	499.020	64.5	1.195	65.695
588003.1	1323409	467.299	63.1	1.036	64.136
589821.4	1323415	421.446	62.7	0.964	63.664
591628.8	1323420	367.255	63.1	1.118	64.218
593447.2	1323426	232.371	63.7	1.135	64.835
595265.5	1323431	143.506	64.4	1.003	65.403
597083.8	1323437	158.707	64.4	0.832	65.232
598891.3	1323443	249.507	63.5	0.650	64.150
600709.7	1323449	276.036	61.3	0.585	61.885
584382.4	1321596	645.422	67.2	1.838	69.038
586200.8	1321601	525.866	64.5	1.313	65.813
588008.3	1321607	457.441	62.5	1.136	63.636
589826.8	1321612	442.217	61.4	1.094	62.494
591634.3	1321618	328.287	61.2	1.061	62.261
593452.8	1321623	218.587	61.6	1.158	62.758
595271.2	1321629	144.012	62.2	1.335	63.535
597089.7	1321635	184.554	62.7	1.026	63.726
598897.2	1321640	290.201	62.5	0.800	63.300
600715.7	1321647	313.662	61.5	0.722	62.222
584387.5	1319794	648.064	67.5	1.631	69.131
586206	1319799	586.385	64.3	1.385	65.685
588013.6	1319804	536.291	61.7	1.227	62.927
589832.1	1319809	481.862	59.8	1.217	61.017
591639.8	1319815	355.163	58.9	1.012	59.912
593458.3	1319821	302.092	58.8	1.031	59.831
595276.9	1319826	279.427	59.3	1.080	60.380
597095.5	1319832	296.205	60.1	0.956	61.056
598903.1	1319838	354.206	60.8	0.977	61.777

600721.7	1319844	386.303	61	1.129	62.129
584392.5	1317980	595.824	67.8	1.346	69.146
586211.2	1317985	557.499	64.2	1.197	65.397
588018.9	1317990	503.431	60.9	1.075	61.975
589837.5	1317996	452.613	58.2	0.984	59.184
591645.3	1318001	391.207	56.5	0.904	57.404
593464	1318007	418.502	55.8	0.980	56.780
595282.6	1318013	411.384	56	1.017	57.017
597101.3	1318018	388.249	56.9	0.914	57.814
598909.1	1318024	426.459	58.4	1.117	59.517
600727.8	1318030	481.983	59.8	2.092	61.892

8.9 Appendix I: Land Bouguer gravity data (caldera)

Date	Time (GMT)	Station	Easting (UTM 16P)	Northing (UTM 16P)	Elevation (masl)	Free Air Gravity (mGal)	Bouguer Anomaly (no terrain corrections)	Terrain Corr (mGal)	Final Bouguer normalized to A1 (mGal)
13/01/2010	16:00	Coyote_1	592796.3	1327279	286.1289	-1.90892	0.985816	0.585703	1.571519
13/01/2010	16:30	Coyote_1_return	592796.3	1327279	286.1289	-1.79949	1.095243	0.585703	1.680946
13/01/2010	17:30	Coyote_2	592830.6	1327194	281.6008	-4.34106	-0.9719	0.650675	-0.32122
13/01/2010	18:00	Coyote_2a	592874.7	1327024	288.3944	-1.93417	0.723198	0.72155	1.444749
13/01/2010	18:30	Coyote_3	592860.7	1327115	290.1043	-0.96598	1.512237	0.722861	2.235098
13/01/2010	19:40	Coyote_4	592868.9	1326828	295.5533	-0.06643	1.840858	0.741067	2.581925
13/01/2010	20:10	Coyote_4a	592872.3	1326748	291.4363	-1.7957	0.542954	0.70772	1.250674
14/01/2010	19:40	Boug _3	590806.1	1325357	514.9486	9.204055	-11.8758	2.523482	-9.35231
14/01/2010	20:05	Boug _5	590792.6	1325446	495.1206	7.024925	-11.9774	2.22175	-9.7557
14/01/2010	20:22	Boug_6	590756.7	1325528	481.58	6.012327	-11.5713	2.089494	-9.48183
14/01/2010	20:45	Boug_7	590724.8	1325615	468.3672	5.438571	-10.7607	1.913959	-8.84675
15/01/2010	17:15	Bat_1	590648.8	1324602	500.1603	5.985653	-13.5448	1.931445	-11.6133
15/01/2010	17:58	Choc_3	590762	1324579	494.7702	5.782457	-13.1832	1.838168	-11.345
15/01/2010	18:24	Choc_7	590841.9	1324538	495.6473	6.449624	-12.6079	1.898991	-10.7089
15/01/2010	18:43	Choc_9	590867	1324500	496.4377	6.447366	-12.693	1.935595	-10.7574
15/01/2010	20:50	Choc_12a	590861.9	1324411	487.3903	6.38553	-11.8069	1.759377	-10.0475
15/01/2010	21:14	Choc_16	590862.1	1324338	476.8501	2.862453	-14.2256	1.585205	-12.6404
15/01/2010	21:28	Choc_18	590840.3	1324284	465.1581	1.926185	-13.9369	1.393295	-12.5436
17/01/2010	17:02	bunker_2	590485.2	1325274	527.2686	10.0241	-12.3466	3.106989	-9.23959
17/01/2010	17:16	Plateau_2	590462.1	1325314	525.9783	11.23952	-10.996	2.945444	-8.05052
17/01/2010	17:26	Plateau_3	590430.1	1325349	528.7738	11.96894	-10.5594	3.020373	-7.53908
17/01/2010	17:41	Plateau_4	590394.6	1325379	529.3511	11.69308	-10.8958	3.077812	-7.81798
17/01/2010	17:55	Plateau_5	590345	1325393	526.2587	10.65603	-11.6088	2.98902	-8.61982
17/01/2010	18:08	Plateau_6	590299	1325387	525.9542	10.57775	-11.6552	2.99891	-8.6563
17/01/2010	18:18	Plateau_7	590259.7	1325421	537.8563	12.34682	-11.1332	3.693598	-7.43959
17/01/2010	19:30	Valley_6	590752.6	1325266	528.413	10.92267	-11.5679	2.800911	-8.767
17/01/2010	19:35	Valley_5	590724.1	1325310	527.0832	9.671929	-12.6793	2.827295	-9.85203
17/01/2010	19:40	Valley_4	590704.6	1325353	529.1776	9.087383	-13.4833	3.070213	-10.4131
17/01/2010	19:45	Valley_3	590653.7	1325356	530.8999	8.505988	-14.2452	3.196155	-11.049
17/01/2010	19:50	Valley_2	590603.7	1325359	534.8893	8.679473	-14.4897	3.409782	-11.0799
17/01/2010	19:56	Bunker_4/Valley_1	590553.9	1325356	540.5792	9.178269	-14.587	3.592336	-10.9947
17/01/2010	20:04	Bunker_3	590519.7	1325312	537.3579	11.5703	-11.8575	3.352487	-8.50499
17/01/2010	20:18	Valley_6	590752.6	1325266	528.413	10.60667	-11.8839	2.800911	-9.083
17/01/2010	20:43	Boug_7	590724.8	1325615	468.3672	5.308642	-10.8906	1.913959	-8.97668
17/01/2010	20:49	Boug_8	590709.2	1325700	462.4021	7.155135	-8.41916	1.907455	-6.5117
17/01/2010	20:56	Boug_9	590713.1	1325800	448.983	6.181646	-7.98666	1.814229	-6.17243
17/01/2010	21:01	Boug_10	590724.3	1325892	436.1136	5.722857	-7.09706	1.734409	-5.36265
17/01/2010	21:06	Boug_11	590701.1	1325983	422.4664	4.88785	-6.50218	1.588545	-4.91363

17/01/2010	21:11	Boug_12	590669.5	1326067	410.2575	4.270043	-5.8408	1.488293	-4.3525
17/01/2010	21:18	Boug_13	590669.3	1326067	409.0836	6.686463	-3.30138	1.467719	-1.83366
17/01/2010	21:23	Boug_14	590596.3	1326236	386.9888	2.803108	-4.86975	1.33261	-3.53714
17/01/2010	21:30	Boug_15	590573.6	1326327	374.4293	1.833273	-4.52367	1.2432	-3.28047
18/01/2010	18:14	B4			529.4494	8.674426	-13.9247		
18/01/2010	20:56	Coyote_1	592796.3	1327279	286.1289	-2.00592	0.888816	0.585703	1.474519
19/01/2010	16:28	Coyote_6	592868.7	1326829	295.4977	-0.02055	1.892566	0.740188	2.632754
19/01/2010	16:41	Coyote_7	592875.8	1326731	294.8111	-0.76796	1.217099	0.735501	1.952599
19/01/2010	16:48	Coyote_8	592875.1	1326737	291.6906	-2.86704	-0.55504	0.710803	0.155768
19/01/2010	16:58	Coyote_9	592911.8	1326652	296.8982	-2.5641	-0.79771	0.800759	0.003044
19/01/2010	17:32	Coyote_10	592938.3	1326564	304.6441	-0.08826	0.866545	0.985204	1.851749
19/01/2010	17:48	Coyote_11	593015	1326499	306.1806	1.861104	2.654921	1.141981	3.796902
19/01/2010	17:56	Coyote_12	593071.1	1326445	292.557	-0.53762	1.683614	0.915266	2.59888
19/01/2010	18:11	Coyote_13	593092.9	1326364	283.5444	-1.77564	1.389882	0.872865	2.262747
19/01/2010	18:35	Coyote_14	592990.2	1326331	272.4543	-5.31767	-0.99018	0.986016	-0.00416
19/01/2010	19:35	Coyote_15	593002.2	1326278	282.595	-1.83086	1.434139	0.985389	2.419528
19/01/2010	19:41	Coyote_16	593057.2	1326106	278.762	-2.9753	0.691298	1.068556	1.759854
19/01/2010	20:08	Coyote_17	593102.8	1326014	266.6737	-5.59869	-0.66554	1.086758	0.42122
19/01/2010	20:15	Coyote_18	593138.2	1325942	267.7277	-3.94136	0.88136	1.120134	2.001494
19/01/2010	20:24	Coyote_19	593170.8	1325852	254.315	-7.74161	-1.51358	1.157842	-0.35574
20/01/2010	16:14	Bat_1				-51.329			
20/01/2010	16:34	Choc_18	590845.9	1324278	464.3752	1.392285	-14.3887	1.384749	-13.004
20/01/2010	16:50	Choc_22	590810.6	1324215	469.0974	4.179606	-12.0962	1.41992	-10.6763
20/01/2010	17:07	Choc_26	590762	1324113	464.2057	3.337258	-12.426	1.363211	-11.0628
20/01/2010	17:18	Choc_30	590757.7	1324028	456.9619	2.928586	-12.0757	1.298732	-10.777
20/01/2010	17:35	Choc_34	590777.6	1323933	440.542	0.410357	-12.8735	1.056533	-11.817
20/01/2010	18:02	Choc_38	590804.6	1323835	436.7788	0.374012	-12.5156	1.008946	-11.5067
20/01/2010	18:26	Choc_42	590733.6	1323779	436.2849	0.780386	-12.0575	0.98867	-11.0688
20/01/2010	19:20	Choc_46	590642.5	1323737	431.7985	-1.14619	-13.514	0.910899	-12.6031
20/01/2010	19:27	Choc_50	590620.4	1323650	430.5323	-2.18139	-14.4165	0.89291	-13.5236
20/01/2010	19:34	Choc_54	590552.6	1323590	431.3063	-2.898	-15.2142	0.892866	-14.3214
20/01/2010	20:00	Choc_58	590492.3	1323525	433.0946	-3.85206	-16.3557	0.917584	-15.4381
21/01/2010	17:48	Boug18	590547.4	1326610	339.4612	-0.53419	-3.22735	0.98174	-2.24561
21/01/2010	18:00	Boug19	590613.4	1326694	328.8304	-0.56977	-2.14908	0.926756	-1.22233
21/01/2010	18:11	Boug20	590710.5	1326734	321.9786	-0.98081	-1.84223	0.890266	-0.95196
21/01/2010	18:25	Boug21	590797.5	1326767	324.87	1.281869	0.117505	0.914993	1.032497
21/01/2010	19:25	Boug22	590883.6	1326793	315.0611	-0.16067	-0.29731	0.862387	0.565078
09/02/2010	17:00	Coyote_20	593232	1325790	255.9985	-5.70285	0.348797	1.104931	1.453728
09/02/2010	17:09	Coyote_21	593320.4	1325778	242.3418	-8.14947	-0.66694	1.019147	0.352206
09/02/2010	17:45	Coyote_22	593408.3	1325756	232.411	-9.6262	-1.10317	0.994146	-0.10903
09/02/2010	18:01	Coyote_23	593485.5	1325710	233.5443	-9.28539	-0.88111	0.935651	0.054544
09/02/2010	18:13	Coyote_24	593564.4	1325665	229.463	-9.75703	-0.92512	0.867515	-0.05761
09/02/2010	19:42	Coyote_25	593635.7	1325610	229.6267	-8.93936	-0.12461	0.867335	0.742726
09/02/2010	19:52	Coyote_26	593719.6	1325595	229.6806	-8.46833	0.340771	0.872659	1.21343

09/02/2010	20:02	Coyote_27	593812.5	1325600	224.7209	-9.71097	-0.38221	0.811636	0.429427
09/02/2010	20:12	Coyote_28	593912.3	1325596	221.8988	-9.91891	-0.29447	0.781302	0.486831
10/02/2010	17:07	Choc_58			429.377	-4.91517	-17.0293		
10/02/2010	17:26	Choc_59	590416.6	1323556	430.3356	-5.0915	-17.306	0.85225	-16.4538
11/02/2010	16:45	MAS01	591035.9	1325133	600.1073	17.28339	-12.719	6.911329	-5.80763
11/02/2010	16:55	MAS02	591008.9	1325102	593.8859	13.91329	-15.4372	6.233462	-9.20375
11/02/2010	17:15	MAS03	590982.4	1325068	586.846	16.49049	-12.1224	5.564214	-6.5582
11/02/2010	17:20	MAS04	590961	1325028	585.0871	15.21157	-13.217	5.287449	-7.92959
11/02/2010	17:30	MAS05	590946.6	1324986	585.6421	15.21064	-13.2761	5.236394	-8.03973
11/02/2010	17:45	MAS06	590949.2	1324938	586.4481	14.8576	-13.7136	5.209938	-8.50367
11/02/2010	18:00	MAS07	590969.5	1324896	588.1485	14.79876	-13.9506	5.274737	-8.67587
11/02/2010	18:10	MAS08	591009.6	1324873	590.7698	14.65904	-14.365	5.499045	-8.86593
11/02/2010	18:24	MAS09	591053.6	1324851	593.3367	16.58787	-12.7051	5.863297	-6.8418
11/02/2010	18:38	MAS10	591098.3	1324828	596.7247	16.10052	-13.5474	6.149632	-7.39778
11/02/2010	18:46	MAS11	591138.4	1324803	602.6126	16.23333	-14.0315	6.687624	-7.34389
11/02/2010	19:28	MAS12	591162.4	1324762	607.4074	13.25904	-17.5082	6.994027	-10.5142
12/02/2010	17:08	NP1	590095.3	1324904	537.2321	11.00168	-12.4129	3.970418	-8.44251
12/02/2010	17:25	NP02	590121.6	1324942	528.579	11.93766	-10.5703	3.751032	-6.81928
12/02/2010	18:06	NP03	590162.1	1324982	510.023	14.17345	-6.39032	3.553782	-2.83654
12/02/2010	18:37	NP04	590198.2	1325050	498.7509	9.051235	-10.3315	2.916268	-7.41523
12/02/2010	18:49	NP05	590225.2	1325085	494.9175	8.838879	-10.1422	2.626668	-7.51554
12/02/2010	18:56	NP06	590248.8	1325116	495.2198	9.383005	-9.62976	2.46944	-7.16032
12/02/2010	19:05	NP07	590278.2	1325151	494.8818	9.611536	-9.36581	2.359159	-7.00666
12/02/2010	19:10	NP08	590305.3	1325186	495.0317	9.778671	-9.21439	2.343452	-6.87093
12/02/2010	19:14	NP09	590333.6	1325225	494.843	9.666973	-9.30631	2.390868	-6.91544
12/02/2010	19:21	NP10	590360.7	1325263	496.2868	9.854833	-9.26973	2.415785	-6.85394
15/02/2010	17:19	NP11	590408	1325318	530.3869	14.5386	-8.1588	3.098021	-5.06077
15/02/2010	17:45	NP12	590407.9	1325319	530.4943	11.42773	-11.2809	3.101872	-8.17905
15/02/2010	19:56	T2	590913.6	1324769	554.2979	43.12231	17.91964	3.495658	21.4153
16/02/2010	17:46	Coyote_29	594000.8	1325570	227.119	-7.23285	1.844643	0.894276	2.738918
16/02/2010	18:04	Coyote_30	594025.8	1325491	231.1552	-5.38325	3.271352	1.110208	4.38156
16/02/2010	18:16	Coyote_31	593983.8	1325410	215.9279	-8.82951	1.420531	0.866183	2.286714
16/02/2010	18:34	Coyote_32	594001.6	1325326	211.5345	-9.71483	0.995532	0.863167	1.858699
16/02/2010	18:45	Coyote_33	594061.6	1325253	206.3984	-10.5859	0.66261	0.819208	1.481818
16/02/2010	19:49	Coyote_34	594104.3	1325173	200.0246	-13.2244	-1.30809	0.760296	-0.5478
16/02/2010	19:58	Coyote_35	594156.1	1325116	197.5646	-13.7867	-1.61262	0.747014	-0.86561
16/02/2010	20:02	Coyote_36	594174.7	1325041	198.9336	-13.2054	-1.17478	0.778466	-0.39632
16/02/2010	20:14	Coyote_37	594132.1	1324975	195.0186	-14.1684	-1.7276	0.796517	-0.93108
17/02/2010	17:36	LAG1	595257	1323754	137.4662	-22.3132	-3.84228	0.792712	-3.04957
17/02/2010	17:44	LAG2	595211.6	1323908	145.2683	-21.1252	-3.47184	0.779969	-2.69187
17/02/2010	17:55	LAG3	595214	1323909	146.0771	-23.1943	-5.62563	0.783713	-4.84192
17/02/2010	18:07	LAG4	595213.1	1323907	145.3088	-24.7408	-7.09161	0.780206	-6.3114
17/02/2010	18:15	LAG5	595115.7	1323991	156.667	-23.0278	-6.56872	0.797279	-5.77144
17/02/2010	18:25	LAG6	594922.9	1324108	162.451	-20.8843	-5.03123	0.744117	-4.28711

17/02/2010	18:34	LAG7	594763.8	1324105	170.6141	-20.0887	-5.09087	0.780046	-4.31082
17/02/2010	18:42	LAG8	594640.4	1324227	172.6784	-20.4837	-5.70218	0.755731	-4.94645
17/02/2010	18:52	LAG9	594619.3	1324394	182.1659	-18.2073	-4.41989	0.777928	-3.64196
17/02/2010	19:05	LAG10	594458.1	1324463	193.4096	-14.2675	-1.65813	0.839943	-0.81819
17/02/2010	19:15	LAG11	594337	1324608	195.9932	-13.837	-1.49828	0.839476	-0.6588
17/02/2010	19:28	LAG12	594171.5	1324686	194.2735	-13.8763	-1.35741	0.796931	-0.56048
17/02/2010	19:45	LAG13	594158.6	1324854	196.6934	-13.744	-1.47868	0.801937	-0.67674
18/02/2010	17:34	Boug_29	591072.3	1326882	309.2427	-0.75929	-0.2863	0.827159	0.540855
18/02/2010	18:00	Boug_30	591165.6	1326868	314.7481	0.534403	0.430561	0.863106	1.293667
18/02/2010	18:20	Boug_31	591250.6	1326837	314.4269	0.019176	-0.05101	0.862728	0.811714
18/02/2010	18:31	Boug_32	591344.4	1326873	318.2731	0.932175	0.459	0.956767	1.415767
18/02/2010	18:40	Boug_33	591440.4	1326860	318.3243	1.016269	0.53773	0.959733	1.497463
18/02/2010	19:56	Boug_34	591532.2	1326823	318.2375	0.804074	0.33463	0.945769	1.280399
18/02/2010	20:09	Boug_35	591624.3	1326856	313.7429	1.041047	1.042524	0.9109	1.953424
18/02/2010	20:16	Boug_36	591726.2	1326836	309.5524	0.090619	0.531156	0.854904	1.38606
18/02/2010	20:23	Boug_37	591822	1326865	310.3396	0.248039	0.606097	0.839765	1.445863
18/02/2010	20:30	Boug_38	591910.6	1326901	315.798	1.224454	1.010609	0.898445	1.909054
18/02/2010	20:37	Boug_39	592012.2	1326905	315.0874	1.602545	1.463153	0.865561	2.328713
18/02/2010	20:46	Boug_40	592114.9	1326907	314.7784	1.80756	1.700543	0.902491	2.603034
18/02/2010	20:53	Boug_41	592217.2	1326892	310.697	1.657658	1.978269	0.831765	2.810034
18/02/2010	21:00	Boug_42	592319.7	1326876	307.8428	0.486917	1.106577	0.743842	1.85042
19/02/2010	17:53	NIN_1	590149.2	1325087	503.5871	9.959574	-9.92987	3.084676	-6.8452
19/02/2010	18:00	NIN_2	590200.3	1325092	502.7324	10.56843	-9.23147	2.769046	-6.46242
19/02/2010	18:07	NIN_3	590258.3	1325111	501.2487	11.13014	-8.51431	2.631454	-5.88285
19/02/2010	18:16	NIN_4	590304.6	1325073	500.8923	10.74156	-8.86554	3.311142	-5.5544
19/02/2010	18:23	NIN_5	590320	1325116	500.0914	11.0273	-8.49588	2.942637	-5.55325
19/02/2010	18:30	NIN_6	590341	1325153	499.6304	10.98138	-8.4935	2.77254	-5.72096
19/02/2010	18:38	NIN_7	590343	1325211	499.2265	11.04284	-8.38972	2.497412	-5.89231
19/02/2010	18:51	NIN_8	590255.8	1325162	498.2005	10.40108	-8.92399	2.383892	-6.5401
02/03/2010	18:00	Road1	592522.3	1326841	319.5572	-0.09143	-0.69915	0.87289	0.173741
02/03/2010	18:15	Road2	592569.4	1326927	321.0233	3.77962	3.018294	0.904356	3.92265
02/03/2010	18:30	Road3	592631.8	1327002	324.5117	2.49324	1.366417	1.016288	2.382705
02/03/2010	20:33	Road4	592655.4	1327034	332.6142	-1.50193	-3.4777	1.318416	-2.15928
02/03/2010	20:45	Road5	592675.6	1327058	332.9332	-1.68033	-3.68952	1.38222	-2.3073
02/03/2010	20:52	Road6	592680.9	1327094	334.9655	-0.88676	-3.10888	1.536836	-1.57204
02/03/2010	21:00	Road7	592673.3	1327129	324.1865	-3.75699	-4.84974	1.192942	-3.6568
02/03/2010	21:15	Road8	592669.2	1327165	321.0795	-3.33484	-4.10206	1.172775	-2.92928
02/03/2010	21:35	Road9	592679	1327205	315.5035	-3.41001	-3.593	1.094336	-2.49866
02/03/2010	21:53	Road10	592699.9	1327228	313.025	-3.08584	-3.00915	1.052729	-1.95642
03/03/2010	17:20	Lavaflow1	590537.8	1326773	327.1655	-0.15957	-1.56445	0.901565	-0.66288
03/03/2010	18:21	Lavaflow7	590285.8	1327284	312.4724	-0.01374	0.12085	0.679264	0.800114
03/03/2010	18:39	Lavaflow8	590249.6	1327374	301.792	-1.41156	-0.15792	0.592502	0.434579
03/03/2010	19:25	Lavaflow9	590205.4	1327459	305.4751	0.040959	0.908695	0.639758	1.548453
03/03/2010	19:34	Lavaflow10	590155.6	1327545	306.4682	0.393008	1.156692	0.668035	1.824728

03/03/2010	19:40	Lavaflow11	590486	1326857	326.4337	6.72163	5.393429	0.879631	6.27306
03/03/2010	19:47	Lavaflow12	590418.3	1326926	328.5984	7.45694	5.901933	0.889517	6.79145
03/03/2010	19:56	Lavaflow13	590359.8	1327006	323.7521	6.583129	5.535892	0.798991	6.334884
03/03/2010	20:11	Lavaflow14	590316.4	1327096	321.2431	6.110827	5.326471	0.75348	6.079951
03/03/2010	20:18	Lavaflow15	590291.1	1327188	319.1353	6.467798	5.904287	0.741673	6.64596
06/03/2010	16:11	Lavaflow16	589848.1	1327992	289.459	-1.33401	1.211814	0.542344	1.754158
06/03/2010	16:22	Lavaflow17	589850.4	1327988	289.1498	-2.29922	0.279001	0.539369	0.81837
06/03/2010	16:31	Lavaflow18	589815.7	1328079	290.6204	-1.70049	0.723652	0.563351	1.287002
06/03/2010	16:46	Lavaflow19	589795.5	1328175	293.5097	-0.82344	1.297969	0.603231	1.9012
06/03/2010	17:09	Lavaflow20	589814.4	1328274	294.7739	-1.19054	0.798415	0.610747	1.409162
06/03/2010	17:24	Lavaflow21	589863.5	1328366	286.8011	-0.92794	1.896365	0.561685	2.458051
06/03/2010	17:33	Lavaflow22	589922.7	1328450	285.2297	-0.26317	2.725781	0.545249	3.271031
06/03/2010	17:42	Lavaflow23	589987.1	1328528	284.4529	-0.32394	2.746395	0.525715	3.27211
06/03/2010	17:50	Lavaflow24	590083.8	1328542	283.4225	-0.40555	2.77275	0.493017	3.265767
06/03/2010	18:00	Lavaflow25	590185.3	1328531	285.5555	0.596684	3.551496	0.49727	4.048766
06/03/2010	18:51	Lavaflow26	590286.7	1328527	283.6032	0.136555	3.29592	0.46505	3.76097
06/03/2010	18:57	Lavaflow27	590392.6	1328517	284.409	0.645906	3.720843	0.470384	4.191227
06/03/2010	19:09	Lavaflow28	590471.6	1328478	284.9156	1.017454	4.039312	0.473177	4.512489
06/03/2010	19:17	Lavaflow29	590406.3	1328402	287.299	1.118678	3.890815	0.491054	4.381869
06/03/2010	19:27	Lavaflow30	590347.1	1328321	287.4642	0.570345	3.325173	0.50899	3.834163
06/03/2010	19:34	Lavaflow31	590271.7	1328251	289.5961	0.311559	2.843018	0.545083	3.388101
06/03/2010	19:43	Lavaflow32	590207.8	1328172	293.0794	0.655022	2.821518	0.562939	3.384457
06/03/2010	19:48	Lavaflow33	590127.8	1328113	297.0164	1.459993	3.213989	0.575212	3.789201
06/03/2010	19:59	Lavaflow34	590035.1	1328061	292.4543	0.189522	2.421512	0.533644	2.955156
06/03/2010	20:07	Lavaflow35	589972	1327984	292.8737	-0.16138	2.026665	0.532465	2.559129
06/03/2010	20:13	Lavaflow36	589907.7	1327905	298.7885	1.154294	2.722619	0.627025	3.349644
06/03/2010	20:18	Lavaflow37	589834.4	1327831	297.1012	0.617819	2.362931	0.619962	2.982892
06/03/2010	20:26	Lavaflow38	589759.8	1327761	296.8095	0.382076	2.15775	0.620681	2.778431
06/03/2010	20:31	Lavaflow39	589662.9	1327727	294.2494	-0.46813	1.575774	0.603481	2.179256
06/03/2010	20:40	Lavaflow40	589574.2	1327667	295.4477	-0.39022	1.528137	0.639577	2.167713
06/03/2010	20:48	Lavaflow41	589570.6	1327576	298.2662	-0.47609	1.146962	0.681793	1.828755
06/03/2010	20:56	Lavaflow42	589577.8	1327480	300.2751	-0.86916	0.543406	0.700415	1.243821
06/03/2010	21:05	Lavaflow43	589532.3	1327388	298.0382	-1.71912	-0.07218	0.669909	0.597728
06/03/2010	21:10	Lavaflow44	589530.7	1327288	299.0358	-1.74344	-0.20102	0.690244	0.489222
06/03/2010	21:18	Lavaflow45	589556.9	1327187	307.5546	-0.71442	-0.06456	0.768395	0.70383
06/03/2010	21:25	Lavaflow46	589562.6	1327084	313.8981	-0.26604	-0.28082	0.764505	0.483681
06/03/2010	21:34	Lavaflow47	589622.1	1327011	319.5687	0.246299	-0.36262	0.784477	0.421855
08/03/2010	19:30	Ted	591067.6	1325193	593.9374	15.63731	-13.7186	6.549576	-7.16902
08/03/2010	19:50	Aidan	591100.8	1325235	597.2264	15.03618	-14.6643	6.908166	-7.75616
08/03/2010	20:00	Evan	591137.2	1325268	591.2852	13.93686	-15.1412	6.520405	-8.62075
08/03/2010	20:11	Compton	591176.3	1325300	594.2628	15.49149	-13.8985	6.862956	-7.03555
08/03/2010	20:20	Nic	591221.1	1325332	583.2229	13.16924	-15.0641	6.135372	-8.92868
08/03/2010	20:30	Slater	591267.6	1325372	577.8771	12.92883	-14.7443	5.900336	-8.84401
08/03/2010	20:40	Graham	591298.6	1325398	576.768	12.94068	-14.6163	5.836562	-8.77974

09/03/2010	17:30	Crescent_2b	590026.8	1323681	424.6216	-6.81661	-18.4324	0.902785	-17.5297
09/03/2010	19:52	Crescent_5	588674.6	1324719	361.2493	-11.4098	-16.3858	1.979174	-14.4067
09/03/2010	20:00	Crescent_6	588578	1324876	347.1663	-12.2109	-15.7113	2.108036	-13.6033
09/03/2010	20:12	Crescent_7	588638.9	1325058	336.9666	-9.66683	-12.0986	1.587605	-10.511
09/03/2010	20:22	Crescent_8	588766.3	1325151	333.0162	-8.76133	-10.7792	1.37927	-9.39994
09/03/2010	20:39	Crescent_9	588877.8	1325286	325.4769	-8.18904	-9.41699	1.196471	-8.22052
09/03/2010	20:51	Crescent_10	588990.7	1325341	325.353	-9.16988	-10.3849	1.191588	-9.19326
10/03/2010	16:15	Km21_1	591910.5	1326945	306.3143	-0.62587	0.153941	0.764714	0.918655
10/03/2010	16:22	Km21_2	591875.6	1327025	301.5988	-0.59702	0.676859	0.739889	1.416748
10/03/2010	16:33	Km21_3	591836.1	1327116	298.4515	-0.34087	1.262763	0.707781	1.970545
10/03/2010	16:39	Km21_4	591880	1327214	297.6919	0.218252	1.901473	0.685005	2.586478
10/03/2010	16:47	Km21_5	591886.8	1327317	295.2129	0.754623	2.697581	0.68486	3.382441
10/03/2010	16:55	Km21_6	591880.3	1327418	291.0502	1.336315	3.71542	0.68098	4.3964
10/03/2010	17:04	Km21_7	591867.7	1327519	287.4774	1.919363	4.672808	0.668506	5.341314
10/03/2010	17:09	Km21_8	591883.2	1327624	287.282	2.690118	5.464036	0.676162	6.140198
10/03/2010	17:19	Km21_9	591935.1	1327707	290.078	3.480626	5.961593	0.710782	6.672376
10/03/2010	17:26	Km21_10	591985	1327783	291.6868	4.266103	6.578508	0.722515	7.301023
10/03/2010	17:34	Km21_11	592037	1327862	292.3101	4.818714	7.065813	0.747699	7.813512
10/03/2010	17:43	Km21_12	592131	1327992	283.4436	2.602113	5.778199	0.578226	6.356425
10/03/2010	17:49	Km21_13	592222.6	1328127	283.8885	3.237097	6.366569	0.54779	6.914359
10/03/2010	17:56	Km21_14	592285.7	1328210	284.2271	3.866461	6.960456	0.535827	7.496284
10/03/2010	18:03	Km21_15	592369.4	1328346	282.2048	3.868396	7.174278	0.495468	7.669746
10/03/2010	18:11	Km21_16	592409.5	1328441	280.3816	3.73119	7.228098	0.487163	7.715261
10/03/2010	18:17	Km21_17	592446	1328528	279.8185	3.876385	7.432291	0.480507	7.912799
10/03/2010	18:27	Km21_18	592504.9	1328676	279.3481	4.037215	7.642408	0.473152	8.11556
10/03/2010	18:33	Km21_19	592564.8	1328819	279.0884	3.890597	7.522999	0.491709	8.014708
10/03/2010	19:10	Km21_20	592727.3	1328805	286.6324	4.506833	7.348812	0.60087	7.949682
10/03/2010	19:25	Km21_21	592943.7	1328701	288.4748	3.572279	6.221221	0.590351	6.811572
10/03/2010	19:31	Km21_22	593033.2	1328627	294.8728	5.216811	7.195403	0.749191	7.944594
10/03/2010	19:38	Km21_23	593127.5	1328513	298.5451	5.805287	7.399113	0.855384	8.254498
10/03/2010	19:49	Km21_24	593231.8	1328374	298.359	5.499871	7.113196	0.905492	8.018688
10/03/2010	19:58	Km21_25	593392	1328144	296.4688	5.280243	7.091615	0.882017	7.973632
10/03/2010	20:07	Km21_26	593293.7	1328138	288.288	4.137813	6.806328	0.744008	7.550336
11/03/2010	16:32	SAN01	591343.9	1325432	582.235	16.18966	-11.9401	6.282915	-5.6572
11/03/2010	16:40	SAN02	591391.6	1325445	589.1036	16.46209	-12.3873	6.887479	-5.49987
11/03/2010	16:50	SAN03	591444.7	1325435	599.217	17.11174	-12.7973	7.624977	-5.17235
11/03/2010	16:59	SAN04	591501.9	1325449	605.334	17.73924	-12.8107	8.384906	-4.42583
11/03/2010	17:09	SAN05	591560.5	1325440	612.9057	16.78032	-14.563	8.721484	-5.8415
11/03/2010	17:17	SAN06	591667.1	1325457	605.0454	17.18193	-13.3378	7.46629	-5.87153
11/03/2010	17:28	SAN07	591568.6	1325378	621.796	18.11916	-14.1556	9.333353	-4.82227
11/03/2010	17:43	SAN08	591591.9	1325332	627.9991	18.77369	-14.151	9.638924	-4.5121
11/03/2010	18:01	SAN09	591602.6	1325274	632.256	29.36604	-4.00469	9.844122	5.839427
11/03/2010	18:08	SAN10	591635.3	1325229	626.3398	34.05991	1.30905	9.504923	10.81397
11/03/2010	18:17	SAN11	591659.8	1325178	623.3421	33.70963	1.272847	8.98066	10.25351

16/03/2010	16:06	Lag01	595142.5	1326499	229.4862	-6.03667	2.792804	0.935891	3.728695
16/03/2010	16:15	Lag02	594950.4	1326471	214.0552	-6.2747	4.171553	0.725246	4.896799
16/03/2010	16:31	Lag03	595237.3	1326343	188.0992	-9.48742	3.678378	0.81297	4.491348
16/03/2010	16:43	Lag04	595505.4	1326220	169.3895	-11.9257	3.200391	0.828213	4.028604
16/03/2010	16:52	Lag05	595606.3	1325950	163.4565	-12.8244	2.923318	0.798141	3.721459
16/03/2010	17:00	Lag06	595720.8	1325681	150.2676	-15.7588	1.370836	0.748708	2.119544
16/03/2010	17:11	Lag07	595660.4	1325387	143.9842	-16.9432	0.844788	0.69342	1.538208
16/03/2010	17:20	Lag08	595483.2	1325151	137.3249	-17.9167	0.56899	0.751284	1.320274
16/03/2010	17:31	Lag09	595550.5	1324873	139.2136	-18.1429	0.144905	0.715823	0.860728
16/03/2010	17:52	Lag10	595518.1	1324559	144.6128	-17.0937	0.628428	0.910898	1.539326
16/03/2010	18:02	Lag11	595505	1324256	149.9052	-18.9601	-1.79257	0.830344	-0.96223
16/03/2010	18:14	Lag12	595336.8	1323955	146.8397	-21.245	-3.75624	0.796405	-2.95983
16/03/2010	18:28	Lag13	595245.9	1323677	136.7923	-22.6451	-4.1036	0.815954	-3.28764
16/03/2010	18:44	Lag14	595336	1323404	140.4895	-22.8239	-4.66978	0.840478	-3.8293
16/03/2010	18:58	Lag15	595337.3	1323117	137.9971	-25.7502	-7.33491	0.913575	-6.42133
16/03/2010	19:09	Lag16	595246.9	1322850	144.0346	-24.489	-6.70629	0.969716	-5.73658
16/03/2010	19:18	Lag17	595099.4	1322597	132.8639	-28.4667	-9.5136	0.965649	-8.54795
16/03/2010	19:25	Lag18	594943	1322392	146.3133	-26.2572	-8.71326	0.94246	-7.7708
16/03/2010	19:40	Lag19	594766.1	1322148	143.4293	-28.3404	-10.4943	1.103969	-9.39034
16/03/2010	19:50	Lag20	594655.1	1321891	142.6456	-29.5111	-11.5829	1.216995	-10.3659
16/03/2010	20:00	Lag21	594654.4	1321620	137.567	-28.5028	-10.0425	1.429478	-8.61302
16/03/2010	20:17	Lag22	594744.9	1321471	136.0412	-32.9811	-14.3609	1.452618	-12.9083
19/03/2010	16:04	MONT01	589590.5	1326923	328.4688	0.51872	-1.02271	0.78534	-0.23737
19/03/2010	16:20	MONT02	589515.2	1326846	331.2313	0.104912	-1.72596	0.745848	-0.98011
19/03/2010	16:39	MONT03	589556.9	1326774	334.02	-0.21062	-2.33368	0.739695	-1.59398
19/03/2010	17:48	NIN01	592803.8	1327337	294.9582	2.102647	4.072291	0.682006	4.754297
19/03/2010	17:54	NIN02	592823.2	1327389	288.8245	0.837633	3.449936	0.598428	4.048364
19/03/2010	18:02	NIN03	592844.9	1327440	288.8541	1.231035	3.840236	0.599871	4.440108
19/03/2010	18:14	NIN04	592867.4	1327492	288.8437	1.389172	3.999463	0.597188	4.596651
19/03/2010	18:26	NIN05	592896.1	1327548	289.6445	1.361876	3.888263	0.62556	4.513823
19/03/2010	18:38	NIN06	592900.5	1327600	295.4979	4.953973	6.86707	0.74775	7.61482
19/03/2010	18:46	NIN07	592938.3	1327660	295.8971	3.29553	5.166801	0.894416	6.061217
19/03/2010	18:53	NIN08	592967.5	1327715	290.6286	3.03294	5.456218	0.895917	6.352135
19/03/2010	19:01	NIN09	592973.1	1327770	293.236	4.140994	6.291082	0.985903	7.276985
19/03/2010	19:11	NIN10	592967.2	1327843	292.4791	4.57723	6.806622	0.901481	7.708102
19/03/2010	19:18	NIN11	592975.2	1327899	285.3365	3.583417	6.561174	0.710971	7.272145
19/03/2010	19:26	NIN12	592993.2	1327954	281.3218	3.389252	6.78765	0.61084	7.39849
19/03/2010	19:37	NIN13	593028.1	1328016	277.1615	3.106626	6.94092	0.529514	7.470434
19/03/2010	19:42	NIN14	593077.6	1328051	275.3897	3.558128	7.578062	0.519702	8.097764
19/03/2010	19:54	NIN15	593163.4	1328106	273.4955	3.393565	7.611964	0.501743	8.113707
19/03/2010	20:02	NIN16	593231.8	1328121	277.8116	3.506595	7.272774	0.571641	7.844416
19/03/2010	20:29	NIN17	593578.5	1327947	296.7632	3.070999	4.851524	0.808711	5.660235
19/03/2010	20:41	NIN18	593754.2	1327731	299.9718	2.657821	4.102166	0.874781	4.976947
19/03/2010	20:53	NIN19	593906.7	1327539	299.4557	0.657671	2.15609	0.87397	3.03006

19/03/2010	21:03	NIN20	594117.6	1327274	288.1054	-1.05479	1.632856	0.849417	2.482273
19/03/2010	21:20	NIN21	594305.2	1327044	276.6373	-1.20833	2.680884	0.820047	3.500931
19/03/2010	21:32	NIN22	594541.9	1326764	253.8801	-5.17939	1.094209	0.671653	1.765862
19/03/2010	21:46	NIN23	594837.7	1326638	245.0999	-5.28487	1.908678	0.788202	2.696881
19/03/2010	21:59	NIN24	595140.9	1326632	236.7618	-5.79299	2.274179	0.706674	2.980853
24/03/2010	16:38	MONT01	589460.9	1326481	340.7601	-3.28301	-6.11226	0.747191	-5.36506
24/03/2010	16:49	MONT02	589467.4	1326557	325.9326	-4.33098	-5.60668	0.83629	-4.77039
24/03/2010	16:59	MONT03	589403	1326617	325.5262	-2.70436	-3.93748	0.794573	-3.1429
24/03/2010	17:10	MONT04	589429.9	1326709	326.2235	-1.99943	-3.30561	0.725535	-2.58007
24/03/2010	17:18	MONT05	589449.2	1326824	326.464	-1.08983	-2.42121	0.707465	-1.71374
24/03/2010	17:26	MONT06	589391.3	1326900	324.0264	-1.8224	-2.89837	0.709762	-2.18861
24/03/2010	17:36	MONT07	589412.4	1326976	324.0512	-1.69898	-2.77756	0.741635	-2.03592
24/03/2010	18:18	MONT09	589454.7	1327041	311.9027	-2.53387	-2.33958	0.762703	-1.57688
24/03/2010	20:10	COMA01	592413.2	1326694	313.8142	0.12229	0.116297	0.821812	0.938109
24/03/2010	20:17	COMA02	592443.8	1326610	317.0017	-0.10477	-0.44473	0.877336	0.432607
24/03/2010	20:30	COMA03	592452.4	1326526	328.583	0.16649	-1.3869	1.038946	-0.34796
24/03/2010	20:34	COMA04	592465.2	1326455	336.7928	5.711894	3.298318	1.123801	4.422119
24/03/2010	20:48	COMA05	592419.8	1326376	342.6253	0.471312	-2.55336	1.187936	-1.36543
24/03/2010	20:58	COMA06	592419.9	1326376	343.3002	1.738364	-1.35703	1.202107	-0.15492
24/03/2010	21:12	COMA07	592389	1326278	340.0357	0.979951	-1.7734	1.160095	-0.6133
24/03/2010	22:33	CARRETERA01	595330.5	1326631	212.7262	-11.7079	-1.12244	0.521495	-0.60094
25/03/2010	16:12	CERJITO01	590722.3	1323417	423.0878	-4.38708	-15.8422	0.889402	-14.9528
25/03/2010	16:25	CERJITO02	590927.3	1323319	422.4852	-0.48859	-11.8806	1.011294	-10.8693
25/03/2010	16:40	CERJITO03	591209.1	1323312	413.5758	-4.29375	-14.7523	1.05815	-13.6941
25/03/2010	17:04	CERJITO04	591356.6	1323097	394.2373	-7.35489	-15.7872	1.008157	-14.7791
25/03/2010	17:20	CERJITO05	591547.8	1322948	375.7401	-8.06801	-14.5623	0.988434	-13.5739
25/03/2010	17:37	CERJITO06	591656.1	1322645	345.2539	-13.0234	-16.3235	0.792096	-15.5314
25/03/2010	17:46	CERJITO07	591838.1	1322457	335.5282	-13.7725	-16.0536	0.84902	-15.2046
19/01/2011	16:02	GRADIENT_BASE	591962.7	1329124	280.7945	4.315301	7.768947	0.522637	8.291584
19/01/2011	16:16	GRADIENT01	591722.5	1329224	281.0357	3.890007	7.318381	0.543378	7.861759
19/01/2011	16:34	GRADIENT02	591425.8	1329343	288.9735	3.031985	5.628676	0.548465	6.177141
19/01/2011	17:00	GRADIENT03	591164	1329373	298.0851	4.006215	5.648238	0.587179	6.235417
19/01/2011	17:17	GRADIENT04	590883.6	1329402	303.9522	4.342094	5.369392	0.592654	5.962046
19/01/2011	17:24	GRADIENT05	590603.2	1329431	306.8027	4.263283	4.991919	0.593801	5.58572
19/01/2011	17:46	GRADIENT06	590336.8	1329459	308.2883	3.720565	4.293548	0.603704	4.897252
19/01/2011	18:01	GRADIENT07	590062	1329482	310.1217	3.190142	3.57103	0.630344	4.201374
19/01/2011	18:16	GRADIENT08	589795.6	1329531	310.6759	1.234941	1.557763	0.662108	2.219871
19/01/2011	18:35	GRADIENT09	589547.3	1329707	300.2571	-0.91867	0.495778	0.60159	1.097368
19/01/2011	20:00	GRADIENT10	589317.6	1329964	285.0589	-3.27103	-0.26419	0.581978	0.317791
19/01/2011	20:13	GRADIENT11	589100.7	1330199	269.9813	-5.80774	-1.22114	0.587476	-0.63367
19/01/2011	20:27	GRADIENT12	588921.2	1330402	264.5153	-7.23196	-2.07266	0.571303	-1.50136
19/01/2011	20:42	GRADIENT_BASE	591962.7	1329124	280.7945	4.315301	7.768947	0.522637	8.291584
19/01/2011	21:06	A1	592423.4	1326777	313.757	0.026982	0.026982	0.811514	0.838495
20/01/2011	16:37	Ninmas01	595655.4	1326649	223.7514	-7.79025	1.640088	0.866904	2.506993

20/01/2011	16:47	Ninmas02	595956.5	1326661	218.8504	-6.76755	3.176286	1.279647	4.455933
20/01/2011	16:57	Ninmas03	596257.3	1326664	219.4579	-10.0658	-0.18558	0.826603	0.64102
20/01/2011	17:05	Ninmas04	596495.3	1326507	218.7152	-10.6976	-0.73957	0.741492	0.001919
20/01/2011	17:19	Ninmas05	596779.6	1326287	221.309	-10.3711	-0.68485	0.529329	-0.15552
20/01/2011	17:37	Ninmas06	596971.5	1326078	224.4702	-10.3558	-1.00077	0.477497	-0.52327
20/01/2011	18:01	Ninmas07	597166.9	1325841	235.9922	-10.6949	-2.54707	0.520985	-2.02608
20/01/2011	18:10	Ninmas08	597322.4	1325562	233.5327	-11.4948	-3.0893	0.473518	-2.61578
20/01/2011	18:18	Ninmas09	597461	1325280	233.7451	-12.6011	-4.21789	0.543239	-3.67465
20/01/2011	18:27	Ninmas10	597613.1	1325007	234.7177	-13.7337	-5.4524	0.590173	-4.86222
20/01/2011	18:36	Ninmas11	597750.5	1324751	236.1868	-14.4186	-6.29123	0.582092	-5.70913
20/01/2011	18:46	Ninmas12	597874.7	1324532	238.5294	-14.9526	-7.07058	0.540544	-6.53004
20/01/2011	19:20	Ninmas13	598022.4	1324281	237.6644	-16.0029	-8.03025	0.471544	-7.55871
20/01/2011	19:32	Ninmas14	597994.5	1324115	237.2147	-16.4971	-8.4774	0.492172	-7.98522
20/01/2011	19:44	Ninmas15	597691.7	1324107	232.6569	-17.3896	-8.89234	0.739987	-8.15236
20/01/2011	19:53	Ninmas16	597437.2	1324126	235.8394	-15.6253	-7.46152	2.312095	-5.14943
20/01/2011	20:05	Ninmas17	597476.8	1323770	240.5473	-15.8735	-8.203	2.935518	-5.26748
20/01/2011	20:16	Ninmas18	597728	1323474	234.2965	-19.801	-11.4755	0.839079	-10.6364
20/01/2011	20:39	Ninmas01	595655.4	1326649	223.7514	-7.78255	1.647788	0.866904	2.514693
21/01/2011	16:21	NINTOW01	595821.9	1326977	220.0309	-8.3929	1.427248	0.422915	1.850163
21/01/2011	16:36	NINTOW02	595820.9	1327346	221.4718	-7.17729	2.491895	0.372708	2.864603
21/01/2011	16:46	NINTOW03	595860.6	1327623	215.7291	-8.45121	1.819666	0.303398	2.123064
21/01/2011	16:55	NINTOW04	595902.9	1327955	215.3738	-8.12561	2.182488	0.32149	2.503978
21/01/2011	17:05	NINTOW05	595946.1	1328235	213.2197	-8.92451	1.609285	0.330664	1.939949
21/01/2011	17:15	NINTOW06	595988.7	1328559	211.6717	-9.79815	0.897837	0.341746	1.239583
21/01/2011	17:27	NINTOW07	595999.5	1328842	210.1143	-10.8376	0.021543	0.343462	0.365005
21/01/2011	17:36	NINTOW08	595987.8	1329116	207.4559	-11.864	-0.72632	0.311166	-0.41516
21/01/2011	17:44	NINTOW09	596031.4	1329412	205.4404	-11.81	-0.46115	0.308277	-0.15287
21/01/2011	17:53	NINTOW10	596094.6	1329702	203.3993	-13.6391	-2.07642	0.305302	-1.77112
21/01/2011	18:03	NINTOW11	596130.7	1330004	201.7471	-14.8574	-3.12156	0.312015	-2.80955
21/01/2011	18:15	NINTOW12	596101.7	1330332	196.5375	-16.1646	-3.88297	0.293324	-3.58964
21/01/2011	18:29	NINTOW13	596111.5	1330550	190.4325	-17.5143	-4.59299	0.291409	-4.30158
21/01/2011	18:38	NINTOW14	596088.5	1330819	188.7462	-18.2655	-5.16745	0.286163	-4.88128
24/01/2011	18:09	Nintow16	591324.5	1324753	603.0933	14.98174	-15.3335	6.960836	-8.37263
24/01/2011	18:24	Nintow17	591398.4	1324746	610.6343	14.82388	-16.2814	7.499184	-8.78226
24/01/2011	18:34	Nintow18	591449.7	1324729	631.4455	14.1582	-19.1276	9.047587	-10.08
24/01/2011	18:47	Nintow19	591513.8	1324760	610.5804	14.93867	-16.161	7.429438	-8.73156
24/01/2011	19:06	Nintow20	591595.2	1324832	601.0264	16.175	-13.9237	6.636689	-7.28697
24/01/2011	19:37	Nintow21	591662.5	1324925	611.2173	16.70631	-14.4601	7.282066	-7.17803
24/01/2011	19:54	Nintow22	591693.4	1324999	623.9413	17.20603	-15.2935	8.361177	-6.93235
24/01/2011	20:07	Nintow23	591719.9	1325081	625.7941	18.79206	-13.9016	8.445021	-5.45661
24/01/2011	20:21	Nintow24	591678.5	1325156	616.0114	17.76219	-13.9065	8.237136	-5.66938
24/01/2011	20:30	Nintow25	591631	1325227	616.2758	17.77165	-13.9248	8.763702	-5.16105
24/01/2011	20:45	Nintow26	591564	1325306	626.1407	19.31845	-13.4116	9.521952	-3.8896
24/01/2011	20:55	Nintow27	591490.7	1325346	627.0541	17.9885	-14.8372	9.701449	-5.13575

24/01/2011	21:10	Nintow28	591402.5	1325373	603.1168	17.25964	-13.058	7.79718	-5.26085
24/01/2011	21:20	Nintow29	591314.2	1325342	596.115	16.72524	-12.8588	7.369236	-5.48958
24/01/2011	21:29	Nintow30	591228	1325291	598.0145	16.401	-13.3821	7.475627	-5.90646
24/01/2011	21:42	Nintow31	591141.3	1325237	597.6762	16.60196	-13.1457	7.183934	-5.96174
24/01/2011	21:49	Nintow32	591083.2	1325188	594.0541	16.70249	-12.6656	6.703732	-5.9619
24/01/2011	22:37	A1	592423.4	1326777	313.757	0.026982	0	0.811514	0.811514
27/01/2011	16:57	Piedquem01	592124.6	1329428	273.2435	-1.62582	2.618979	0.471788	3.090767
27/01/2011	17:06	Piedquem02	591979.8	1329756	260.0692	-3.86129	1.763846	0.446981	2.210827
27/01/2011	17:17	Piedquem03	591792.1	1330040	257.7535	-3.57816	2.289608	0.49331	2.782918
27/01/2011	17:42	Piedquem04	591731.9	1330394	236.755	-6.47933	1.588552	0.474246	2.062797
27/01/2011	17:50	Piedquem06	591619	1330782	218.1264	-9.01874	1.000958	0.431239	1.432197
27/01/2011	18:03	Piedquem07	591613.5	1331106	206.0685	-11.0036	0.279432	0.420824	0.700257
27/01/2011	18:16	Piedquem08	591643.7	1331456	193.4888	-13.5578	-0.95666	0.416034	-0.54063
27/01/2011	18:24	Piedquem09	591692.4	1331972	178.7378	-17.1224	-2.97577	0.392531	-2.58324
27/01/2011	18:35	Piedquem10	591595.4	1332336	170.2876	-18.7542	-3.72219	0.379198	-3.34299
27/01/2011	19:09	Piedquem11	591487.6	1332629	164.132	-19.9671	-4.29015	0.3777	-3.91245
27/01/2011	19:25	Piedquem12	591259.2	1333023	153.3941	-21.6726	-4.87056	0.38871	-4.48185
27/01/2011	19:37	Piedquem13	591121.6	1333525	144.3822	-23.2447	-5.49847	0.37951	-5.11896
27/01/2011	19:48	Piedquem14	591161.7	1334017	123.5953	-26.8255	-6.90129	0.380436	-6.52086
27/01/2011	19:57	Piedquem15	591109.8	1334352	119.7129	-27.3563	-7.02537	0.358186	-6.66719
27/01/2011	20:24	Piedquem01	592124.6	1329428	273.2435	-1.62422	2.620579	0.471788	3.092367
07/02/2011	16:49	BORDE01	587400.8	1324976	532.3583	0.375184	-22.5288	3.452187	-19.0766
07/02/2011	16:58	BORDE02	587338.6	1325325	503.7824	-0.47759	-20.3875	4.773319	-15.6142
07/02/2011	17:05	BORDE03	587268.7	1325738	476.2347	-0.15867	-17.1823	4.382553	-12.7997
07/02/2011	17:13	BORDE04	587183.1	1326121	458.0369	-1.86017	-16.9771	3.24168	-13.7354
07/02/2011	17:24	BORDE06	587150.8	1326472	432.9825	-1.32755	-13.8194	1.922116	-11.8973
07/02/2011	17:35	BORDE08	587127.2	1326887	397.0549	-6.41658	-15.1441	0.982826	-14.1613
07/02/2011	17:43	BORDE08	587150.3	1326859	403.0248	-8.05841	-17.4114	1.051815	-16.3596
07/02/2011	17:57	BORDE10	587068.2	1327251	380.9248	-8.40869	-15.4462	0.827427	-14.6188
07/02/2011	18:10	BORDE12	586976.2	1327663	361.0644	-9.50412	-14.4608	0.737779	-13.723
07/02/2011	18:21	BORDE13	586778.5	1327960	338.6949	-11.5762	-14.189	0.672943	-13.5161
07/02/2011	18:32	BORDE14	586683.2	1328267	326.8011	-13.1946	-14.5613	0.67981	-13.8815
07/02/2011	18:46	BORDE15	586666.2	1328665	310.3777	-14.6187	-14.2646	0.643276	-13.6214
07/02/2011	19:36	BORDE16	586481.9	1329081	295.7241	-16.939	-15.0496	0.6777	-14.3719
07/02/2011	19:45	BORDE17	586946	1329034	297.5925	-14.4	-12.7063	0.65096	-12.0554
07/02/2011	19:52	BORDE18	587468.9	1329091	303.7411	-11.2036	-10.1542	0.6293	-9.52488
07/02/2011	20:03	BORDE19	588025.5	1329180	313.3132	-7.43161	-7.38511	0.626881	-6.75823
07/02/2011	20:14	BORDE20	588810.3	1329333	314.0832	-0.65595	-0.69012	0.812178	0.122054
07/02/2011	20:22	BORDE21	589413.1	1329385	319.3503	3.479083	2.893045	1.061462	3.954507
08/02/2011	16:34	BCNT01	591028.7	1324100	461.8972	4.023059	-11.4983	1.44134	-10.057
08/02/2011	16:57	BCNT02	590999.6	1323820	433.7774	0.636441	-11.9387	1.079739	-10.859
08/02/2011	17:30	BCNT03	591356.5	1323986	449.1114	2.884081	-11.2977	1.471083	-9.82659
08/02/2011	17:50	BCNT04	591650.3	1324377	435.1895	1.85428	-10.8688	2.215815	-8.653
08/02/2011	18:45	BCNT05	592900.4	1324858	310.253	-5.42767	-5.06053	1.541982	-3.51855

08/02/2011	19:04	BCNT06	593043.6	1325157	282.2295	-6.17464	-2.87135	1.464539	-1.40681
08/02/2011	17:05	Kunz01	596405.3	1326679	219.8296	-10.064	-0.22277	0.604494	0.381726
08/02/2011	17:19	Kunz02	596721.2	1326609	220.3362	-10.368	-0.57987	0.474575	-0.10529
08/02/2011	17:28	Kunz03	596950.9	1326429	223.9002	-10.0829	-0.66814	0.460054	-0.20809
08/02/2011	17:35	Kunz04	597189.1	1326220	227.5454	-10.4368	-1.404	0.448962	-0.95504
08/02/2011	17:45	Kunz05	597228.8	1326016	232.6118	-10.9957	-2.49371	0.445352	-2.04836
08/02/2011	17:55	Kunz06	597239.3	1325693	236.9474	-8.60077	-0.55304	0.515367	-0.03768
09/02/2011	16:00	A4	590612.9	1326695	323.7794	-2.50748	-3.55758	0.910705	-2.64687
09/02/2011	18:25	Novac011	588791.8	1325161	328.7911	-9.99552	-11.5707	1.326855	-10.2439
09/02/2011	18:51	Novac012	588918.4	1325252	326.5339	-9.65598	-10.9947	1.222182	-9.77249
09/02/2011	19:05	Novac013	589042	1325377	329.0233	-8.36731	-9.96684	1.202398	-8.76444
09/02/2011	19:18	Novac014	588970.4	1325612	318.8367	-9.27015	-9.80238	1.054677	-8.7477
09/02/2011	19:29	Novac015	588899	1325813	311.0452	-9.19286	-8.90873	0.972167	-7.93657
09/02/2011	19:39	Novac016	588994.6	1325957	321.4763	-6.59989	-7.40868	0.94404	-6.46464
09/02/2011	19:49	Novac017	589134.7	1326035	329.2667	-5.70226	-7.32729	0.944208	-6.38308
09/02/2011	20:00	Novac019	589296.7	1326185	341.9172	-3.81214	-6.76262	0.891222	-5.8714
09/02/2011	18:55	Novac21	588872.8	1325221	325.9366	-9.78072	-11.0568	1.236697	-9.82014
09/02/2011	19:02	Novac22	588973.7	1325298	326.2946	-9.44814	-10.7618	1.209586	-9.55218
09/02/2011	19:14	Novac23	588996.9	1325495	322.7748	-9.1353	-10.0801	1.114443	-8.96569
09/02/2011	19:25	Novac24	588938.5	1325719	315.0663	-8.80908	-8.94626	0.997661	-7.9486
09/02/2011	19:35	Novac25	588924.2	1325901	315.0913	-7.72803	-7.86783	0.945867	-6.92196
09/02/2011	19:45	Novac26	589081.6	1325980	324.1402	-6.37385	-7.46175	0.938705	-6.52304
09/02/2011	19:55	Novac27	589217.5	1326133	335.8738	-4.79653	-7.11382	0.904279	-6.20954
15/02/2011	16:04	Bat_1	590646	1324602	505.4318	7.129896	-12.9528	2.068977	-10.8839
15/02/2011	17:50	Ted_1	590129	1323676	423.8761	-6.76321	-18.3009	0.86357	-17.4374
15/02/2011	18:24	Ted_2	590031.9	1323680	422.1408	-7.38918	-18.7451	0.893673	-17.8514
15/02/2011	18:43	Ted_3	589956	1323698	420.6619	-7.76639	-18.9674	0.956982	-18.0104
15/02/2011	19:16	Ted_4	589901.4	1323708	419.8194	-8.12684	-19.2395	1.066342	-18.1732
15/02/2011	19:35	Ted_5	589801.1	1323726	419.3821	-8.4673	-19.5342	1.306557	-18.2276
15/02/2011	19:51	Ted_6	589698.5	1323736	415.7491	-9.26487	-19.9511	1.595343	-18.3557
15/02/2011	20:03	Ted_7	589563.7	1323785	409.6982	-10.2789	-20.3311	1.487989	-18.8431
15/02/2011	20:49	Ted_9	589335.2	1323904	402.8903	-10.762	-20.101	1.481363	-18.6196
15/02/2011	21:09	Ted_10	589206.1	1323972	403.9766	-11.1152	-20.5679	1.608173	-18.9598
15/02/2011	21:23	Ted_11	589010	1324178	399.2234	-11.3536	-20.3083	1.636217	-18.6721
16/02/2011	15:41	Borde_01	587400.8	1324976	532.3583	66.54978	43.64583	3.452187	47.09802
16/02/2011	15:55	Village_01	589873.1	1329287	276.8627	0.710111	4.575711	0.801243	5.376955
16/02/2011	16:45	Village_02	589894.3	1329113	275.934	0.986859	4.949763	0.564443	5.514207
16/02/2011	16:54	Village_03	589900.7	1328919	277.0917	0.15283	3.994436	0.505634	4.50007
16/02/2011	17:09	Village_04	589924.8	1328766	277.3141	-0.34671	3.471594	0.482131	3.953725
16/02/2011	17:18	Village_05	589895.7	1328596	275.1827	-0.77149	3.270128	0.479662	3.74979
16/02/2011	17:33	Village_06	589872.5	1328433	277.2441	-0.6993	3.126341	0.522674	3.649015
16/02/2011	17:54	Village_07	590038.6	1328547	284.7485	0.056956	3.096322	0.521117	3.617438
16/02/2011	18:50	Village_08	590266.8	1328528	288.0188	1.111927	3.808647	0.512286	4.320933
16/02/2011	19:00	Village_09	590470.2	1328477	288.3632	1.682284	4.342919	0.511704	4.854623

8.10 Appendix J: Microgravity data (summit area)

Point_ID	Height_m	Easting (UTM 16P)	Northing (UTM 16P)	First reading	Feb-93	Apr-94	Oct-94	Mar-96	Mar-97	Feb-98	Sep-98	Feb-99	Jun-99	Mar-00	Jan-04	Mar-08	Mar-09	Jan-10	Mar-11
Delta_Nind	499.2921	590298.4	1325201	Mar-08	-	-	-	-	-	-	-	-	-	-	-	-	0.046	0.052	-0.031
Nindiri	498.585	590298.8	1325201	Feb-99	-	-	-	-	-	-	-	-	-0.044	-0.023	-	-	-	-	-
Zopilotes	539.7667	589970.2	1325146	Mar-08	-	-	-	-	-	-	-	-	-	-	-	-	0.0485	0.039	-0.002
Pecho_Viejo	540.4568	590050.1	1324995	Mar-08	-	-	-	-	-	-	-	-	-	-	-	-	0.031	0.008	-0.048
Teatro	538.8775	590235.3	1324912	Jan-04	-	-	-	-	-	-	-	-	-	-	-	-0.056	-0.06167	-0.065	-0.108
Bat1	508.1565	590646	1324602	Jan-10	-	-	-	-	-	-	-	-	-	-	-	-	-	-	-0.02
A9	525.9264	590785.9	1324703	Feb-93	-	-0.08	-	-0.113	-0.064	-0.066	-0.083	-0.183	-0.15	-0.137	-0.171	-	-0.164	-0.172	-0.162
B4	538.5463	590758.1	1325172	Jan-04	-	-	-	-	-	-	-	-	-	-	-	-	-0.00936	0.004	-0.043
Guru	593.9622	591051.4	1325143	Mar-09	-	-	-	-	-	-	-	-	-	-	-	-	-	-0.005	0.014
Edge	526.5325	590451	1325227	Mar-97	-	-	-	-	-	0.004	-0.04	-0.056	-0.12	-0.114	-0.104	-0.0575	-0.09	-0.073	-0.13
E3	516.29	590633.4	1324680	Feb-93	-	0	-	-	-	-	-	-	-	-	-0.076	-	-0.006	-0.063	-0.102
A8	572.6873	590901.7	1324933	Feb-93	-	-0.071	-	-0.052	-0.055	-0.068	-0.083	-0.085	-0.083	-0.076	-0.14	-0.14	-0.137	-0.142	-0.149
B2	538.1112	590728.4	1325208	Apr-94	-	-	-	0.029	-0.015	-0.023	-0.034	-0.035	-0.094	-0.081	-0.121	-0.1125	-	-	-
A11	516.5332	590484.4	1324615	Mar-97	-	-	-	-	-	-0.036	-0.051	-0.063	-0.105	-0.107	0	-	0.061	0.007	-0.035
A10	522.4791	590400.2	1324629	Feb-93	-	-0.08	-	-0.065	-0.024	-0.053	-0.072	-0.074	-0.131	-0.127	-0.179	-	-0.1	-0.152	-0.009
A7	534.0615	590740.9	1325301	Feb-93	-	-0.078	-0.088	-0.051	-0.054	-0.056	-0.074	-0.082	-0.139	-0.135	-0.191	-0.1485	-	-	-0.013
Pedro	530.3625	590349.5	1325384	Mar-97	-	-	-	-	-	-0.012	-0.05	-0.052	-0.123	-0.111	-0.097	-0.0355	-0.066	-0.058	-0.102
Pedro2	533.4776	590220.8	1325443	Feb-99	-	-	-	-	-	-	-	-	-0.045	-0.053	-0.043	-0.015	0.004	0.045	-0.041

8.11 Appendix K: InSAR data

Master date	Slave date	Time Spanned (days)	Approximate B_{perp} (m)	Track	Frame	Orientation
10th Oct. 2007	25th Feb. 2008	138	339	165	230	Ascending
10th Oct. 2007	12th Oct. 2008	368	-987	165	230	Ascending
25th Nov. 2007	25th Feb. 2008	92	282	165	230	Ascending
25th Feb. 2008	12th Oct. 2008	230	-1406	165	230	Ascending
12th Oct. 2008	27th Nov. 2008	46	102	165	230	Ascending
27th Nov. 2008	14th Apr. 2009	138	736	165	230	Ascending
30th Aug. 2009	30th Nov. 2009	92	-183	165	230	Ascending
30th Nov. 2009	18th July 2010	230	302	165	230	Ascending
30th Nov. 2009	15th Jan 2010	46	-26	165	230	Ascending
2nd June 2010	18th July 2010	46	-45	165	230	Ascending
15th Jan 2010	2nd June 2010	138	373	165	230	Ascending
27th Sep. 2007	28th Dec. 2007	368	508	470	3380	Descending
28th Dec. 2007	29th Mar. 2008	92	74	470	3380	Descending
29th Mar. 2008	14th May 2008	46	-302	470	3380	Descending
29th Sep 2008	14th Nov. 2008	46	-114	470	3380	Descending
14th Nov. 2008	1st Apr. 2009	138	542	470	3380	Descending